IJEST

ISSN: 0973-6255
Vol. 15 No.1&2
January - December 2021

Indian Journal of Engineering, Science, and Technology

A Refereed Research Journal

Published by

BANNARI AMMAN INSTITUTE OF TECHNOLOGY

(Autonomous Institution Affiliated to Anna University, Chennai - Approved by AICTE - Accredited by NAAC with "A+" Grade)

Sathyamangalam - 638 401 Erode District Tamil Nadu India | Ph: 04295-226340 - 44 Fax: 04295-226666

E-mail: ijest@bitsathy.ac.in | www.bitsathy.ac.in

Stay Ahead

Indian Journal of Engineering, Science, and Technology

IJEST is a refereed research journal published half-yearly by Bannari Amman Institute of Technology. Responsibility for the contents rests upon the authors and not upon the IJEST. For copying or reprint permission, write to Copyright Department, IJEST, Bannari Amman Institute of Technology, Sathyamanagalam, Erode District - 638 401, Tamil Nadu, India.

Indian Journal of Engineering, Science, and Technology

ISSN: 0973-6255

Volume 15 Number 1&2 **January - December 2021**

CONTENTS

PERFORMANCE ANALYSIS OF AUTOMOBILE RADIATOR USING MWCNT NANO-FLUID

Amarkarthik Arunachalam and Vinoth Kumar Jayakumar
Department of Mechanical Engineering,
Bannari Amman Institute of Technology, Sathyamangalam -638 401, Erode District, Tamil Nadu
E-mail: amarkarthik@bitsathy.ac.in, vinothkumar@bitsathy.ac.in

Abstract

Traditional fluids (water and glycol) have poor heat transfer capability when paired with a car radiator. The performance of vehicle radiators employing water and multiwalled carbon nanotube nanoparticles (MWCNT) nanofluid as the working fluid was investigated in an experimental investigation. The heat transfer rate and fluid outlet temperature of various flow rates ranging from 0.2 to 0.5 m^3/hr are investigated and compared. Nanofluids were made with volume concentrations of MWCNT nanoparticles of 0.0167 percent, 0.034 percent, and 0.0667 percent in water. Because temperature fluctuations have the least impact on system performance, the fluid inlet condition is set to 50°C. In the experiment, the largest increase in heat transfer rate was 4.56 percent when compared to the base fluid.

Keywords: *Heat transfer rate, MWCNT, Nanoűuid, Performance, Radiator*

1. INTRODUCTION

For heat dissipation, most engineering systems rely on traditional coolants. In most heat transfer systems, nanofluids (basic fluids dispersed with nanoparticles) now perform much better than other heat transfer methods. To avoid fouling, precipitation, and a rise in pressure drop, proper precautions must be followed. It is important to expand the size of the heat transfer system or the performance of the cooling fluid in order to improve the heat transfer system's performance. It helps to increase the coolant's performance due to structural constraints.

Peyghambarzadeh [1] examined the performance of a radiator utilising Al2O3Waternanofluid at flow rates ranging from 2 to 5 litres per minute and coolant inlet temperatures ranging from 37 to 49°C. They found that a 1% volume concentration nanofluid increased heat transfer rate by 45% when compared to water, and that variations in coolant inlet temperature had little effect on performance. Sharma [2] performed an experimental investigation on a radiator employing Al/water nanofluids of 0.2% vol. con. and 0.3 vol. con. with intake coolant fluid temperatures ranging from 45 to 55°C. For 0.3% vol. con., they achieved a 23.563% improvement in heat transmission coefficient. Selvam *et al.*[3]reported an 88% increase in Nusselt number for 0.5% vol. con. GnP/(water/EG) nanofluid at 35°C and a 90% increase at 40°C for 0.5% vol. con. GnP/(water/EG) nanofluid.

Oliveira [4] investigated the use of 0.05-0.16 wt. percent MWCNT/water in an automotive radiator with a coolant intake temperature range of 50°C to 80°C and found that 0.16 wt % nanofluid resulted in a 17% reduction in heat transfer. Ali [5] evaluated the performance of a radiator using 0.01% -0.3% vol. con. ZnO/Water nanofluid for intake temperatures of 45 C-55 C and found that utilising 0.2% vol. con. nanofluid resulted in a 46.5% improvement. Ali [6] conducted an experimental investigation on a radiator employing 0.06, 0.09, and 0.12 vol. % MgO/water nanofluid, and found that 0.12 vol. % resulted in a 31% increase in heat transfer rate. Naraki [7] investigated the use of 0.04-0.4% CuO/water nanofluid, which resulted in an 8% increase in overall heat transfer coefficient for the 0.4 vol.% nanofluid.

Hussain[8] studied the overall performance of a radiator using a 1% -2.5% vol. con. SiO2/Water nanofluid for an intake temperature of 60°C-80°C and a coolant flow rate of 2-8 lit/min. They were able to get a 46% improvement by using 2.5% vol. con. Nanofluid. Ahmed *etal.*[9] investigated the incorporation of TiO2/water nanofluid of 0.1% vol. con., 0.2 % vol. con., and 0. 3 vol. con. in radiators with inlet coolant fluid temperatures ranging from 20 to 80°C, and found that the 0.3% vol. con. had the highest overall heat transfer coefficient of 2050 W/m2K (23.563%).

Palaniapan[10] studied the usage of a 2% vol.con. Fly ash nanofluid in an automotive radiator for Reynolds numbers 4000-8000, finding that the 2 percent vol.con. nanofluid resulted in a 43.7% increase in heat transfer at Reynolds number 8000. In the literature, there is no study of tungsten trioxide nanofluid in an automotive radiator. Tungsten trioxide nanoparticles are a type of semiconductor frequently utilised in photo thermal systems; nevertheless, this type of particle has not previously been used as a working fluid additive in automobile radiators, to the authors' knowledge at this concentration range. As a result, the current research aims to see how different concentrations of MWCNT / water nanofluids affect radiator performance.

2. METHODOLOGY

2.1 Analysis of heat transfer rate

Calculation of heat transfer rate in radiator is obtained by using Eq. (1)& Eq. (2).

$$Q = mc_p (T_i - T_0) \quad (1)$$

$$Q = h A (T_b - T_w) \quad (2)$$

The nanofluid's specific heat capacity can be calculated by using Eq. (3) [11]

The density of nanofluid is calculated from the following Eq. (4) [11]

(4)

$$c_{p,nf} = \frac{(1-\varphi)\rho_{bf}c_{p,bf} + \varphi\rho_n c_{p,n}}{(1-\varphi)\rho_{bf} + \varphi\rho_n} \quad (3)$$

nofluid is calculated from the following Eq. (5) [11]

(5)

$$\rho_{nf} = (1-\varphi)\rho_{bf} + \varphi\rho_n$$

The viscosity of nanofluid is calculated from the following Eq. (6) [11]

(6)

$$k_{nf} = \frac{k_n + (n-1)\,k_{bf} - \varphi(n-1)(k_{bf} - k_n)}{k_n + (n-1)\,k_{bf} + \varphi(n-1)(k_{bf} - k_n)}$$

can be calculated using the Eq. (7)[11]

$$Nu_{exp} = \frac{h_{exp}\, x\, D_h}{k} \quad (7)$$

$$\mu_{nf} = \mu_{bf}(1 + 2.5\,\varphi)$$

2.2 uid and experimentation

2.2.1 MWCNT nanofluid synthesis

All chemical compounds were used as obtained, with no additional processing and of diagnostic quality. Nano Research Labs, Jharkhand, India is a supplier of MWCNT nanoparticles. The nanoparticles are 40-50 nm in size and have a purity of 99.9%. Nanofluid is prepared utilising a two-step approach due to its ease of creation. To prevent or limit agglomeration, MWCNT nanoparticles are first ground in a mortar. Following that, appropriate mass fractions of MWCNT nanoparticles are added to distilled water, and the mixture is manually stirred for a minimum of 10 minutes. The produced mixture is sonicated for 4 hours in an ultrasonic bath (ANALAB, India) at a frequency of 30 kHz and a power of 1000 watts. Three distinct nanofluids with volume concentrations of 0.0166%, 0.0334%, and 0.06667% are created. Finally, a Zeta potential analyzer is used to test the stability of the nanofluid.

2.2.2 Experimentation

A vehicle radiator with a fan, reservoir, connectors, rotameter, pump, thermometers, heater, small fuses, tubes, and an expansion resource make up the experimental setup. A thermometer was also used to measure the radiator's air input and output temperatures, coolant inlet and output temperatures, front and rear surface temperatures, and coolant inlet and output temperatures. The experiment took place in Erode, India, at the Bannari Amman Institute of technology. The pump is used to circulate the operational fluid into the radiator (500W). When the working fluid is circulated, it first enters the radiator, then moves to a 20-liter tank and continues the process. The constant temperature bath is used to keep the heat gain from the solar collector cold. Water and nanofluid flow rate adjustment with three-way valve, rotameter for desired flow rate up to 4 l/min, and pressure indicator tables 1 and 2 show the radiation specifications and test conditions for experimentation. The experiment apparatus is shown in schematic form figure 1.

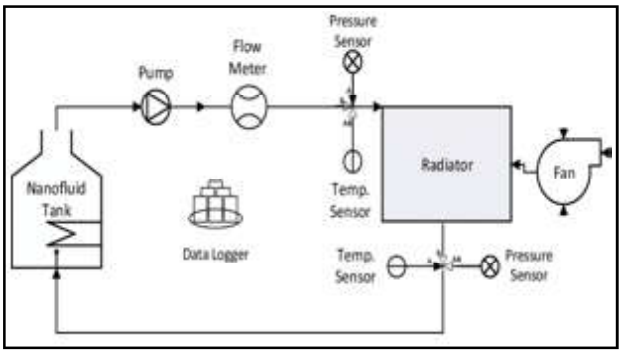

Fig. 1 Experimental setup in schematic form

Table 1 Radiator Specifications

Parameter	Value (cm)
Radiator height	2.2
Radiator length	38.4
Radiator width	33
Fin length	1
Fin thickness	0.008
Width of the radiator tube	0.2
Distance between adjacent fins	0.1

Table 2 Experiment test condition

Parameter	Water based Nano fluid
Reynolds number	200-600
Volumetric flow rate (m^3/hr)	0.2 to 0.5
Inlet temperature (K)	323
Nanoparticle	MWCNT
Nanoparticle concentration (vol. %)	0-0.0667%

3.RESULTS AND DISCUSSION

The working fluids in this investigation are MWCNT nanofluid with concentrations of 0.0167, 0.0334, and 0.0667 vol % for flow rates of 0.2, 0.3, 0.4, and 0.5 m^3/hr, respectively. Figure 3 shows an increase in heat transfer rate as flow rate and nanoparticle concentrations increase. At high flowrates, mixing fluctuation caused by the action of dispersion and chaotic movement of the nanoparticles results in an increase in heat transfer coefficient. Increased heat transmission was seen when the volume concentration of nanoparticles added to the base fluid was increased. Figure 2 illustrates radiator outlet temperatures, T_{out}, as a function of the radiator's fluid volume flow rate. It has been discovered that adding nanoparticles to the base fluid causes the radiator outlet temperature to drop.It may be deduced that an equal mass flow rate in a heat transfer system tends to lower fluid outlet temperature, improving the radiator's thermal performance. Figure 3 also shows how the heat transfer rate depreciates as the volume flow rate through the system increases. The cause for this could be due to an increase in fluid velocity as a result of the increased volume flow rate. As a result, the coolant would only be in contact with the air cycled via the fan for a short time, resulting in a rise in the coolant's exit temperature. All of the statistics in Figure 4 were found for a radiator fluid inlet temperature of 54^0C.

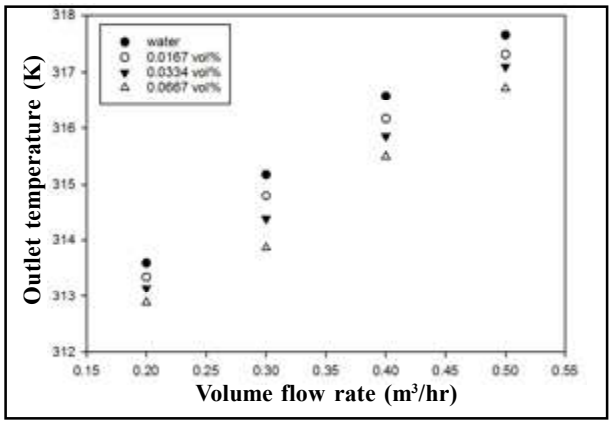

Fig.2. Coolant fluid outlet temperature based on variation of volume flow rate

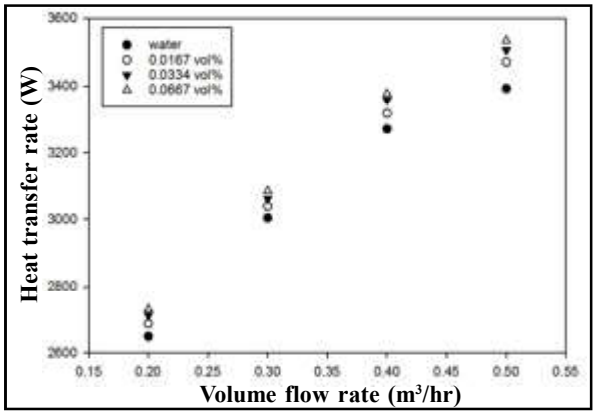

Fig. 3 Heat transfer rate based on volume flow rate variation

Finally, in automotive radiators, replacing traditional cooling fluid with nanofluid would improve heat transfer rate. When nanoparticles are mixed with the base fluid and used with the radiator, the heat transfer rate increases. As a result, there's a chance that the radiator's size and weight will be reduced. As a result, fuel economy would be enhanced and environmental emissions would be lowered.

4. CONCLUSION

The effects of MWCNT /Water nanofluids in an automotive radiator were investigated in this study. Heat transfer rates for the use of (MWCNT /Water) nanofluid increased significantly when compared to the basic fluid. The largest increase in heat transfer rate was 4.56% for 0.067 vol % of (MWCNT /Water) nanofluid under the optimum conditions. The heat transfer rate improved as the flow rate of nanofluid increased in the experiments. The heat transfer rate was also raised as the volume

concentration rose. The findings show that utilizing nanofluids can increase the rate of heat transmission. As a result, scientists have a promising technique of improving incredibly tiny and effective car radiators. The weight of the radiator is reduced, which saves fuel consumption. Furthermore, it can provide efficient heat transfer and extend the life of vehicle components.

Nomenclature	*Nondimensionals*
A area [m^2]	*Nu* Nusselt Number
C_p specific heat at constant pressure [J/kgK]	*Re* Reynolds Number
h Heat transfer coefficient [W/m^2K]	*Subscripts*
k thermal conductivity [W/mK]	*b* bulk mean
m mass flow rate [kg/s]	*bf* base fluid
Q heat transfer rate [W]	*exp* experiment
T temperature [°C]	*h* hydraulic
wt mass concentration	*i* inlet
Greek letters	*n* nanoparticles
μ dynamic viscosity [kg/ms]	*nf* nanofluid
ρ density [kg/m^3]	*o* outlet
φ volumetric concentration	*w* wall

REFERENCES

[1] S.M. Peyghambarzadeh, S.H. Hashemabadi, M.S. Jamnani and S.M. Hoseini, "Improving the Cooling Performance of Automobile
Radiator with Al_2O_3/water Nanofluid", doi:10.1016/j.applthermaleng.2011.02.029, Appl. Therm. Eng., 2011, pp.1833-1838.

[2] S. Sharma, "Fabricating An Experimental Setup to Investigate the Performance of an Automobile Car Radiator by Using Aluminum
/ Water Nanofluid, doi:10.1007/s10973-018-7224-9, J. Therm. Anal. Calorim, Vol.9, 2018.

[3] C. Selvam, D.M. Lal and S. Harish, "Enhanced Heat Transfer Performance of an Automobile Radiator Withgraphene Based Suspensions", doi:10.1016/j.applthermaleng.2017.05.076, Appl. Therm. Eng., Vol.123, 2017, pp.50-60.

[4] G.A. Oliveira, E.M. Cardenas Contreras and E.P. BandarraFilho, "Experimental Study on the Heat Transfer of MWCNT/Water Nanofluid Flowing In a Car Radiator", doi:10.1016/j.applthermaleng.2016.05.086, Appl. Therm. Eng., Vol.111, 2017, pp.1450-1456.

[5] H.M. Ali, H. Ali, H. Liaquat, H.T. Bin Maqsood and M.A. Nadir, "Experimental Investigation of Convective Heat Transfer Augmentation for Car Radiator Using ZnO-water Nanofluids", doi:10.1016/j.energy.2015.02.103. Energy, Vol.84, 2015, pp.317-324.

[6] H. Ali, M. Azhar, M. Saleem, Q. Saeed and A. Saieed, "Heat Transfer Enhancement of Car Radiator Using Aqua Based Magnesium Oxide Nanofluids ", doi:10.2298/TSCI150526130A., Therm. Sci., Vol.19, 2015, pp.2039-2048.

[7] M. Naraki, S.M. Peyghambarzadeh, S.H. Hashemabadi and Y. Vermahmoudi, "Parametric Study of Overall Heat Transfer Coefficient of CuO/water Nanofluids in a Car Radiator", doi:10.1016/j.ijthermalsci.2012.11.013., Int. J. Therm. Sci., Vol.66, 2013, pp.82-90.

[8] A.M.Hussein, R.A.Bakar and K.Kadirgama, "Case Studies in Thermal Engineering Study of Forced Convection Nanofluid Heat Transfer in the Automotive Cooling System, Case Stud. doi:10.1016/j.csite.2013.12.001., Therm. Eng., Vol.2, 2014, pp.50-61.

[9] S.A. Ahmed, M. Ozkaymak, A. Sцzen, T. Menlik and A. Fahed, "Improving Car Radiator Performance by Using TiO_2-water Nanofluid", doi:10.1016/j.jestch.2018.07.008, Eng. Sci. Technol. an Int. J. 2018, pp.996-1005.

[10] B.Palaniappan and V.Ramasamy, "Thermodynamic Analysis of Fly Ash Nanofluid for Automobile (heavy vehicle) Radiators", doi:10.1007/s10973-018-7844-0, J. Therm. Anal. Calorim, 2018.

[11] DevireddySandhya, Mekala Chandra Sekhara Reddy and Veeredhi Vasudeva Rao, "Improving the Cooling Performance of Automobile Radiator with Ethylene Glycol Water Based TiO_2", doi:10.1016/j.icheatmasstransfer.2016.09.002, Int.Comm.in Heat and Mass Transfer Nanofluids.

FOLDABLE BIKE TROLLEY

K.P. Boopathiraja, M.K.Y. Paarthasarathy, J.Abhishek Vincent and S.B.Deva
Department of Mechanical Engineering,
Bannari Amman Institute of Technology, Sathyamangalam - 638 401, Erode District, Tamil Nadu
E-mail: boopathiraja@bitsathy.ac.in, paarthasarathy.me20@bitsathy.ac.in

Abstract

Foldable bike trolleys are designed to eliminate people carrying goods carriers such as rice bags; therefore, our foldable trolleys help to carry goods in light load vehicles. It is made of mild steel plate, and a hinge is provided for folding the plate easily according to the load requirement. This trolley can be disconnected at any time, and a braking system is provided to stop the trolley easily. In modern times, our lives depend on machines for every task, which will cause many health problems, so we have planned to design and fabricate another way for carrying small loads from one place to another in an eco-friendly manner.

Keyword: *Compact, Eco friendly, Foldable, Load requirement, Small loads.*

1. INTRODUCTION

In many developing countries people live in regions away from the main transport infrastructure. This makes transport services are expensive. Many villages are not part of road networks and the lack of transport is a constraint on income generating activities such as taking products to markets and to transport equipment and materials needed for a small enterprise. The bike is the most common wheeled vehicle in the world. Till today major transport will be happen on bike in rural as well as suburban areas [1]. Because of its efficiency, low cost and versatility, the bike is extensively used by people for personal transport and for the movement of goods. A variety of different methods are used in rural and urban areas to carry loads on bikes, but the weight and volume that can be carried in safety is limited by the strength of the machine, and by problems of stability and control [2]. Some carry load by tying a rope with the carrier attachment. The problem while carrying load was unbalance, due to which people weren't able to carry load, labours used to carry loads in their heads and bike was just limited to transportation [3]. From the observation the problem faced by people in rural as well as urban, our research got an idea of working. This research reduces the human effort to an extent and to balance while carrying the load, also maintaining human comfort. The bike trolley enables user an easy drive while carrying loads so even a kid can ride it easily without the risk of unbalance. Apart from household purpose even labours can use the trolley for carrying load through places. Another important feature is the trolley detachable so the user can not only use while driving the bicycle but also can be used as a trolley while detaching it [4]. The bike trolley has considerable potential for meeting many local transport needs in because of the following characteristics:

- It offers considerable flexibility because it is easily detachable from the bike
- It aims heavy loads to be transported safely by bike
- It can be manufactured locally and purchased by bicycle owners to increase the utility of their vehicles. Bike is the most common wheeled vehicle in the world. Because of its high efficiency, low-cost and versatility, the bicycles are mostly used in developing countries for personal transport and for the movement of goods. A variety of different methods are used in rural and urban areas to carry loads on bikes, but the weight and volume that can be carried in safety is limited by the strength of the machine, and by problems of stability and control. So to overcome this type of problem, bike trolleys were introduced. The trolley is attached to the bike and is used as medium for transporting the goods. The bike trolley has considerable potential for meeting many local transport needs in various aspects. Trolleys are commonly used in certain parts of European countries but are rarely used in the other developing world [5]. The evidence indicates that this is not because the technology is inappropriate, but because it is unknown. As transporting goods through bike is the cheapest mode and does not require any external source for operations, so it has potential in the market. Trolleys are, by definition, attached but not rigidly connected carrying goods while maintaining its stability. Two bike

frames are attached to the chassis of the trolley. By providing a dual pedalling mechanism to power the trolley manually.

The main objective for fabrication of this trolley can bring about a change in daily life cleaning purpose for garbage cleaners under Swatch Bharath scheme.

2. DESCRIPTION OF EQUIPMENTS

2.1 Plate

Sheet metal is formed by an industrial process that makes the metal into thin or flat pieces. Sheet metal is one of the basic formations used in metal works, and it can be cut and bent into a variety of shapes [6]. Countlessly every object is fabricated from sheet metal. Thickness can vary within tolerance limit; Thin sheets are considered as foil or leaf, and thicker than 6 mm (0.25 in) are considered plate steel or "structural steel".

Fig.1 Aerial view and side view of the trolley

Sheet metal are generally available in two types they are flat pieces or coiled strips. The coils are formation is by running a continuous sheet of metal through a roll slitter. In most of the world, sheet metal thickness is consistently specified in millimetres. In US, the thickness of sheet metal is commonly specified by a traditionally, non-linear measurement known as its gauge. The largest gauge number indicates that the metal is thinner. Commonly used steel sheet metal ranges vary from 30 gauge to about 7 gauge. This Gauge values are differs between ferrous (iron-based) metals and nonferrous metals such as aluminium or copper. Thickness of copper is measured in ounce that representing the weight of copper contained in an area of one square foot. Product manufactured from sheet metal should need to maintain a uniform thickness for good results.

Fig.2 Steel plate

There are many different metals can be made into sheet metal formation, such as asluminium, brass, copper, steel, tin, nickel, and titanium. For decorative purpose some improtant sheet metals include they are silver, gold, and platinum (platinum sheet metal is also utlized as a catalyst)[7].

Sheet metal used in automobile, truck (lorry) bodies, airplane fuselages, roofs for buildings (architecture), and many other applications. Sheet metal from iron and other materials having high magnetic permeability are also known as laminated steel cores those are generally used in transformers and electric machines. Historically, sheet metal was used as armour worn by cavalry, and sheet metal continues to have many decorative uses, including in horse tack. Sheet metal workers are generally known as "tin bashers" (or "tin knockers"), a name derived from the hammering of panel seams when installing tin roofs. In this research sheet of length 105mm, breadth 55mm and thickness of 3mm is used.

2.2 Tyre

Fig.3 Tyre used for trolley

A tyre is major element for transport a vehicle. Tyres are used on bikes, cars, lorry, wheelchairs and hand cycles, especially for racing. Bike tires provide an important source of suspension, it generate the lateral forces necessary for balancing and turning, and it generate the longitudinal forces necessary

for propulsion and braking [8]. Although the use of a pneumatic tire greatly reduces rolling resistance compared to the use of a rigid wheel or solid tire, the tires are still typically the second largest source, after air drag, of power consumption on a level road. The modern detachable pneumatic bike tire contributed to the popularity and eventual dominance of the safety bike.

2.3 Square Rod

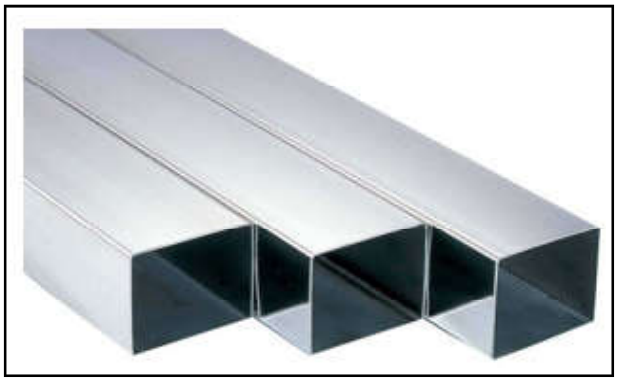

Fig.4 Hollow Rod

Metal rods are the combination of metals and alloys that designed in the pattern of round bars or square rod, rectangular or flat bars, square bars, hexagons, and other patterns of bar stock. These shapes also come in billet form and generally include a cross-section based on the shape of rod or bar stock. Reinforcing bars are also a type of metal rods that are used to give strength or internally sustain the concrete and masonry structures. Some other forms of metal rods includes coil stock and hollow tube stock.

2.4 Hinge

A hinge is a mechanical bearing that connects two rigid objects to produce movement between them, typically it allows only a limited angle of rotation between them. Two objects connected by an ideal hinge rotate relative to each other about a fixed axis of rotation: all other translations or rotations being prevented, and thus a hinge have one degree of freedom. Hinges will be made up of flexible material. Biologically, many joints function act as hinges like the elbow joint [9].

The Hitch used is of simple shuttle type. The working is simple and works perfectly regarding the load to be carried by a bicycle. Hitch of this type are simple in construction and easy to make. The numbers of components required are low and so cost of construction is relatively lower than other types available.

Fig.5 Hinge support

The attachment and detachment of hitch of this type is simple. And due to its easy working saves time while removing and attaching it.

2.5 Bearing

A bearing is an element that constrains relative motion to the desired motion, and reduces friction between moving or rotating parts. The design of the bearing may vary with some condition, for example, provide for free linear movement of the moving part or for free rotation around a fixed axis or it may prevent a motion by controlling the vectors of normal forces that bear on the moving parts [10]. Most bearings facilitate the desired motion by minimizing friction. Bearings are classified according to the type of operation, the motions allowed, or to the directions of the loads (forces) applied to the parts.

Rotary bearings hold the rotating components such as shafts or axles within the system, and transfer axial and radial loads from the source of the load to the structure supporting it. The simplest form of bearing is the plain bearing, consists of a shaft rotating in a hole. Lubrication is used to reduce friction. In the ball bearing and roller bearing, it reduce sliding friction, Rolling elements such as rollers or balls with a circular cross-section are located between the journals of the bearing assembly. A wide variety of bearing designs exists to allow the demands of the application to be correctly met for maximum efficiency, reliability, durability and performance.

2.6 Brake

Most brakes commonly use friction between two surfaces pressed together to convert the kinetic energy of the moving object into heat, though other methods of energy conversion may be employed. For example, regenerative braking converts much of the

energy to electrical energy, which may be stored for later use. Other methods convert kinetic energy into potential energy in such stored forms as pressurized air or pressurized oil. Eddy current brakes use magnetic fields to convert kinetic energy into electric current in the brake disc, fin, or rail, which is converted into heat. Still other braking methods even transform kinetic energy into different forms, for example by transferring the energy to a rotating flywheel.

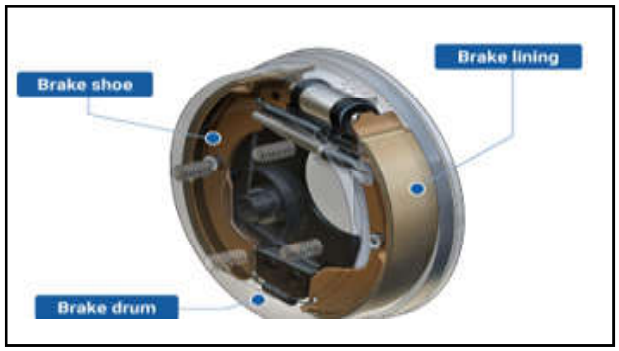

Fig.6 Brake

Brakes are generally applied to rotating axles or wheels, but may also take other forms such as the surface of a moving fluid (flaps deployed into water or air). Some vehicles use a combination of braking mechanisms, such as drag racing cars with both wheel brakes and a parachute, or airplanes with both wheel brakes and drag flaps raised into the air during landing.

2.7 Shaft

A shaft is an rotating machine element, usually circular in cross section, which is used to transmit power from one part of the machine to another part, or from a another machine which produces power to a machine which absorbs power. The various members such as pulleys and gears are mounted on it.

Fig.7 Shaft

2.8 Brake Wire Cable

Generally cables are used for braking on bikes with cable-pull brakes. They consist of two parts they are inner cable of braided stainless steel wire and outer cable housing, and it will work by transmitting force using a combination of tension on the inner cable and compression to the housing.

3. RESULT & DISCUSSION

This trolley is used as the general purpose of goods carrier. It is designed in a manner which eliminates people carrying loads such as rice bags with help of light load carrying vehicles. It is made of mild steel plate of 3mm thickness where hinge is provided for folding the plate easily according to the load requirement. This trolley can be disconnected at any time and braking system is provided to stop the trolley easily.

The arrangement consists of adjustment joint which plays a vital role in our process. In order to align the wheel based on the sliding surfaces this joints are used. Two wheels are placed for every single joint, and this joint is fitted to a frame which supports the container of the trolley for transferring the materials. When the trolley is tending to slide on the uneven floor area of the workshop, then it activates the joints based upon the sliding surfaces due to the automatic adjustment of the joints the wheels which are fitted to it align automatically. This alignment will stabilize the movement of the trolley even when they are operated in the uneven environment. For using this trolley with the motor bike in Indian road we have to follow the rule ‘Motor vehicle act’.

4. CONCLUSION

In this research, the materials and parts used to attain foldable bike trolley. The concept of weld and sheet metal cutting are understood clearly. This research helps to carry loads of 150kg from one place to another place by means of any type of two wheeler, where it is available in maximum houses. The use of braking system in bike trolley makes efficient stopping of vehicles at required places reducing slip. This attachment can be fitted and removed based on requirement. In future, features such as brake light system and indicator system can be fixed to indicate the turning of trolley to reduce accidents.

REFERENCES

[1] M. C. Chen, "Bicycle Foldable To Align Front and Rear Wheels along a Transverse Direction of the Bicycle", Google Patents, 2005.

[2] P.Kanasagara, J. Mandliya, K.Bhatt and R.Bhandari, "Design and Fabrication of Tricycle Fold Around the Bag and Utilized as a Trolley", 2018, academia.ed.

[3] "Cycling Mobility through Product and Process Innovations in Bicycle Design", Vol.41, pp.1501.

[4] R.S. Khurmi and J.K. Gupta, "A Text Book of Workshop Technology: Manufacturing Processes", S.Chand Limited, Machine-shop practice, 2008, pp.551.

[5] L. Cowan, P. Rebecca, L. Evelyn, A. Schwartz, M. Chino and J. Chapa, "Folding Bike| Inhabitant - Green Design, Innovation, Architecture, Green Building".

[6] M. A. Maleque, M. S. Hossain and S. Dyuti, "Material Properties and Design Aspects of Folding".

[7] M. Arunachalam, "A Typical Approach in Conceptual and Embodiment Design of Foldable", Vol.87, No.19.

[8] D. Norman, "Emotion & Design: Attractive Things Work Better", Interactions, Vol.9, No. 4, pp.36-42.

[9] P. Cox, "The Role of Human Powered Vehicles in Sustainable Mobility", Vol. 34, No. 2, 2005.

PHARMACEUTICAL PREDICTIONS OF SECONDARY PLANT METABOLITES

G. Sivaranjani and K. Sadasivam
Department of Physics,
Bannari Amman Institute of Technology, Sathyamangalam -638 401, Erode Distrct, Tamil Nadu
Email: dftsada@gmail.com

Abstract

Minnesota functional (M06-2X) and suitable basis set 6-311 G(d,p) is applied to explore the best radical scavenger of the derivatives of cinnamic acid including caffeic acid (Compound A) and p-coumaric acid (Compound B). All computational studies are carried out in three different phases such as gas, polar (water) and nonpolar (ethanol). Donor-acceptor (DAM) analysis is employed to identify good antioxidant. Appropriate drug candidate is examined by the interaction between ligand and protein, this can be achieve via molecular docking analysis. Toxicity range of the secondary metabolite is found in absorption distribution metabolism excretion and toxicity (ADMET) analysis. Consuming all the analysis, the most preferential radical scavenger compound amid the cinnamic acid is determined.

Keywords: *Donor-acceptor map, Molecular docking, Toxicity, Lipinski' rules and Ghose rules*

1 INTRODUCTION

An imbalance is raised between the antioxidant and pro-oxidant are due to the generation of reactive oxidative species (ROS) and free radicals in the cell. Harmful UV radiation produces the number of ROS components including superoxide anion radical $O_2^{-\bullet}$, hydroxyl radical $HO^{\bullet}$, alkyl radical $R^{\bullet}$, peroxy radical $RO^{\bullet}$, nitric oxide radical $ROO^{\bullet}$ and lipin hydroperoxide radical $LOOH$). Diabetes, cancer, Parkinson's, Alzheimer disease, cardiovascular diseases and aging are associated by oxidative stress. Antioxidant which employed to protect cells from reactive oxidative species (ROS) and reduce the free radical [1].

Generally, antioxidant quenches the free radicals and prevents cellular damages. Antioxidant is characterized into two ways: a) enzymatic antioxidant (free radicals are converted into hydrogen peroxide (H_2O_2) after removal or break down of free radicals) and b) non-enzymatic antioxidant (terminating the bond of the free radicals). Moreover, non-enzymatic antioxidant is categorized to natural antioxidant and synthetic antioxidant. Natural antioxidant including phenolic groups, flavonoids, vitamin E, vitamin C and vitamin A are highly available in plant sources such as leaves, flowers, stem, barks and roots [2].

Density functional theory (DFT) is employed to investigate the potent antioxidant and suitable drug candidate in secondary metabolites. Cinnamic acid derivatives including caffeic acid and p-coumaric acid are naturally available in plants such as coffee, vegetables and fruits that are more facile used as an antioxidant, an antidiabetic, an antimicrobial and antiaging [3]. Chemical structures of caffeic acid (Compound A) and p-coumaric acid (Compound B) are depicted in Fig. 1.

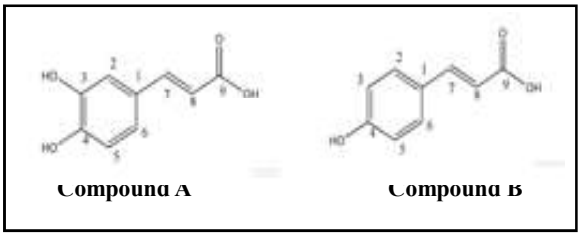

Fig. 1 Structure and atom numbering

2. QUANTUM CHEMICAL TECHNIQUE

All computational studies are carried out in Gaussian 16W software along the higher level of theory M06-2X/ 6-311 G (d,p) basis set is employed. Both TEST and Drug Likeness Tool (DruLiTo) softwares are employed to examine the toxicity of the compounds. Binding efficiency of the protein with ligand are detected through Swiss target prediction and cavity-detection guided blind docking (CB Dock 2) [4].

3. RESULTS AND DISCUSSION

3.1 Donor Acceptor Mapping (DAM)

The DAM is established the radical scavenging ability of the compound through electron donating or accepting tendency is illustrated in Fig. 2 with four different sectors. The best antioxidant is represented in sector 1 including higher R_a and lower R_d magnitudes indicates the good electron donating and accepting ability. Good antioxidant and bad antioxidant are observed at both sector 2 and sector 3 correspondingly, depends upon the magnitudes R_d and R_a. The good antioxidant is found at sector 4 which specifies the capacity of quenching free radicals [5, 6]. The magnitudes of R_a and R_d are computed and complied in Table 1 using the relations (1) and (2).

$$R_a = \frac{\omega^+}{\omega_F^+} \quad (1)$$

$$R_d = \frac{\omega^-}{\omega_{Na}^-} \quad (2)$$

The values of R_d and R_a are plotted for three different phases, both Compound A and Compound B exhibits good radical scavenging nature revealed in Figure 3a and 3b.

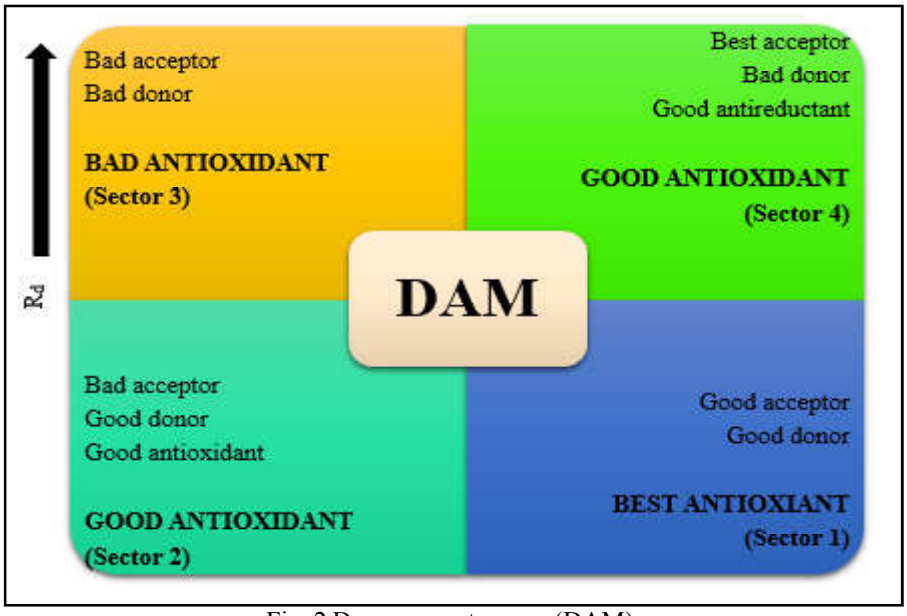

Fig. 2 Donor acceptor map (DAM)

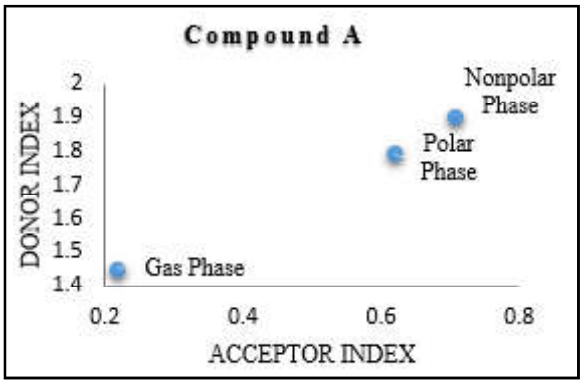

Fig. 3 (a) A graph is plotted for Compound A against donor index R_d and acceptor

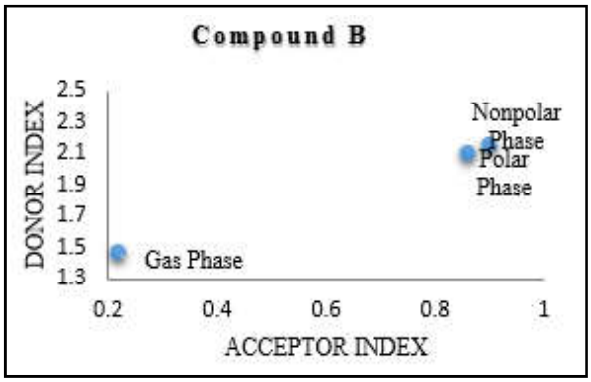

Index R_a for three different environments

Fig. 3 (b) DAM graph is plotted for Compound B in three phases (gas, polar and nonpolar) against donor and acceptor indices.

3.2 Molecular Docking

Molecular docking is a structural-activity relationship which characterize the scoring function of ligand with protein [7, 8]. Generally, docking comprise the estimation of scoring function of the Compound A and Compound B with the protein is demonstrated in Figure 4. In the case of Compound A, V143, V121 and H94 are the effective binding sites which binds with the carbon atoms

attached with benzene ring and the oxygen atom of acid group respectively. The T200 and V121 are the important binding sites of Compound B which binds with the carbon and oxygen atoms of the ligand. These effective protein binding sites with ligand are more prone in all two compounds which are found to be suitable drug candidates.

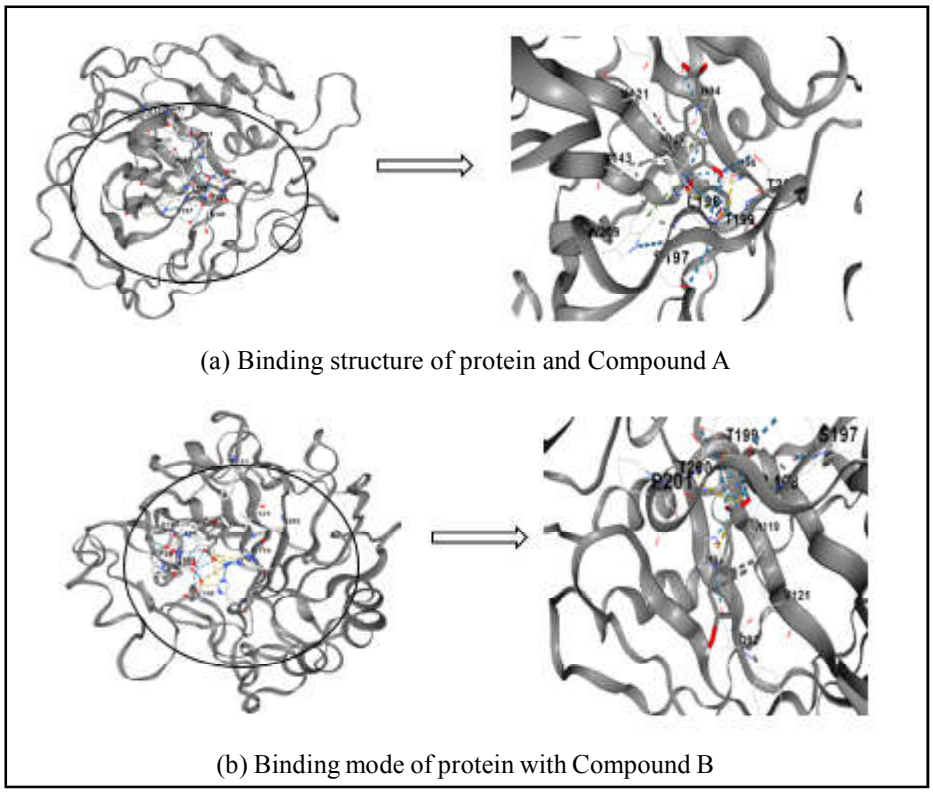

(a) Binding structure of protein and Compound A

(b) Binding mode of protein with Compound B

Fig. 4 Molecular docking

3.3 ADMET

ADMET (absorption, distribution, metabolism, excretion and toxicity) analysis is involved to establish the physicochemical properties of the compounds [9]. Compliance of Lipinski's R05, Ghose' rules and Veber's criteria with chosen compounds will estimate the toxicity and Drug likeness are explored and predicted in Table 2 and 3. The best drug candidate is obtained whether the compound violates any one of the rules. Oral rat LD_{50} and mutagenicity (M) is computed with the aid of TEST software [10, 11]. Analyzing the results from Table 2, both the compounds is observed to be less toxic and are preferential for drug fabrication due to maximum and minimum magnitudes of LD_{50} and M (Table 3) respectively.

Table 1 Donor (R_d) and Acceptor (R_a) Indices

Compounds	Gas phase		Polar phase		Nonpolar phase	
	Donor index, R_d	Acceptor index, R_a	Donor index, R_d	Acceptor index, R_a	Donor index, R_d	Acceptor index, R_a
Compound A	1.458	0.224	1.893	0.706	1.792	0.621
Compound B	1.460	0.221	2.145	0.897	2.104	0.856

Table 2 ADMET analysis

Compounds	Log P	HBD	HBA	MW	AMR	nAtom	nRB	PSA
Compound A	0.97	3	4	180.16	47.16	13	2	77.76
Compound B	0.95	2	3	164.16	45.13	12	2	57.53

Table 3 Lethal Dose (LD_{50}) and Mutagenicity (M) Analyses

Compounds	LD_{50}	M
Compound A	3484.34	0.24(-)
Compound B	2806.93	0.32(-)

4. CONCLUSION

Density functional theory is utilized to explore the preferential radical scavenger and pharmaceutical candidate among the chosen compounds. Compound A and Compound B are found to be good antioxidant from the results of DAM analysis. Both Compound A and Compound B are concluded as the suitable drug candidate for pharmaceutical purposes and is determined from the investigations of molecular docking. From the results of ADMET analysis, it is observed that both the compounds having less toxicity range and hence it is appropriate for drug fabrication.

REFERENCES

[1] S.B.Nimse and D.Pal, "Free Radicals, Natural Antioxidants, and their Reaction Mechanisms", RSC Advances, Vol. 5, 2015, pp. 27986-28006.

[2] K.B. Pandey, S.I. Rizvi, "Plant Polyphenols as Dietary Antioxidants in Human Health and Disease", Oxidative Medicine and Cellular Longevity, Vol. 2, 2009, pp. 270-278.

[3] Nam Yi Kim, Nguyet Tran Trinh, Sang Gun Ahn and Soo A Kim, "Cinnamaldehyde Protects Against Oxidative Stress and Inhibits the TNF á Induced Inflammatory Response in Human Umbilical Vein Endothelial Cells", International Journal of Molecular Medicine, Vol. 46, 2020, pp.449-457.

[4] Maciej Spiegel, "Current Trends in Computational Quantum Chemistry Studies on Antioxidant Radical Scavenging Activity", Journal of Chemical Information and Modeling, Vol. 62, 2022, pp. 2639-2658.

[5] P.C.Sumayya, Godsa Merin Babu and K.Muraleedharan, "Quantum Chemical Investigation of the Antiradical Property of Avenanthramides, Oat Phenolics", Heliyon, Vol.7, 2021, pp.e06125.

[6] Maciej Spiegel, "Current Trends in Computational Quantum Chemistry Studies on Antioxidant Radical Scavenging Activity", Journal of Chemical Information and Modeling, Vol. 62, 2022, pp. 2639-2658.

[7] A. Sagaama and N. Issaoui, Comput Biol Chem, Vol.88, 2020, pp.107348.

[8] Evki Adem, Volkan Eyupoglu, Iqra Sarfraz, Azhar Rasul, Ameer Fawad Zahoor, Muhammad Ali, Mohnad Abdalla, Ibrahim M Ibrahim and Abdo A Elfiky, "Caffeic Acid Derivatives (CAFDs) as Inhibitors of SARS-CoV-2: CAFDs-based Functional Foods as a Potential Alternative Approach to Combat COVID-19", Phytomedicine, Vol. 85, 2020, pp.153310.

[9] Q.S.Obu, H. Louis, J.O. Odey, I.J. Eko, S. Abdullahi, T.N. Ntui and O.E.Offiong, "DFT, ADMET and Molecular Docking Investigations for the Antimicrobial Activity of 6,62 -Diamino-1,12 ,3,32 -tetramethyl-5,52 -(4-chlorobenzylidene)bis[pyrimidine-2,4(1H,3H)-dione]", Molecules, Vol. 1244, 2021, pp.130880.

[10] Jia, C.-Y., Li, J.-Y., Hao, G.-F., Yang, G.-F, "A Drug-likeness Toolbox Facilitates ADMET Study in Drug Discovery", Drug Discovery Today, Vol. 25, 2019, pp.248-258.

[11] Brenda Manzanilla and Juvencio Robles, "Antiradical Properties of Curcumin, Caffeic Acid Phenethyl Ester, and Chicoric Acid: A DFT Study", Journal of Molecular Modeling, Vol. 28, 2022, pp. 1-14.

SYNTHESIS OF FLUORESCENCE CHEMOSENSOR USING BENZIMIDAZO QUINOLINE AS FLUOROPHORE - EDTA BASED CHELATING GROUP AS IONOPHORE

Malathi Mahalingam[1], Manikandan Irulappan[2] and Venil Chidambaram Kulandaisamy[3]
[1&2]Department of Chemistry,
Bannari Amman Institute of Technology, Sathyamangalam -638 401, Erode District, Tamil Nadu
[3]Department of Biotechnology,
Anna University, Regional Campus, Coimbatore - 641 046, Tamil Nadu
E-mail: malathimahalingamm@bitsathy.ac.in

Abstract

2,2'-(2-(3-(1H-benzo[d]imidazol-2-yl)quinolin-2-yloxy)ethylazane diyl) diacetic acid - an EDTA based fluorescence probe 1 is prepared in three steps, start from the benzimidazole quinoline 2. The newly synthesized compound in each stage of synthesis is purified through chromatography techniques and characterized by FT-IR and NMR spectral studies. The optical properties of the synthesized compounds are analyzed using spectrophotometer and spectrofluoro meter. The synthesized Quinoline-EDTA compounds 1a-d are used to study the metal binding abilities as fluorescence sensors for the metal ions Ca2+, Na+, K+, Fe2+, Fe3+, Cu2+, Ni2+ Co2+ and Zn2+. A notable sensing property is identified in aqueous medium for zinc ion.

Keywords: *EDTA sensor, Emission properties, Fluorescence, Metal binding, Ionophore-fluorophore, Quinolines*

1. INTRODUCTION

Calcium ions (Ca^{2+}) play a crucial role in various cellular functions. The following are the few examples like signal Transduction, where calcium ions act as second messengers in signal transduction pathways and relaying information from extracellular signals to the interior of the cell [1]. Calcium ions are essential for muscle contraction in both smooth and skeletal muscles. It also plays a critical role in neurotransmitter which release at synapses and as cofactors for various enzyme activities [2]. The concentration of calcium ion various from 100 mM at rest to 1 μM[3]. Accordingly, the measurement of calcium ions in cellular medium becomes essential for the biological diagnosis processes [4]. Even though there are some promt one- and two-photon fluorescent probes are available,[5] it has been narrowed down to some specific structural motifs.

Recently, the development of chemosensor associated with fluoroionophore has attracted great attention [6]. The concept is detailed as follows. Fluoroionophore is a compound combining the fluorophore and ionophore, where ionophore binds selectively to target ion and fluorophore generates a fluorescence signal with respect to binding of ionophore [7].

Depending on the nature of functionality and extended resonance interaction of fluorophore and ionophore, the fluorescence properties such as fluorescence intensity and wavelength лmax, can be qualitative and quantitative [8]. In addition, the sensitivity of fluorophore is associated with the ionic recognition ability of the ionophore, if the fluorophore may be perturbed by coordination of cation. Accordingly, the current paper concentrates the synthesis of such heterocyclic fluorescent probe by combining benzimidazolequinoline (BIQ) as fluorophore and ethylene amino acid functionality as calcium and magnesium ion capturing ionophore unit.

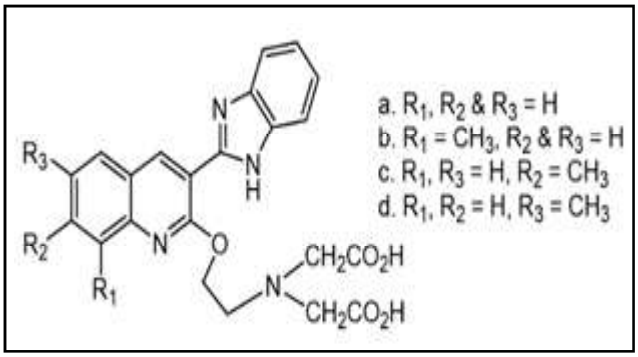

Fig.1 Target quinoline derivatives (1a-d)

Reported studies reveals that EDTA ethylen ediaminetetra acetic acid) and BAPTA (1,2-bis (o-aminophenoxy) ethane-N,N,N',N'-tetraacetic acid) types of chelating groups show optical signals for the Ca2+ and Mg2+ ions [9]. All creates a curiosity to synthesize a receptor with BIQ fluorophore and EDTA based chelating group as ionophore as given in Figure 1.

2. EXPERIMENTAL PART

2.1 Compound 4a-d

The mixture of ethanol amine and KOH (1:1 mole ratio) in the THF (5 mL) solvent medium is stirred for 15 min. To this mixture 1 mol of quinoline benzimidazole compound 2a-d is added and refluxed for 15 min [10]. The product formation is confirmed by TLC analysis. The solvent is removed under reduced pressure. The crude is washed with brine solution and then extracted with ethyl acetate. The organic layer is condensed and adsorbed for the column chromatography. The pure white product is isolated in the 30 % petroleum ether and ethyl acetate medium. Yield 65-70%, Melting point 212-225 °C.

2.2 Compounds 6a-d

Quinoline ethanolamine 4a-d and ethyl-2-bromoacetate 5 (1:2 molar ratio respectively) in acetonitrile medium are stirred at room temperature. To this mixture 1 mL of triethylamine is added in drop. The whole reaction medium is stirred further an hour.

The product formation is confirmed by TLC analysis. Then the content of the reaction mixture is reduced and the crude is subjected to silica gel column chromatography using petroleum ether and ethyl acetate medium (2 %) which yields the pure diacetate product. Yield 40-46 %; Melting point 125-135 °C.

2.3 Compounds 1a-d

Ethanol and potassium hydroxide mixture is stirred for 10 min. To this, quinoline diacetate compound 6a-d is added and refluxed for 2 h. The product formation is confirmed by TLC. The reaction mixture is condensed under reduced pressure. The product is purified by column chromatography using petroleum ether and ethyl acetate mixture (12%). Yield 40-48 %; Melting point 252-269 °C.

2.4 Stock solution: Metal binding studies

The required concentration of 1b stock solution is prepared using 10 % aqueous ethanolic solution. The respective metal salt solutions are prepared in the double distilled water or ethanol (if the metal is insoluble in aqueous medium). Ca(ClO4)2, Na(ClO4), K(ClO4), Fe(NO3)3, FeSO4, CuSO4, NiSO4, CoSO4 and Zn(NO3)2, compounds are used in the preparation of respective metal ion solution.

3. RESULTS AND DISCUSSION

3.1 Synthesis of target derivative1a-d

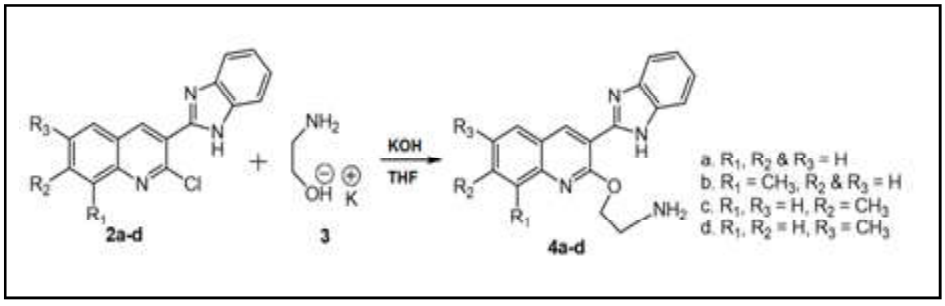

Fig. 2 Synthesis of intermediate 1a-d

The target sensor compound 1a-d is synthesized in three steps. In the first step, 2-(3-(1*H*-benzo[*d*]imidazol-2-yl)quinolin-2-yloxy)ethanamine derivatives (4a-d) is prepared from the BIQ (2a-d) through condensation reaction with the ethanol amine. Initially the ethanol amine was converted to its potassium salt in the THF solvent. To this reaction mixture, the precursor (2a-d) was added and refluxed for 15 min. The product formation was confirmed by TLC. The structure of the product was confirmed by the spectral (IR, ^{1}H-, ^{13}C- NMR) and analytical studies.

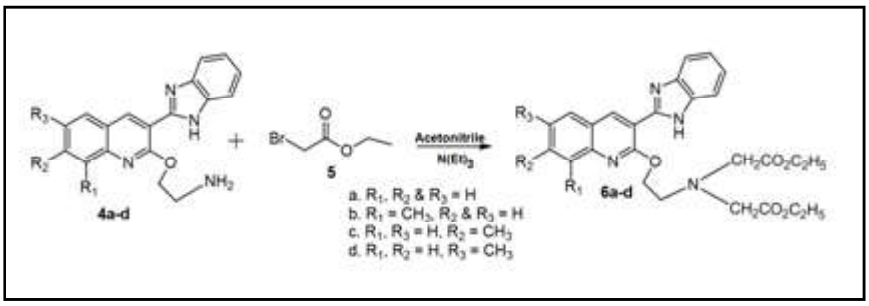

Fig. 3 Synthesis of target intermediate 6a-d

In the next step the compounds (4a-d) are converted to diethyl 2,2'-(2-(3-(1H-benzo[d]imidazol-2-yl)quinolin-2-yloxy) ethylazanediyl) diacetate derivatives (6a-d) through condensation reaction with ethylbromo acetate. The reaction was performed at room temperature using acetonitrile solvent medium containing triethylamine as a base.

The formation of the product was confirmed by thin layer chromatography (TLC). The isolation of the product from the reaction mixture was done by column chromatography using petroleum ether and ethyl acetate. The structure of the compounds (6a-d) is confirmed by spectral studies (IR, ^{1}H-, ^{13}C- NMR).

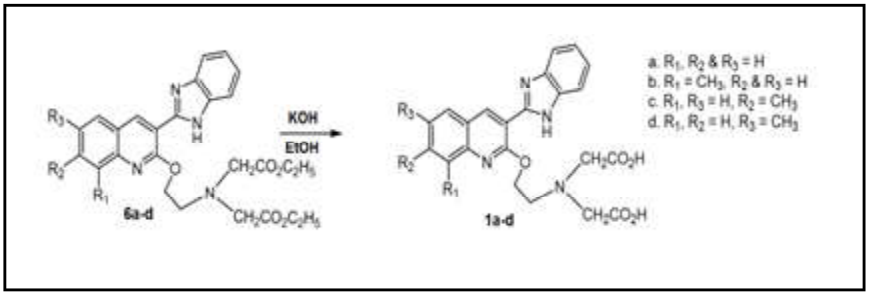

Fig. 4 Synthesis of target compound 1a-d

The final step is only the hydrolysis of diacetate compound 6a-d to get the target compound di-acid compound (1a-d). The structure of the recrystallized product 1a was confirmed by the spectral (IRFigs. 4.7-4.9).

4. METAL CATION BINDING STUDIES

The absorbance and the corresponding fluorescence spectra of compounds (**1a-d**) were recorded in the different solvent mediums such as toluene, dioxane, CH_2Cl_2, $CHCl_3$, DMSO, ethanol and 10 % aqueous ethanolic solution. From the spectral data it was concluded that all the compounds (**1a-d**) notable the photophysical properties. Hence the metal binding affinity of the synthesized receptor (**1a-d**) was analyzed by taking one of its derivative **1b**. The fig. 5 shows the absorbance and emission spectra of the receptor **1b**.

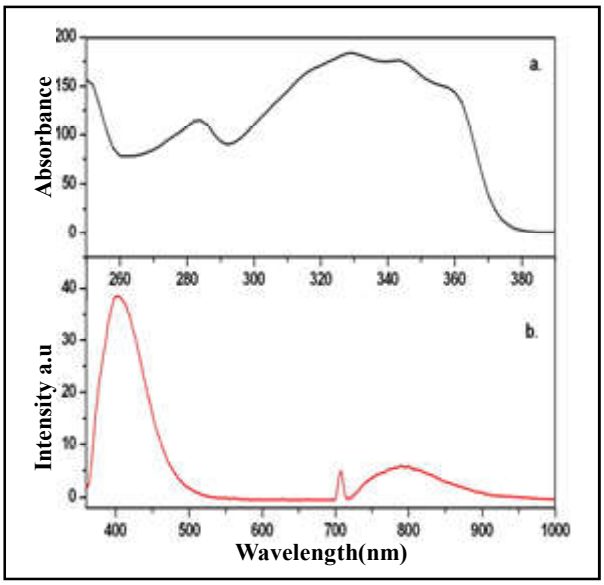

Fig. 5 Absorption and emission spectrum target compound 1b

The metal binding affinity of the receptor (**1b**) is primarily analyzed by the spectrofluorimetric analysis instead of UV-vis absorption technique since the fluorimetric measurement is highly qualitative.[8] 3 μM concentration of **1b** in 10 % aqueous ethanolic solution with Tris-HCl buffer (pH =7) is used as receptor stock solution. In fluorescence binding analysis, both the blank and the receptor solution with the metal ions are excited at λ_{exc} 707 (double excitation) and the resulting emission spectra is measured in the wavelength range 360 to 1000 nm for all binding analysis. 10 μM concentration of the Ca^{2+}, Na^{+}, K^{+}, Fe^{2+}, Fe^{3+}, Cu^{2+}, Ni^{2+} Co^{2+} and Zn^{2+} ions were used and the resulting fluorescence changes are presented in the figure 6. The fluorescence signals show the specific binding of the receptor molecule towards the Fe^{2+}, Fe^{3+} and Zn^{2+} ions.

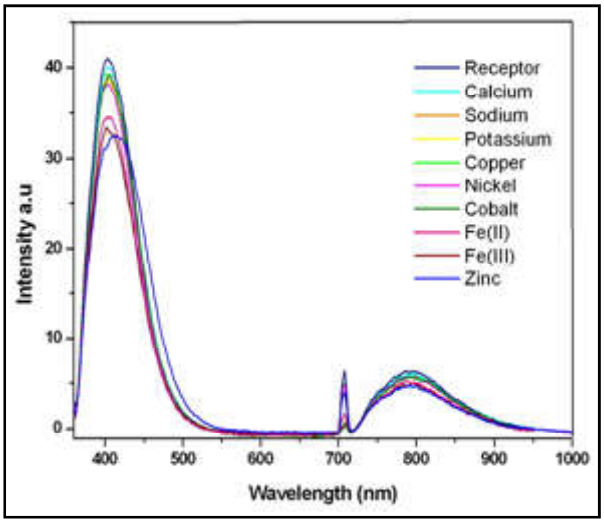

Fig. 6 Fluorescence titration of compound 1b with metal ions

The Fe^{2+} and Fe^{3+} ions results fluorescence quenching which illustrates basic affinity and capability of the ions with the fluorophore unit (BIQ) of the receptor molecule **1b**. However, a notable fluorescence enhancement is noted in the wavelength 500 to 550 nm range for the Zn^{2+} ion shows. Based on the results a fluorescence titration is performed using the receptor compound (**1b)** with the Zn^{2+} ion and resulting fluorescence changes are presented in the Figure 7. The increase of Zn^{2+} ion concentration results fluorescence quenching of the receptor characteristic peaks at the $\dot{e}_{max}$ 401 and 790 nm. Simultaneously, a shift in fluorescent enhancement is noticed around 450 to 500 nm which is indicated in the figure 7.

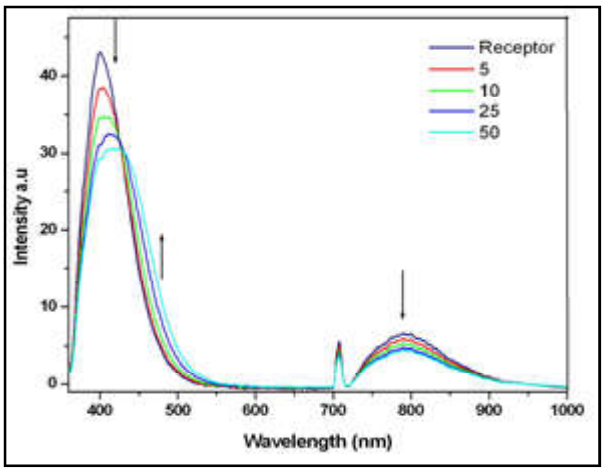

Fig.7 Fluorescence titration spectra of 1b upon addition of Zn^{2+} cations

5. METAL BINDING MECHANISM

The following points details the mechanism for the metal binding

- In the fluorophore and ionophore combined receptor system 1b, may bind with the Ca^{2+} and Mg^{2+} ions. But the bounded complex cannot influence the internal charge transfer of the BIQ fluorophore unit. Hence no change in the fluorescence signal reflates for the presence of Ca^{2+} and Mg^{2+} ions since the receptor has basic binding sites.
- The fluorescence quenching of the receptor in the presence of Fe^{2+} and Fe^{3+} ions are normally expected because of the observed affinities of the BIQ dipodal system [11]. But the fluorescence enhancement of the receptor in the presence Zn^{2+} is quite a significant. These results further support the affinity of the BIQ fluorophore towards the transition metal ions. The following charge transfer mechanism is proposed for this fluorescence enhancement.

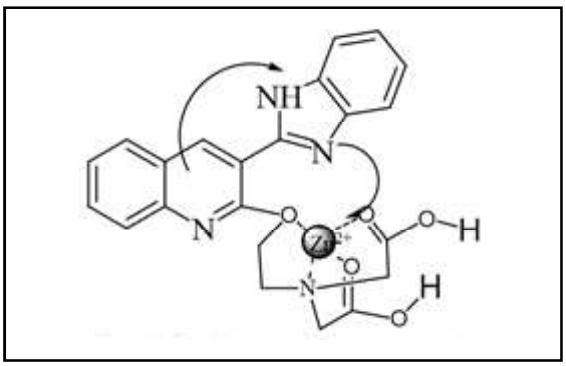

Fig. 8 Proposed metal binding

The observed results illustrates that the combination of the BIQ fluorophore 2a-d and any ionophore units will result a charge transfer fluorescence sensor specifically for transition metal cations. Because these transition metal ions can influence the ICT of the BIQ unit during binding with ionophore unit.

REFERENCES

[1] M. J. Berridge, M. D. Bootman and H. L. Roderick, Nat. Rev. Mol. Cell Biol. Vol.4, 2020, pp.517. (b) S. Orrenius, B. Zhivotovsky, P. Nicotera, Nat. Rev. Mol. Cell Biol. Vol.4, 2021, pp.552. (c) R. Rizzuto, T.Pozzan, Physiol. Rev. 86, 2016, pp.369.

[2] M. Wibo, N. Morel, T. Godfraind and T. Biochim, Biophy. Acta. 1981, pp.649. (b) E. Carafoli, Physiol. Reviews. Vol.71,1991, pp.129,

[3] A. J.Caride, A. G.Filoteo, A.Enyedi, A. K.Verma, J. T.Penniston, Biochem. 316, 353, 2016. (b) G. R.Monteith, Y.Wanigasekara, B. D. J. Roufogalis, Phamacol and Toxicol Methods, Vol.40, 2018, pp.183.

[4] A. K.Campbell,R. A. Daw, M. B.Hallett, J. P. Luzio, Biochem J. Vol.194, No.2,1981, pp. 551. (b) M. B.Hallett, A.K.Campbell, Nature, Vol.295, No.5845, 1982, pp.155. (c) M. B. Hallett, P. Fuchs, A. K.Campbell, Biochem J. Vol.206, No.3, 1982, pp.671.

[5] Q. P.Lloyd, M. A. Kuhn, C. V. J. Gay, Biol. Chem., Vol.270, 1995, pp.22445. (b) E. F.Etter, M. A. Kuhn, F. S. J. Fay, Biol. Chem. Vol.13, 1994, pp.10141. (c) Y. Tojyo, A.Tanimura, Y. Matsumoto, Biochem. Bioresearch Commun, Vol.240, 2017, pp.189.

[6] A. W. Czarnik, Acc. Chem. Res. Vol.27, 1994, pp.302. (b) B.Valeur, I. Leray, Coord. Chem. Rev. Vol.205. No.3, 2018. (c) De A. P. Silva, H. Q. N.Gunaratne, T.Gunnlaugsson, A. J. M. Huxley, C.P. McCoy, J. T.Rademacher, T. E.Rice, Chem. Rev. Vol.97, 1997, pp.1515. (d) L.Fabbrizzi, A. Poggi, Chem. Soc. Rev. Vol.97, 1994, 197. (e) L. Fabbrizzi, M. Lincchelli, P. Pallavicini, Acc. Chem. Res. Vol.32, 2019, pp.846. (f) V. Amendola, L. Fabbrizzi, M. Lincchelli, C.Mangano, P.Pallavicini, L.Parodi, A.Poggi, Coord. Chem. Rev. Vol.646, 2019, pp.190.

[7] R. Y.Tsien, Biochemistry, Vol.19, 1980, pp.2396.

[8] A. P. Demchenko, TRENDS in Biotechnology, Vol.23, No.9, 2021, pp.456.

[9] T. Dhanapal, Ph.D., Thesis Entitled "Synthetic Studies on Indoloquinoline Alkaloids and Fusced Quinoline Heterocycles", Submitted to Bharathiar University, India

[10] O. Meth-Cohn, B.Narine, Tetrahedron Lett. Vol.23, 1978, pp.2045.

[11] "Quinolines Part-I", Edited by Gurnos Jones, University of Keele, Staffordshire, Wiley-interscience publication. John wiley & sons. 1977, London, New York.

A STUDY ON LEVEL OF ADAPTABILITY, TECHNICAL ISSUES AND OTHER CHALLENGES OF VIRTUAL CLASSROOM

S. Murugappan and S. Nagarajan
Department of School of Management Studies (SMS)
Bannari Amman Institute of Technology, Sathyamangalam - 638 401, Erode District, Tamil Nadu

Abstract

This paper analysis the students' adaptability, technical issues and other challenges on online learning. It specifically found the profile of the respondents in terms of Age, Sex, Socio-economic status, Location from where they are attending the online classes, Apps preferred by the students and Internet Service Provider (ISP). Furthermore, it is determined the problems faced by the students during online class along geographical location, adaptability level and technical issues. Friedman Test (One-way ANOVA) was used to rank the factors belonging to Adaptability level, Technical issues and other challenges. The researchers have used the tools like Mann Whitney U Test and Kruskal Wallis Test to accomplish the research objectives. Further it was found that there pints are positive with regard to adaptability. They are namely Virtual Class makes the students to fell entirely different, Minimal in-person contact with classmates in Virtual Classroom does not pull the students interest level other than this we have the following factors are in negative aspects like students are preferring to attend the physical class and they also felt that virtual class was not creating the college environment.

Keywords: *Adaptability, On-line learning, Students Challenges, Technical Issues*

1. INTRODUCTION

It is education that takes place over the Internet that is known as online learning. It is referred to as "e-learning," among other labels, when it is done online. Although online learning is a sort of "distance learning," which is an umbrella word for any learning that takes place over a distance rather than in a traditional classroom, it is only one type of distance learning. The usage of a network environment is essential for this type of learning, which is significant. When students learn in this type of environment, they are not learning in a physical location in the traditional sense, but rather in a shared "space," which is sometimes referred to as the "cyberspace." According to Smith et. al (2013), a learning network classroom is any location where students require access to a personal computer, a modem, and a telephone line, satellite dish, or radio link in order to participate. Also, he concluded that learning networks are groups of people that gather to learn together at a time, location, and pace that is convenient for them.

1.1 Objectives of the Study

- To identify the profile of the students in terms of Age, Age, Sex, Socio-economic status, Location from where they are attending the online classes, Apps preferred by the students and Internet Service Provider (ISP).
- To analyze the adoption of on-line learning and Technical issues faced by the students during online learning.
- To analyze problems faced by the students in online learning.

2. REVIEW OF LITERATURE

Fischer *et al.* (2015) made an important contribution to the diffusion of digital media in higher education. The researchers found that the detailed analysis of the frequency distribution over the seven years reflects the intensity of scientific discussion towards e-learning trends, and conclusions about the didactical or technical potentials of innovations can be introduced. Specifically, they found the development potential of learning management, mobile learning, virtual worlds, e-portfolio, social media and Massive Open Online Courses are crucial for elearning in German higher education.

Moravec *et al.* (2015) showed how e-learning tools impact students' achievement. The study was attended by nearly 2000 students. According to Moravec et al. (2015), the study compares the results of questions from the area of law where the tool was provided in a pilot version with the results of questions, where the e-learning tool was not provided. The researchers found that the e-learning tools have affected the students' results.

Nevertheless, the belief of the e-learning tool may possibly have a negative effect on students who will depend on given materials was disproved.

Beurs *et al.* (2015) argued that randomized researches investigating the impact of training of mental health professionals in suicide prevention guidelines are limited. The researchers evaluated whether professional benefited from an e-learning supported train-the-trainer program aimed at the application of the Dutch multidisciplinary suicide prevention guideline. 45 psychiatric departments from all over the Netherlands were clustered in pairs and selected randomized. All of the staff of psychiatric departments was trained by peers with an e-learning supported train-the-trainer program. Multi level analyses were employed to find if variation between conditions was due to differences between individual professionals or departments. The study found that the intervention resulted in an improvement of individual professionals. At the three month follow up, professionals who received the intervention demonstrated greater guideline adherence, enhanced selfperceived knowledge and superior confidence as providers of care than professionals who were only exposed to traditional guideline dissemination. Also, the analyses showed that enhanced guideline adherence was found among nurses but not among psychiatrists and psychologists, and there was no significant effect of the intervention on team performance.

3. RESEARCH METHODOLOGY

3.1 Profile of the Sample Respondent

Sample Size

- Total number of Students are 2010 from I, II and III Year of B.E., B.Tech.

Gender

- Number of Male Members: 1277 (63.53%)
- Number of Female Members: 733 (36.47%)

Location of the Respondent

- Rural Area: 925 (46.02%)
- Semi Urban Area: 528 (26.27%)
- Urban Area: 557 (27.71%)

District

- 90% of the sample respondents are from the 16 Districts of Tamilnadu. It has been furnished below

Table 1 Sample Respondents are From the 16 Districts of Tamilnadu

Sl. No.	City	No. of Students	% of Students	Running %
1	Coimbatore	510	25.37%	25.37%
2	Erode	446	22.19%	47.56%
3	Salem	155	7.71%	55.27%
4	Namakkal	154	7.66%	62.94%
5	Nilgiris	70	3.48%	66.42%
6	Karur	69	3.43%	69.85%
7	Tiruchirappalli	60	2.99%	72.84%
8	Dindigul	59	2.94%	75.77%
9	Krishnagiri	53	2.64%	78.41%
10	Madurai	48	2.39%	80.80%
11	Dharmapuri	43	2.14%	82.94%
12	Virudhunagar	35	1.74%	84.68%
13	Cuddalore	31	1.54%	86.22%
14	Tirunelveli	27	1.34%	87.56%
15	Theni	27	1.34%	88.91%
16	Vellore	22	1.09%	90.00%

Table 2 Number of Samples Across Year of Study

Year	No.of Students	% of Students
I	695.00	34.58%
II	769.00	38.26%
III	546.00	27.16%
Grand Total	2010.00	100.00%

Table 3 Number of Students Across the Departments

Branch	No of Students	% of Students	Running %
Electronics and Communication Engineering	255	12.69%	12.69%
Computer Science and Engineering	253	12.59%	25.27%
Mechanical Engineering	247	12.29%	37.56%
Electrical and Electronics Engineering	188	9.35%	46.92%
Electronics and Instrumentation Engineering	158	7.86%	54.78%
Biotechnology	152	7.56%	62.34%
Information Technology	100	4.98%	67.31%
Civil Engineering	96	4.78%	72.09%
Mechatronics	91	4.53%	76.62%
Food Technology	81	4.03%	80.65%
Agriculture Engineering	74	3.68%	84.33%
Textile Technology	65	3.23%	87.56%
Computer Technology	54	2.69%	90.25%
Fashion Technology	54	2.69%	92.94%
Aeronautical Engineering	47	2.34%	95.27%
Information Science and Engineering	37	1.84%	97.11%
Biomedical Engineering	28	1.39%	98.51%
Automobile Engineering	17	0.85%	99.35%
Computer Science and Business System	13	0.65%	100.00%
Grand Total	2010	100.00%	

Apps used by the Faculty Members / Department

- Google Classroom: 1935 (96.27%)
- Other Apps: 60 (2.99%)
- Zoom: 14 (0.70%)
- Go-Brunch: 1 (0.05%)

Preferred Gadget for the Virtual Class

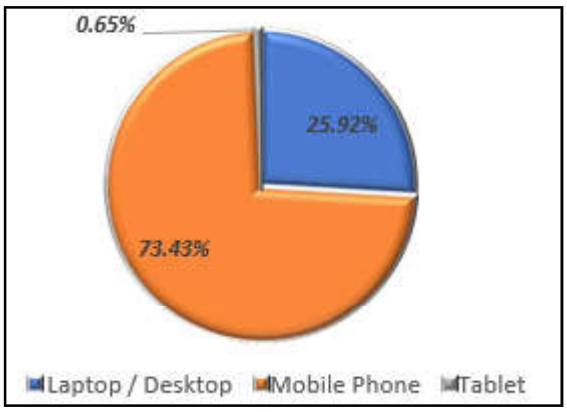

Apps Preferred by the Students

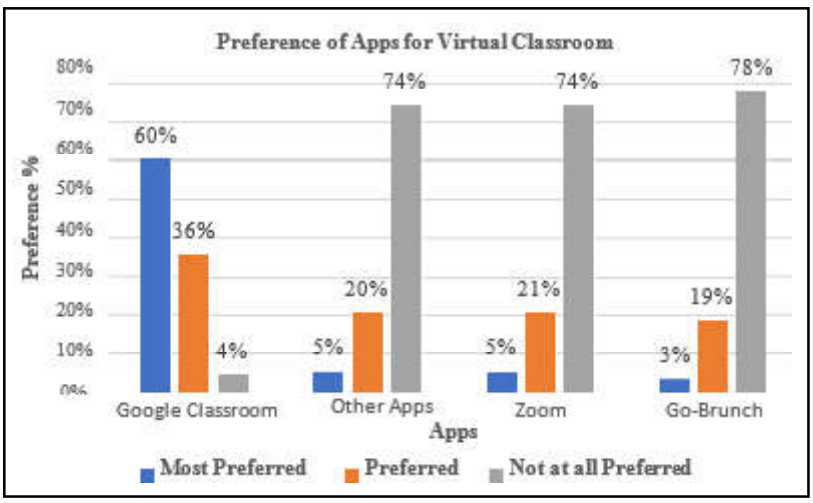

Internet Service Provider used by the Respondents and Number of Connections

No. of Connections	No. of Students	% of Students
One	1721	85.62%
Two	263	13.08%
Three	21	1.04%
Four	3	0.15%
Five	2	0.10%
Grand Total	**2010**	**100.00%**

Internet Service Provider	No. of Students	% Out of 2010
Jio	1298	64.58%
Airtel	585	29.10%
Vodafone Idea	200	9.95%
BSNL	163	8.11%
Others	20	1.00%
Jio Fiber	15	0.75%
ACT Fibernet	10	0.50%
Airtel Fiber	5	0.25%
Hathway	2	0.10%
GTPL	1	0.05%
Grand Total	**2299**	**100.00%**

4. Analysis and Interpretation

4.1. Virtual Classroom Adaptability Level

4.1.1 Overall Adaptability Level

Twelve factors have been used to measure the level of adaptability of Virtual Classroom. They have been measured by Five Point Likert Scale. Average Ratings of various factors are arranged in descending order and the same have been furnished below.

Adaptability Factors	Average of Rating	Standard Deviation of the Rating
Virtual Classroom makes the learning entirely different - ASQ1	3.9	0.9
Minimal in-person contact with classmates in Virtual Classroom does not pull my interest level - ASQ6	3.7	1.0
It does not take much time to accustomed to the Virtual Classroom - ASQ3	3.3	1.0
I accept the new learning circumstances with an open mind and heart - ASQ9	3.3	1.1
As, I am being evaluated at the end of every Virtual Class, My understanding has been improved - ASQ12	3.1	1.1
My concentration towards class has improved due to Virtual Class - ASQ11	2.8	1.1
My surrounding is not a great impediment for the Virtual Classroom - ASQ10	2.7	1.1
There is no resistance to change to adapt to the Virtual Classroom - ASQ2	2.6	1.0
I am not having the feel of isolation in the Virtual Classroom - ASQ4	2.5	1.1
There is no ineffectiveness due to minimal in-person contact with Professors in Virtual Classroom - ASQ8	2.3	1.0
Traditional Classroom is not preferable than the Virtual Classroom - ASQ7	1.8	1.0
College Environment can be created in the Virtual Class - ASQ5	1.7	1.0
Grand Total	2.8	1.2

Note: Likert Scale Rating – Ranges from Strongly Agree (5) to Strongly Dis-agree (1)

From the above table, it is very clear that most of the respondents felt that Virtual Classroom makes their learning entirely different. At the same time, they have clearly stated that Traditional Classroom cannot be replaced by the Virtual Classroom. Moreover, College Environment cannot be created by Virtual Classroom.

Based on the above mean value, we can group the factors as follows;

- **Highly Positive Points**
  - i Virtual Class makes the students to fell entirely different. (ASQ1)
  - ii Minimal in-person contact with classmates in Virtual Classroom does not pull the students interest level. (ASQ6)

- **Positive Points**
  - i Students took less time to adapt to the Virtual Class. (ASQ3)
  - ii They accepted the new learning circumstances with an open mind and heart. (ASQ9).
  - iii Evaluation at the end of the Virtual Class helps them to improve their understanding level. (ASQ12).
- **Negative Points**
  - i They refused that the Virtual Class helps to improve their concentration level. (ASQ11)
  - ii Their surrounding in their home is a great impediment to the Virtual Class. (ASQ10)
  - iii Even though they took less time to adapt to the Virtual Class, resistance to change to Virtual Class is more. (ASQ2)
  - iv They are having the feel of isolation in the Virtual Class. (ASQ4)
  - v Due to less in-person contact with the Professors, they felt that the Virtual Class is not the effective as compared to Traditional Class. (ASQ4)
- **Highly Negative Points**
  - i They are preferring the Traditional Class than the Virtual Class. (ASQ7)
  - ii Virtual Class is not able to create a College Environment. (ASQ5)
  - iii The above insights can be traced easily by our naked eyes through visualizing the Box and Whisker Plot presented in the next page.

Box and Whisker Plot

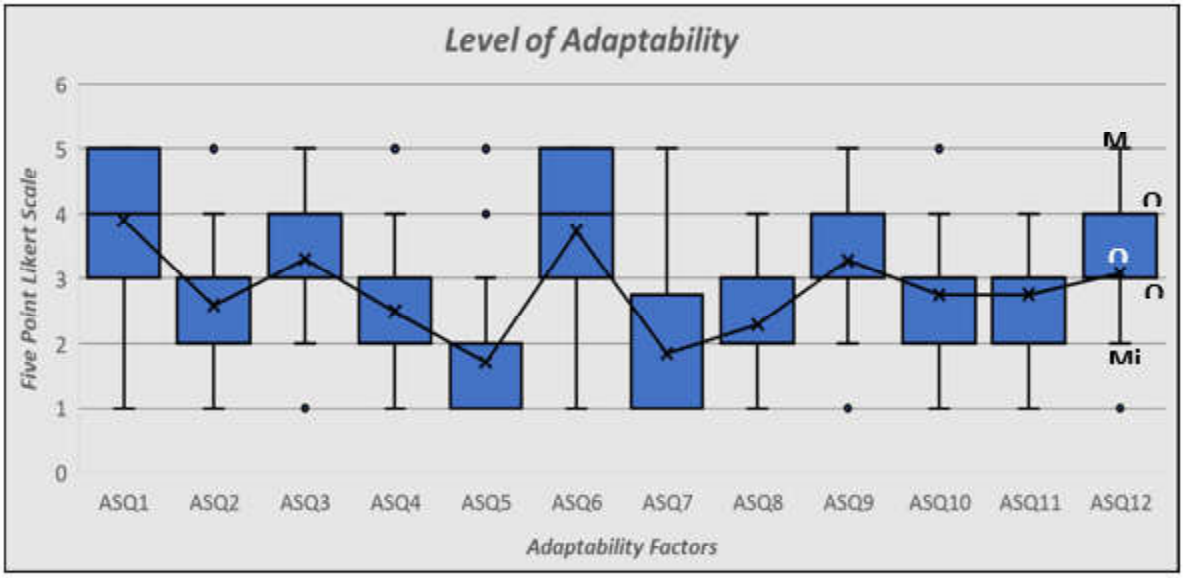

Note: Connecting line indicates the mean value. Dots are outliers. Minimum Value, First Quartile (Q 1), Second Quartile (Q 2) i.e. Median, Third Quartile (Q 3) and Maximum Value of all the twelve factors presented through Box and Whisker Plot. From the above graph we can group the factors. ASQ1 and ASQ6 are one group. ASQ3, ASQ9 and ASQ12 are another group. ASQ2, ASQ4, ASQ8, ASQ10 and ASQ11 are forming another group. Finally, ASQ5 and ASQ7 form another group.

The above interpretations are explored using the graphical presentation and simple mean value. The same results were obtained through the Friedman Test (One Way Repeated Measure ANOVA) and the results are furnished below.

Hypothesis:

Null Hypothesis **(H0):** Twelve Factors used to measure the Adaptability Level of Virtual Class are not significantly different.

Alternate Hypothesis **(H1):** Twelve Factors used to measure the Adaptability Level of Virtual Class are significantly different.

Level of Significance:

The level of significance preferred in this research study is 5%. Therefore, confidence level is 95%.

Friedman Mean Rank Table

Adaptability Factors	Mean Rank
Highly Positive Points	
Virtual Classroom makes the learning entirely different	9.56
Minimal in-person contact with classmates in Virtual Classroom does not pull my interest level	8.76
Positive Points	
I accept the new learning circumstances with an open mind and heart	8.07
It does not take much time to accustomed to the Virtual Classroom	7.95
As, I am being evaluated at the end of every Virtual Class, My understanding has been improved	7.43
Negative Points	
My concentration towards class has improved due to Virtual Class	6.37
My surrounding is not a great impediment for the Virtual Classroom	6.25
There is no resistance to change to adapt to the Virtual Classroom	5.90
I am not having the feel of isolation in the Virtual Classroom	5.66
There is no ineffectiveness due to minimal in-person contact with Professors in Virtual Classroom	5.02
Highly Negative Points	
Traditional Classroom is not preferable than the Virtual Classroom	3.69
College Environment can be created in the Virtual Class	3.34

Test Statistics[a]

Particulars	Values
No of Respondents	2010
Chi-Square	7663.842
Degrees of Freedom (df)	11
Asymptotic Sig.	.000

Note: a. Friedman Test

From the Test Statistics table, we can conclude that the Asymptotic Significant Value is less the significance level of 5% i.e. .05. Therefore, we can reject the null hypothesis and accept the alternate hypothesis.

Therefore, we can conclude that the factors used to measure the Adaptability Level of Virtual Classroom are significantly differently rated by the sample respondents. Similarly, it has been decided to check the Adaptability Level between Male and Female, B.E. and B.Tech. Students, among the First, Second and Third Year Students, among the Rural, Semi-Urban and Urban Students. These results are furnished below;

4.2 Adaptability vs Demographic Factors

Between Male and Female – Mann Whitney U Test

Hypothesis:

Null Hypothesis **(H0):** There is no significant difference in the Adaptability Level between Male and Female candidates.

Alternate Hypothesis **(H1):** There is significant difference in the Adaptability Level between Male and Female candidates.

Level of Significance:

The level of significance preferred in this research study is 5%. Therefore, confidence level is 95%.

Mean Rank Table - Adaptability Overall Score

Gender of the Respondent	No. of Students	Mean Rank	Sum of Ranks
Male	1277	979.11	1250327.50
Female	733	1051.47	770727.50
Total	**2010**	-	-

Test Statistics[a]

Particulars	Values
Mann-Whitney U	434324.50
Wilcoxon W	1250327.50
Z	-2.697
Asymptotic Sig. (2-tailed)	.007

Note a. Grouping Variable: Gender of the Respondent

From the Test Statistics table, it is very clear that the Asymptotic Significant value is lower the researcher's preferred significance level of 5%. Therefore, we can

conclude that the there is a significant difference between Male and Female members Adaptability Level of Virtual Class. From the Mean Rank table, it is obvious that Female members' Adaptability Level is higher than the Male members.

4.3 Technical Issues and Other Challenges in Virtual Classroom

Overall Technical Issues and Other Challenges

Technical Factors	Average of Rating	Standard Deviation of the Rating
Storage space is not at all an issue in the Virtual Class - TIQ12	3.52	1.07
Use of Laptop / Desktop makes the Classroom more effective - TIQ2	3.44	1.07
I am always getting technical assistance to tune / join to the Virtual Class - TIQ4	3.32	1.03
OS version / Browser compatibility issue does not impediment the participation in Virtual Class - TIQ6	3.31	1.00
The app I am using for Virtual Classroom is user friendly - TIQ14	3.08	1.06
Use of Mobile Phone makes the Virtual Classroom more effective - TIQ1	2.99	1.09
Audio quality in the Virtual Class is too good - TIQ8	2.75	1.09
Both Analytical Course and Theoretical Course are more effective in Virtual Class - TIQ11	2.67	1.07
The materials shared via Virtual Classroom App is not difficult to view while I am attending the Virtual Class - TIQ13	2.54	1.10
Video quality in the Virtual Class in too good - TIQ9	2.51	1.10
Virtual Class does not consume that much data usage - TIQ7	2.32	1.22
Lack of high bandwidth does not result in ineffective Virtual Class - TIQ3	2.25	0.96
Continuously seeing the display / monitor does not make my eye too dry - TIQ10	1.92	1.03
Poor internet connectivity does not result in ineffective Virtual Class - TIQ5	1.85	1.01
Grand Total	2.75	1.19

Note: Likert Scale Rating – Ranges from Strongly Agree (5) to Strongly Dis-agree (1)

From the above table, it is very clear that Storage Space, Use of Laptop / Desktop, Technical Assistance and OS Version / Browser Compatibility are not at all an issue in the Virtual Class. At the same time Eye Irritation (Dry Eye) and Poor Internet Connectivity are the major impediment in the Virtual Class. Based on the above mean value, we can group the factors as follows;

- **Very Least Bothering Technical Issues and Other Challenges**
  - i Storage space is not at all an issue in the Virtual Class - TIQ12
  - ii Use of Laptop / Desktop makes the Classroom more effective - TIQ2
  - iii I am always getting technical assistance to tune / join to the Virtual Class - TIQ4
  - iv OS version / Browser compatibility issue does not impediment the participation in Virtual Class - TIQ6
- **Least Bothering Technical Issues and Other Challenges**
  - i The app I am using for Virtual Classroom is user friendly - TIQ14
  - ii Use of Mobile Phone makes the Virtual Classroom more effective - TIQ1
- **Moderately Bothering Technical Issues and Other Challenges**
  - i Audio quality in the Virtual Class is too good - TIQ8
  - ii Both Analytical Course and Theoretical Course are more effective in Virtual Class - TIQ11
  - iii The materials shared via Virtual Classroom App is not difficult to view while I am attending the Virtual Class - TIQ13
  - iv Video quality in the Virtual Class in too good - TIQ9

- **More Bothering Technical Issues and Other Challenges**
  i Virtual Class does not consume that much data usage - TIQ7
  ii Lack of high bandwidth does not result in ineffective Virtual Class - TIQ3

- **Most Bothering Technical Issues and Other Challenges**
  i Continuously seeing the display / monitor does not make my eye too dry - TIQ10
  ii Poor internet connectivity does not result in ineffective Virtual Class - TIQ5 the next page.

Box and Whisker Plot

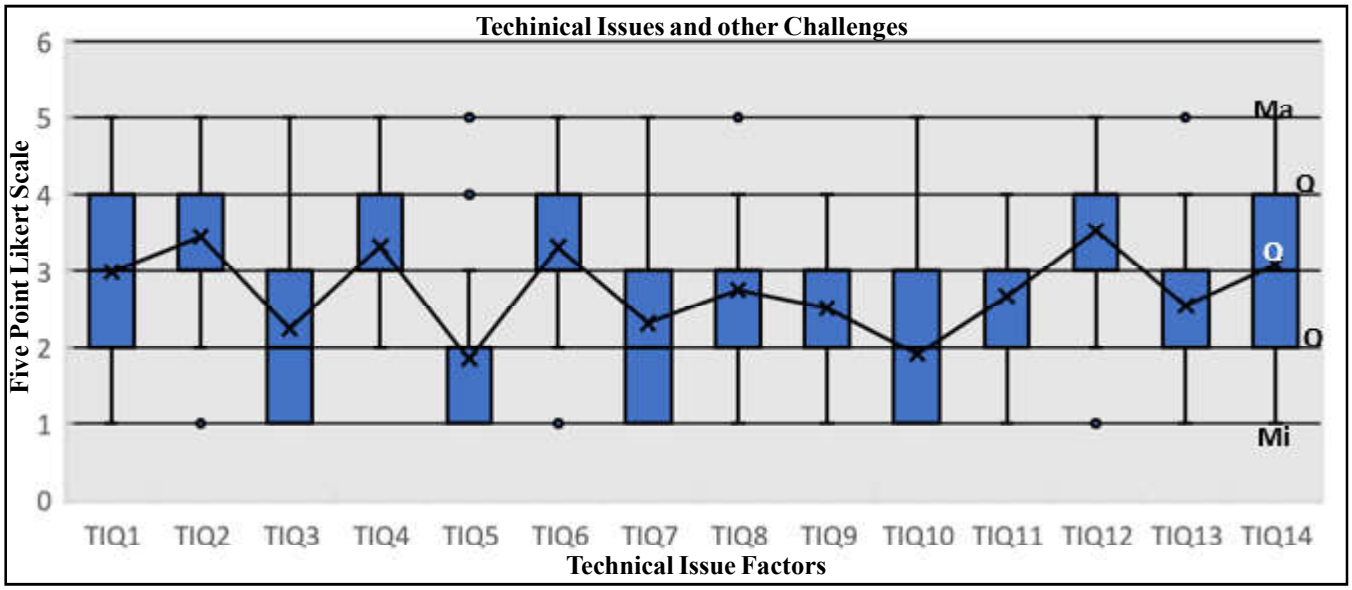

Note: Connecting line indicates the mean value. Dots are outliers. Minimum Value, First Quartile (Q 1), Second Quartile (Q 2) i.e. Median, Third Quartile (Q 3) and Maximum Value of all the fourteen factors presented through Box and Whisker Plot.

From the above graph we can group the factors. TIQ12, TIQ2, TIQ4 and TIQ6 are one group. TIQ14 and TIQ1 are another group. TIQ8, TIQ11, TIQ13 and TIQ9 are forming another group. TIQ7 and TIQ3 are forming another group. Finally TIQ10 and TIQ5 form another group.

The above interpretations are explored using the graphical presentation and simple mean value. The same results were obtained through the Friedman Test (One Way Repeated Measure ANOVA) and the results are furnished below.

Hypothesis:

Null Hypothesis **(H0):** Fourteen Factors used to measure the Technical Issues and Other Challenges are not significantly different.

Alternate Hypothesis **(H1):** Fourteen Factors used to measure the Technical Issues and Other Challenges are significantly different.

Level of Significance:

The level of significance preferred in this research study is 5%. Therefore, confidence level is 95%.

Test Statistics[a]

Particulars	Values
No of Respondents	2010
Chi-Square	6256.189
Degrees of Freedom (df)	13
Asymptotic Sig.	.000

Friedman Mean Rank Table

Technical Issue Factors	Mean Rank
Very Least Bothering Technical Issues and Other Challenges	
Storage space is not at all an issue in the Virtual Class	10.06
Use of Laptop / Desktop makes the Classroom more effective	9.88
OS version / Browser compatibility issue does not impediment the participation in Virtual Class	9.36
I am always getting technical assistance to tune / join to the Virtual Class	9.34
Least Bothering Technical Issues and Other Challenges	
The app I am using for Virtual Classroom is user friendly	8.74
Use of Mobile Phone makes the Virtual Classroom more effective	8.44
Moderately Bothering Technical Issues and Other Challenges	
Audio quality in the Virtual Class is too good	7.58
Both Analytical Course and Theoretical Course are more effective in Virtual Class	7.14
The materials shared via Virtual Classroom App is not difficult to view while I am attending the Virtual Class	6.87
Video quality in the Virtual Class in too good	6.72
More Bothering Technical Issues and Other Challenges	
Virtual Class does not consume that much data usage	6.00
Lack of high bandwidth does not result in ineffective Virtual Class	5.84
Most Bothering Technical Issues and Other Challenges	
Continuously seeing the display / monitor does not make my eye too dry	4.61
Poor internet connectivity does not result in ineffective Virtual Class	4.42

Note: Friedman Test

From the Test Statistics table, we can conclude that the Asymptotic Significant Value is less than the significance level of 5% i.e. .05. Therefore, we can reject the null hypothesis and accept the alternate hypothesis. Therefore, we can conclude that the fourteen factors used to measure the Technical Issues and Other Challenges are significantly different. An Overview of Internet Connectivity Issue Across Location Category

5. FINDINGS

5.1. Adaptability Level

A. Twelve Factors used to measure the Adaptability Level of Virtual Class are significantly different.

- **Highly Positive Points**

i Virtual Class makes the students to fell entirely different. (ASQ1)

ii Minimal in-person contact with classmates in Virtual Classroom does not pull the students interest level. (ASQ6)

- **Positive Points**

i Students took less time to adapt to the Virtual Class. (ASQ3)

ii They accepted the new learning circumstances with an open mind and heart. (ASQ9).

iii Evaluation at the end of the Virtual Class helps them to improve their understanding level. (ASQ12).

- **Negative Points**

i They have denied to accept that the Virtual Class helps to improve their concentration level. (ASQ11)

ii Their surrounding in their home is a great impediment to the Virtual Class. (ASQ10)

iii Even though they took less time to adapt to the Virtual Class, resistance to change to Virtual Class is more. (ASQ2)

iv They are having the feel of isolation in the Virtual Class. (ASQ4)

v Due to less in-person contact with the Professors, they felt that the Virtual Class is not the effective as compared to Traditional Class. (ASQ4)

- **Highly Negative Points**

i They are preferring the Traditional Class than the Virtual Class. (ASQ7)

ii Virtual Class is not able to create a College Environment. (ASQ5)

B. Female candidate's adaptability level is significantly higher than the Male candidates.

C. Both B.E. and B.Tech. Programmes are having similar adaptability level.

D. Rural Students' adaptability level is lower than the

Poor Internet Connectivity does not Result in Ineffective Virtual Class

Rating	% of Students			Cumulative %			Total % of Students	Total Cumulative %
	Rural Area	Semi Urban Area	Urban Area	Rural Area	Semi Urban Area	Urban Area		
Strongly Dis-agree	52.32%	47.92%	38.42%	52.32%	47.92%	38.42%	47.31%	47.31%
Dis-agree	26.38%	33.52%	34.29%	78.70%	81.44%	72.71%	30.45%	77.76%
Neutral	14.05%	13.26%	17.77%	92.76%	94.70%	90.48%	14.88%	92.64%
Agree	4.65%	3.98%	5.39%	97.41%	98.67%	95.87%	4.68%	97.31%
Strongly dis-agree	2.59%	1.33%	4.13%	100.00%	100.00%	100.00%	2.69%	100.00%
Grand Total	100%	100%	100%				100%	

Across District

District Name	No of Students					% of Students					Total No of Students
	1	2	3	4	5	1	2	3	4	5	
Coimbatore	242	156	76	25	11	47.45%	30.59%	14.90%	4.90%	2.16%	510
Cuddalore	10	16	3	2		32.26%	51.61%	9.68%	6.45%	0.00%	31
Dharmapuri	21	11	5	4	2	48.84%	25.58%	11.63%	9.30%	4.65%	43
Dindigul	26	18	7	7	1	44.07%	30.51%	11.86%	11.86%	1.69%	59
Erode	222	136	59	15	14	49.78%	30.49%	13.23%	3.36%	3.14%	446
Karur	30	25	9	2	3	43.48%	36.23%	13.04%	2.90%	4.35%	69
Krishnagiri	25	17	6	2	3	47.17%	32.08%	11.32%	3.77%	5.66%	53
Madurai	25	14	9			52.08%	29.17%	18.75%	0.00%	0.00%	48
Namakkal	68	46	32	4	4	44.16%	29.87%	20.78%	2.60%	2.60%	154
Nilgiris	43	17	7	3		61.43%	24.29%	10.00%	4.29%	0.00%	70
Salem	66	41	32	9	7	42.58%	26.45%	20.65%	5.81%	4.52%	155
Theni	15	9	2	1		55.56%	33.33%	7.41%	3.70%	0.00%	27
Tiruchirappalli	24	16	14	5	1	40.00%	26.67%	23.33%	8.33%	1.67%	60
Tirunelveli	11	9	4	2	1	40.74%	33.33%	14.81%	7.41%	3.70%	27
Vellore	8	10	3	1		36.36%	45.45%	13.64%	4.55%	0.00%	22
Virudhunagar	20	14	1			57.14%	40.00%	2.86%	0.00%	0.00%	35
Grand Total	**856**	**555**	**269**	**82**	**47**	**47.32%**	**30.68%**	**14.87%**	**4.53%**	**2.60%**	**1809**

Note: Strongly Dis-agree (1), Dis-agree (2), Neutral (3), Agree (4), Strongly Agree (5)

1.2 Technical Issues and Other Challenges

Fourteen Factors used to measure the Adaptability Level of Virtual Class are significantly different.

- **Very Least Bothering Technical Issues and Other Challenges**
  - i Storage space is not at all an issue in the Virtual Class - TIQ12
  - ii Use of Laptop / Desktop makes the Classroom more effective - TIQ2
  - iii I am always getting technical assistance to tune / join to the Virtual Class - TIQ4
  - iv OS version / Browser compatibility issue does not impediment the participation in Virtual Class - TIQ6
- **Least Bothering Technical Issues and Other Challenges**
  - i The app I am using for Virtual Classroom is user friendly - TIQ14
  - ii Use of Mobile Phone makes the Virtual Classroom more effective - TIQ1
- **Moderately Bothering Technical Issues and Other Challenges**
  - i Audio quality in the Virtual Class is too good - TIQ8
  - ii Both Analytical Course and Theoretical Course are more effective in Virtual Class - TIQ11
  - iii The materials shared via Virtual Classroom App is not difficult to view while I am

attending the Virtual Class - TIQ13

iv Video quality in the Virtual Class in too good - TIQ9

- **More Bothering Technical Issues and Other Challenges**
  - i Virtual Class does not consume that much data usage - TIQ7
  - ii Lack of high bandwidth does not result in ineffective Virtual Class - TIQ3
- **Most Bothering Technical Issues and Other Challenges**
  - i Continuously seeing the display / monitor does not make my eye too dry - TIQ10
  - ii Poor internet connectivity does not result in ineffective Virtual Class - TIQ5

B. Both the Male and Female have similar Opinion about the Technical Issues and Other Challenges.

C. Both the Programmes have similar Opinion about the Technical Issues and Other Challenges.

D. Rural and Semi Urban Students' Technical Issues & Other Challenges are higher than the Urban and Semi-Urban Students.

E. First and Second Year Students' Technical Issues & Other Challenges are higher than the Third Year Students.

F. Poor Internet Connectivity Issue is common across Location Category, District and Year of Study and between Gender, Programme.

6. CONCLUSION

In the light of findings, the study concluded that the respondents' profile are contributory factors for their online learning. i.e: location from where they are connecting the application to attend the online class, Internet services provider etc., Moreover, the blended learning be sustained as a modality of instruction to address the need of students who have poor connectivity due to their geographical location and their inability to acquire the needed gadgets like cell phones, laptop, tablets etc. Further, The findings and implications of the study served as the basis for policy formulation (online learning) and modification so the intellectual and educational needs of the students will be addressed.

REFERENCES

[1] A. Abante, *et.al*. "A Comparative Analysis on the Challenges of Online Learning Modality and Modular Learning Modality
: A Basis for Training Program", International Journal of Multidisciplinary Research and Analysis, Vol.4, No.4, 2021, pp.463-476.

[2] Martin, "Adaptability and High School Students' Online Learning During COVID-19: A Job Demands-Resources Perspective", Front. Psychol., 17 August 2021.

[3] R. Ancheta and Helen Ancheta, "The New Normal in education: A Challenge to the Private Basic Education", Institutions in the Philippines.2020.

[4] D. Xu and S.S. Jaggars, "Performance Gaps between Online and Face-To-Face Courses: Differences across Types of Students and Academic Subject Areas", J. Higher Educ. Vol.85, 2016, pp.633-659.

[5] C.Wladis, K.M. Conway and A.C. Hachey, "The Online STEM Classroom-who Succeeds? An Exploration of the Impact of Ethnicity, Gender, and Non-Traditional Student Characteristics in the Community College Context", Commun. Coll. Rev. Vol.43, 2015, pp.142-164.

[6] E.G.Beale, P.M. Tarwater and V. H. Lee, "A Retrospective Look at Replacing Face-Toface Embryology Instruction with Online Lectures in a Human Anatomy Course", Am. Assoc. Anat., doi: 10.1002/ase.1396, Vol.7, 2014, pp.234-241.

[7] R.Biel and C.J. Brame, "Traditional Versus Online Biology Courses: Connecting Course Design and Student Learning In an Online Setting", J. Microbiol. Biol. Educ., doi: 10.1128/jmbe.v17i3.1157, Vol.17, 2016, pp.417-422.

CARBON FOOTPRINT: AN IMPACT ON GLOBAL WARMING

R. Geethamani[1], S.Kanmani[2] and B. Soundara[3]
Department of Civil Engineering
[1]Bannari Amman Institute of Technology, Sathyamangalam - 638 401, Erode District, Tamil Nadu.
[2]KPR Institute of Engineering and Technology, Coimbatore - 641 407, Tamil Nadu.
[3]Anna University, CEG Campus, Chennai - 600 025, Tamil Nadu.
E-mail: geethamanir@bitsathy.ac.in, kanmani.s@kpriet.ac.in, soundra_iit@yahoo.co.in

Abstract

The fundamental destination of this report is to present the data gathered among different individuals at BIT campus, Sathyamangalam, Erode District, about the use of each kind of vitality and to compute the level of Carbon dioxide proportionate. In this examination, a technique has been built for gauging normal people individual carbon impression datum, the relationship between environmental change and the arrival of carbon dioxide. The total quantity of carbon di oxide chemical compound that is let into the atmosphere by human activities, industries, households is calculated in Carbon Footprint calculations. This Carbon Footprint Calculator has been used for examining the results by obtaining relevant information from the individuals. The main objective for carbon footprint is to calculate the amount of carbon di oxide emitted into atmosphere every year. One of the main objectives of this analysis is to facilitate the identification of measures for the reduction of greenhouse gas emission. It includes 3R initiatives (i.e.,) Reduce, Reuse and Recycle. The carbon foot print is a subset of data covered by normal life cycle. This study is intended to create awareness among the people about the relationship between day to day activity of human beings, greenhouse gas emission (especially carbon di oxide) and global warming.

Keywords: *Carbon foot print; Carbon di-oxide emission; Green House Gases, Global warming.*

1. INTRODUCTION

A carbon impression is the amount of ozone depleting substances, most importantly CO2, produced into the air by human activity. Most of the people think that Carbon Foot Print (CFP) is a new thing and they are not aware that it is a part of our day to day activities. Waste water treatment plants, Catalytic converter and diesel particulate filters used in automobiles form major part of carbon di oxide emission. Nuclear power plants contribute less Carbon footprint(CFP) to the country[1].

CFP can be reduced by incorporating changes in the supply chain by the producers of different goods. The key aspects of Life Cycle Assessment (LCA) are the identification and quantification of raw materials used and waste generated by them, effect of the wastes generated on the environment and possible amendments available to reduce the impact on the environment and thereby improve the current status [2].

Different carbon foot print assessment standards were compared to analyze their differences, deficiencies and similarities. Principles and calculation methods were analyzed in detail. Green House Gas (GHG), ISO 14047 standards were also analyzed comparatively. Certain guidelines were framed based on the analyses but still improvement is needed [3]. The carbon footprint mainly applies to countries, cities, personal, products and organizations etc. The emission of greenhouse gases during the life cycle of a system was the concept used to assess the impact of regular human activities to increased global warming. [4], [5], [6].

Quantification of Carbon dioxide emission in three municipalities in Greece was made using three different carbon foot print approaches, to know the significant effect on increasing price of domestic healing oil and gasoline which affected their energy consumption. From the study it was found that high carbon dioxide emission was due to the consumption of more electrical energy and carbon dioxide emission due to buildings was low.[7].

Though carbon dioxide is a natural component of air, its high concentration and short time exposure or low concentration for a long time exposure causes threat to human health and the environment [8].

To efficiently manage the greenhouse gases emission and in corporate suitable measures to reduce them, the

carbon foot print calculation plays a vital role in the present scenario. From the analysis, the sources of carbon dioxide emission, their intensity etc., can be identified which helps in the optimization for improvement and efficiency [9].

Household-level footprint calculator can be used to integrate geo demographic information using user input data which allows the users to estimate their carbondioxide emission and compare with standard global values. This carbon foot print calculator tool serves as an awareness platform for the community to know about their carbon dioxide and to have a control of it [10].

The objective of this study is to determine the carbon dioxide released into the atmosphere and to compare the estimation between the country average and world target. In developed countries like US the carbon dioxide emission is 19.8 tons/capita/year [11]. Global average carbon dioxide emission is 4.5 tons/capita/year [12]. India's average carbon dioxide emission is 1.8 tons/capita/year [13].

In order to promote sustainable development, the carbon foot print has to be reduced. The circular economy which is governed by 3Rs ie., Reduce, Reuse and Recycle helps in the reduction of carbon foot print. Awareness about the benefits of 3Rs practice help us to reduce carbon foot print and global warming considerably[14].

2. CAUSES AND EFFECTS OF CARBON FOOTPRINT

2.1 Causes of Carbon Footprint

Burning of fossil fuels release carbon into the atmosphere causes global warming and increases the greenhouse gas. Modern way of life is the main significant reason for the increase of carbon dioxide. Food, industrial revolution, air planes are also play a major role for the cause of carbon footprints. Chief carbon inputs are home appliances, airplanes, cars, condenser, boilers, tumble driers. Secondary carbon inputs are vehicles and other external uses, imported food, fast food, eating large quantity of meat, cool drinks and drinkable water [4], [5],[6].

2.2 Effects of Carbon Footprint

Outcome of carbon footprint is the major changes in climatic conditions. GHGs that are emitted consist mainly of CO2 that is up to 80%. It results in decrease in the marine life that includes sea mammals and other water animals. It occurs mainly due to the injection of plastics that emit more amount of carbon and affects their digestive systems. It also results in the depletion of natural resources, erosion of soil, deforestation. They affect the ecological balance and cause habitat destruction.[7],[8],[9].

2.3 Reduction of Carbon Footprint

Air travel is the largest component of carbon foot print. This can be reduced by going through train. The important lifestyle change of the carbon footprint is to eat less meat. Home eating is the biggest component of carbon foot print. This can be eliminated if the loft is insulated and cavity of wall is filled by using solid brick or stone walls. Old gas and oil boilers should be avoided. Usage of more electric vehicles should be encouraged. LED bulbs should be used instead of halogen bulbs. Awareness should be given for the usage of solar panels [7], [11].

CFP is considered to be an important step in reducing the carbon emission since it represents the quantity of carbon di oxide emitted by a person/ organization/ country/ world. This will help to reduce the carbon emission by the public by creating awareness about the pollution each individual is emitting [15].

In addition to normal activities, the activities which will reduce the carbon foot print in construction industry have also been identified. The standard materials used for concrete were replaced with materials which may result in low carbon emission [16].

3. STUDY AREA

Bannari Amman Institute of Technology(BIT) is an educational institution offering many undergraduate and post graduate programmes including Master of Business Applications. It is nestled nearby the banks of Bhavani River in Sathyamangalam Town. The campus has spacious and the earth hugging buildings punctuated with landscaped courtyards.

3.1 Source of Carbon Footprint at BIT

The main source of carbon foot print at BIT may include books, magazines, newspapers, computers, motor vehicles, mobile phones, cars, Air conditioners, etc.,. It

may also include the sewage treatment plant and wasted food from the mess.

4. METHODOLOGY

To create awareness among the individuals about their contribution to carbon di oxide emission, a random survey was conducted among the individuals at Bannari Amman Institute of Technology. A widget was used to calculate carbon emissions. A questionnaire was prepared based on the data to be fed in the widget. This tool is used to calculate the carbon emissions of a trip or annual commute or our overall lifestyle.

The step by step procedure for carbon emission calculations using the widget is explained below.

- Country in which the respondent is residing is first entered.
- Carbon footprint calculations are typically based on annual emissions from the previous 12 months. From/ to period is entered.
- Next, the appropriate tab required (ie., house, flights, cars, motor bike, Bus and rails, Secondary) is chosen to calculate the part of respondent's life style.
- In this study the tabs House and Secondary are selected to calculate the carbon emissions.
- House carbon foot print calculator is chosen first and consumption of each type of energy is entered.
- Secondary carbon foot print calculator is then chosen and the amount spent on different items such as food and drink products, Pharmaceuticals, Clothes, textiles & shoes, Paper based products (eg. Books, magazines, newspapers), Computers and IT equipment, television, radio and phone, motor vehicle (excluding fuel cost), furniture and other manufactured goods, hotels, restaurants and pubs, telephone, mobile/cell phone call costs, banking and finance (mortgage & loan interest payments), insurance, education, Recreational, cultural and sporting activities were entered.
- Based on the entered data, secondary foot print is estimated.
- Using the result tab, individual carbon foot print was estimated and is compared with Country's average and Global average.

From this comparison, whether the carbon di oxide emission by the individuals exceeded or prevailed within the desirable limit was found. The carbon dioxide emission varied from person to person depending on their way of living. By the survey, the individuals were made aware of the quantity of carbon dioxide emitted by them into the environment.

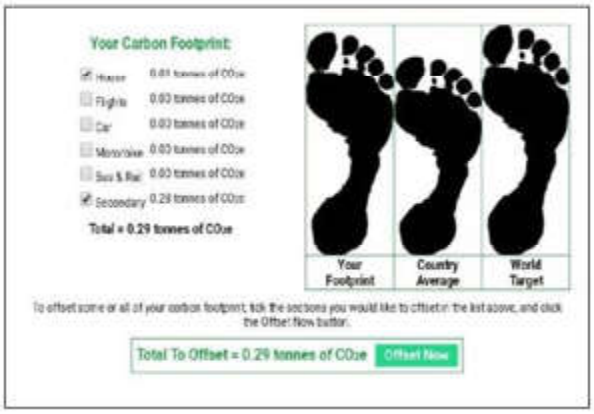

Fig. 1 Carbon foot print 0.09 tonnes of CO2 emission

Figure 1 represents the carbon footprint of an individual as 0.09 tonnes/capita. When compared to the country's average value 1.7 tonnes/capita, this value is very less.

Fig. 2 Carbon foot print 0.29 tonnes of CO2 emission

This is when compared to the country's average value 1.7 tonnes/capita, is vey less. Fig.2 represents the carbon footprint of an individual as 0.29 tonnes/day.

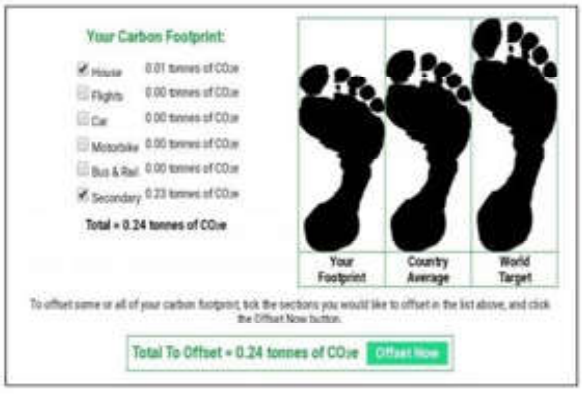

Fig. 3 Carbon foot print 0.24 tonnes of CO2 emission

Figure 3 Carbon foot print 0.24 tonnes of CO2 emission. This when compared to the country's average value 1.7 tonnes/month, is very less.The carbon foot print values in Fig.1, Fig.2, Fig. 3 are around 5.00%, 16.11% and 13.33% respectively when compared to country's average. The values when compared with global standards are around 2.00%, 6.44% and 5.33%. Though the values are less when compared to the Global Standards, they too contribute to carbon dioxide emission and global warming.

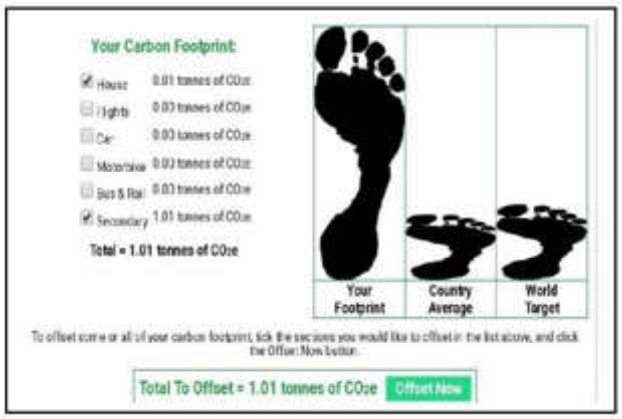

Fig.4 Carbon foot print 1.01 tonnes of CO2emission

Figure 4 represents the carbon footprint of an individual as 1.01 tonnes /capita. This when compared to the country's average value 1.7 tonnes/capita, is less, but when compared to other individuals, this is the highest contributing to carbon di oxide emission.

Fig.5 Carbon foot print 0.34 tonnes of CO_2 emission

Figure 5 represents the carbon footprint of an individual as 0.34tonnes /capita. This when compared to the country's average value 1.7 tonnes/capita, is less.

The carbon foot print values in Fig.4, Fig.5, Fig.6 when compared to country's average are around 56.11%, 16.11% and 18.89% respectively. The values when compared with global standards are around 22.44%, 6.44% and 7.56%.

From the survey it can be inferred that though the individuals are living in the same area, their carbon dioxide emission value may differ due to different income groups (LIG – Low Income Group, MIG – Middle Income Group, HIG – High Income Group) they belong to. This reveals the tendency of human beings about the usage of resources. More the income that the individual earns, more is his/her tendency to move to the comfort zone with sophisticated life style.

The table 1 shows the comparison between the carbon foot print that an individual generates with respect to Country's and World's Average.

Table 1 Comparison of Individual, Country and Global Carbon Footprint

Sl. No.	Individual Carbon Footprint	Country' s Carbon footprint	Global Carbon Footprint
(Average) (Tonnes/capita/year)			
1	0.09	1.8	4.5
2	0.29	1.8	4.5
3	0.24	1.8	4.5
4	1.01	1.8	4.5
5	0.29	1.8	4.5
6	0.34	1.8	4.5

India's average Carbon dioxide emission is 1.8 tons/ capita estimated in 2017 and it is around 40% of Global Carbon dioxide emission of 4.5 tons/capita for one year. This is when compared to developed countries is around 22.73%.

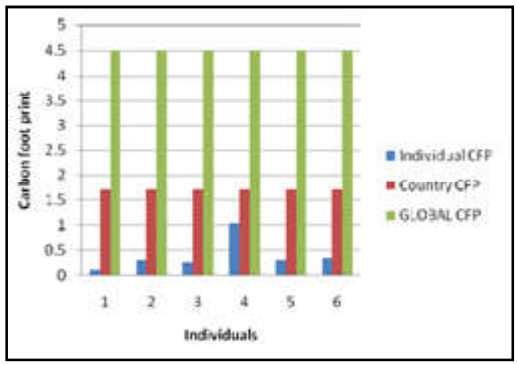

Fig.6 Comparison graph for Individual, Country and Global carbon footprint.

Figure 6 represents the Carbon footprint for different individuals and their carbon di oxide concentrations were compared with Country and Global average carbon di oxide emissions. From the comparison it was identified that none of the individuals CO2 emission exceeded the country as well as global CO2 emission.

5. DISCUSSION

Figure 6 represents the Carbon foot print for five different individuals and their carbon di oxide emission levels were compared with Country and Global average carbon di oxide emission levels. From the comparison it was identified that none of the individuals CO2 emission exceeded the country as well as global CO2 emission.

The graph shows that Indian's emit less CO2 when compared to the global and developed countries standard limit of CO2 emission. This review was conducted among 20 individuals in close- by urban region Sathyamangalam. Five surveys were shown for sample. From the study it was inferred that the carbon dioxide emission into the atmosphere varied with respect to the lifestyle of the people. The lowest carbon dioxide emission was found to be 0.04 tonnes per capita and the highest was found to be 1.01 tonnes per capita. Both the upper and lower levels are within the country average and global average.

6. CONCLUSIONS

From the survey conducted for carbon foot print at Bannari Amman Institute of Technology, it can be concluded that the life style of the people here is such that their carbon di oxide emissions were far below the country's and global emission standards. Though the Carbon foot print is well below the prescribed levels, awareness has been created among the individuals about their contribution towards carbon di oxide emission which leads to global warming.

Estimated per individual, India's discharges are still low, at just 1.8 tons of CO2 per capita or, in other words 2.5 times lesser than the world normal of 4.5 tons. However, those outflows have been developing consistently, with a normal development rate over the previous decade of 6%. Though it is within the limits there is a chance for increase in CO2 emission in the near future. So to reduce global warming and other effects on the environment the usage of sources of CO2 emission should be minimized to the maximum possible.

This survey may create awareness about the present condition of carbon dioxide emissions and may motivate the individuals to change their way of living, so that their contribution to Global warming will be minimized.

REFERENCES

[1] Matthias Fink beiner, "Carbon Foot Printing Opportunities and Threats", Int J Life Cycle Assess, Vol.14, 2009, pp 91-94.

[2] "Carbon Footprints in the Supply Chain: The Next Step for Business", The Carbon Trust; November 2006.

[3] Tao Gao, Qing Liu and Jianping Wang, "A Comparative Study of Carbon Foot Print and Assessment Standards", International Journal of Low-Carbon Technologies, Vol.9, No.3, 1st September 2014, pp.237-243.

[4] T. Wiedmann and J. Minx, "A Definition of Carbon Footprint [J]", ISA Res Rep 2007, Vol.7, 2007, pp.1-7.

[5] B.P. Weidema, M.Thrane and P.Christensen, "Carbon Footprint", [J] Ind Ecol, Vol.12, 2008, pp.3-6.

[6] K. Angelakoglou, G. Gaidajis, K. Lymperopoulos and P. N. Botsaris, "Carbon Footprint Analysis of Municipalities-Evidence from Greece", Journal of Engineering Science and Technology Review, Vol.4, 2015, pp.15-23.

[7] P.Freund, S.Bachu, D.Simbeck, K. Thambimuthu and M. Gupta, "Properties of CO2 and Carbon-based Fuels", IPCC special report on Carbon Dioxide and Storage. Annex I: 2012, pp. 384-400.

[8] L. Cucek, J.J. Klemes and Z. Kravanja, "A Review of Footprint Analysis Tools for Monitoring Impacts on Sustainability", Journal of Cleaner Production , Vol.34, 2012, pp.09-20.

[9] Sarah E. West, Anne Owen, Katarina Axelsson and Chris D. West, "Evaluating the Use of a Carbon Footprint Calculator, Communicating Impacts of Consumption at Household Level and Exploring Mitigation Options", Journal of Industrial Ecology, Vol.20, 2015, pp.396-409.

[10] https://www.theguardian.com/environment/datablog/2009/sep/02/carbon -emissions-per-person-capita.

[11] M.G.G. Awanthi and C.M. Navaratne, "Carbon Footprint of an Organization: A Tool for Monitoring Impacts on Global Warming", Procedia Engineering, https://doi.org/10.1016/j.proeng.2018.01.094, Vol. 212, 2018, pp.729-735.

ECO-FRIENDLY APPLICATIONS OF NATURAL WASTE MATERIALS IN CONSTRUCTION

S.M. Sanjaikumar, G. Sureshkumar and V. Jayanthi
Bannari Amman Institute of Technology, Sathyamangalam - 638 401, Erode District, Tamil Nadu

Abstract

A sustainable solution for solid waste management suffers many practical hindrances during implementation due to the prevailing conflicts in socio-economic development goals. In order to provide practically feasible solutions for this multi-faceted issue, there is a need for an integrated approach combining various seemingly incoherent concepts. One such approach is presented in this study, where rice husk, hyposludge, and chicken feather are effectively used as active ingredients in concrete design. In this approach, the fine aggregate used in cement mortar is partially replaced by rice husk, hyposludge, and chicken feather for preparing M20-grade concrete and further tested for its behavioural strength. The results are found to be promising, suggesting that the replacement of waste materials will increase the strength behaviour of concrete as well as its thermal insulation. The resultant green concrete is envisaged to motivate further refinement to reduce its adverse impacts in the built environment. The results of the present study indicate the possibility of confluences of approaches in effectively handling waste management problems for achieving sustainable solutions in material reuse in concrete manufacturing.

Keywords: *Environment, Green concrete, Rice husk, Sustainable technology, Thermal insulation*

1. INTRODUCTION

The present-day world is witnessing the construction of very challenging and aesthetic structures. Concrete is the most common material used in construction worldwide. High strength, durability, and workability are the promising results that make it versatile, and it is used in almost all major construction projects. The total world consumption of concrete per year is about one tonne for every living human being. Man consumes no material except water in such tremendous quantities. [1]

Progressive activities like globalisation, privatisation, etc. ultimately lead to the consumption of large quantities of precious natural resources. This eventually leads to a faster depletion of natural resources and increases the cost of building structures as well. "We have to put an end to those bad, long-standing habits of squandering natural resources. Sustainable building materials can be the solution" Here, the principle of sustainability has to come into play. Development without damaging the environment or meeting the needs of future generations is referred to as "sustainable development. At present, the demand for a more sustainable way of building is no longer a matter of personal choice, and the sector has been regulated for the purpose of implementing measures that improve the infrastructure's and buildings' environmental behaviour. Here, effective replacement of natural waste materials could either be used as an additive or as a partial replacement to the conventional ingredients of concrete so that the existing natural resources could be saved to the maximum extent possible and could be made available for the future generation. In this process, natural and environmentally friendly wastes like rice husk ash, hypo sludge, and chicken feather have been tried as feasible substitute materials for conventional materials in concrete.

2. DESIGN MIX MATERIALS

2.1. Cement

The Ordinary Portland Cement of 53 grades conforming to IS: 8112- 1989 is being used. Tests were conducted on the cement like Specific gravity, consistency tests, setting tests, soundness, Compressive strength N/mm2 at 28 days.

Table 1 Properties of 53 Grade Cement

Sl. No.	Physical Properties of Grade cement	Requirements as per IS:8112-1989
1	Specific gravity	3.10-3.15
2	Standard consistency (%)	30-35
3	Initial setting time (hours, min)	30 (minimum)
4	Final setting time (hours, min)	600 (maximum)
5	Compressive strength N/mm2 at 28 days	53 N/mm2 (minimum)

Fig.1 Ordinary portland cement

2.2 Fine Aggregate

The particles of size ranging from 4.75 mm to 150 microns are termed as fine aggregate. The river sand is used as fine aggregate conforming to the requirements of IS: 383. The river sand is washed and screened, to eliminate deleterious materials and oversize particles.

Table 2 Properties of Fine Aggregate

Property	Fine Aggreagte (River Sand)
Fineness modulus	3.1
Specific Gravity	2.767
Water Absorption (%)	1.2
Bulk density (gm/cc)	1.78

Fig.2 River sand

2.3. Coarse Aggregate

The particles of size ranging from 4.75 mm to 37.5 mm are termed as coarse aggregate. Coarse aggregate of 20 mm maximum size is used.

Table 3 Properties of Coarse Aggregate

Property	Coarse Aggregate (20 mm)
Type	Angular
Density	1560 kg/m3
Specific gravity	2.63
Fineness modulus	7.54
Water absorption (%)	0.48%

Fig.3 Angular course aggregate

2.4. Water

Water is an important ingredient in the cement mortar, as it actually contributes to the chemical reaction with cement. Since it helps to form the strength-giving cement gel, the quantity and quality of water are required to be looked into very carefully.

2.5. Rice Husk Ash(RHA)

Rice husk is an agro-waste material that is produced in about 100 million tonnes. Approximately 20 kg of rice husk are obtained for 100 kg of rice. Rice husks contain organic substances and 20% inorganic material. Rice husk ash (RHA) is obtained by the combustion of rice husk. The most important property of RHA that determines pozzolanic activity is its amorphous phase content. RHA is a highly reactive pozzolanic material suitable for use in lime-pozzolana mixes and for Portland cement replacement. RHA contains a high amount of silicon dioxide, and its reactivity with lime depends on a combination of two factors, namely the non-crystalline silica content and its specific surface.

Fig 5 Rice husk ash (RHA)

2.6. Hypo Sludge

Hypo sludge is a type of waste obtained by paper production. The material is a by-product of the de-inking and re-pulping of paper. The utilization of hypo sludge as cement replacement material introduces many benefits from economical, technical and environmental points of view. Hypo sludge contains, low calcium and maximum calcium chloride and minimum amount of silica. Hypo sludge behaves like cement because of silica and magnesium properties. This silica and magnesium improve the setting of the concrete

Fig.6 Hypo sludge

2.7 Chicken Feathers

Chicken feathers are waste products of the poultry industry. Billions of kilograms of waste feathers are generated each year by poultry processing plants, creating serious solid waste problem. Chicken feathers possess good durability and resistance to degradation because of the extensive cross-linking and strong covalent bonding within its structure.

Fig.7 Chicken feathers

3. DESIGN MIX METHODOLOGY

A cement mortar mix 1:1.5:3 was designed as per IS: 10262: 2019 methods and the same were used to prepare the test samples Three cubes, each of size 150mm x 150 mm x 150 mm are to be cast with the mortar. The design mix proportion is done in Table 5 and 6.

Table 5 Mix Design Proportions

Material	% to be Replaced with Cement	% to be Replaced with Fine Aggregate	Weight (in gms)
RHA	12.5	-	516.7
Hypo sludge	10	-	413.4
Chicken Feather	-	3	231.04

Table 6 Proportions of Materials to be Replaced

	Cement	Fine Aggregate	Coarse Aggregate	Water
By weight [in gms]	4133.4	7470.4	13046.4	186000

4. EXPERIMENTAL METHODOLOGY

4.1 Compression Test

150 mm X 150mm X 150mm concrete cubes were casting using M20 grade concrete. Specimens with ordinary Portland cement (OPC) and OPC replaced with RHA and hypo sludge, Fine aggregate replaced with chicken feather at 12.5%, 10% and 3% levels respectively were cast. After 24 hours, the specimens were removed from the mould and subjected to water curing for 28 days. After curing, the specimens were tested for compressive strength using a compression testing machine of 2000 kN capacity.

Fig.8 Compression test

4.2. Split Tensile Strength Test

Split tensile strength of concrete is usually found by testing plain concrete cylinders. Cylinders of size 150mm x 300 mm were casting using M20 grade concrete Specimens with ordinary Portland cement (OPC) and OPC replaced with RHA and hypo sludge, Fine aggregate replaced with chicken feather at 12.5%, 10% and 3% levels respectively were cast.

Fig.9 Split Tensile Strength test

After 24 hours, the specimens were removed from the mould and subjected to water curing for 28 days. After curing, the specimens were tested.

5. EXPECTED RESULT

5.1 Workability

Jayraj Vinodsinh Solanki et.al (2013) has observed that as the percentage of hypo sludge in the mix increases the slump decreases. The mix has shown good workability and the workablilty was found to be less as compared to conventional M-20 grade concrete.

5.2 Compressive Strength

Dr. A.M. Pande et.al (2013) suggested that higher percentages of RHA replacement lead to decrease in the compressive strength. However, 10% replacement of cement with RHA attained the targeted compressive strength addition of RHA instead of cement not only improve compressive strength, but also durability representations can be observed in normal or conventional concretes. Mixes show higher compressive rather than normal concrete. Replacement of 12.5 % of cement with rice husk ash in matrix causes reduction in utilization of cement and expenditures. Also, can improve quality of concrete at the age of 90 days.[1] It was found out that the concrete tends to achieve 85-100 % for 12.5 % RHA.

Sumit A Balwaik et.al (2010) investigated that the compressive, splitting tensile and flexural strength increased up to 10% addition of waste paper pulp.
Dr. Jayeshkumar Pitroda et.al found out that the Compressive strength of the concrete increased when the percentage of replacement was increased up to 40%. Further replacement of cement reduced the compressive strength. Replacement of cement with hypo sludge material gave maximum compressive strength at 30% replacement.[2]

According to Merrit (1976), “Cement served as the binder of the aggregates, and with cement content increasing, the strength is also increasing”. Thus, the resulting compressive strength gradually decreases as the feather level increases unless the quantity of cement is increased. Amit Kumar Sharma et.al (2016) has drawn out a fact that as the feathers replaces fine aggregates in increasing manner, the compressive strength decreases. Therefore, the varying ratios of fine aggregate with respect to the chicken feathers affected the compressive strength of the specimens. It indicates that

the compressive strengths of the specimens are inversely proportional to the increase of the feather levels.[4].

5.3 Split Tensile Strength

It is observed that in split tensile strength of M20 grade concrete, the strength of concrete has increased with 10% replacement of hypo sludge with cement as compare to conventional concrete.

6. CONCLUSION

The concrete was found to be performing better than normal concrete, in properties such as workability and compressive strength. As disposal of wastes, by-products are a major problem in today's world due to limited landfill space as well as its rising prices for disposal, utilization of these wastes in concrete will not only provide economy but also help in reducing disposal problems. "Little drops of water make the mighty ocean"- Small steps towards sustainability to create a better environment for the future generations.

REFERENCES

[1] Dr. A.M. Pande, S.G.Makarande, International Journal of Engineering Research and Applications (IJERA) ISSN: 2248-9622 www.ijera.com Vol. 3, Issue 1, January -February 2013, pp.1718-1723

[2] Dr. Jayeshkumar Pitroda, "Gainfull Utilization of Hypo Sludge in Construction Industry- A Review", International Conference on "Engineering: Issues, opportunities and Challenges for Development", ISBN: 978-81-929339-3-1.

[3] Rushabh A. Shah and Prof. Jayeshkumar Pitroda, "Effect of Hypo Sludge as Partial Replacement With Cement In Mortar", Iarm Vol.1, No.3, April 2013.

[4] Amit Kumar Sharma, "Chicken Feather as a Substitute of Fine Aggregate in Mortar", International Journal of Advances in Engineering & Scientific Research, ISSN: 2349 –3607 (Online) ISSN: 2349 –4824 (Print), Vol.3, No.6, Dec-2016, pp.35-48.

[5] Min-Hong Zhang and V. Mohan Malhotra, "High-Performance Concrete Incorporating Rice Husk Ash as a Supplementary Cementing Material", November 1996, ACI Materials Journal Vol.93, No.6, pp.629-636.

[6] Jayraj VinodsinhSolanki and Jayeshkumar Pitroda, "Investigation of Low Cost Concrete Using Industrial Waste as Supplementary Cementitious Materials", International Journal of Engineering Science and Innovative Technology (IJESIT), Vol.2, No.1, January 2013, pp.81.

DESIGN AND DEVELOPMENT OF NEW PORTABLE WATER FILTER SYSTEM FOR DRINKING WATER PURPOSE

PS.Vijayanand[1], NV. Manjunath[2], V.Jayanthi[3], V. Vijayakumar[4], S. Jagan[5], A.Kathiralagan[6] and G. Suresh Kumar[7]

[1&4]Department of Chemistry, [2,3,5,6&7]Department of Civil Engineering,
Bannari Amman Institute of Technology, Sathyamangalam - 638 401, Erode District, Tamil Nadu
E-mail: vijayanandps@bitsathy.ac.in, vijayps6@yahoo.co.in

Abstract

About one-fifth of people on earth lack the access to safe drinking water, a condition that resulted in the death of 2.2 million people in 2004, as per the records of United Nations. Hence research on clean water usage is being a prime concern in many developing countries. Contaminated water plays threatening in numerous lives in these localities, for which a number of efforts are being made for accessing safe purified drinking water. This study was conducted to design a water filter system which is both economic and easy to use which can act as antimicrobial one. A prototype design water filter was constructed by using the layers of gravel, sand, activated charcoal, and polypropylene micron filter, silver nanoparticles coated polypropylene fiber containing compartments were built for carrying out water purification. Complete water analysis was done, and the removal of suspended impurities, microorganism in each layer was analyzed. It is discussed with six important water quality parameters improvements such as electrical conductivity, pH, total dissolved solids, hardness, alkalinity, chloride content during the treatment process. A significant change of coliform bacterial count between UV treatments together with this sand, Charcoal filter, silver nanoparticles coated fiber are observed. This study also demonstrated that the proposed design of water filter system is efficient in removal of turbidity, odor, and microbial content of polluted water. The results are also compared with commercial ceramic filter.

Keyword: *Activate carbon, Micron filter sliver, Nanoparticles, Polypropylenefibre, Water.*

1.INTRODUCTION.

Water is the main component in our body. Human being body consists mainly of water (on average about 70%).[1] Human being liver, for example, is about 90% water, brain 85%, blood 83% and even the bones 35%. [2]. Therefore, consuming enough water in our daily life is a must to stay hydrated and healthy. According to the World Health Organization (WHO) in 2007, over 1 billion people lack access to safe water supplies. This has led to widespread microbial contamination of drinking water. Water-associated infectious diseases claim up to 3.2 million lives each year, approximately 6% of all deaths globally. The burden of disease from inadequate water, sanitation, and hygiene totals 1.8 million deaths and the loss of greater than 75 million healthy life years. [3] It is well established that investments in safe drinking water and improved sanitation show a close correspondence with improvement in human health and economic productivity. Water is one of the natural resources that are essential for human people and other living organisms.

Water can be classified by clean water (consumable water) and dirty water (inconsumable water; further treatment is required prior to using). [4] Clean water is required for supporting people daily life and activity, such as drinking and cooking, bathroom uses, wash, and other purposes. Quality of clean water can support welfare and health for people [5]. On the contrary, bad water quality has direct correlation to the health of users.

Nowadays, clean water supply becomes one of the main issues in the world, especially for developing country. With this shortage of clean water, people activity is disturbed; Further, this can give negative pact to the country in general. The process to purify water is a must. Otherwise, the clean water cannot be distributed. [6] Many methods have been reported to treat and purify dirty water. One of the popular methods are combination of filter and physicochemical process system (namely filter system). [4] Although electrolysis is well-known as the best method to purify the water, the process is impractical for the practical uses. [7] In short of the filter

process, the water is through into the filter system. The filter system screens the larger component via hard screening, adsorption, and simple chemical reaction. To achieve this method, combination of filtering system, activated carbon, coagulant, and alum is typically used. In filtering system based on hard screening process, textile fibers are typically used for filtering large floating or sinking component. [8] However, this is ineffective when the water containing colloidal component. For activated carbon, the process is basically used adsorption process for removing impurities, including organic compound. [9] Typically, this activated carbon process is effective for eliminating odor in the water. [10] Then, in the case of coagulant, this step is typically used for water with high level of turbidity. Coagulant can be from either inorganic compound (e.g. aluminum salt and iron) or organic compound (e.g. polyacrylic amide and polyethylene mina). Many types of portable water filters available, with varying degrees of effectiveness, can be used together with chemical purification.

There are several methods of water purification. The main ones are:

- Distillation,
- Ion exchange
- Reverse osmosis
- Microporous filtration
- Ultra-filtration
- Photo-oxidation

Thus, the requirement for the facile process that can afford the production of clean water is required. Here, the purpose of this study was to introduce our simple home-made water treatment system for solving the clean water supply problem in rural area. We designed a water system using several inexpensive materials: activated sand, activated carbon, micron fibre filter. Hence this research paper mainly focused on the fabrication of prototype water filter cartridge for water purification. The performance also compared with commercial available ceramic filter.

2. METHODOLOGY

The methodology of the design a new gravity based filtration system by using is the layers of gravel, sand, activated charcoal, and polypropylene micron filter, silver nanoparticles coated polypropylene fiber containing compartments were built for carrying out water purification as starting materials. The purified water after the removal of the physical, chemical and biological impurities at several stages has been analyzed. The efficiency of the filter and also regeneration of the filter has been tested.

3.FILTER MEDUIM

The filter medium is a porous and also semipermeable one barrier placed across the flow of water to hold back all the suspended materials. The cylindrical hollow filter cartridge is having a combination of filter pads consists five layers; activated carbon, silica sand, and mineral sand.

Fig.1 Designed water filter and B. commercial ceramic filter

Fig.2 Represent the commercial ceramic filter which is purchased from sea zone industry.

4. ACTIVE CARBON

Active carbon is unique and versatile adsorbents. The preparation of activated carbon by using the coconut shell as a source of biomass material and it is impregnated in

concentrated sulfuric acid for period of 48 hours. After that it has been washed, dried and completely grinded by mortar to get the fine particles. They are extensively used for water purification for a removal of undesirable odour, colour, taste, and other organic and inorganic impurities. The prepared activated carbon is a form of carbon that has been processed to make it extremely porous and thus to have a very large surface area available for adsorption or chemical reaction. Adsorption is a removal process where particles are bound to an adsorbent particle surface by either chemical or physical attraction. It is most effective in removing organic contaminants and other particles from water. Most importantly, activated carbon filtration will remove chlorine from the water where chlorine is greatly used in water treatment as disinfectant.

Other than that, activated carbon does remove some organic chemicals such as trihalomethanes (THM), pesticides, industrial solvents (halogenated hydrocarbons), polychlorinated biphenyls (PCBs), and polycyclic aromatic hydrocarbons (PAHs). Activated carbon is not suitable for removing suspended biological material. This can be done in an element that combines adsorption with biological activity by utilizing the other filter media particles such as sand, polypropylene micron fiber.

Fig.3 Preparation of activated carbon by impregnation method

5. SILICA SAND

Silica sand (quartz) is pure crystalline sand, the most common mineral on the earth's surface. Silica sand has been used in water filtration systems for many years to put finishing touches on clean water. It removes the acidic components from the water, and thereby brings about a pH-balance of body fluids. Besides, it also removes toxic chemicals and other hazardous materials from water much more effectively and at lower cost.

Fig.4 Preparation of sand for filtration media

6. GRAVEL MATERIALS

Layers of gravel can trap large particles and help to oxygenate the water. If there are smaller gravel below, they will filter out smaller particles. Then there's small size gravel which would continue the process like sand. Filter Gravel is an extremely effective filter media because of its ability to hold back precipitates containing impurities. Filtration quality depends upon the size, angularity, density of packing and hardness to ensure proper filtering

7. MINERAL SAND

Mineral sands contain suites of minerals with high specific gravity known as 'heavy minerals', which include economically important minerals rich in titanium, zirconium and rare earths. Mineral sand is used in water filtration because it releases minerals to the water. Furthermore, it adjusts the water pH to mildly alkaline. Thus, healthy water can be obtained. The upper filter cap is received inside an open top portion of the cartridge. The cartridge also includes a lower filter cap with a water outlet. The lower filter cap is received inside an open bottom portion of the cartridge.

8. POLYPROPYLENE BASED SILVER NANOCOMPOSITES FIBRE LAYER

For the preparation of silver nanoparticle polypropylene nanocompites the following procedure has been adopted. Synthesis of poly m-toluidine-silver nanocomposites10 ml of silver nanoparticle colloid were diluted into 70 ml of distilled water. The waste of polypropylene micron fibre from RO plant is collected, the dirt and the impurities are washed with saturated solution oxalic acid and sodium solution in equal proportion. The fibre is washed again and again with

fresh water and dried. The bleached fibre is then soaked into the colloidal solution slowly under sonication. The fibre composites has been formed centrifuged, and washed with double distilled water, acetone, and methanol. The product was dried in a vacuum oven at 50 °C for about 24 h.

Fig.5 Preparation of polypropylene fiber by bleaching

9. FTIR SPECTRUM

The most prominent peaks of polypropylene are assigned to asymmetric stretching of CH3 (2950 cm "1), asymmetric stretching of CH2 (2916 cm "1), CH3 stretching (2866 cm "1), CH3 symmetric bending (1454 cm "1 and 1375 cm "1), C-H wagging and CH3 rocking vibration (1167 cm "1), CH3 rocking vibration and C-C stretching (997 cm "1 and 973 cm "1), and C-H rocking vibration (841 cm "1). The absorption spectrum confirms the chemical structure of the pure polypropylene and also composites.

10. TURBIDITY TEST

Turbidity is the cloudiness or haziness of a fluid caused by individual particles (suspended solids) that are generally invisible to the naked eye. The measurement

Fig.6 Preparation of polypropylene based silver nanocomposites

of turbidity is a key test of water quality. Fluids can contain suspended solid matter consisting of particles of many different sizes. While some suspended material will be large enough and heavy enough to settle rapidly to the bottom container if a liquid sample is left to stand (the settle able solids), very small particles will settle only very slowly or not at all if the sample is regularly agitated or the particles are colloidal.

These small solid particles cause the liquid to appear turbid. WHO establishes that the turbidity of drinking water shouldn't be more than 5 NTU (Nephelometric Turbidity Units), and should ideally be below 1 NTU. The designed water filter will remove the turbidity causing chemical substance in all the layer such as sand, gravel, carbon and polypropylene layers. The test results show that the value of turbidity all below 1 NTU which passes the minimum requirement by WHO. There are some differences in the turbidity level of sample water obtained from designed and also comparing with commercial ceramic filter. This shows that the efficiency of the filtration.

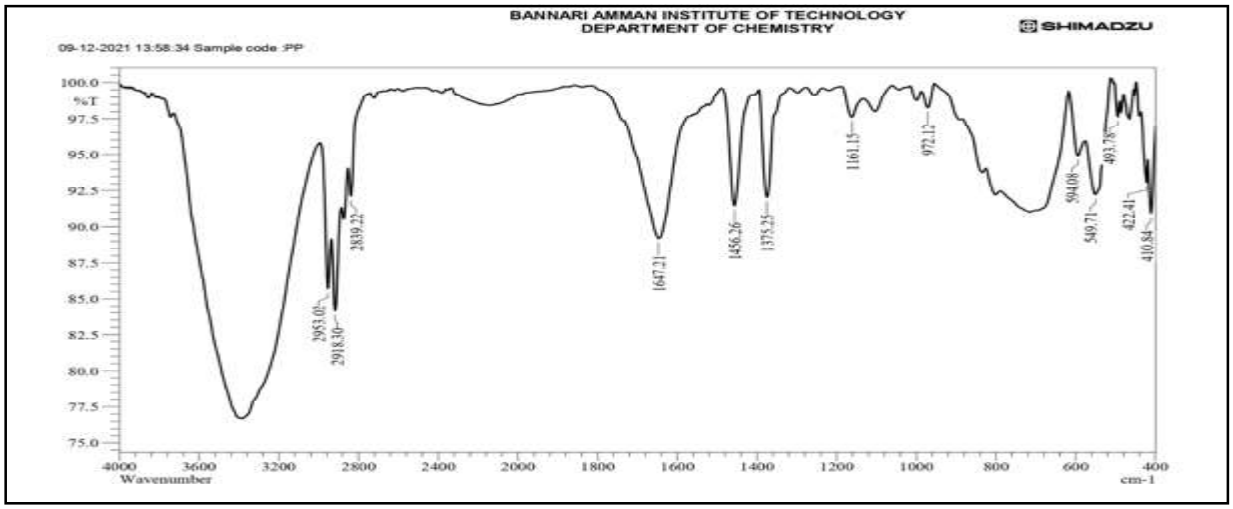

Fig.6 FT-IR spectrum of polypropylene micron fiber silver nanocomposites

Table 1 Turbidity Test

TEST	Input water data	Designed filter (Filtered water data)	Commercial Ceramic filter (Filtered water data)
PH	9.3	8.0	9.0
CONDUCTIVITY(µS/cm)	1454	600	1400
TDS(PPM)	727	300	700
HARDNESS(PPM)	678	250	600

11. CONCLUSION

The design portable ecofriendly gravity based water filter are fabricated into prototype model successfully and the quality of purified water has been analyzed The information about the technology, feasibility of using this technology and on design, construction, and operations to best performance has been studied. The water filter comprises a cylindrical structure container with several layers of filtration media to filtrate the water. The water analysis indicates the removal of considerable amount of dissolved hardness causing salt, complete removal of suspended impurities, removal of bacterial impurities. The regeneration of the filter system by washing alkali and acidic solution is also undertaken. The designed filter provides an easier way to get safe, clean, and healthy and hot water. The designed water filter shows better performance than of the commercial ceramic based filter. wash. The water from this filter has been tested using various tests to prove that the quality of water is meeting the standards.

REFERENCES

[1] WHO, World Health Organization, "Ecosystems and Human Health: Some Findings From the Millennium Ecosystem Assessment", Report Published by WHO, 2007.

[2] HDR Engineering Inc. (2002). Handbook of public water systems. (2nd Ed.), Hoboken New Jersey, John Wiley and Sons, Inc.

[3] K. Sutherland, "Filters and Filtration Handbook. (5th Ed.), Butterworth Heinemann is an imprint of Elsevier, 2008.

[4] A E. Valentina, S.S.Miswadi and L.Latifah, "Pemanfaatan Arang Eceng Gondok Dalammenurunkan Kekeruhan, COD, BOD Pada Air Sumur Indonesian, Journal of Chemical Science, Vol.2, No.2, 2013, pp.84-89

[5] V. Damiati, A. Lumangkun and M. Dirhamsyah, "Partisipasi Masyarakat Dalam Melestarikan Kawasan Hutan Lindung Gunung Buduk Sebagai Sumber Air Bersih Di Desa Idas KecamatanNoyan Kabupaten Sanggau Jurnal Hutan Lestari, Vol.3, No.1, 2015, pp.142-149.

[6] Peraturan Menteri Kesehatan No. 416 Tahun 1990 Tentang: Syarat-syarat Dan Pengawasan Kualitas Air.

[7] M. El-Harbawi, "Design of A Portable Dual Purposes Water Filter System", Journal of Engineering Science and Technology, Vol.5, No.2, 2010, pp.165-175.

[8] T.H. Inazaki, P.B. de Moraes, G. Regis, P.R.M.Lopes, R.N.Montagnolli, A.C.S.Piao and ED.Bidoia, "Wastewater Containing 1, 2-dihydro-2, 2, 4 Trimethylquinoleyn Treated By Electrolysis and Respirometric Method Hydrology: Current Research", Vol.1, No.1, 2011, pp.100-101

[9] A. Herlambang, "Teknologi Penyediaan Air Minum Untuk Keadaan Tanggapdarurat", Jurnal Air Indonesia, Vol.6, No.1, 2011, pp.52-63.

[10] B. Ramavandi, "Treatment of Water Turbidity And Bacteria By Using Coagulant Extracted From Plant Ago Ovata", Water Resources and Industry, Vol.6, 2014, pp.36-50.

COMPARATIVE STUDY ON DEEP LEARNING BASED ANOMALY DETECTION TECHNIQUES FOR SECURITY SURVEILLANCE SYSTEMS

K.Ganagavalli[1], V. Santhi[2] and V. Krishnamoorthy[3]
[1&3]Bannari Amman Institute of Technology, Sathyamanagalam - 638 401, Erode District, Tamil Nadu
[2]PSG College of Technology, Coimbatore - 641 004, Tamil Nadu
E-mail:ganagavalli@bitsathy.ac.in

Abstract

Recently the occurrence of crime activities and terrorism has begun to increase significantly. Most of the attacks are taking place in public areas. Now-a-days CCTV surveillance has become a major part in all public places and private places. They are used for monitoring the context and produces enormous amount of data on daily basis. Monitoring such videos with manpower is impracticable. An automatic system for monitoring and analyzing those video data is required. So making use of this video surveillance for preventing violent activities and attacks will be more helpful to the society. Deep learning based anomaly detection systems can be used for monitoring the public activity and protecting them during crucial times. Automatic anomaly detection systems will be applied on the surveillance data and they can be used for analyzing the behavior people. Based on the analysis, abnormal activities can be easily detected and notified to the concern administration. This system can be implemented in any public or private areas, to prevent violent and criminal activities before head. In this paper deep learning based anomaly activity detection system has been proposed.

Keywords*: Anomaly detection, Abnormal behavior, Anomaly activities.*

1. INTRODUCTION

In recent years, video surveillance has become one of the major tool for analyzing the crime scenes and crime activities. The technology advancement in automated system has brought a crucial tool for discovering the crime activities and also be used for preventing such events beforehand. Most of the automated systems uses artificial intelligence based deep learning methodologies for these types of applications. The Intelligent video analysis applications are used in real time for detecting violence in an early stage and prevent the occurrence of sensitive event during public gathering and in other events.

While designing an automated anomaly detection system, there may be many difficulties to be considered. For example if we are analyzing human behavior, it may change based on the environment and context. The activity will differ when a person is associated in a group and different whenever he is alone. In a group a person with his friends may interact with some gesture or communicate through some actions. But a lone person can be attacked by someone else using the same actions. So there may be a possibility of generating false positives and false negatives. So the implementation part may face many issues while taking into action. The abnormal activity detection can also be implemented by considering the conditions of the foreground, speed of the person, size and texture available on the context. So automated anomaly detections are application specific and they are more specific to the context of an organization.

Anomaly detection systems can be applied in residential areas, private organizations and environments where security is one of the main concerns. They can also be useful for monitoring the patients in a hospital and also be used for elderly monitoring system. This type of system can also be employed in restricted areas for monitoring the abnormal movements from unauthorized personalities. In this paper we are going to discuss about the anomaly detection system that is used for security purpose. This system will be employed inside a campus to monitor the activities of the employees and for detecting any unusual events and protecting the professionals from any violent activities. For this purpose , here we have proposed using three deep learning methodologies which are illustrates in the upcoming chapters.

1.1 Human Behavior Analysis

The framework for analyzing human behavior is depicted in the following diagram Figure 1. The

framework takes input from the video surveillance camera installed in the particular premises. The input video is segmented into several frames and fed into the system for preprocessing. The preprocessing step scans the video frames, analyze the background and illumination conditions of the frame. It will eliminate the background and applies resizing and adjustment of brightness in the frames. The preprocessing phase also removes the unwanted noise from the input video frames.

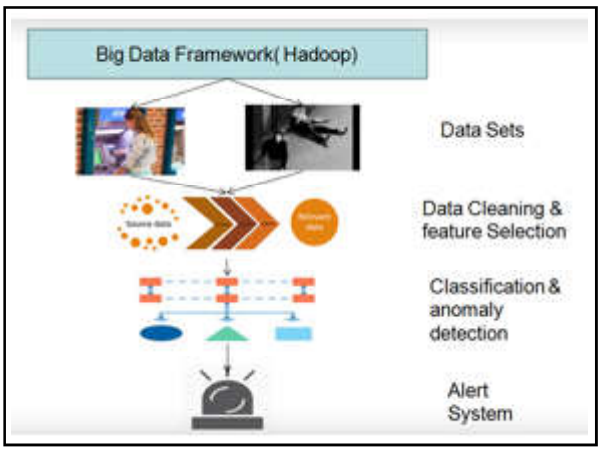

Fig.1 Anomaly Detection system

Once the preprocessing is completed, the data will become error free and noise free. From this data, the features with high impact on the human behavior will be selected for further processing. This process is called as feature selection. The features that will change / determine the activity will be considered for further processing in the upcoming phases. Once the suitable features are selected, deep learning algorithms will be applied on the preprocessed data. Different algorithms can be applied. Based on the algorithm, the behavior will be classified as normal activity and abnormal activity. The normal activities include behaviors like walking, sitting, running, lying and etc.

Fig.2 Normal Human Activities

Some examples of normal human activities are specified in Figure 2.

The abnormal activity may include actions like beating, stabbing, kicking, jumping and fighting. Once the activities are classified, they will be collected into a group and if there are any abnormal events present in the given frame, then the system will send an alert to the concern authority for taking necessary actions. As the video surveillance data is large in volume, they may be stored in Big data framework like Hadoop for easy access and management.

2. DATASET

The dataset used in this paper is Human Activity Recognition Using Smartphone Data Set which is available in the UCI Machine learning Repository. It consists of data being recorded in using Smartphone. The dataset was collected from a group of 30 volunteers in the age ranging from 19 to 48 years. Each person in the group was instructed to perform normal activities like walking, stair climbing, standing, sitting and lying. The movement of the object is recorded in x,y,z axis using the accelerometer. Their activity was recorded and their movements were analyzed based on the sensor data available in the Smartphone such as accelerometer and gyroscope. The dataset contains totally 561 features related to human behavior. They are triaxial acceleration, velocity, the activity label and an identifier that represents the experimenter who acted as a subject in the experiment.

3. ANOMALY DETECTION METHODOLOGIES

3.1 1D Convolutional Neural Networks (CNN)

Convolutional Neural Network is mainly used for image classification and analysis applications. In this paper, the video data is converted into frames which can be considered as image sequences. So convolutional neural network algorithm can be applied for achieving the result. One dimensional convolutional neural network process the data in one direction which means, the kernel of 1-D CNN moves in only one direction. So this technology is mainly used for handling time series data. The following data given in Figure 1 specifies the time series data that is collected from mobile accelerometer for activity classification in the dataset specified in section 2. This data is used for recognizing the normal actions like walking, standing, sitting and jumping. The collected data is specified in two dimensions in which the first dimension denotes the time steps and the second one denotes the values collected through accelerometer.

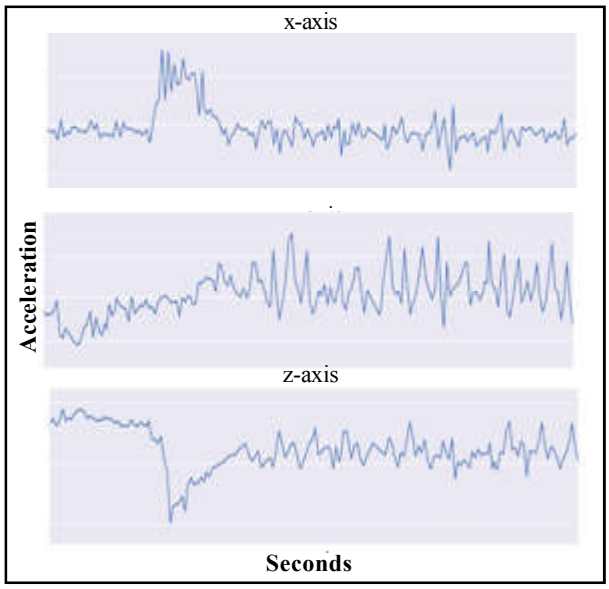

Fig.3 Data from Accelerometer

The sliding movement of the kernel of 1-D CNN is specified in the following diagram Figure 4.

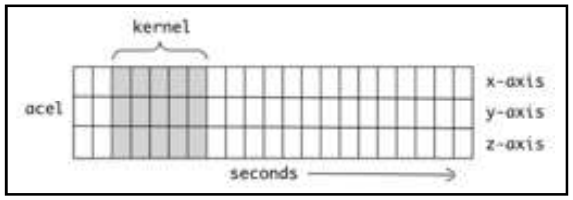

Fig.4 Kernel movement of 1-D CNN

The one dimensional convolutional neural network algorithm is applied on the given data set and used for detecting abnormal events if there is any. The algorithm is implemented in the following procedure:

1. Initialize and import the dataset
2. Model fitting
3. Evaluating the results
4. Alert the authority

In the first step, the dataset will be loaded into the model. Once the data is loaded, it will be preprocessed and necessary features will be selected for implementation. The data will be divided into two parts such training data and test data before deploying the algorithm. The CNN algorithm will be applied on the data which reshaped and to be made that will perfectly fit into the algorithm. The results of the algorithms will be analyzed and summarized. If there is any data present other than the normal events specified in the previous section 2, they will be considered as abnormal events. Once the results are summarized, the occurrence of abnormal events will be notified to the authority for making necessary action through an alert system.

The summarization and accuracy of the classification algorithm 1-D CNN is specified in the following diagram Figure 5.

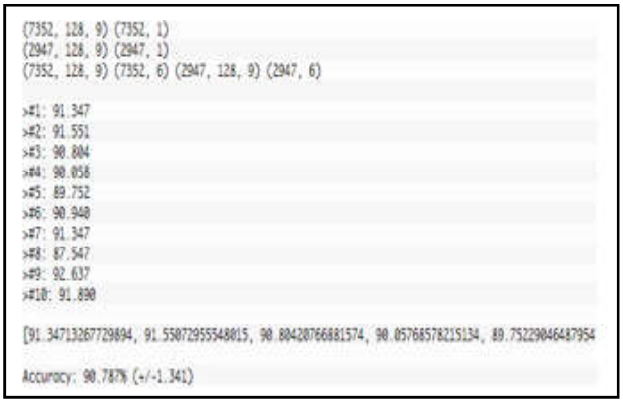

Fig.5 Accuracy for 1-D CNN

The performance of the 1-D convolutional neural network can be improved by applying some tweaking to the hyper parameters used in the model.

3.2 Multi-headed Convolutional Neural Networks

The performance of anomaly detection methodology can be improved by applying variant of the Convolutional Neural Networks. One of the most widely used such variant is multi-headed convolutional neural networks. In this methodology we are going to design a model with multiple heads. This model will be able to capture the input data from the base network and forward the activations to the different heads available in the models. Unlike the single dimensional CNN, the multi-headed CNN reads the input data with different sized kernel using its each head. Suppose we are using a three headed CNN model, the kernel size can be defined as 5, 7 and 11. Each of them may have different kernel size which lets the model to analyze the data with different ruling instead of producing the same result. In this paper we have used the Keras library for implementing the CNN model.

The plotting of multi-headed CNN is specified in Figure 6 where each head is reading the same data but handling the data with different kernel size. Each head in the convolution layer is independent of others. Each branch in the CNN model is defined as an individual head. For deploying a multi-head CNN model, here we have employed multiple single headed CNN that are summarized into single channel. At the end of the algorithm, the collective results from different heads will be summarized and given as a result with classification label whether it is a normal event or abnormal events.

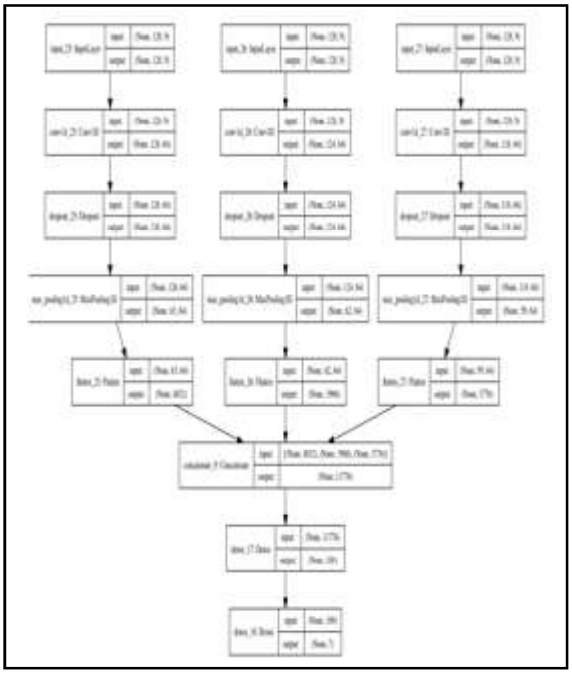

Fig.6 Processing in multi-head CNN

The following diagram Figure 8 specifies the model definition and evaluation of multi-headed CNN model.

Here in this model, three heads have been defined where each of them is a single dimensional CNN model. Each head is defined with a kernel size of (5, 7, 11) respectively. The batch size is defined as 0, 10 and 32.

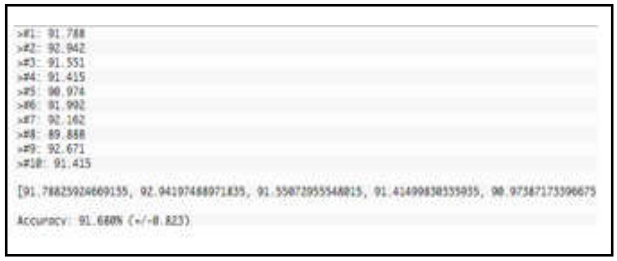

Fig.7 Accuracy of Multi-headed CNN

This model is an improved version of previous model specified in section 3.1 where the same architecture is used but with multiple heads and different kernel size. This model can be enhanced by improving the data preprocessing part and by applying some regularization techniques. Varying the learning rate, batch size and epochs can also be used for getting better results.

3.3 LSTM based Convolutional Neural Network Model

For improving the performance of anomaly detection system, the recurrent neural network models like LSTM can be combined with Convolutional Neural Network model. As most of the recurrent neural networks algorithm lies with a shortfall of short term memory, they tend to suffer from gradient vanishing problem during the back propagation process. Anomaly detection process is used for handling long sequence of video frames, in which past frames will provide some information for understand the present frame. So Recurrent neural networks cannot be able remember the past information. So we are going for an enhanced version of RNN. LSTM is recurrent neural network model which is capable of handling problems with long dependency. For example they are most helpful in handling video analysis applications.

In this paper we are going to use a LSTM based CNN model for detecting the anomalies. This model uses LSTM architecture for handling sequential data like video. In this model, the convolutional neural network model is used for feature identification and feature extraction. The LSTM model is used for classification of human activities into normal and abnormal activities.

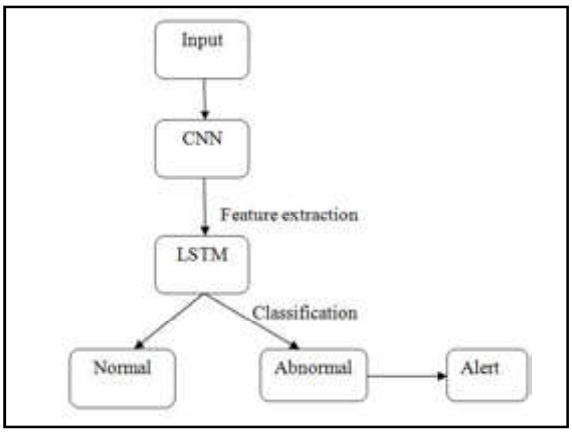

Fig.8 LSTM CNN Architecture

The LSTM based CNN architecture is specified in the Figure 8. The convolutional neural network model in the given architecture divides the video into sequence of frames and handles each frame as an individual image.

The CNN model takes the video frame as input and generates the abstract information from the given image for better feature selection. The CNN model converts each frame in the video sequence into a vector representation for further processing. The features extracted from CNN will be flattened and given as input to the LSTM model. Next the LSTM model take the data and apply the mechanism for classifying the activities of human present in the video sequence. The activities can be classified into normal or abnormal events. As

specified in the data set, the video sequence will be assigned with labels for each and every activity. The presence of abnormal activities will be notified to the concern authority for taking actions.

The LSTM model takes the features and reshapes them into desired time steps for each subsequence. Initially the time steps have been fixed as 128. LSTM model divides the data into four subsequences with time steps of 32 for each sequence. The accuracy of the given model is specified in Figure 9.

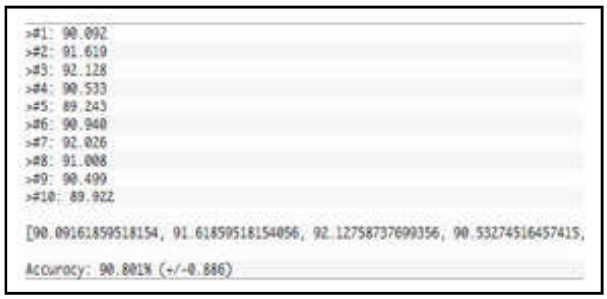

Fig.9 Accuracy of LSTM based CNN model

The accuracy of the model can be improved by using variants of LSTM like stacked LSTM and bidirectional LSTM. We can also tune the hyper parameters in the given dataset for achieving more sophisticated result.

4. COMPARISON OF RESULTS

In this paper we have focused on three algorithms that are used for anomaly detection in human behavior analysis. Each algorithm will have their advantages and limitation. For this comparison we have used the same dataset

Human Activity Recognition Using Smartphone Data Set from the UCI repository. The number of samples in the given dataset considered for processing is 10299 which contain 561 features. The prediction results of each algorithm are specified in the previous sections. The comparison of the results is given below in diagram Figure 10.

From the above given chart we can conclude that multi-headed CNN provides better performance than other two algorithms. This work can be extended and improved by tuning the hyper-parameters and also by applying variants of these algorithms.

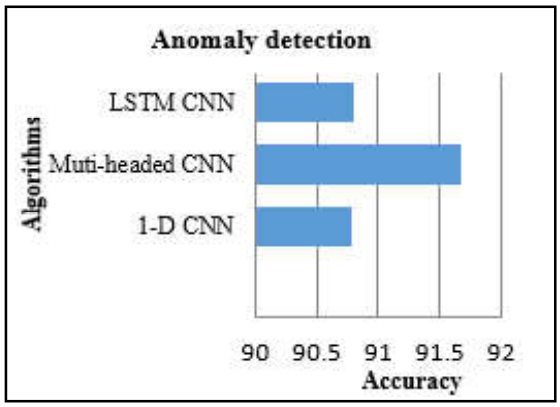

Fig.10 Comparison of Results – CNN, Mutiheaded CNN, LSTM-CNN

5. CONCLUSION

Anomaly detection system is mainly used as a surveillance mechanism for ensuring the privacy and security of public areas, large gatherings and private organizations. In this paper, we have discussed about three deep learning methodologies used for detecting the abnormal events and also for analyzing the human behavior. Each algorithm is employed on the dataset and achieved the given accuracy. Based on the comparison of results, multi-headed convolutional neural network model achieve higher accuracy than the other two algorithms. As the video sequence is processed in terms of frames, convolutional neural network models will perform very well and their performance can also be improved by tuning the hyper parameters. This work can also be extended by using other frameworks like Yolo and other variants of CNN.

REFERENCES

[1] F.Luque Sanchez, I.Hupont, S.Tabik and F.Herrera, "Revisiting Crowd Behaviour Analysis through Deep Learning: Taxonomy, Anomaly Detection, Crowd Emotions, Datasets, Opportunities and Prospects, Inf Fusion.doi: 10.1016/j.inffus.2020.07.008. Epub 2020 Jul 29. PMID: 32834797; PMCID: PMC7387290, Dec.2020, Vol.64, pp.318-335.

[2] G.Sreenu and M.S.Durai, "Intelligent Video Surveillance: A Review through Deep Learning Techniques for Crowd Analysis", J. Big Data, Vol.6, No.1, 2019, pp.48.

[3] Davide Anguita, Alessandro Ghio, Luca Oneto, Xavier Parra and Jorge L. Reyes-Ortiz, "A Public Domain Dataset for Human Activity Recognition

Using Smartphones", 21th European Symposium on Artificial Neural Networks, Computational Intelligence and Machine Learning, ESANN 2013. Bruges, Belgium 24-26 April 2013.

[4] R.Olmos, S.Tabik, F. Herrera, "Automatic Handgun Detection Alarm In Videos Using Deep Learning", Neurocomputing, Vol. 275, 2018, pp.66-72.

[5] S. Bashbaghi, E.Granger, R.Sabourin and M. Parchami, "Deep Learning Architectures for Face Recognition in Video Surveillance", in Deep Learning in Object Detection and Recognition, Springer, 2019, pp.133-154.

[6] H.Swathi, G.Shivakumar and H.Mohana, "Crowd Behavior Analysis: A Survey", in International Conference on Recent Advances in Electronics and Communication Technology (ICRAECT), 2017, pp.169-178.

[7] M. Sabokrou, M. Fathy, M. Hoseini and R. Klette, "Real-time Anomaly Detection and Localization in Crowded Scenes", in IEEE conference on Computer Vision and Pattern Recognition Workshops, 2015, pp. 56-62.

[8] G.Ciaparrone, F.L.Sanchez, S.Tabik, L.Troiano, R.Tagliaferri and F.Herrera, "Deep Learning in Video Multi-Object Tracking: A Survey", Neurocomputing, Vol.381, 2020, pp.61-88.

[9] X. Zhang, Q.Zhang, S.Hu, C.Guo and H.Yu, "Energy Level-Based Abnormal Crowd Behavior Detection", Sensors, Vol.18 , No.2, 2018, pp.423.

[10] R.Hinami, T.Mei and S.Satoh, "Joint Detection and Recounting Of Abnormal Events by Learning Deep Generic Knowledge", in Proceedings of the IEEE International Conference on Computer Vision, 2017, pp. 3619-3627.

[11] K.Singh, S.Rajora, D.K.Vishwakarma, G.Tripathi, S. Kumar and G.S. Walia, "Crowd Anomaly Detection Using Aggregation of Ensembles of Fine-Tuned Convnets", Neurocomputing, Vol.371, 2020, pp.188-198.

[12] M. Yang, S.Rajasegarar, S.Erfani and C.Leckie, "Deep Learning and One-class SVM based Anomalous Crowd Detection", in 2019 International Joint Conference on Neural Networks (IJCNN), 2019, pp.1-8.

[13] Y. Feng, Y. Yuan and X. Lu, "Learning Deep Event Models for Crowd Anomaly Detection", Neurocomputing, Vol.219, 2017, pp.548-556.

[14] C. Viroli and G.J. McLachlan, "Deep Gaussian Mixture Models", Stat. Comput., Vol.29, No.1, 2019, pp.43-51.

[15] A. Ramchandran and A.K. Sangaiah, "Unsupervised Deep Learning System for Local Anomaly Event Detection in Crowded Scenes", Multimedia Tools Appl., 2019, pp.1-21.

[16] M.Ravanbakhsh, M.Nabi, H.Mousavi, E. Sangineto and N.Sebe, "Plug-and-play CNN for Crowd Motion Analysis: An Application in Abnormal Event Detection", in 2018 IEEE Winter Conference on Applications of Computer Vision (WACV), 2018, pp.1689-1698.

[17] Wang, Jun & Xia and Limin, "Abnormal Behavior Detection in Videos using Deep Learning", Cluster Computing. 22. 10.1007/s10586-018-2114-2, 2019.

[18] R. Jayaswal and M. Dixit, "A Framework for Anomaly Classification Using Deep Transfer Learning Approach", Revue d'Intelligence Artificielle, https://doi.org/10.18280/ria.350309, 2021, Vol. 35, No. 3, pp. 255-263.

[19] A.J. Suresh and J.Visumathi, "Inception ResNet Deep Transfer Learning Model for Human Action Recognition Using LSTM", Materials Today: Proceedings. https://doi.org/10.1016/j.matpr.2020.09.609, 2020.

[20] R. Nayak, U.C. Pati and S.K.Das, "A Comprehensive Review on Deep Learning-Based Methods for Video Anomaly Detection", Image and Vision Computing, 106: 104078. https://doi.org/10.1016/j.imavis.2020.104078, 2020.

[21] I.P.Febin, K.Jayasree and P.T. Joy, "Violence Detection in Videos for an Intelligent Surveillance System Using
MoBSIFT and Movement Filtering Algorithm", https://doi.org/10.1007/s10044-019-00821-3, Pattern Analysis and Applications, 2020, Vol.23, No.2, pp.611-623.

[22] M.Ramzan, A.Abid, H.U. Khan, S.M.Awan, A.Ismail, M. Ahmed and A.Mahmood, "A Review On State-Of-The-Art Violence Detection Techniques", https://doi.org/10.1109/ACCESS.2019.2932114, IEEE Access, Vol.7, 2019, pp.107560-107575.

[23] F.U.M.Ullah, A.Ullah, K.Muhammad, I.U. Haq and S.W. Baik, "Violence Detection Using Spatiotemporal Features with 3d Convolutional Neural Network", https://doi.org/10.3390/s19112472, Sensors, Vol.19, No.11, 2019, pp.2472.

[24] V.Dandage, H.Gautam, A.Ghavale, R.Mahore, P.A.Sonewar, "Review of Violence Detection System Using Deep Learning", International Research Journal of Engineering and Technlogy (IRJET), Vol.6, No.12, 2019, pp.1899-1902.

[25] A. Khaleghi, M.S.Moin, "Improved Anomaly Detection in Surveillance Videos Based On A Deep Learning Method", In 2018 8th Conference of AI & Robotics and 10th RoboCup Iranopen International Symposium (IRANOPEN), https://doi.org/10.1109/RIOS.2018.8406634, 2018, pp.73-81.

[26] P. Zhou, Q. Ding, H. Luo and X.Hou, "Violent Interaction Detection in Video Based On Deep Learning", Journal of Physics: Conference Series, Vol.844, No.1, 2017, pp.012044.

[27] P. Bilinski and F.Bremond, "Human Violence Recognition and Detection in Surveillance Videos", In 2016 13th IEEE International Conference on Advanced Video and Signal Based Surveillance (AVSS), https://doi.org/10.1109/AVSS.2016.7738019, 2016, pp.30-36.

[28] I. Serrano Gracia, O. Deniz Suarez, G.Bueno Garcia and T.K.Kim, "Fast Fight Detection", PloS One, e0120448. https://doi.org/10.1371/journal.pone.0120448, Vol.10, No.4, 2015.

[29] S.K.Venu, "An Ensemble-Based Approach by Fine-Tuning the Deep Transfer Learning Models to Classify Pneumonia from Chest X-ray Images", arXiv preprint arXiv:2011.05543, 2020.

[30] Z. Li and J.Ye, "Abnormal Behavior Recognition Based On Transfer Learning", In Journal of Physics: Conference Series, : https://doi.org/10.1088/1742-6596/1213/2/022007, Vol.1213, No.2, 2019, pp.022007.

[31] D. Arifoglu and A.Bouchachia, "Activity Recognition and Abnormal Behaviour Detection with Recurrent Neural Networks", Procedia Computer Science, https://doi.org/10.1016/j.procs.2017.06.121,Vol.110, 2017, pp.86-93.

[32] J. Ruchi and D. Manish, "Human Behavior Dataset (HBD21). Mendeley Data, 1. https://doi.org/10.17632/xh9pgb3w8c.1, 2021.

[33] R.K.Tripathi, A.S.Jalal and S.C.Agrawal, "Suspicious Human Activity Recognition: A Review", Artificial Intelligence Review, https://doi.org/10.1007/s10462-017-9545-7, 2018, Vol.50, No.2, pp.283-339.

[34] R. Jayaswal and J.Jha, "A Hybrid Approach for Image Retrieval Using Visual Descriptors", https://doi.org/10.1109/CCAA.2017.8229, In 2017 International Conference on Computing, Communication and Automation (ICCCA), 2017, pp. 1125-1130.

DRIVER DROWSINESS DETECTION USING DEEP LEARNING TECHNIQUES

Philo Sumi and G. Kishor
Department of Computer Science and Engineering,
Bannari Amman Institute of Technology, Sathyamangalam - 638 401, Erode District, Tamil Nadu
E-mail: philosumi@bitsathy.ac.in

Abstract

Driver drowsiness detection is a critical issue in ensuring road safety. Road accidents are significantly impacted by driver weariness, which is thought to be a factor in 20% of collisions. These mishaps can have devastating effects, including fatalities, physical harm, and monetary losses. Therefore, detecting driver drowsiness in real- time is crucial in preventing accidents and saving lives. The present study involves positioning a camera in a direct manner towards the driver's face and recording real- time video has been created as a way for detecting tiredness in drivers. Once the video has been recorded, keep an eye on the subject's eyes and face to look for signs of fatigue. The technology employed in this study has the capacity to track eye location and determine whether or not they are open. The device alerts the driver with a warning signal if it detects drowsiness. The length of eye closure can also be determined by looking at the proportion of time the eyes are closed over the course of a given interval. The technology determines that the motorist is falling asleep, if their eyes are closed cumulatively more often than a standard value.

Keywords: *Driver Drowsiness, Detection, Deep Learning, RetinaFace Pytorch, Mediapipe*

1. INTRODUCTION

One out of every four automobile accidents is caused by drowsy driving. This practice poses a significant risk, particularly when combined with the effects of fatigue. What's particularly concerning about drowsy driving is that it doesn't necessarily involve a driver completely nodding off at the wheel; it can simply manifest as a moment of brief sleepiness when the driver is not fully focused on the road. Given the gravity of this issue, we believe it's imperative to create a drowsiness detection system, particularly during the early stages, to help prevent accidents. Our proposed solution involves developing a detection system that can identify key signs of drowsiness and provide an alert before it's too late.

Drowsiness Detection has two main stages such as Face Detection and Drowsiness Detection. RetinaFace Pytorch is the model used for face detection and Mediapipe is used for iris tracking and detection in real-time video streams. The project's goal is to detect driver drowsiness and alert them when necessary so accidents can be avoided. Based on whether a person's eyes are open or closed, the project uses a deep learning model to assess their level of drowsiness. The concept directly impacts the automotive industry, improving driving safety and reducing the number of fatalities in crashes brought on by drowsy driving.

2. RELATED WORKS

H. Guan *et al.* (2018) [1] proposed a real-time driver drowsiness detection system that employs a convolutional neural network (CNN) framework to analyze facial images and determine if the driver is drowsy. The system comprises three primary components: face detection, feature extraction, and drowsiness classification. On the other hand, M. Zabihi *et al.* (2020) [2] introduced a driver drowsiness detection system that uses physiological signals, including electroencephalogram (EEG), electrocardiogram (ECG), and photoplethysmogram (PPG), in conjunction with a well-designed CNN architecture. The aim of this system is to detect drowsiness based on the physiological signals of the driver.

S. Zhang *et al.* (2019) [3] present a real-time driver drowsiness detection system that employs a convolutional neural network (CNN) architecture and electroencephalogram (EEG) signals. The system's objective is to identify drowsiness in real-time by analyzing EEG signals obtained through sensors attached to the driver's scalp.

H. Kim *et al.* (2018) [4] introduce a driver assistance system that employs deep learning techniques

to detect drowsiness. The system comprises three main steps: data acquisition, feature extraction, and drowsiness classification. In the data acquisition step, a camera captures facial images of the driver. The images are then preprocessed and relevant features are extracted using a deep neural network in the feature extraction step. Finally, the extracted features are classified as either drowsy or non-drowsy by a fully connected layer in the drowsiness classification step.

A. Nour *et al.* (2018) [5] propose a driver drowsiness detection system that uses electroencephalogram (EEG) signals and a convolutional neural network (CNN) architecture. The system aims to detect drowsiness by analyzing the brainwave activity of the driver, which is obtained from EEG sensors placed on the driver's scalp.

"Real-time driver drowsiness detection using facial landmarks and convolutional neural networks" by J. Li *et al.* (2017) [6] proposes a driver drowsiness detection system based on facial landmarks and a convolutional neural network (CNN) architecture. The system aims to detect drowsiness based on the driver's facial expressions, which are acquired from a camera placed on the dashboard.

"Driver drowsiness detection using hybrid deep neural network" by Y. Liu et al. (2018) [7] proposes a driver drowsiness detection system based on a hybrid deep neural network (DNN) architecture. The system aims to detect drowsiness based on a combination of features from facial images and electroencephalogram (EEG) signals. "Driver drowsiness detection using heart rate variability and convolutional neural networks" by S. Kim et al. (2018) [8] proposes a driver drowsiness detection system based on heart rate variability (HRV) signals and a convolutional neural network (CNN) architecture. The system aims to detect drowsiness based on the driver's HRV, which is acquired from a wearable device.

"Driver drowsiness detection using a hybrid approach of feature extraction and deep learning" by S. Wu et al. (2021) [9] proposes a driver drowsiness detection system based on a hybrid approach of feature extraction and deep learning techniques. The system aims to detect drowsiness based on facial images and electroencephalogram (EEG) signals. "Driver drowsiness detection using multi-level feature fusion and deep learning" by J. Li et al. (2021) [10] proposes a novel method for detecting driver drowsiness using multi-level feature fusion and deep learning techniques. The proposed method consists of three main steps: data acquisition, feature extraction, and drowsiness classification. "Real-time driver drowsiness detection using physiological signals and deep learning" by W. Chen et al. (2019) [11] presents a method for detecting driver drowsiness in real-time using physiological signals and deep learning techniques. The proposed method uses two physiological signals, electroencephalography (EEG) and photoplethysmography (PPG), to detect driver drowsiness. EEG measures the electrical activity of the brain and PPG measures the blood volume changes in the fingertip. These signals are acquired from the driver using wearable sensors and processed to extract relevant features, such as power spectral density and pulse rate variability. After the relevant features are extracted, they are fed into a deep neural network for drowsiness classification. In this study, the authors employ a long short-term memory (LSTM) network, which is a recurrent neural network that is capable of capturing the temporal dependencies of the physiological signals.

A novel approach for driver drowsiness detection using wavelet transform and deep learning" by H. Mirzaei et al. (2019) [12] proposes a new method for driver drowsiness detection that combines wavelet transform and deep learning techniques. The proposed method uses electroencephalogram (EEG) signals to detect driver drowsiness. The EEG signals are first preprocessed using wavelet transform to extract the frequency and time- domain features. The authors then use a convolutional neural network (CNN) to classify the extracted features and detect driver drowsiness.

S. Lee *et al.* (2020) [13] present a method for detecting driver drowsiness in real-time using a combination of facial landmarks and a convolutional neural network (CNN). The proposed method involves detecting facial landmarks from video frames using a pre- trained model and feeding these landmarks into a CNN for feature extraction and drowsiness classification in real-time.

Y. Cai *et al.* (2020) [14] propose a driver drowsiness detection method that utilizes multiple physiological signals and deep learning. This method integrates various physiological signals including electroencephalogram (EEG), electrooculogram (EOG), electromyogram (EMG), and heart rate (HR) signals to detect driver drowsiness. The signals undergo feature extraction through signal processing techniques and are

subsequently inputted into a deep learning model for classification.

The article "Driver drowsiness detection based on physiological signals and deep learning" authored by M. Jiang et al. (2021) [15] presents an innovative strategy for detecting driver drowsiness using deep learning and physiological signals. This approach utilizes a range of physiological signals, including EEG, EOG, and EMG, to monitor the driver's drowsiness. To achieve this, the signals undergo signal processing techniques to extract relevant features that are then fed into a deep learning model to classify the level of drowsiness.

3. PROPOSED WORK

This section discusses the proposed framework for the model. The workflow of this work is as follows. The first and foremost step is to design a GUI using Tkinter Framework that gives a good-looking user experience etc.

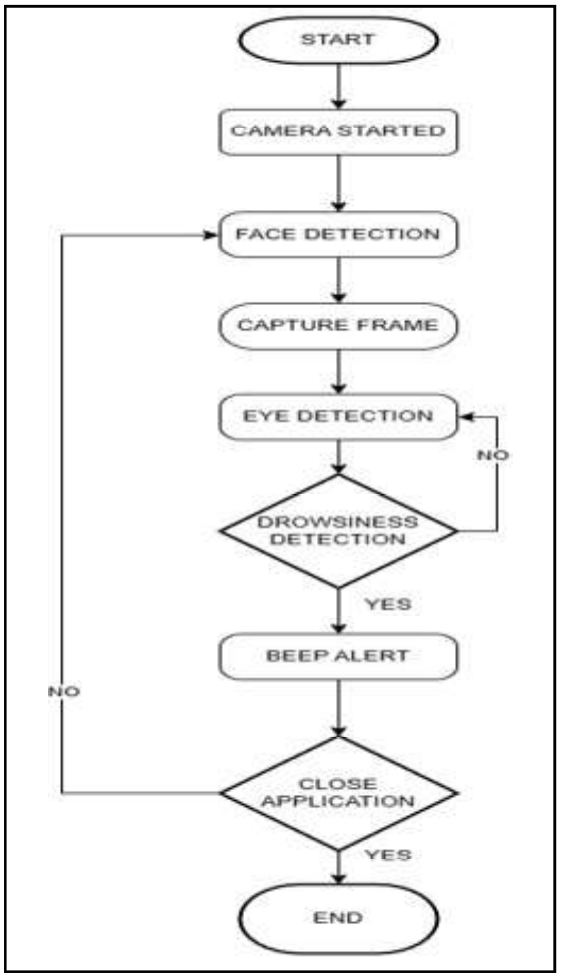

Fig.1 Workflow of proposed framework

Then placing the camera in the right position to collect the stream was one of the changing tasks. The actual challenge comes here which is to choose the right face detection and key point generation Algorithms. There are lots of face detection and key point generation algorithms are there in the Market yet picking the right algorithm is something fundamental. Coding the face detection algorithm and key point generation algorithm was the next step. And connecting these two algorithms was one of the hardest parts of this project. The next step is to create an end-to-end training and testing pipeline. The last but not the least step is to connect the testing pipeline with the GUI.

3.1Face Detection

The face detection part is doing with RetinaFace Pytorch. To carry out pixel-wise face localization, Retinaface implements three subtasks in a single shot. The tasks are Face Detection, 2D Face Alignment, and 3D Face Reconstruction utilizing a mesh decoder. Previous techniques, such as Mask and MTCNN, give a revolutionary cascaded structure for determining facial landmarks. For more accurate face localization, Rcnn used a technology called 3D mask reconstruction. These concepts were integrated by Retinaface to create a reliable model that surpasses the SOTA. The method incorporates three main concepts: Context modelling, Single Stage Method, and Feature Pyramid. Understanding these ideas and their importance is vital before we get into the model architecture since they underpin the model's success. The feature pyramid is a feature extractor that produces feature maps at several scales from a single image. Contrary to two stage methods (such as Faster R-CNN), single stage methods just need one iteration over the whole network to provide the bounding boxes of the object to be detected. To help with the localization process using DCN, the goal is to learn contextual information from the photos. With the exception of not having a rigid kernel grid, deformable convolutional networks (DCN) function very similarly to CNN's convolutional blocks. Instead, a parameter that controls the grid points enables it to be more adaptable to the object's various feature scales. We chose this model by comparing other 5 models with the face detection in worlds largest selfie. And we got the conclusion like in the table 1.

Table 1

MODEL	NUMBER OF FACES DETETED
RatinaFACE	99
MTCNN	107
DSFDDetector	210
RetinaNetResNet50	179
RetinaNetMobileNetV1	136
RatinaFace_Pytorch	367

Fig. 2 Comparison of 6 face detection algorithm with world's largest selfie

3.2 Key Point Generation

The process of mechanically identifying and localising the important landmarks on the human eye, such as the pupil, iris, corners, and eyelids, is known as eye keypoint generation. Computer vision techniques and deep learning models are typically used for this activity because they can examine photos or video frames captured by the human eye and precisely pinpoint the locations of these crucial areas. Pre-built Iris landmark identification solution from Mediapipe enables precise iris tracking and detection in real-time video streams. The Mediapipe Python API gives easy access to the Iris landmark detection module, making it simple to include the module into Python-based computer vision or machine learning applications

The iris is recognized and tracked by the Iris landmark identification module using a deep neural network. To identify the essential iris patterns and properties, a huge collection of iris photos is used to train the network. In order to extract characteristics and carry out additional analysis, the module returns a set of iris landmark points that correspond to the iris's boundary.

The Eye Aspect Ratio (EAR) calculation can be used to determine whether or not the eyes are closed:

$$\mathbf{EAR} = \frac{\|P_2 - P_6\| + \|P_3 - P_5\|}{2\|P_1 - P_4\|}$$

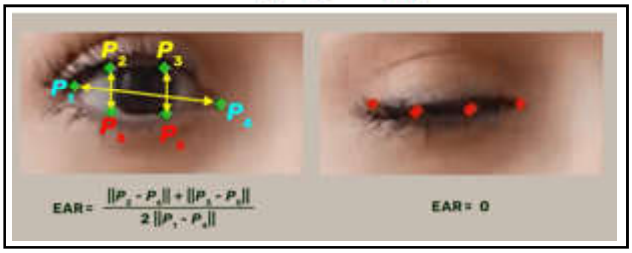

Fig.3 EAR Calculation for open and close eyes

A deep neural network that has been trained on a sizable dataset of iris images forms the foundation of the Mediapipe Iris landmark identification module architecture. The neural network is made up of a number of convolutional, pooling, and fully connected layers that have been trained to identify the essential iris patterns and features. A set of 68 landmark points that represent the borders of the iris, eyelids, and eyelashes are the neural network's output. The size, location, and orientation of the iris in the input image can be determined using the landmark points' representation as a set of (x, y) coordinates. To increase the precision and robustness of the landmark recognition method, the Mediapipe Iris landmark detection module also incorporates extra processing steps, such as iris detection and tracking. The module recognizes and tracks the iris in real-time video streams using a variety of approaches, including image filtering, segmentation, and optical flow. As a result, the module may continue to preserve precise landmark point placements even when the eye moves or the lighting changes.

Steps for Inference in Mediapipe:

- Install Mediapipe: The Mediapipe library needs to be installed on your computer first. Run the command below in your terminal to install the library using pip: pip set up mediapipe
- Import the module: Once Mediapipe has been installed, use the following command to import the Iris landmark detection module into your Python script: mp import from mediapipe
- Initialize the module: You must create an instance of the mp.solutions to initialise the Iris landmark detection module.
- Read the input image: Using your favourite computer vision library or function, read the input image or video frame that you wish to analyse.

- Process the input image: The Iris landmark detection module's iris.process() method can be used to process the input image. This method returns a Landmark object that has the iris landmark points and accepts an input image as input.
- Extract the iris landmarks: By using the landmark attribute on the Landmark object, you may extract the iris landmark points. 68 (x,y) coordinate pairs that represent the iris boundary, eyelids, and eyelashes are listed in this feature.
- See the landmarks: Using your choice visualisation library or function, you may see the iris landmarks on the input picture or video frame.

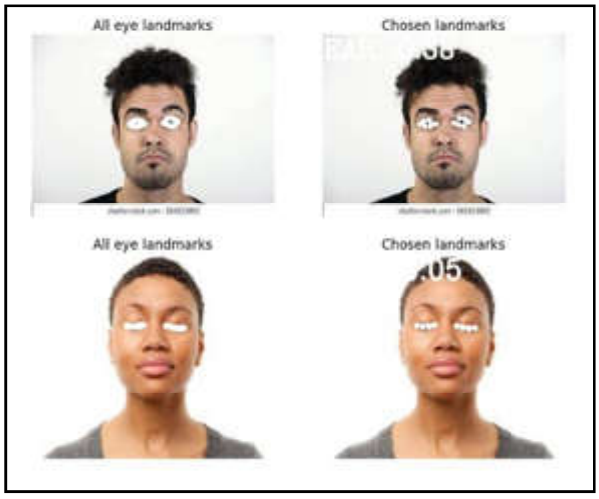

Fig. 4. Eye landmarks detected for Open and Close Eye

3.3 Alert The Driver

To identify changes in the driver's eye shape, measure the ratio of the distance between some important eye sites, such as the distance between the upper and lower eyelids. For instance, if the driver's eyes begin to close, the ratio will alter as the space between their upper and lower eyelids narrows. Then one alert will pass to the driver.

3.4 Tkinter (GUI)

Python offers several options for GUI creation (Graphical User Interface). The most popular GUI method is Tkinter, compared to all the others. Tkinter, which is part of all common Python distributions, is the de facto method for creating Graphical User Interfaces (GUIs) in Python. In our project we are using latest version of tkinter (0.16.0).

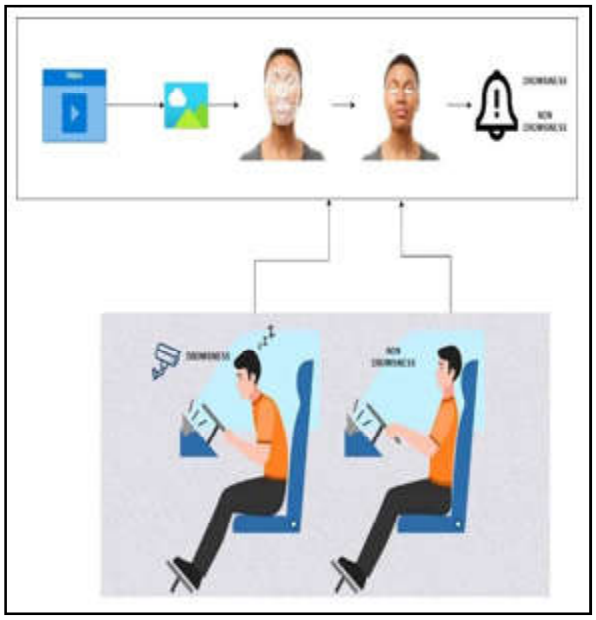

Fig.5 Model Architecture

Table 2

Test Condition	System Behavior	Expected Result
Straight face, Eyes Open, good light without Glasses	Non-Drowsy	Non-Drowsy
Tilted face, good light, Eyes closed, No Glasses	Drowsy	Drowsy
Tilted face, Eyes closed, good light, with glasses	Drowsy	Drowsy

Fig.6 Testcase Results

4. RESULTS AND DISCUSSION

The system is intended to find the drowsiness of the person during driving. Face of a person is getting detected using Retina Face pytorch. And checking his

eyes with mediapipe to check whether he is active or not. If the driver is not active for a threshold time that is set before will consider as inactive. Here checking some scenarios for the system (Table II). Here the 3 test conditions and the model's response are marked. The real result from the model also included for the testcases considered.

5. CONCLUSION

A vital use of computer vision and machine learning is the identification of driver drowsiness, which can help avoid accidents and save lives. In this project, we've shown how to create a real-time driver drowsiness detection system that can identify and warn drivers when they start to get sleepy or distracted using the Mediapipe framework. To follow the driver's head and eye movements in real-time video feeds, our technology combines face and eye landmark detection. After that, we examine the eye and head movement patterns to look for indicators of distraction or tiredness. The technology warns the driver through visual and audio alarms if it notices that they are starting to get sleepy or distracted. Our technology has been tested in a number of real-world situations and has proven to be very accurate and resilient in spotting distraction and sleepiness. The system is simple to integrate into current driver assistance systems or to utilise in cars on its own. Overall, by assisting in the reduction of accidents brought on by sleepy or distracted drivers, our driver drowsiness detection technology has the potential to dramatically increase road safety.

REFERENCES

[1] H. Guan *et al.,* "Real-time Driver Drowsiness Detection Using a Convolutional Neural Network-Based Framework", 2018.

[2] M. Zabihi *et al.,* "Driver Drowsiness Detection Based On Physiological Signals Using a Convolutional Neural Network", 2020.

[3] S. Zhang *et al.,* "Real-time driver drowsiness detection using EEG Signals and a Convolutional Neural Network", 2019.

[4] H. Kim *et al.,* "Deep Learning-Based Drowsiness Detection for a Driver Assistance System", 2018.

[5] A. Nour *et al.,* "Driver drowsiness detection using EEG and convolutional neural networks", 2018.

[6] J. Li, *et al.*, "Real-time Driver Drowsiness Detection Using Facial Landmarks and Convolutional Neural Networks", 2017.

[7] Y. Liu *et al.*, "Driver Drowsiness Detection Using Hybrid Deep Neural Network", 2018.

[8] S. Kim et al., "Driver Drowsiness Detection Using Heart Rate Variability and Convolutional Neural Networks", 2018.

[9] S. Wu *et al.,* "Driver Drowsiness Detection Using a Hybrid Approach Of Feature Extraction and Deep Learning", 2021.

[10] J. Li *et al.* "Driver Drowsiness Detection Using Multi-Level Feature Fusion and Deep Learning", 2021,

[11] W. Chen *et al.* "Real-time Driver Drowsiness Detection Using Physiological Signals and Deep Learning", 2019.

[12] H. Mirzaei *et al.* "A Novel Approach for Driver Drowsiness Detection Using Wavelet Transform and Deep Learning", 2019.

[13] S. Lee *et al.* "Real-time Driver Drowsiness Detection Using a Convolutional Neural Network and Facial Landmarks", 2020.

[14] Y. Cai *et al.* "Driver Drowsiness Detection Using Multiple Physiological Signals and Deep Learning", 2020.

[15] M. Jiang *et al.* "Driver drowsiness detection based on physiological signals and deep learning", 2021.

COMPUTATIONAL STUDY ON FLOW CHARACTERISTICS OF A TAPERED WING WITH MODIFIED RAKED WINGTIP FOR REGIONAL AIRCRAFT

M.S. Prasath, G.Sivaraj, D. Lakshmanan and P. Vadivelu
Department of Aeronautical Engineering,
Bannari Amman Institute of Technology, Sathyamangalam - 638401, Erode District, Tamil Nadu
E-mail: prasathms@bitsathy.ac.in, sivarajg@bitsathy.ac.in

Abstract

A wingtip is an essential part of an aircrafts located the tip of the wing of an aircraft. It helps to reduce the vortices created at the tip of the wings. Thereby reducing the drag produces and increases the fuel efficiency of the particular aircraft. This paper compares a conventional wing with a raked wingtip and highlights the advantages of having a raked wingtip over a conventional wing in reducing the coefficient of drag (C_D). The reduced C_D eventually helps increasing the fuel efficiency of the aircraft. The percentage of induced drag reduction is carried out in conceptual approach. This comparison was conducted numerically by using simulation model of turbulence k-e realizable. The model was designed using CATIA software and the CFD simulations were carried out for different velocities with respect different angle of attack varying from 0^o to 18^o. Apart from the C_D, other parameters like Coefficient of Lift (C_L), and C_L/C_D of conventional wing and wing with raked wingtips were found and compared. The raked wingtip can be also be retrofitted after the delivery of the aircraft to its operator as it is not a complex in structure and design.

Keywords: Computational fluid dynamics, Induced drag, Raked wingtip, Regional aircraft

1. INTRODUCTION

The current scenario of airlines, the passenger aircrafts face on several challenges and problems. Such as, the fuel efficiency, maintenance costs, noise reduction, aging fleet, etc. In response to these challenges, the aerospace industry is developing new materials and technologies for the next generation of passenger aircraft wings. These include lighter and stronger materials, such as composites and advanced alloys, as well as more efficient aerodynamics and propulsion systems. These advances will help airlines in their environmental performance, and provide passengers with a more comfortable and convenient flying experience. Among them the fuel consumption plays a major role. Due to rising fuel prices and increasing environmental concerns, the airlines focus on reducing their fuel consumption and emissions.

Drag increases the fuel consumption of an aircraft, as the engines have to work harder to overcome the resistance caused by the drag. This increases the cost of fuel and reduces the range of the aircraft, making it less economically viable for airlines to operate. Increased drag can also increase the wear and tear on the engines, airframe, and other components, leading to higher maintenance costs. Higher fuel consumption and maintenance costs directly increase the operating costs of an aircraft, which can make it more difficult for airlines to operate profitably. Increased drag reduces the range of an aircraft, which can limit its operational capabilities and make it less economically feasible for airlines to operate long-haul routes. Drag can also affect the comfort of passengers, as increased turbulence and noise can make for a rougher, less comfortable flight.

By reducing drag, airlines can increase the fuel efficiency, reduce their maintenance and operating costs, increase their range, and provide passengers more comfortable and efficient flying experience. This makes drag reduction as a major part in the economics of aircraft operations and one that airlines must carefully consider when designing and operating their aircraft. There are several ways to reduce drag in aircraft wings, including, streamlining, winglets, laminar flow, vortex generators, leading edge devices: installing leading edge devices, such as slats or flaps, can increase lift and reduce drag by altering the shape of the wing and encouraging more efficient air flow, engine placement and materials used. These methods can be used individually or in combination to reduce drag and improve the efficiency of aircraft wings.

The Induced drag is produced by the passage of an air through the airfoil. Air flowing over the top of a wing tends to flow inwards because the decreased pressure over the top surface is less than the pressure outside the wing tip. Induced drag is the increase in the drag component which depends on the angle of attack and is caused by the airflow around the wing tips caused by the pressure difference between the lower and upper surfaces of the wing at the tips [1]. Drag is the aerodynamic force that opposes an aircraft's motion through the air. It is generated by every part of the airplane with respect to the difference in velocity between the solid object and the fluid. This drag can be reduced by various methods and it depends on the type of drag acting on the aircraft. [2].

The induced drag is caused by uneven pressure on certain wing tip between the top (pressure side) and lower surface (suction side). However, near the wing tip, the high pressure air from the lower surface moves to the top which causes the stream curved like figure 1 below [3].

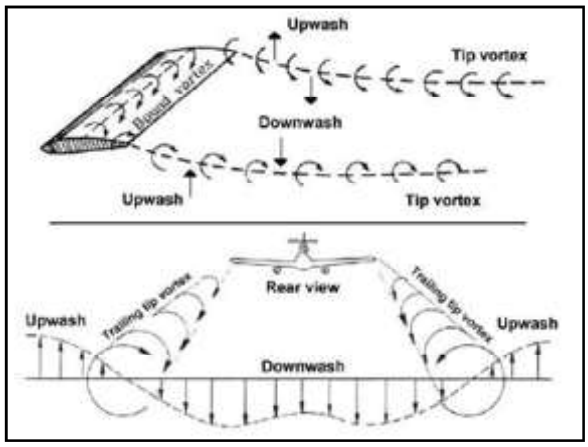

Fig.1 Wingtip vortices cause downwash which reduces the effective angle of attack [3]

Winglets are small vertical fins that are attached to the tips of the wings of an aircraft. They are used in passenger aircraft to improve aerodynamics and reduce fuel consumption. Winglets work by redirecting the air flow to the tips of the wings, creating a vortex that decreases drag and increases lift. Winglets help to reduce drag by redirecting the air flow that would otherwise escape from the tips of the wings, creating a vortex that decreases drag and increases lift. This means that the engines don't have to work as hard to overcome the resistance caused by the drag, reducing fuel consumption. Winglets can also improve the lift-to-drag ratio of an aircraft, making it more aerodynamically efficient. This means that the aircraft can fly further using the same amount of fuel, reducing fuel consumption and operating costs. By reducing drag and improving the lift-to-drag ratio, winglets can increase the range of an aircraft, allowing it to fly further without refuelling. This can make it more economically feasible for airlines to operate long-haul routes, reducing their operating costs. By reducing fuel consumption, winglets can also reduce the carbon emissions produced by an aircraft, making it more environmentally friendly [3]. There are many kinds of wing tip devices which are operated in different manners; the major role of wingtip devices is to reduce an aircraft's drag. In addition to that, the application of winglets decreases the drag and increases the fuel efficiency of commercial passenger aircrafts [4]. Raked wing tip is a wing tip which has a sweep angle higher than the rest of the wing; this feature is implemented in some boing commercial planes to increase fuel efficiency, take-off and climb performance [5]. This raked wing tip increases the wing aspect ratio and decrease the lift-induced drag. This raked wingtip was inspired from the birds in nature as they have wing and tail portions with curved profile makes them to fly efficiently [6]. In conclusion, winglets help to reduce fuel consumption in aircraft by improving aerodynamics, reducing drag, increasing the lift-to-drag ratio, increasing range, and reducing emissions. These benefits make winglets an important part of modern aviation technology and a key factor in the economics of aircraft operations.

2. CONCEPTUAL DESIGN AND METHODOLOGY

The methodology of this research consists of design and numerical simulations. The design process starts with the modelling of wings using the CAD modelling tool CATIA. Both the wing models (with and without wingtips) were designed in the CATIA. The wingtip was created with 0^{o} angle and the reference line lays over the lateral axis of the wing configuration. And then the numerical simulation starts with the pre-processing. The models were discretised and meshed before the analysis process. Since it is a 3 dimensional model, a 3D domain was created and followed three dimensional unstructured meshing processes.

The meshed models were imported to the numerical simulation CFD solver. Ansys Fluent was selected as the solver of choice for CFD simulations. The CFD simulations were carried out using K-E model with necessary boundary conditions. The models were tested for various angle of attacks ranging from 0^{o} to 18^{o}. The completed methodology was shown in below Figure2.

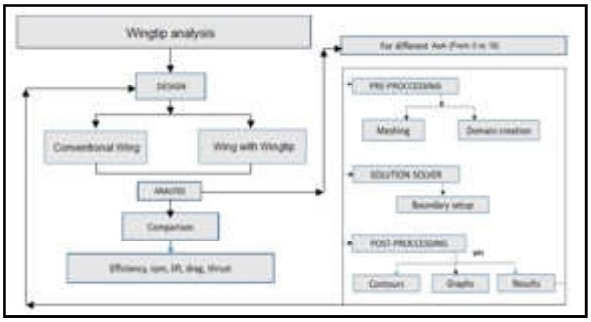

Fig.2 Methodology

3. DESIGN CONSIDERATION

The purpose of this research is to simulate and compare the wing configuration models. The design part of the research starts with airfoil selection. This can be done by importing proper airfoil coordinates to the CAD modeling software i.e., CATIA. The NACA 43018 and NACA 43013 aerofoils shown in fig.3 are the choice of airfoil for this research. The modeling was done with the dimensions as specified in the Table 1.

Table 1 Parameters of Wing Configuration

Wing Type	Conventional Wing	Conventional Wing with Raked wingtip
Wing root cross section airfoil	NACA 43018	NACA 43018
Wing tip cross section airfoil	NACA 43018	NACA 43013
Sweep angle	-	60o
Wing span length	27320 mm	28922 mm
Wing semi span length	13660 mm	14461 mm
Taper ratio	0.5	0.5
Wing root chord length Cr	2864 mm	1689 mm
Wing tip chord length Ct	1689 mm	337 mm
Aspect ratio	11.99	11.99

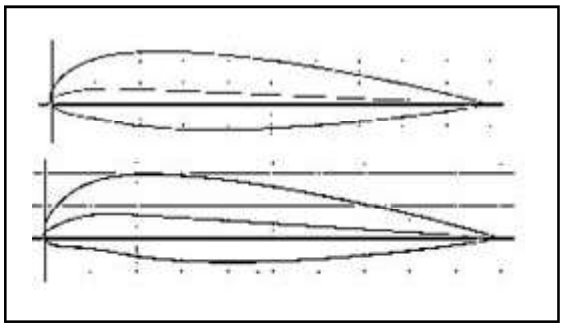

Fig.3 NACA 43018 and NACA 43013

The airfoil NACA 43018 was used for both the wing models and for the wingtip, NACA 43013 was chosen. Both the aerofoils have similar aerodynamic characteristics, but the NACA 43013 is better suited for the wing tip design. The CAD models of the wing configurations are shown in below figure 4 and figure 5.

The model without winglet is referred as Conventional wing [Fig.4]. This conventional type wing model is used short-range and trainer aircrafts. The cross-section of this airfoil has camber in it creates lift at zero angle of attack. The conventional wing is drafted CATIA V5 with semi span length 13660mm, wing root chord of 2864mm and wing tip chord length of 1689mm.

On the other case, in the raked wing tip [Figure 5], the leading edge of the tip section has greater sweep angle than the leading edge of main wing. Leading edge of raked wingtip has been made in dependent with sweep reference line and sweep line.

The conventional wing with raked wingtip is drafted CATIA V5 with semi span 13660mm, raked tip span 1602mm, raked wingtip root chord 1689mm and tip chord 337mm.

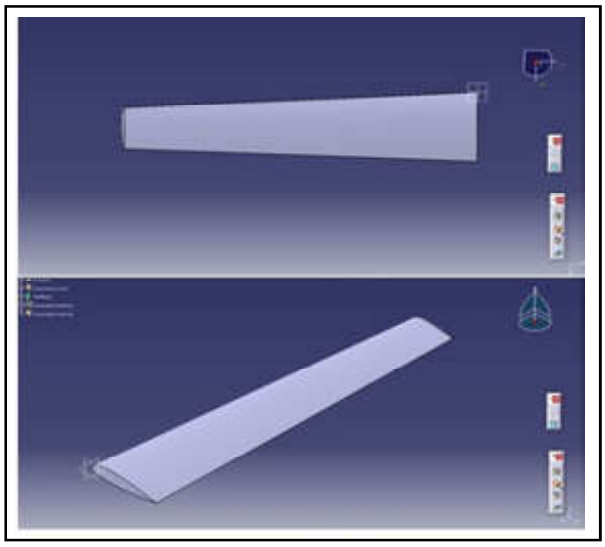

Fig.4 CAD Model of Conventional Wing (Top & Isometric View)

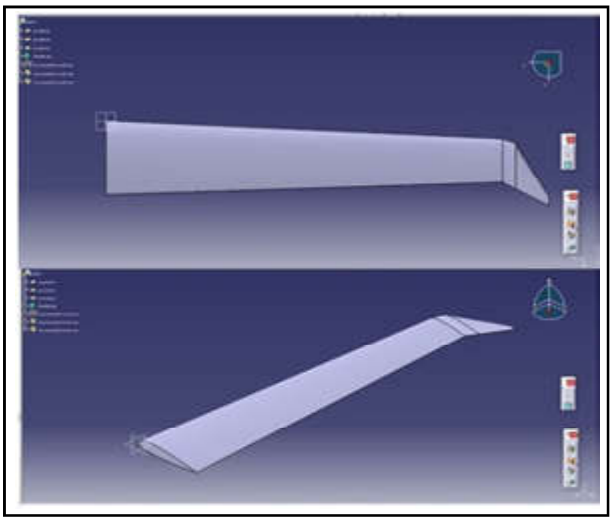

Fig.5 CAD Model of Wing with Raked Wingtip
(Top & Isometric View)

4. MESHING

Meshing is an inevitable part of any CFD simulation. The CAD model of this research work was further discretised using the Meshing tool available in ANSYS Workbench. Since it is a 3D model, a three dimensional domain [Fig.6] was created around the wing model with necessary spacing needed for the flow and circulations. Three dimensional unstructured meshing was chosen as the meshing choice for the domain and tetrahedral & hexahedral elements were used in the meshing process as shown in Fig.8 [10]. A grid independence study was performed [Fig.8] to select the right meshing for the model and the nodes along the element size were given in table.2**.** Since the coefficients are concentrated, the Y+ value of 30 layers [Fig.7] are given to capture the flow over the wing. Fine mesh was preferred over the coarse mesh to improve the overall quality of the result [11].

A grid independence study was done to choose between different mesh sizes. A total of three mesh sizes were studied for the C_p values. C_p values of grid independency are shown in Table 2.

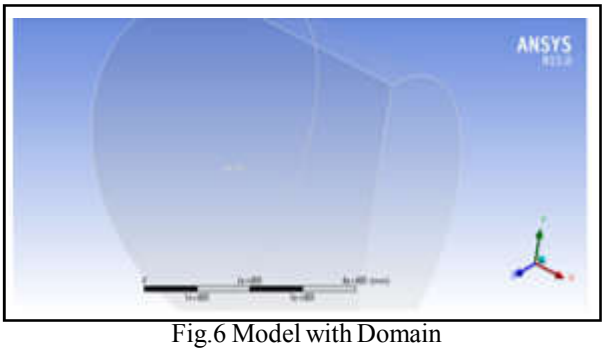

Fig.6 Model with Domain

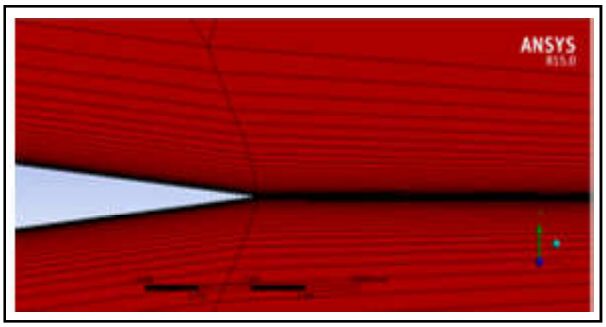

Fig.7 Bondary layer mesh

Table 2 Grid independent Study of Airfoil 43018

Meshing	No. of Nodes	No. of Elements	Cp
Coarse	6275	32021	-1.212 to 0.946
Medium	12115	62057	-1.131 to 0.901
Fine	28777	148551	-1.028 to 0.854

Fine mesh was preferred over the coarse mesh to improve the overall quality of the result. Also the boundary conditions for the simulation were specified in the meshed model as shown in figure 8.

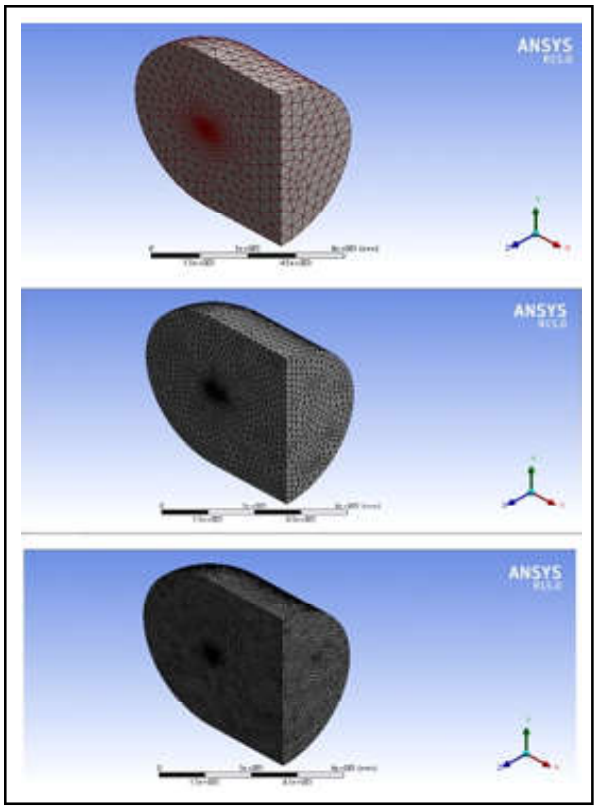

Fig.8 Grid Independence study

5. SOLVER SETUP FOR THE CFD SIMULATIONS

The numerical simulations were carried out using the CFD Solver ANSYS FLUENT. The meshed models of

conventional wing and wing with wingtip are imported to the CFD solver. The parameters taken for the analysis are at the cruise level flight condition and boundary conditions were given as in the Table.3. Since, the regional aircrafts fly at subsonic speed range, Pressure based solver is used with turbulence models [12]. K-epsilon model was chosen as the turbulence model for this research as they give better Reynolds averaging compared to other models in external flow simulations [13]. Simulations were carried out up to which the residual plot seems to be converging at the 6000 iterations.

Table 3 Flow Conditions

Parameter	Values
Solver	Pressure Based
Turbulence Model	K-e
Velocity, v	140m/s
Pressure, P	36284.576 Pa
Density, ρ	0.5234679 kg/m3
Temperature, t	238.75 K
Angle of Attack, α	0,3,6,9,12,15,18

5. RESULT AND DISCUSSIONS

5.1 Coefficient of Pressure (Cp)

5.1.1 Case-1: C_p at $\alpha = 0$

The entire numerical simulations were carried out for a constant velocity of 140m/s (cruising velocity of regional aircrafts). This study of winglets starts with an angle of attack (б) of 0°. Both the wing models were analysed for the velocity and the coefficient of pressure was plotted below (fig.9). It shows that the Cp varies from -1.028 to 0.854 for the conventional wing and -1.093 to 0.826 for the wing with wing tip. It is noted that the wing with wingtip has better Cp distributions at the tip.

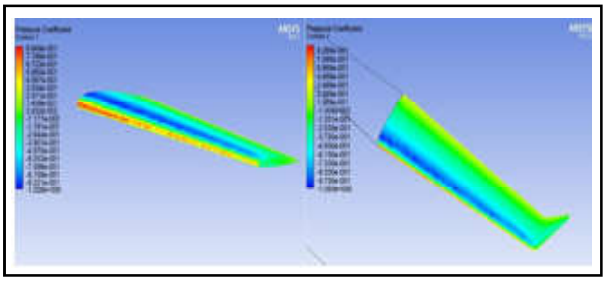

Fig.9: C_p at $\alpha = 0$

5.1.2 Case-2: CP at $\alpha = 3$

Similarly, the same wing models were analysed for the same velocity of 140m/s with an angle of attack of 6o. It shows that the leading edge of the wings experience more Cp compared to other parts of the wing with -0.820 and -0.833 on both the wings respectively. The Cp of the Wingtip model was gradually extending up to the tip portion.

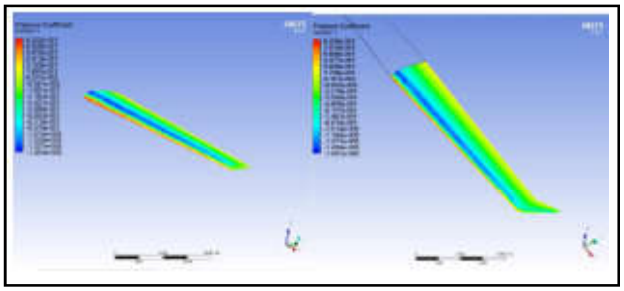

Fig.10 C_p at a $\alpha = 3$

5.1.3 Case-3: CP at $\alpha = 6$

Now the models were tested at an angle of 6o and it is clear that the Cp of wingtip model has extended over the tip portion of the wing comparing to the conventional wing model. The lower Cp at the tip portion of conventional wing generates the drag leading to trailing vortex.

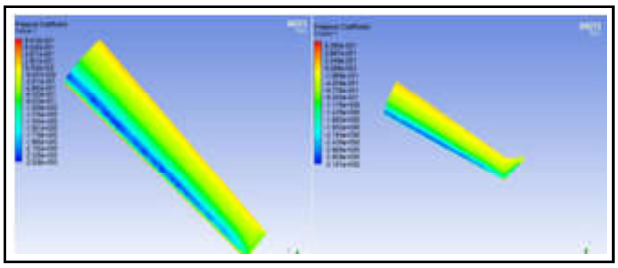

Fig.11 C_p at $\alpha = 6$

5.1.4 Case-4: CP at $\alpha = 9$

From the contour plots, it is clear that the increasing angle of attack decreases the pressure distribution in the wing with wingtip model and it advantageous for a wing to have winglets at higher velocities with respect to higher angle of attack.

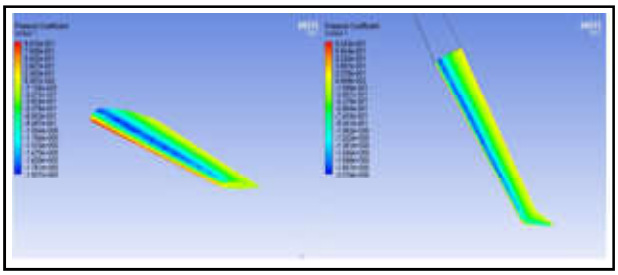

Fig.12 C_p at $\alpha = 9$

5.1.5 Case-5: CP at $\alpha = 12$

Similar to the previous angle, at 12o also has lower values of Cp distribution exactly at the tip portions. The

curve end in the winglet portion of the wing makes it possible to have smooth flow at this region. As a result, it increases the lift production.

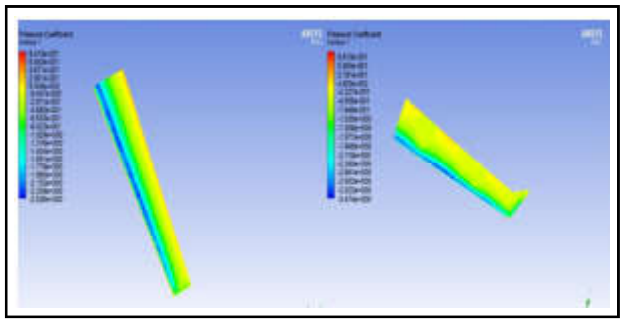

Fig.13 C_p at $\alpha = 12$

5.1.6 Case-6: CP at α = 15

For the angle of 15o, the Cp values are varying from -0.841 to -0.871 on both the models respectively. It is noted that the Cp values in wingtip model is slightly higher than the Cp distribution in conventional wing model.

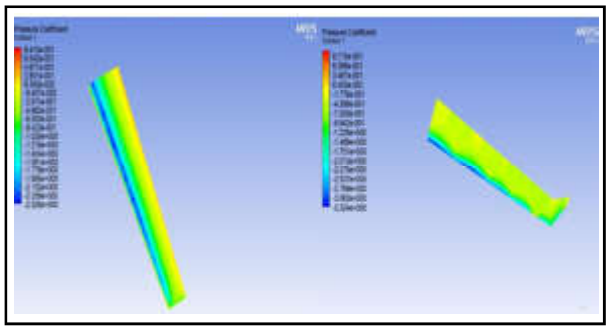

Fig.14 C_p at $\alpha = 15$

5.2 Coefficient of Lift (CL)

The coefficient of lift is dimensionless and relates the lift force generated by the body to fluid density, velocity and reference surface area. The CL depends on certain parameters like angle of attack, Mach number and Reynolds number. The CL was found for both the wing models and the results are tabulated as follows in Table.4

Table 4 Angle of Attack vs. Coefficient of Lift (CL)

Angle of Attack (Degree)	CL (Conventional Wing)	CL (Wing with Raked Wing Tip)
0	0.233	0.255
3	0.500	0.547
6	0.754	0.826
9	0.979	1.070
12	1.148	1.243
15	1.195	1.228
18	1.112	1.155

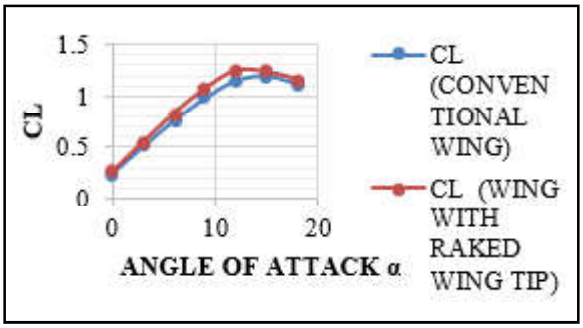

Fig.15 Lift Coefficient Vs. AoA.

The above graph shows that the C_L is increasing gradually with respect to the increasing angle of attack (б). For the conventional wing, C_L was maximum at 15° as 1.195 and for the wing with wingtip the C_L was maximum at 12° 1.243. It is clear that the wing with wingtip has higher C_L at lower angle of attack (б). This concludes that the implementation of raked wing tip increase the surface area of the wing and thus increasing the coefficient of lift compared to the conventional wing without wingtip.

5.3 Coefficient of Drag (C_D)

The coefficient of drag is the dimensionless number used to relate the drag force or resistance of the body in the fluid atmosphere. The effect of form drag, interference drag and the drag due to lift are comprised in the coefficient of drag. The C_D was found for both the wing models and the results are tabulated as follows in Table.5

Table 5 Angle of Attack vs. Coefficient of Drag (CD)

Angle of Attack (Degree)	CD (Conventional Wing)	CD (Wing with Raked Wing Tip)
0	0.028	0.029
3	0.035	0.037
6	0.054	0.058
9	0.081	0.086
12	0.113	0.121
15	0.150	0.168
18	0.199	0.230

A graph was plotted for the coefficient of drag against the angle of attack (б). It is observed that the C_D is gradually increases with increasing angle of attack (б) and the wing with raked wingtip experiences lesser drag compared to the wing without the wingtip. Thus results in a decreased coefficient of drag.

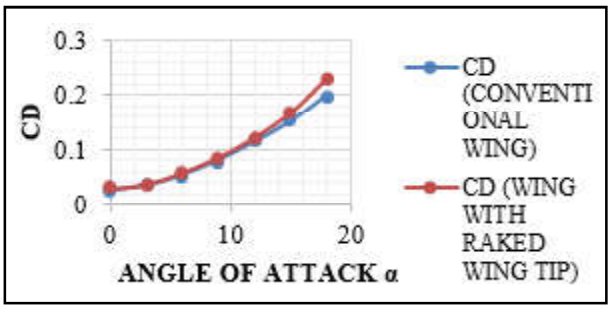

Fig.16 Coefficient of Drag vs. AoA

5.4 Lift To Drag Ratio:

The lift to drag ratio give the overall aerodynamic aspect on a airfoil/wing. The C_L/C_D was found for both the wing models and the results are tabulated as follows in Table.6.

Table 6 Angle of Attack vs. C_L/C_D

Angle of Attack (Degree)	*C_L/C_D (Conventional Wing)*	*C_L/C_D (Wing with Raked Wing Tip)*
0	8.367	8.909
3	14.086	14.779
6	13.853	14.365
9	12.129	12.501
12	10.123	10.292
15	7.971	6.918
18	5.608	5.010

Then the CL/CD was plotted against the Angle of Attack. From the graph, it is clear that the curve was increasing up to 14.086 and 14.779 for both the wing models at angle of attack (б) = 3°. And further on increasing the angle of attack, the curve gradually falls all the way down to 5.608 and 5.010 at (б) = 3°. From these curves, it is clear that the wing with raked wingtip has slightly higher lift to drag ratio compared to the wing without the wingtip.

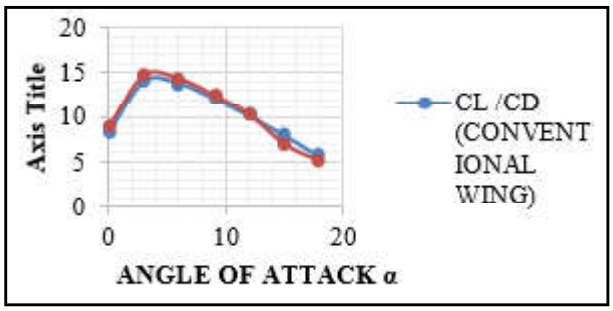

Fig.17 C_L/C_D vs. AoA.

6. CONCLUSION

Thus, from the above results we can conclude that the implementation of wingtips on aircrafts increases their lift coefficients (CL) at lower angle of attack compared to the conventional wing without the wingtips. This also improves the overall lift to drag ratio (CL/CD) of the wing compared to the conventional wing. Overall the induced drag is reduced for wing with raked wing tip for regional aircraft. From the induced drag estimation results the induced drag for wing with raked wing tip is less than the induced drag for conventional wing. This shows that by fixing the raked wing tip devices for regional aircraft will reduce the induced drag.

REFERENCES

[1] W. F. Phillips, D. F. Hunsaker and J. J. Joo, "Minimizing Induced Drag with Lift Distribution and Wingspan", AIAA journal, https://doi.org/10.2514/1.C035027, 2018.

[2] Kaoruko Eto, Yusuke Kondo, Koji Fukagata and Naoko Tokugawa, "Assessment of Friction Drag Reduction on a Clark-Y Airfoil by Uniform Blowing", AIAA journal, https://doi.org/10.2514/1.J057998, 2019.

[3] Setyo Hariyadi Suranto Putro, S. Sutardi and Wawan Aries Widodo, "Numerical Study of Aerodynamic Analysis on Wing Airfoil NACA 43018 with the addition of Forward and Rearward Wingtip Fence", Proceedings of the International Mechanical Engineering and Engineering Education Conferences (IMEEEC), DOI: 10.1063/1.4965745, 2016.

[4] Jingeleski and J. David, "Aerodynamic Analysis of Variable Geometry Raked Wingtips for Mid-Range Transonic Transport Aircraft", ProQuest Dissertations And Theses, Masters Abstracts International, 2012, Vol.57, No.02, pp.55.

[5] J. P. L. G. M. Barrios and G. M. P. Herman, "Reducing Drag by Modifying the Winglet Design", The Philippine Physics Society Physics Fair, 2017, pp.1-29.

[6] D. Liu, B. Song and W. Yang, *et al.,* "A Brief Review on Aerodynamic Performance of Wingtip Slots and Research Prospect", J Bionic Eng., https://doi.org/10.1007/s42235-021-00116-6, Vol.18, 2021, pp.1255-1279.

[7] Gavrilovic, N. Nikola, Boљko P. Raљuo, George S. Dulikravich and Vladimir B. Parezanoviж, "CommercialAircraft Performance Improvement Using Winglet", Numerical Study of Aerodynamic Analysis on Wing Airfoil NACA 43018 with the addition of Forward and Rearward Wingtip Fence, FME Transaction Vol. 43, 2015.

[8] Khamis Ali Al Sidari and G.R.Rameshkumar, "Design of Winglet Device for Aircraft", in International Journal of Multidisciplinary Sciences and Engineering, Vol.7, No.1, 2016.

[9] A. Rajesh, A.S. Praveen and Dr. M.S. Ganesha Prasad, "Design and Analysis of UCAV Wing with a without Winglet by Varying the Cant Angle", IJERT, Vol.4, No.5, 2015, pp. 351-354.

[10] T. Seshaiah, B. Vasu, K.V.K. Reddy and P.Bridjesh, "Analysis on Air Craft Winglet at Different Angles by using CFD Simulation", Materials Today: Proceedings, Vol.49, 2021, pp. 275-283.

[11] N.K. Mishra, A.S.Kumar, B.Shashank, K.S.Vamsi, S. Annem, B.D.Rao and K.Sundararaj, "Numerical Investigation of a Finite Wing Section with a Bleed Hole Allowing Boundary Layer Suction", AIP Conference Proceedings, Vol.2446, 2022, pp.180054.

[12] L.Praveen and M.S. Anoop, "Modeling and Finite Element Analysis of Composite Propeller Blade for aircraft", AIP Conference Proceedings, Vol.2317, 2021, pp.020027.

[13] K. Shiva Shankar, M.Satyanarayana Gupta and G. Parthasarathy, "Comparative Study of CFD Solvers For Turbulent Fuel Flow Analysis To Identify Flow Nature", International Journal of Mechanical Engineering and Technology Vol.8, Issue.5, 2017.

[14] Xu, Jianhua, Xu., Huijing, Li., Wenping, Song., Zhong-Hua and Han, "An Aerodynamic Design Method of Propeller Airfoils with Geometric Compatibility as Constraints", American Institute of Aeronautics and Asttrauntics, 2019.

SELECTION OF BEARINGS FOR THE TWO-STAGE SPEED REDUCTION GEAR-BOX AND STUDY OF FAILURES ON THE BEARINGS

D.Dinesh, N. Sivaprakash and J. Meer Jaffer Satick
Bannari Amman Institute of Technology, Sathyamangalam - 638 401, Erode District, Tamil Nadu

Abstract

Bearings can be categorized into three areas, they are bearings, automotive products, and precision machinery components. Presently, Bearings are found everywhere from cars to airplanes, from homes to high-tech factories, and from huge construction equipment to small medical instruments. Bearings play a vital role in the cement industry and machinery meets the environmental requirements, smart technologies, and is completely reliable. In this paper, we have discussed the selection of bearings, which have been used in the transmission system of the most important machine named "Crusher". These crushers have a major role in cement preparation as they will be carrying heavy weight and load carrying capacity must be very high. In these crushers, the gearbox plays a major role when they are used to transmit the input power. These gearboxes must be able to withstand continuous high loads with less speed, and, more torque in a slow process. A study of Double stage – Reduction gearbox and the loads acting on the gearbox in order to select suitable bearings with a criterion to meet the basic load rating life of 10^5 hours, for each bearing and the defects on the bearings has been focused.

Keywords: *Bearings, Crushers, Double-stage gearbox*

1. INTRODUCTION

Fatigue failure analysis of a helical gear in a gearbox in 2005 analysed a helical gearbox that is used in vehicles made of AISI 8620 steel. An evaluation of the failed gear was taken to assess its integrity through visualization, chemical analysis, photo documentation, micro-hardness measurement, and metallographic examination. Results indicate that the failure in the teeth was due to fatigue with fatigue crack initiation from destructive pitting and the spalling region at one end because of misalignment. Helical gears are widely used in transmitting power between non-parallel shafts and they can carry high loads with less noise. Failed tooth of the gear was ultrasonically cleaned and was analysed using scanning electron microscopy. Spectrum analysis and micro hardness test revealed that the failed helical gear material was carburized. Destructive pitting appears as larger pits and reason for the failure of the gears. This indicates that the failures are due to several overload conditions. These failures are caused by high concentration stresses at particular areas, foreign materials in gear mesh, improper heat treating, and misalignment. It was concluded that the primary cause of the failure is a misalignment in helical gears.

Sankar S *et al* in 2012 in Failure analysis of bearings in wind turbine generator Gearbox analysed the root cause for the failure of bearings in wind turbine gearbox. A wind turbine gearbox is one which converts low speed and high torque into high speed and low torque. The reliability of bearings in special environments like corrosive, high temperature, and high power is important. Cylindrical roller bearings were used in that multistage gearbox which comprises planetary gears, helical gears, and spur gears. The final step-up ratio of the gearbox was 1:74.917. The bearing material used was EN31 steel. Chemical analysis of the roller and raceway was carried out using ARL Spark Analyser. Visual inspection of the bearing revealed that the scoring seems to appear in rolling elements. It is observed that the bearing was at maximum power and maximum temperature side for continuously two months but within the limit of 80°C The specimen was finely cleaned and analysed by Scanning Electron Microscopy. It is clearly evident that the roller was subjected to tempering. The major conclusions give that the failure of the bearing was not due to the defect in material, not due to misalignment and the failure was due to the presenceof Bauxite elements from the surface.

This is due to premature overloading and tempering of the bearings. SEM microscopy revealed that the failure was fatigue failure due to a high cyclic phenomenon.**2.**

2. EXPERIMENTAL PROCEDURE

One of the most important industries where bearings play a vital role is the Cement industry. Cement is one of the main components in buildings and construction as buildings and construction play a major part in the modern world. In cement industries cement is manufactured by crushing limestone rock and is finely powdered into cement. There are various types of crushers like hammer, impact, jaw, gyratory, and roll for which the gearbox of spur gearbox, helical gear box, bevel gearbox, and Planetary gearboxes are used.

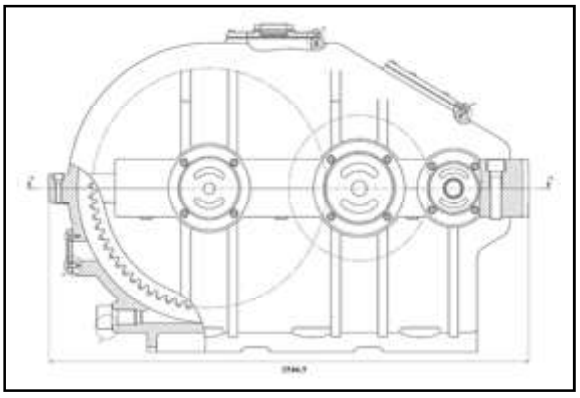

Fig.1 Front view of the gear box.

They all have a different application on based on their functions. This paper focuses on with a Double stage – Reduction gearbox in order to study the loads acting on the gearbox and to select suitable bearings with a criterion to meet the basic load rating life of 10^5 hours, for each bearing. The gearbox as shown in Fig.1 is a two-stage speed reducer (Helical) gearbox. Helical gearboxes are used for their efficient work. Helical gearboxes have n number of advantages and are mostly suited for carrying large loads. Helical gears have teeth that are oriented at an angle called helix angle (φ) to the shaft. Because of this more than one tooth will be in contact with the driven gear during operation which makes helical gears carry more loads. Due to this load sharing between the teeth, helical gears will perform the operation more smoothly and noiseless. The design of this helical gearbox has advantages like inter-changeability of parts and sub-assemblies. This helps in maintaining the economical standards in achieving the highest production.

It consists of three stepped shafts, which are:

- Input shaft
- Intermediate shaft
- Output shaft.

It has four numbers of gears and six numbers of bearings which are needed to be placed as two on each shaft. This gearbox is a speed reducer and it increases torque which will be useful in crushers in the cement industry.

2.1. Forces Acting on the Bearings

Static forces are forces that are due to the self-weight of the components present in the system. This force is the force that keeps the object at rest. It occurs due to the self-weight of the system. These forces are very important for bearing selection. Here the mass of the shaft and gear are considered, and reaction forces at bearings are calculated.

When two gears mesh with each other forces are formed in the gear plane. Depending upon the type of gears, forces are formed. In helical gears, three such forces are formed. They are:

- Tangential Force
- Supporting Force
- Axial (Thrust) Force.

Tangential Force (P) = (Power * d_{p2}) * (60 / (2 ď N))(1)
Supporting Force(S) = (P* tanx) / (cosř) (2)
Axial or thrust force T = P tanř (3)

3. RESULT AND DISCUSSION

The load acting on the bearing due to the self-weight of the gears and bearings is as follows:

3.1. Self-Weight Of the Individual Shafts and Gears

3.1.1 Input shaft

From the analysis, the mass of the Input shaft is 108.712Kg.W=m*g 2*9.81066.4647 N.
Weight of Input shaft (W_{S1}) = 1066.4647 N
C.O.G of Input shaft = 593.5 mm

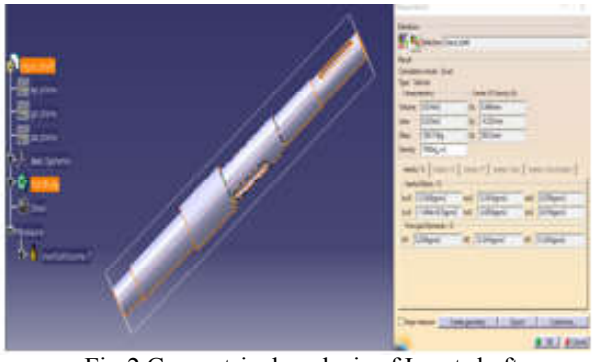

Fig.2 Geometrical analysis of Input shaft

3.1.2 Intermediate Shaft

From the analysis, the mass of the Intermediate shaft is 195.7 Kg.
W=m*g
W=195.7*9.81
W=1919.817 N
Weight of Intermediate shaft (W_{S2}) = 1919.817 N
C.O.G of Intermediate shaft = 499.372 mm

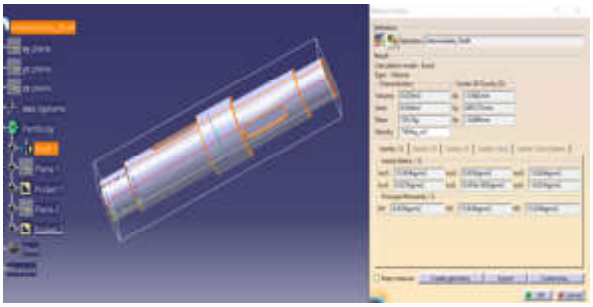

Fig.3 Geometrical analysis of Intermediate shaft

3.1.3 Output Shaft

From the analysis, the mass of the Input shaft is 309.54 Kg.
W=m*g
W=309.154*9.81
W=3032.80074 N
Weight of Output shaft (W_{S3}) = 3032.80074N
C.O.G of Output shaft = 775.273 mm

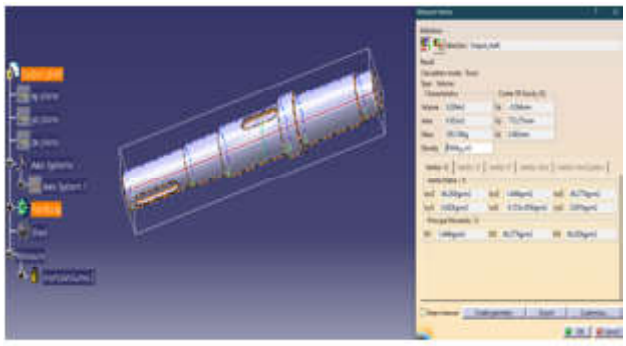

Fig.4 Geometrical analysis of output shaft

The self-weight of the individual gears is listed in Table 1

Name of the Component	Self-weight
Gear 1	454.63464 N
Gear 2	5115.93462 N
Gear 3	1164.47643 N.
Gear 4	19361.03562 N

3.2 Radial Load on the Individual Bearing due to Stationary Load

Each bearing is subjected to two different stationary loads due to the self-weight of the shaft and gears. The function of our bearing is to mainly support the resultant of these two forces (i.e. resultant radial load) for maintaining the system in equilibrium, as well as, to stabilize the gearbox. We can get the resultant forces acting on any bearing in an individual shaft by considering the shaft as a beam and resolving the weights of the gear and shaft about the given bearing.

3.2.1 For Input shaft

From fig,
We have, $R_A+R_B = W_{G1}+W_S$
Thus, $R_A+R_B = 454.63464+1066.4647$
$\rightarrow$ **R_A+R_B = 1521.0993 N** **(4)**
Equating $\Sigma(\text{Moment})_B = 0$,
We have, $R_{A*}(0.85) - W_{G1*}(0.61) - W_{S1*}(0.531) = 0$
$\rightarrow R_{A*}(0.85) - (277.3271) - (566.2927) = 0$

$\rightarrow R_{A*}(0.85) = 843.6198$
$\rightarrow$ **R_A = 992.49 N**
Using R_A in equation (4), We have. **R_B = 528.6093 N**

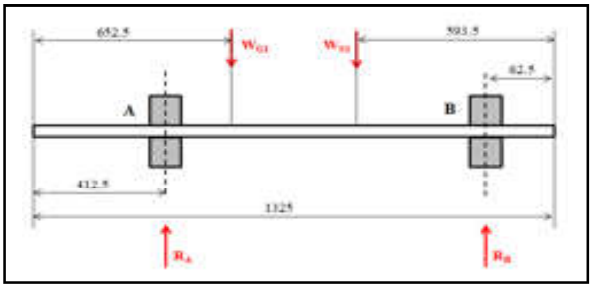

Fig.5 Stationary loads acting in input shaft

3.2.2 Intermediate shaft

From fig,
We have, $R_C + R_D = W_{G2} + W_{S2} + W_{G3}$
Thus, $R_C + R_D = 5115.9346 + 1919.817 + 1164.4764$
$\rightarrow$**R_C+R_D = 8200.228 N (5)**
Equating "$(\text{Moment})_D = 0$,
We have, $R_{C*}(0.85) - W_{G2*}(0.61) - W_{S2*}(0.4268) - W_{G3*}(0.27) = 0$
$\rightarrow R_{C*}(0.85) - (3120.7201) - (314.4086) - (819.3778) = 0$
$\rightarrow R_{C*}(0.85) = 4254.5065$
$\rightarrow$ **R_C = 5005.3017 N**
Using R_C in equation (5), We have. **R_D = 3194.926 N.**

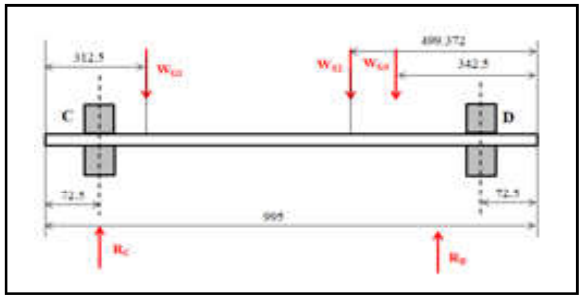

Fig.6 Stationary loads acting on intermediate shaft

3.2.3 Output Shaft

From fig, We have, $R_E + R_F = W_{G4} + W_{S3}$
Thus, $R_E + R_F = 19361.0356 + 3032.8007$
→ **$R_E + R_F$ = 22393.8363 N (6)**

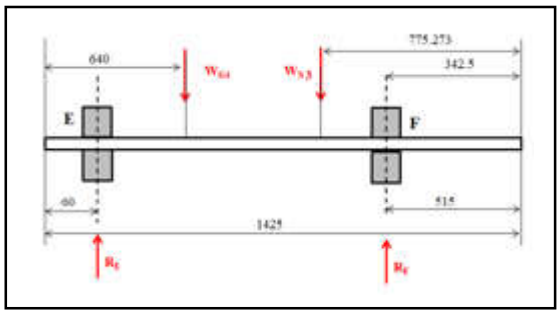

Fig.7 Stationary loads acting in Output shaft

Equating $\Sigma(\text{Moment})_F = 0$,
We have, $R_{E*}(0.85) - W_{G4*}(0.27) - W_{S4*}(0.26) = 0$
→ $R_{E*}(0.85) - (5227.4796) - (788.5281) = 0$
→ $R_{E*}(0.85) = 6016.0077$
→ **R_E = 7077.6561 N**
Using R_E in equation (6), We have, **R_F = 15316.1802 N**

Therefore, the resultant radial loads acting on the individual bearings due to the stationary loads are shown in the below table 2.

Table 2

Bearings	Radial load (N)
A	992.49
B	528.6093
C	5005.3017
D	3197.926
E	7077.6561
F	15316.1812

3.3. Dynamic Load Acting on Gear Mesh

The dynamic loads acting on gears are:
- Tangential load **(P)**
- Supporting load **(S)**
- Thrust (or) axial load **(T).**

These three loads are produced in between two gears whenever they mesh in a dynamic action and hence create two loads in a bearing in two different directions, namely:
- Radial directional (or) Radial load
- Axial directional (or) Thrust load.

The radial load is produced in the bearing due to the individual effect of these three forces and hence the resultant of radial forces is calculated to find the combined radial load acting on the bearing. Also, each bearing in a shaft is subjected to the radial load as it could be easily distributed. However, the axial load cannot be distributed and hence, only one bearing in a shaft is used for nullifying the effect of axial load that is produced.

3.3.1 Gear 1-2

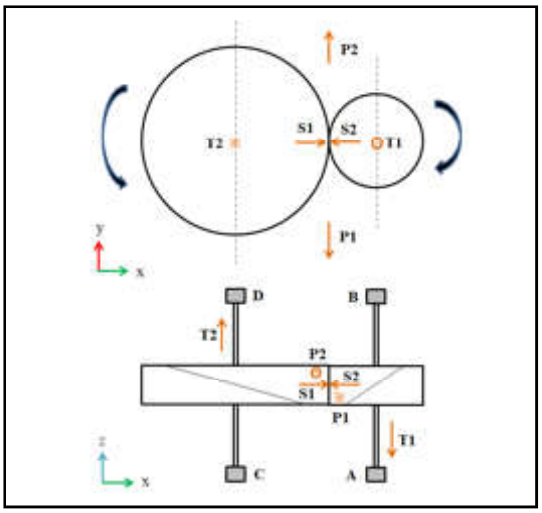

Fig.8 Forces acting in mesh 1-2

Given:

Power = 400 KW;
Speed of Shaft 1 (N_1) = 1000 rpm;
Contact angle (x) = 20Ú
Helix angle (ř) = 6.9Ú
Pitch diameter of gear 1 (d_{p1}) = 252 mm
Pitch diameter of gear 2 (d_{p2}) = 756 mm

We know that, Power = (Torque) * (Angular speed)
→ Power = (P * (d_{p1}/2)) * ((2 * ď * N_1)/60)
On solving, we get,
Tangential force (P) = 30315.2272 N
As we know,
T = P * tan ř
Thrust force (T) = 3637.8272 N
Also we know that,
S = (P * tan x) / (cos ř)
Thus, **Separating force (S) = 11122.8229 N**
Therefore,

→ P1 = P2 = 30315.2272 N
→ S1 = S2 = 11122.8229 N
→ T1 = T2 = 3637.8272 N.

3.3.2 Gear 3-4

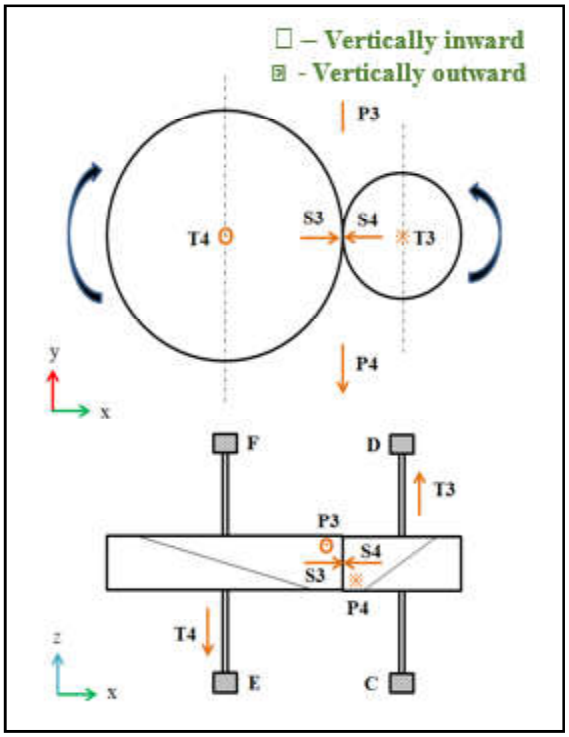

Fig.9 Forces acting in mesh 3-4

→ **Given:**
Power = 400 KW;
Speed of Shaft 1 (N_3) = 333.33 rpm;
Contact angle (x) = 20Ú
Helix angle (ř) = 7Ú
Pitch diameter of gear 3 (d_{p3}) = 360 mm
Pitch diameter of gear 4 (d_{p4}) = 1248 mm
We know that, Power = (Torque) * (Angular speed)
'! Power = (P * (d_{p3}/2)) * ((2 * ď * N_3)/60)
On solving, we get,
Tangential force (P) = 63662.6138 N
As we know,
T = P * tan ř
'! Thrust force (T) = 7811.4027 N
Also we know that,
S = (P * tan x) / (cos ř)
Thus, Separating force (S) = 23345.3088 N
Therefore,
→ P3 = P4 = 63662.6138 N
→ S3 = S4 = 23345.3088 N
→ T3 = T4 = 7811.4027 N.

3.4 Radial Loads Acting On Individual Bearing Due To Dynamic Load

The dynamic loads acting on the individual bearings are calculated and listed in table 3 & 4.

Table 3 Radial Load on Individual Bearing

Load		Bearing A	Bearing B	Bearing C	Bearing D	Bearing E	Bearing F
Radial Load	P (kN)	21.7556 ※	8.5595 ※	41.9778 □	51.9999 □	20.2222 ※	43.4403 ※
	S (kN)	7.9822 (↑)	3.1405 (↑)	0.5666 (↓)	12.7891 (↑)	7.4155 (↓)	15.9297 (↓)
	T (kN)	0.5392 (↑)	0.5392 (↓)	0.0364 (↓)	0.0364 (↑)	5.7344 (↓)	5.7344 (↑)

Table 4 Combined Load and Axial load on Individual Bearing

Load	Bearing A	Bearing B	Bearing C	Bearing D	Bearing E	Bearing F
Combined Radial Load (kN)	23.365	8.9461	41.9822	53.5583	24.1218	44.6207
Axial Load (kN)	3.6378		11.4492		7.8114	

The selected bearing for each position of the gearbox are determined and tabulated in the table 4.

Table 5 Selected Bearings

Position	Bearings
A	NU320E
B	24020CE4
C	NU230E
D	24130CE4
E	NU1036
F	23036CDE4

3.5 Failure of the Bearings

3.5.1 Flaking

This failure causes small pieces of material from raceway or rolling elements comes off from the surface thereby creating rough and coarse texture.

The causes for flaking are:

- Excessive load.
- Poor mounting.
- Moment load.
- Entry of foreign debris or water.
- Poor lubrication.
- Unstable bearing clearance.

Fig.9 Flaking

Counter measures to overcome failures:

- Checking bearing load conditions.
- Improving the mounting method.
- Improving the sealing mechanism and preventing rusting during idle periods.
- Check the bearing internal clearance.

3.5.2 Scoring

Surface damage due to improper loadings and improper lubricants at the surface of the inner ring raceway and rolling elements.

Fig.10 Scoring

Damage causes are:

- Excessive loads, excessive preloads.
- Poor lubrication.
- Particles caught in the surface.
- Shaft bending.
- Poor precision of the shaft and housing.

Counter measures are:

- Check the loading.
- Adjustment of preload.
- Improving the lubrication method and the lubricant.

3.5.3 Fracture

Small pieces of raceway or rolling elements may be broken due to excessive load or shock loads acts locally on a part of a raceway or rolling element.

Damage causes are:

- Impact during mounting.
- Excessive load.
- Poor handling.

Counter measures are:

- Improving the mounting method using proper tools.
- Providing enough backup for the bearing ribs.

Fig.11 Fracture

3.5.4 False brinelling:

Hollow spots that resemble dent marks and are due to wear dent marks are formed in the raceways and rolling elements.

Damage causes are:

- Oscillation and vibration during transportation.
- Poor lubrication.
- Oscillating motion with a small amplitude.

Counter measures are:

- Inner and outer rings packed separately during transportation are required.
- Reduce vibrations by preloading.
- Using of correct lubricant.

Fig.12 False brinelling

4. CONCLUSION

- The selection of each bearing based the radial and axial load criteria has been obtained. It also identified the possible failure of the bearing for the selected type of bearing has been discussed.
- The selected bearing will enhance the fatigue life of each bearing is confirmed through the load calculation as discussed.

REFERENCES

[1] S. Sankar, M. Nataraj and P.V. Raja, "Failure Analysis of Bearing in Wind Turbine Generator Gearbox", Journal of Information Systems and Communication, Vol.3, No.1, 2012, pp.302.

[2] O.Asi, "Fatigue Failure of a Helical Gear in a Gearbox", Engineering Failure Analysis, Vol.13, No.7, 2006, pp.1116-1125.

[3] A. Dhanola and H.C.Garg, "Tribological Challenges and Advancements in Wind Turbine Bearings: A Review", Engineering Failure Analysis, Vol.118, 2020, pp.104885.

[4] G. Singh and K. Sundaram, "Methods to Improve Wind Turbine Generator Bearing Temperature Imbalance for Onshore Wind Turbines", Wind Engineering, Vol.46, No.1, 2022, pp.150-159.

[5] T. Bruce, H. Long and R.S. Dwyer Joyce, "Dynamic modelling of wind turbine gearbox bearing loading during transient events", IET Renewable Power Generation, Vol.9, No.7, 2015, pp.821-830.

PREPARATION, CHARACTERIZATION, AND AC CONDUCTIVITY OF IPANI /BHS FA /AG NANOCOMPOSITE BY DC GLOW DISCHARGE PLASMA

K. Vanitha[1], K. A. Vijayalakshmi[2], M. Revansidddappa[3], S.B. Chalvaraju[4], K. Sadasivam[5] and M. Thirumoorthy [6]

Department of Physics,

[1,5&6] Bannari Amman Institute of Technology, Sathyamangalam - 638 401, Erode District, Tamil Nadu

[2]Sri Vasavi College, Erode - 638 316, Tamil Nadu

[3]PESIT south campus, Bengaluru - 560 085, Karnataka

[4]Bangalore Institute of Technology, Bengaluru - 560 004, Karnataka

E-mail: vanithak@bitsathy.ac.in

Abstract

Polyaniline/Fly ash/silver (IPANI+BHS+Ag) composite films were prepared in different concentrations of FA and surface modified by DC glow discharge plasma. The prepared composite films were characterized by Fourier transform infrared spectroscopy (FTIR), X-ray diffraction (XRD), scanning electron microscopy (SEM), UV and DC conductivity analysis In the IR spectrum a characteristic broad bonds at 3422 and 2984 cm-1 which corresponds to N-H stretching of polyaniline. In XRD both untreated a plasma treated samples there is no crystalline and structural change but, the intensity of the composite was increased after plasma treatment. The SEM images of untreated and plasma treated IPANI based Fly ash and Ag nano composite, which appears to be quite homogeneous) UV visible spectrum is useful in identifying the extent of conjugation in conducting polymers. The DC conductivity of after plasma treatment has some significant increase due to the functional group changes. The AC conductivity behavior maybe variation of ionized gas and different percentage of fly ash of chemical composition. The synthesized composite has good conducting composite as well as the plasma treatment has increased the surface properties.

Key words: *AC Dielectric loss, DC glow discharge plasma, FTIR, SEM, Tangent loss, TG-DTA, UV, XRD*

1. INTRODUCTION

Polymer composites have gained momentum recently because of their exceptional physical properties. Embedding polymers with metals or FA increase the conductivity to many folds. [1, 2]. The most common conducting polymer is polyaniline, which is eco-friendly and synthesized cheaply. This material has numerous applications in corrosion and consumer electronics [3-7]. Due to the flexibility in cost, packing, compatibility and flexibility with the preparation of substrates, the PANI is widely employed in the place of inorganic gas sensors [8, 9]. It has superior optical and electrical properties and is utilized in various applications. [10, 11]. This has excellent interaction capability with oxidizing or reducing agents, which makes it suitable for sensing applications [12-17]. Despite this, it has poor stability caused by polymer degradation, which reduces its capabilities as a potential raw material.

Coal is used as a raw material converted into FA after combustion, and tons of FA is generated globally across all the power stations. Disposal of these FA wastes is still believed to be a significant issue worldwide. However, with rapid urbanization, the applications of FA increased worldwide, not only as the filling material is also used in ceramic technology [18]. BFA (bottom fly ash) is generally composed of alumina silicates. Thus they can be used as structure fills, in soil amendments, for the production of new materials and in various environmental applications.

Additionally, in recent times, materials scientists and engineers have proposed and contrived different techniques to use these unwanted effects for the mixture of some functional composites [19, 20]. Bottom Fly ash can easily combine with calcium hydroxide to form needed compounds. It produces robust and durable concrete that is resistant to harsh chemicals. This can include various toxic substances from trace amounts to per cent levels. To protect the environment or the quality and safety of any products it is added to, the composition of the bottom fly ash product needs to be accurately analyzed before it can be recycled or disposed of. Following microwave

acid digestion, the elemental analysis of coal and coal ash samples can be accomplished using inductively coupled plasma optical emission spectrometry (ICP-OES).

A high specific surface area of metal nanoparticles and a fraction of surface atoms. Among the metal nanoparticles in place of their single physicochemical specific things of catalytic activity, optical, electronic, antibacterial and magnetic properties. Silver shows the highest electrical conductivity surrounded by metals at room temperature and for giving conducting composites, either in organic or inorganic matrices [21, 22]. Plasma treatment is widely used on conducting polymers to improve the surface functional applications via improving the surface functional groups, adhesion, wettability and surface roughness [23].

In the present work, polyaniline-based BHS-Fly ash and silver composite was prepared via in situ polymerization method; consequently, the composite surface properties were increased by plasma treatment.

2 MATERIALS AND METHODS

2.1. Preparation of PANI +BHS+ Ag

Foremost, IPANI/Ag composite is prepared with a concentration of 0.3M $AgNO_3$. Initially, $AgNO_3$ (0.3 M) is dissolved in 1.0 M HNO_3 to produce Ag nanoparticles, and it is added to the organic phase, which contains 0.5g of aniline in 10 ml of $CHCl_3$. Next, ammonium Persulphate (0.1M) is dissolved in HNO3 (1.0 M), and the same is added slowly to the above mixture of organic and aqueous phases. After 5 minutes of mixing, a dark green layer is observed at the interface, gradually converted into an aqueous phase. Finally, the different weight percentage of BHS (5, 10, 15, 20, and 25) is added to the PANI solution with vigorous stirring to achieve homogenous mixing.

After 24 hrs. The top and bottom layers of the aqueous solution are found to have dark green colour indicating the formation of aniline oligomers. The unwanted residues are removed using the Whatman filter paper. It is dried in a vacuum at 40.8oC for 36 h, and pure PANI is collected from the container. Non – Thermal plasma was generated using a dc glow discharge chamber. Atmospheric air was used as a plasma-forming gas. The discharge chamber was first thoroughly cleaned and air-tightened. Then, the air in the chamber was evacuated entirely using the vacuum pump. A gas needle valve allowed the required air pressure, and a Pirani gauge measured the pressure. The circular electrodes inside the chamber were fixed perpendicular to the axis and were separated by a distance is 3cm. The potential is applied between two electrodes. After getting steady discharge plasma, the Ag nano/PANI film surface was exposed perpendicularly to the axis through the Teflon stick. The discharge potential and base pressure were kept constant at 400v and 0.3 bar, respectively. Next, the film was treated, and after the plasma treatment, the treated film was analyzed. The result of the treated film was compared with that of the untreated film.

2.2 AC Conductivity

The AC conductivity IPANI + (5% -25%BHS FA)) +Ag; using Wayne Kerer Precision impedance analyzer 6500B in the frequency range of 20Hz to 1.0 KHz (UK). In the present study, five samples of every composite with variation in their wt. % are explored for their frequency-dependent conductivity.
The equation of the AC conductivity

$$AC = \frac{d}{A} \qquad (1)$$

"d" is the thickness, and "A" is the sample area.
The real (ε') and imaginary (ε") part of the complex dielectric permittivity
(ε = ε'- iε") are computed using the equations

$$\varepsilon' = \left(\frac{C_p}{C_0}\right) \qquad (2)$$

Where, $C_0 = 0.08854 \times \left(\frac{A}{d}\right)$ is the geometrical capacitance whose dimensions are same as the sample.

$$\varepsilon'' = \frac{\varepsilon'}{\left(\omega C_p R_p\right)}$$

According to the pair approximation, frequency-dependent conductivity is evaluated using the relaxation mechanism. Even though the pair approximation technique can provide reliable results at high frequencies, but breaks down at low frequencies. At low frequencies, the percolation path prevails throughout the sample in the DC limit if the DC conductivity is due to the exact electronic transport mechanism between localized states, as is responsible for AC conductivity.

3. RESULTS AND DISCUSSION

3.1 FTIR Analysis

Figure 1 (a) and (b) shows the FTIR spectrum of untreated and plasma-treated polyaniline-based Fly ash and Ag composites. As depicted in fig 1(a), a characteristic broad bond appears at 3422 and 2984 cm^{-1}, corresponding to polyaniline's N-H stretching. The absorption band near 1660 cm^{-1} corresponds to quinoid, and 1530, 1440 cm^{-1} belongs to benzenoid rings. The presence of benzoquinone is witnessed from a peak around 850 cm^{-1}.

The peaks at 1380 and 1290 cm^{-1} correspond to various metal oxides in the Fly ash, as shown in fig1 (b). Absorptions at 1180, 1140 and 997 cm^{-1} correspond to FA constituents in Polyamine-Fly ash composite. In addition, after the plasma treatment, some new bonds are found at 3900, 2300, 2700 and 3100 cm^{-1}, corresponding to -OH, C-H, and C=O. Moreover, the intensities of plasma-treated samples' bonds vary due to the plasma etching process.

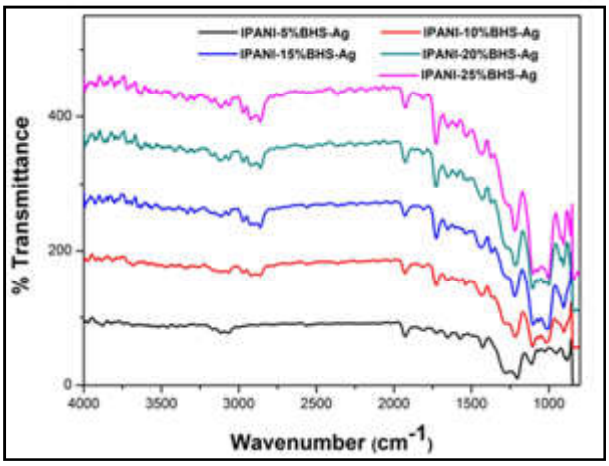

Fig.1(a) FTIR Spectrum of Untreated IPANI-BHS-Ag

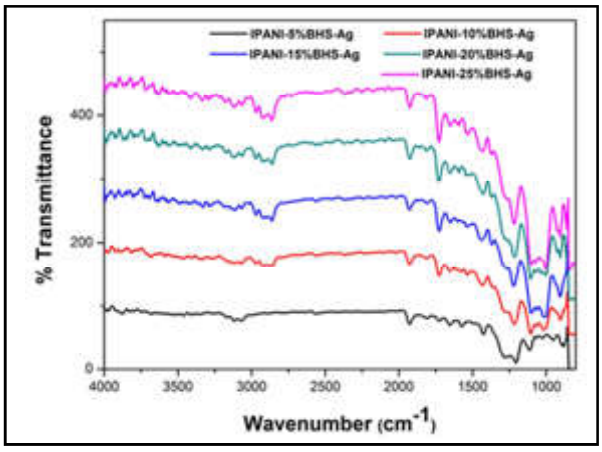

Fig. 1(b) FTIR Spectrum of plasma treated IPANI-BHS-Ag

3.2. XRD Analysis

The XRD patterns of untreated and plasma-treated IPANI-based fly ash and Ag composites are depicted in Figures 2 (a) and (b). The XRD pattern shows polycrystalline nature, and two major broad peaks are observed in 2č = 25.12o and 2č = 37.32o, which have been identified as the single phase of cubic structure with diffraction planes of (110) and (111). However, two other peaks with less intensity are observed at 2č = 8.37o and 2č = 29.13o. No remarkable structural change was observed in both untreated and plasma-treated samples, but the composite intensity increased considerably after plasma treatment, as shown in figure 2(b).

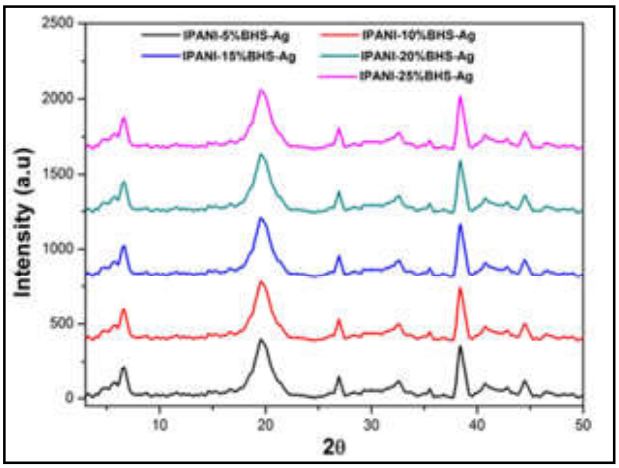

Fig 2 (a) XRD Pattern of Untreated IPANI-BHS-Ag

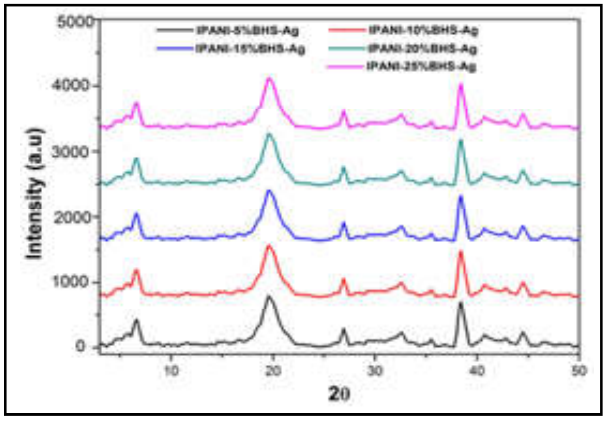

Fig.2 (b) XRD Pattern of Plasma treated IPANI-BHS-Ag

3.3. SEM Analysis

Figures 3 a and 3. b shows the homogeneity of the SEM images of untreated and plasma-treated IPANI-based Fly ash and Ag nanocomposites. As revealed in images (g) and (h), fly ash has hollow spheres with a regular smooth texture on the IPANI surface. After

plasma treatment, some roughness developed on the surface texture of the PANI composite. It is due to the etching of silver particles into the porous area of the polyaniline.

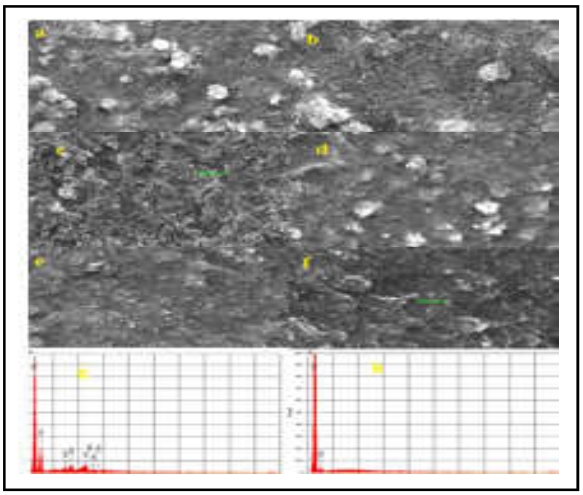

Fig.3 SEM and EDAX Images of Untreated (a, b, c, d, e & k) and Plasma Treated (f, g, h, i, j & l) IPANI-BHS-Ag

3.4. UV-Vis Spectroscopy Analysis

The UV spectrum of untreated and plasma-treated IPANI-based fly ash and Ag nanocomposites are shown in Figures 4 (a) and (b). UV visible spectrum is an efficient tool for identifying the extent of conjugation in conducting polymers. A characteristic bond is observed at 788 nm, attributed to the n-đ* bond, as shown in figure4 (b). There is no bond transition when the weight percentage is between 5 to 10. At the same instant, there is a redshift from 788 nm to 790 nm and 790 nm to 810 nm with a weight percentage of 15 to 25% for FA composites as shown in figure 5(b) with decreasing band gap (4.504 eV to 4.186 eV and 4.186 eV to 3.689 in its transition).

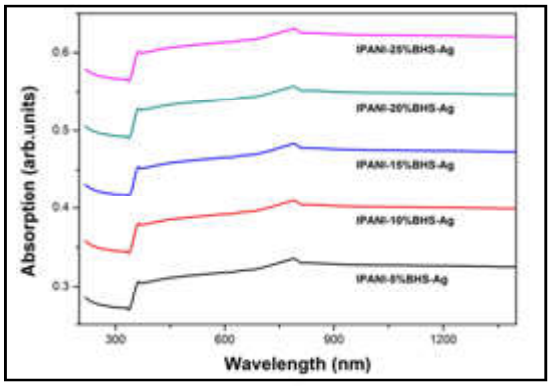

Fig 4 (a) - UV Spectrum of Untreated IPANI-BHS-Ag.

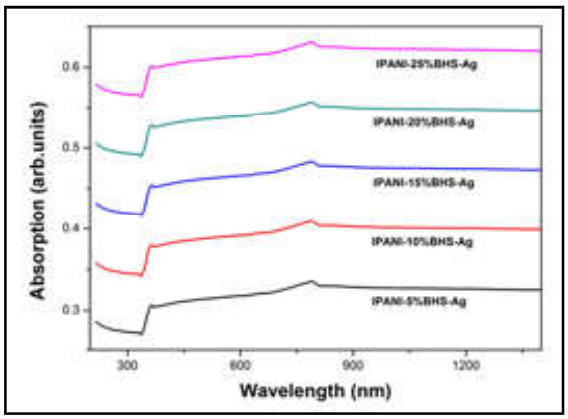

Fig 4 (b) UV Spectrum of plasma treated IPANI-BHS-Ag

3.5 TG-DTA Analysis

TGA is widely used to study all the physical processes involving weight changes to measure a sample's diffusion characteristics and moisture uptake. Figure 5 shows the TG-DTA analysis of untreated (a, c), plasma treated (b, d), IPANI-based FA and Ag composite. In DTA analysis, the sample is stable at 230şC with an endothermic peak at 400oC. This is attributed to the dehydration of IPANI. A 3-5% weight loss is observed within the temperature zone 100ş - 200şC during the first stage. During the second (201ş - 400şC) and third stages (401ş - 700şC), the sample loses 10-20 % and 90% of weight, respectively. The FA increment in the IPANI composite leads to weight loss indicating the interaction of polyaniline with mineral matter contained in the FA. No significant change was observed in the TG-DTA analysis of the plasma-treated sample.

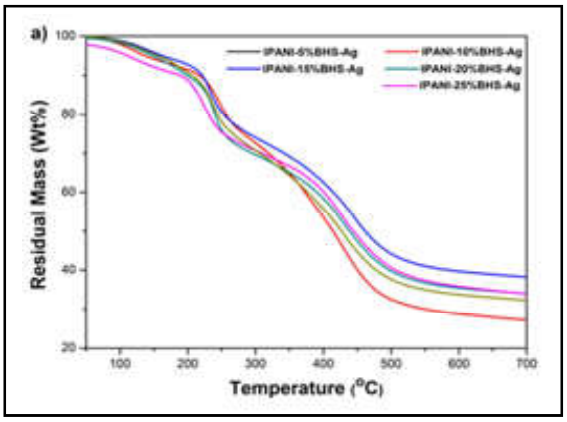

Fig. 5 (a) - TG-DTA Analysis of Untreated IPANI-BHS-Ag

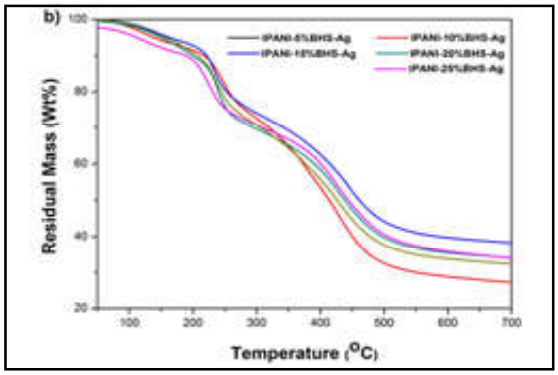

Fig 5 (b) TG-DTA Analysis of Plasma Treated IPANI-BHS-Ag

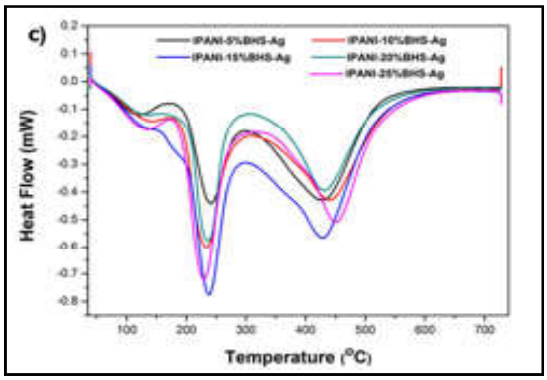

Fig. 5 (c) TG-DTA Analysis of Untreated IPANI-BHS-Ag

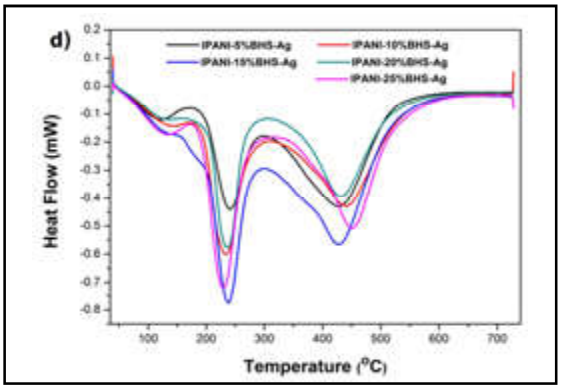

Fig 5 (d) TG-DTA Analysis of Plasma Treated IPANI-BHS-Ag

3.6 DC Conductivity Analysis

A plot of DC conductivity (ó dc) of untreated and plasma-treated IPANI-based FA and Ag nanocomposite versus temperature is shown in Figure 6. It has been observed that the conductivity of the composite increases with an increase in temperature, representing the conducting nature of the polymer composite. The increment in conductivity is due to charge transfer between the polymer chain and the composite material. Moreover, the study established a linear relationship between conductivity and temperature, indicating the behaviour of the disordered conducting polymer. Furthermore, the contribution of Ag may be formed into polarons and bipolarons bonds in the wide band gap of composites. The functional group modification provides enhanced conductivity after the plasm treatment, as presented in Figure 6 (b).

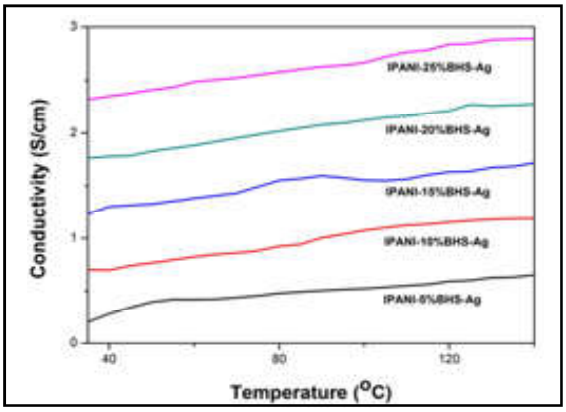

Fig.6 (a) Conductivity Analysis of Untreated IPANI-BHS-Ag

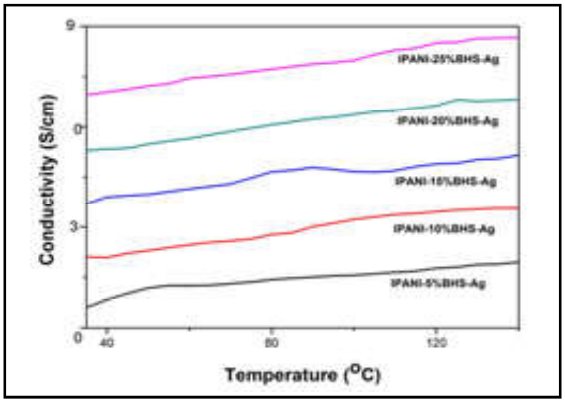

Fig.6 (b) Conductivity Analysis of Plasma Treated IPANI-BHS-Ag

3.7 AC Conductivity

Figure 7 (a) shows the variation of AC response as a function of frequency for untreated Plasma for IPANI + (5% -25% BHS (FA)) + Ag. It is observed that there is a slight increase in the conductivity of all the compositions up to 105 Hz, and the curve appears to be flattened. Among all the compositions, superior conductivity is recorded for ten wt. % BHS FA whereas the remaining compositions have poor conductivity. The decrease in conductivity values may be attributed to the presence of fly ash particles of larger dimensions, which makes the hopping of charge carriers between the favourable sites more difficult.

Figure 7 (b) shows the variation of Ac conductivity as a function of frequency for treated Plasma for IPANI

+ (5% -25% SFA (FA)) + Ag. Like untreated Plasma, the treated Plasma exhibits the same characteristics up to 105 Hz. Similarly, the same sort of trend is observed for ten wt. % BHS FA and all other compositions follow the same tendency as untreated Plasma with a slight increment in conductivity. Because of the formation of excess charge carriers (polarons). In this particular weight percentage of PANI/FA composites, polarization due to hopping conduction dominates.

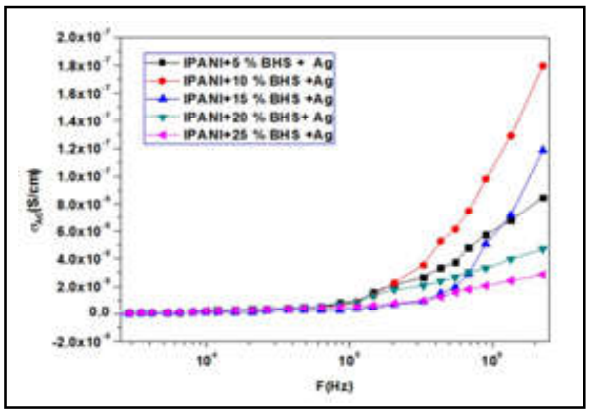

Fig.7 (a) Frequency dependence AC conductivity of untreated IPANI+BHS+Ag

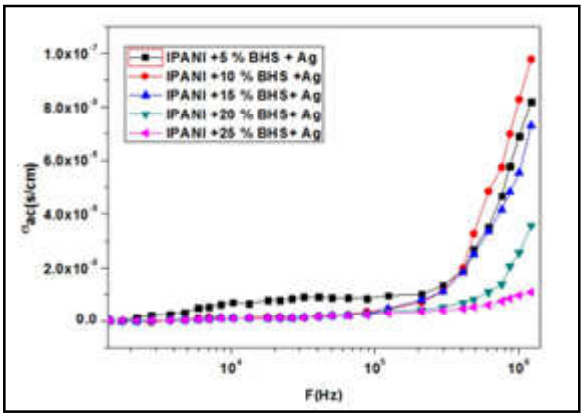

Fig.7 (b) Frequency dependence AC conductivity of plasma treated IPANI+ BHS+ Ag

4. CONCLUSION

With the aid of the in-situ polymerization method, different composite films consisting of Interfacial polyaniline (IPANI) /fly ash(FA)/silver are prepared by various concentrations of FA. It is then subjected to surface modifications using DC glow plasma discharge techniques. Fourier characterizes these samples transforms infrared spectroscopy (FTIR), X-ray diffraction (XRD), scanning electron microscopy (SEM), UV and TG-DTA. The spherical structure is observed for the composite film with 15% FA concentration compared to all other compositions of FA. The exact composition also has excellent transport capacity along with conducting characteristics. This characteristic might positively impact industrial and technological developments as well as relevant application areas.

REFERENCES

[1] A.B. Kaiser, Rep. Prog. Phys.Vol.64, 2001.

[2] A.B. Kaiser, Adv. Mater. Vol.13, 2001, pp.927.

[3] J.E. Albuquerque, L.H.C. Mattoso, D.T. Balogh, R.M. Faria, J.G. Masters and A.G. MacDiarmid, "A Simple Method to Estimate the Oxidation State of Polyanilines", Synthetic Metals, Vol. 113, 2000, pp.19-22.

[4] D.C. Schnitzler, M. S. Meruvia, I. A. H. Mmelgen and A.J.G.Zarbin,"Preparation and Characterization of Novel Hybrid Materials Formed from (Ti,Sn)O2 Nano-Particles and Polyaniline", Chemistry of Materials, Vol.15, No.24, 2003, pp.4658-4665.

[5] F. Huguenin, G.M. Janete, E.A. Ticianelli and R.M. Torresi, "Structural and Electrochemical Properties of Nanocomposites Formed by V2O5 and Poly (3-Alkylpyrroles)", Journal Power Sources, Vol.103, 2001, pp.113-136.

[6] V.A. Samoylov, Q. Hao, M.Y. Shirshov, C. Swart, E. Pringsheim, M.V. Mirsky and O.S.Wolfbeis, "Nanometer- Thick SPR Sensor for Gaseous HCl", Sensors & Actuators, Vol.106, 2005, pp.369-372.

[7] M. Ando, C. Swart, E. Pringsheim, M.V. Mirsky and O.S. Wolfbeis, "Optical Ozone-Sensing Properties of Poly (2-Chloroaniline), Poly (N-Methylaniline) and Polyaniline Films", Sensors & Actuators B, Vol.108, 2005, pp.528-534.

[8] W. Schultze and H. Karabalut, "Electrochemical Copolymerization of M-Toluidine and O-Phenylenediamin", Electrochimica Acta, Vol.50, 2005, pp.1739-1745.

[9] H. Bai and G. Shi, "Gas Sensors Based on Conducting Polymers", Sensor, Vol.2, 2007, pp.267-307.

[10] B.D. Malhotra, A. Chaubey and S.P. Singh, "Prospects of Conducting Polymers in Biosensors", Analytica Chimica Acta, Vol.578, 2006, pp.59-74.

[11] D.C.Trivedi, "Handbook of Organic Conductive Molecules and Polymers", Wiley, Chichester, 1997, pp.505-572.

[12] R. Khan and M. Dhayal, "Chitosan/Polyaniline Hybrid Conducting Biopolymer Base Impedimetric Immunosensor to Detect Ochratoxin-A", Biosensors & Bioelectronics, Vol.24, 2009, pp.1700-1705.

[13] R. Khan, A.Kaushik and A.P. Mishra, "Immobilization of Cholesterol Oxidase onto Electrochemically Polymerized Film of Biocompatible Polyaniline-Triton X-100", Materials Science and Engineering: C, Vol.29, 2009, pp.1399-1403.

[14] R. Khan, P.R. Solanki, A. Kaushik, S.P. Singh, S.Ahmad and B.D. Malhotra, "Cholesterol Biosensor Based on Electrochemically Prepared Polyaniline Conducting Polymer Film in Presence of a Nonionic Surfactant", Journal of Polymer Research, Vol.16, 2009, pp.363-373.

[15] A. Ansari, R. Khan, K.N. Sood and B.D. Malhotra, "Polyaniline-Cerium Oxide Nanocomposite for Hydrogen Peroxide Sensor", Journal of Nanoscience & Nanotechnology, Vol.9, 2009, pp.4679-4685.

[16] A. Kaushik, J. Kumar, M.K. Tiwari, R. Khan, B.D. Malhotra, V. Gupta and S.P. Singh, "Fabrication and Characterization of Polyaniline – ZnO Hybrid Nanocomposite Thin Film", Journal of Nanoscience & Nanotechnology, Vol.8, 2008, pp.1757-1761.

[17] A. Kaushik, R. Khan, V.Gupta, B.D.Malhotra and S.P.Singh, "Hybrid Cross-Linked Polyaniline -WO3 Nano- Composite Thin Film Using Thermal Vacuum Deposition Technique for NOx Gas Sensing", Journal of Nanoscience & Nanotechnology, Vol.9, 2009, pp.1792-1796.

[18] H. Narayan, H.M. Alemu and E. Iwuoha, Phys. Stat. Sol. (a), Vol.203, 2006, pp.3665.

[19] S.C. Raghavendra, S. Khasim, M. Revanasiddappa, M.V.N. Ambika Prasad and A.B. Kulkarni, Bull. Mater. Sci. Vol.26, 2003, pp.733.

[20] S. Bhattacharyya, S.K. Saha, M. Chakravorty, B.M. Mandal, D. Chakravorty and K. Goswami, J. Polym. Sci. (B): Polym. Phys. Vol.39, 2001, pp.1935.

[21] N.V. Blinova, P. Bober, A.J. Hrom_adkov, A.M. Trchov, J.Stejskal and S.J. Proke, "Polyaniline-silver Composites Prepared By the Oxidation of Aniline with Silver Nitrate in Acetic Acid Solutions, Polym. Int., Vol.59, 2010, pp.437-446.

[22] P. Bober, J. Stejskal, A.M. Trchov and S.J. Proke, "Polyaniline-silver Composites Prepared By the Oxidation of Aniline with Mixed Oxidants, Silver Nitrate and Ammonium Peroxydisulfate: The Control of Silver Content", Polymer, Vol.52, 2011, pp.5947-5952.

[23] Kyung Wha Oh, Seong Hun Kim and Eun Ae Kim "Improved Surface Characteristics and the Conductivity of Polyaniline–Nylon 6 Fabrics by Plasma Treatment", Journal of Applied Polymer Science, Vol.81, 2001, pp.684-694.

[24] Khadija Zubair1, Ahmad Ashraf1, Haseeb Gulzar1, M Fayzan Shakir, Yasir Nawab, Z A Rehan and Iqra Abdul Rashid, "Study of Mechanical, Electrical and EMI Shielding Properties of Polymer-Based Nanocomposites Incorporating Polyaniline Coated Graphene Nanoparticles & Nano Express, Vol.2, 2021, pp.010038.

DEVELOPMENT AND ANALYSIS OF SPAGHETTI INCORPORATED WITH AMARANTHUS CAMPESTRIS LEAVES

V. Chelladurai, M. Harini Kiruthika, G. Pavithra and D. Praveen Kumar
Department of Agricultural Engineering,
Bannari Amman Institute of Technology, Sathyamangalam - 638401, Erode District, Tamil Nadu
Email: chelladurai@bitsathy.ac.in, praveenkumard@bitsathy.ac.in

Abstract

Amaranthus campestris is an annual plant. The edible leaves and seeds are sometimes gathered from the wild and used locally. It is a great provider of vitamins A, C, and folate. As far as the health benefits, spaghetti is a complex carbohydrate with a lower glycaemic index which means it doesn't spike your blood sugar rapidly. Extracts of all plant parts of Amaranthus seem to have medicinal benefits, hence our focus of the current study has been to incorporate Amaranthus with spaghetti. The present work aimed to estimate all the quality parameters, namely texture profile analysis, sensory characteristics, water activity and cooking properties of the developed product (spaghetti incorporated with Amaranthus). The colour richness of the product was tested using Hunter's colour lab and found to be light green colour. The suitable drying temperatures of Amaranthus leaves and Amaranthus Spaghetti were found to be 45 ºC and 50 ºC by drying characteristics analysis. Macronutrients such as protein, ash, carbohydrate, fat, fibre were analyzed for the developed Amaranthus spaghetti. The protein value of the developed product is 19.6 g per100 g. The cooking loss of the product was reported as 8.35 % as it was considered acceptable and indicative of good quality spaghetti. The incorporated product Amaranthus campestris enriches the fibre content with 19.5 g of the developed product. These results proved that the developed product can be consumed by toddlers, women, senior citizens.

Keywords: *Amaranthus Spaghetti, Durum wheat, Proximate and cooking quality analysis*

1. INTRODUCTION

In Italy, pasta used to be delivered by making use of tough wheat and formed into lengthy strands conveying this historic meal a ton nearer to modern-day spaghetti. Anyhow, the main Italian interpretation was once practicable pretty close to vermicelli - pasta identifies that proselyte in English as "little twine." Spaghetti is derived from the phrase Spago, which makes an appreciation in English to string or twine. It is a component of every traditional Italian meal. Similar to pasta, water and milled wheat are combined to make spaghetti which is occasionally fortified with vitamins and minerals. Durum wheat semolina is often used to make spaghetti in Italy. Pasta is often made using refined flour, however whole wheat flour can also be used.

The history of pasta feasts had widespread onsets in the Japanese Mediterranean international locations like Greece and a couple of sections of the Middle East and Arabian Peninsula. There, reflections made development aggregate have been unique in colourful approaches to the meals that were once used on generic day-to-day exercise in Ancient Roman Conglomerate. As per the records of archives, the instant launch of Italian pasta got here in India from the Arab supper called "itriyya" which used to be as often as viable portrayed by way of the Greeks as "dry pasta." Excerpts of all plant components of *Amaranthus campestris* look to have medicinal benefits. Notwithstanding toddlers are ready to take fast food sources like maggi, pasta, etc., which are not valuable. So, it would be rearing the most cherished substance, especially for pampers. Several researches had been made to analyze the cooking and nutritional qualities of spaghetti. The optimum cooking time was observed as 12 min for bran containing spaghetti [1]. Similarly, cooking time was observed to be 4 to 16 min for spaghetti made of different cereal materials [2]. The microstructure changes of dough and spaghetti depends on the type of ingredients and the process of cooking [3]. The pre gelatinization on dough properties in making quinoa spaghetti resulted in increased cooking loss percentage and water activity [4]. The digestibility and caloric content of spaghetti was decreased while replacing 50 % of durum wheat semolina with oat bran [5]. The dry spaghetti significantly reduced

the susceptibility of spaghetti to pancreatic digestion in vitro compared to the control at all concentrations [6]. Hence the main focus of our research had been to create awareness of the medicinal components of Amaranthus Spaghetti.

A study has been developed with the main objective of developing and analysing the Spaghetti incorporated with Amaranthus. To achieve this objective following sub-objectives were framed for this study: analyze the drying characteristics of amaranthus spaghetti, determine the chemical compositions using proximate analysis, TPA test to examine the hardness, brittleness, stickiness, evaluate its colour using hunter's color lab, and analyze the properties on cooking qualities of the developed amaranthus spaghetti.

3. METHODOLOGY

3.1 Amaranthus Campestris Leaves

Green leafy vegetables comprise a great variety of bioactive non-nutritive health-promoting compounds together with antioxidants and phytochemicals, which deliver health benefits beyond simple nutrition [7]. Green leaves are an accurate supply of macronutrients specifically carbohydrate, protein, and fibre content. Leafy greens moreover act as anti- diabetic, anti-histaminic, anti-carcinogenic and anti-inflammatory agents because of their practicable richness in antioxidants and phytochemical content.

Fig.1 Amaranthus campestris leaves

3.2 Durum Wheat Flour

Durum wheat is known as pasta wheat or macaroni wheat (Triticum durum or Triticum turgidum subsp. Durum), is a tetraploid species of wheat. It is the second maximum cultivated species of wheat after common wheat, even though it represents almost 5% to 8% of worldwide wheat production (Source: Encyclopedia of Life, 2021). The presence of excessive protein content material in the wheat is the gluten community that's giving excessive power to the dough. Durum consists of 27 % extractable wet gluten, approximately 3 % better than common wheat (T. aestivum L.).

3.3 Amaranthus Spaghetti

Extracts of all plant additives of *Amaranthus campestris* seem to have medicinal benefits. Hence our centre of interest of present-day studies has been to end up with the aware about the healing substances of amaranthus from the fit to be eaten leaves. The entire spaghetti products are fortified with beneficial compounds of Amaranthus spaghetti. The dietary and sensory attribute differs in contrast to present products. In the modern world, the advantages of campestris have been identified to adults and they're ready to intake. When it involves toddlers, it's miles a complicated. In addition, kids are organized for quick food reasserts like Maggie, pasta, cake, etc., which might be now not valuable. So, it'd be rearing maximum loved sustenance for mainly pampers. The methodology of spaghetti making is given in below flow chart.

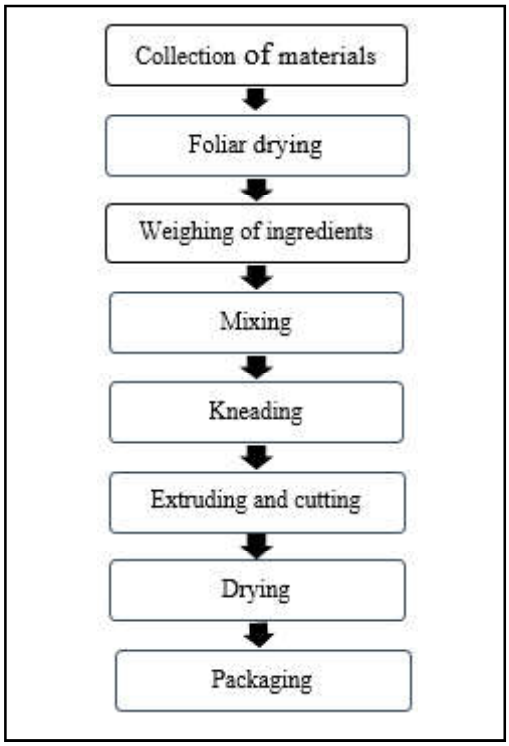

Fig.2 Process Flow chart for making Amaranthus Spaghetti

3.4 Drying of Spaghetti

Drying is utmost difficult and basic parts of making spaghetti. If the pasta dries too excessively, it might break during or after the drying process and obtain an

unfortunate appearance and it may bring down the mechanical strength [8]. Assuming that the spaghetti dries too slowly, it might ruin and become mouldy.Consideration to these lines, the drying process should be carefully executed to keep away from the two previously mentioned results. Whenever the pasta leaves the extruder die, it has a moisture content of 31 %. The final desired moisture of the dried pasta is around 12 %, for the pasta to be unbending and have a long stockpiling life. Here the spaghetti strands were taken as three samples of each 100 g and dried in three different temperatures 50, 60 and 70єC for about 105 minutes.

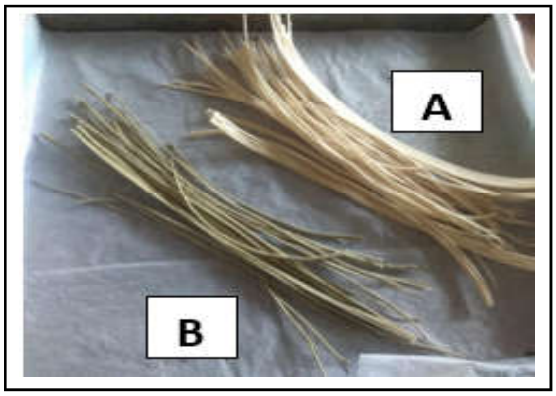

Fig.3 A- Regular Spaghetti, B-Amaranthus Spaghetti

3.5 Instrumental Measurements

3.5.1 Colour Measurements

The color dimension was estimated for the samples - amaranthus powder, dried spaghetti and dried Amaranthus Spaghetti with the aid of using Hunter Color Lab (CIE 1976, Hunter Associates Laboratory, Inc., Virginia, US). The samples were taken, kept in the sample holder and the readings were noted. It is a cleared out that colorimeter which separates the coloration into 3 exclusive dimensions that is the L*, a*, b* values. L* shows the light/darkness of the sample, a* shows red/ green values, b* shows yellow/blue values.

3.5.2 Texture Profile Analysis

The TA-XT2i Texture Analyzer (Stable Micro Systems Ltd., Godalming, and Surrey, UK) ыtted with a 25 kg load cell turned into used. The spaghetti samples have been located adjoining to each other centrally below the compression platen of pasta ыrmness/stickiness rig. The process was carried out by using aluminium cylindrical probe which compresses the sample and the graphical representation was drawn out as a result. The diverse textural parameters are drawn out with the use of the resulted Force-Time Curve.

3.6 Sensory Analysis

The samples of spaghetti have been cooked using distilled water with optimum cooking times. Five panellists were asked to assess the sensory attributes of spaghetti by hedonic scale. The aforementioned textural factors have been tested: hardness, the spaghetti‘s resistance become measured by compressing the noodle strands in opposition to the palate with the tongue. Adhesiveness is evaluated by figuring out the pressure required to cast off the spaghetti with the tongue, that is pressed in opposition to the palate. Chewiness measures the range of chews of constant force application before swallowing. Cohesiveness is measured by the disintegration of spaghetti strands take region below mechanical action. Springiness - at which the product keeps to its unique form after the partial compression.

3.7 Analytical Measurements

3.7.1 Protein Content

Protein content of cooked spaghetti was analyzed by the standard Kjeldhal method (Tulin Equipments, Chennai, Tamil Nadu, India) and expressed in a percent dry basis.

3.7.2 Fat Content

The fat content was estimated by Soxhlet method (Tulin Equipments, Chennai, Tamil Nadu, India).

3.7.3 Fibre Content

The fibre content in the product was estimated using the Fibrotron method (Tulin Equipments, Chennai, Tamil Nadu, India)

3.7.4 Ash Content

The ash content was determined using the sample taken from previous tests (fibre) and it was kept in a muffle furnace (Tulin Equipments, Chennai, Tamil Nadu, India) for 5 hours at 500° C.
Ash content(g) = Crucible weight with sample - Empty crucible weight

3.7.5 pH Value

The pH of the spaghetti was measured by the sample dissolved completely in distilled water using portable pHep pH Tester (Hanna Instruments Manufacturer, Chennai, Tamil Nadu, India).

3.7.6 Water Activity

Water is the most important factors controlling the rate of deterioration of food by either microbial or non-microbial effects. Water activity (5ШNЬ5ШdЬ) is used for the preservation of food, stabilization of the food supply, and developing the different types of shelf-stable food. At first, a small amount (approx. 5 g) of sample was taken, and placed in the sample holder of water activity analyzer (Meter Aqualab PRE, Benchtop Water Activity meter) and the value in the screen was noted down as the water activity of the sample

3.7.7 Calorie value

The total calorie value of the spaghetti was measured using Atwater general factor system which is based on the heat of combustion of carbohydrate, protein, and fat (FAO - Food energy: methods of analysis and conversion factors)

3.8 Cooking Quality Analysis

3.8.1 Optimal Cooking Time

The optimal cooking time was analyzed using AACC Approved Method 66-50 (AACC, 2000).

3.8.2 Cooking Loss

Cooking loss is estimated as the amount of solid substance lost in the cooking water and it was determined by using AACC Approved Method 66-50 (AACC,2000).

3.8.3 Water Absorption

Water absorption is reported as the percent increase in the weight of cooked spaghetti with reference to dry spaghetti by using AACC Approved Method 66-50 (AACC, 2000).

$$\text{Water absorption (\%)} = \frac{W_c - W_{uc}}{W_{uc}} \times 100$$

where,
W_c = Weight of cooked spaghetti (g)
W_{uc} = Weight of uncooked spaghetti (g)

3.8.4. Swelling Index

At optimal cooking time, 50 g of spaghetti was cooked in 750 ml of boiling water. Further the cooked spaghetti was rinsed with 100 ml of cold water and it was drained for 30 seconds. The diameter of spaghetti strands was determined using Vernier caliper before cooking and after cooking. Using the diameters, the swelling index was found by below formula.

$$\text{Swelling index (\%)} = \frac{D_c - D_{uc}}{D_{uc}} \times 100$$

where,
D_c = Diameter of cooked spaghetti (mm)
D_{uc} = Diameter of uncooked spaghetti (mm)

4. RESULTS AND DISCUSSION

4.1 Drying Characteristics of Spaghetti

After extrusion, immediately the spaghetti strands were equally weighed before drying and placed in the tray dryer. Periodically, its weight was calculated until it attains its concurrent value. And this drying experiment was conducted in three different temperatures.

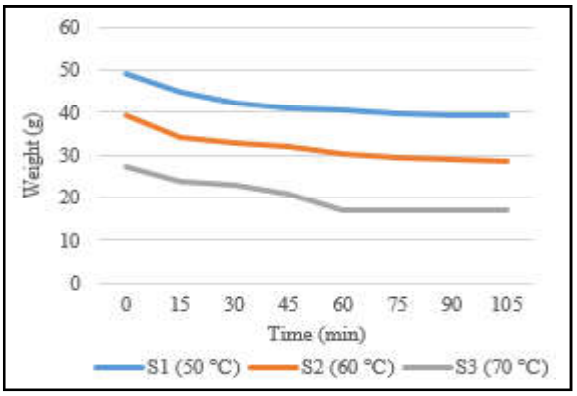

Fig.4 Drying characteristic analysis

By inferring this data, the temperature at 50єC is considered to be the most effective as it decreases gradually and it shows concurrent readings after 1 hour.

4.2 Instrumental Analysis

The hardness of the spaghetti is the peak force of compression. The resulted peak force or hardness of control and the product is found to be 9.8 Kg and 9.7 Kg respectively. The colour evaluation is done to assess the product's colour as it gives immediate impression for the consumers about the freshness, flavor, and quality of the product and also urge them to consume the product. With inference the developed product is green in colour as the a* value was negative.

Table 1 Hardness and Colour Estimation

Sample	Hardness (kg)	Colour Measurements		
		L*	a*	b*
Control	9.8	86.84	1.22	11.87
Product	9.7	67.41	-2.01	18.76

4.3 Analytical Measurement

Macronutrients such as protein, ash, carbohydrate, fat, fibre were analyzed. On reviewing research papers, the protein content of the commercial spaghetti was 18.2% for 100 g of serving whereas the protein value of the newly developed product was 19.6 % for 100 g. The incorporated product Amaranthus campestris enriches the fibre content of the developed product with 19.5% of fibre compared to the commercial spaghetti. The improvement in calorie value of the product (217 kcal) was observed when compared with commercial spaghetti (170 kcal) which might be due to the nutritional value of amaranthus incorporated with spaghetti.

Table 2. Results of Proximate Analysis

	Control	Product
Protein (%)	18.2	19.6
Fat (%)	2.5	3.1
Fibre (%)	15.2	19.5
Ash (%)	1.0	1.4
pH	6.1	6.1
Water activity (a_w)	0.559	0.561
Calorie value (kcal)	170	217

4.4 Cooking Quality Analysis

As per research, the cooking loss of 12% or less was considered acceptable and indicative of good quality spaghetti. Here the cooking loss for the control and product were reported as 8.78% and 8.35% respectively. Optimal cooking time was assessed until the disappearance of white core in the spaghetti. As a result, it takes approximately 7-8 minutes. The total intake of water of the spaghetti while cooking by calculating its weight before and after cooking and percent absorption for control and product were 289.76% and 218.90% respectively.

Table 3 Results of Cooking Quality Analysis

Properties	Control	Product
Optimum cooking time (min)	7.5	8.0
Cooking loss (%)	8.78	8.35
Water absorption (%)	218.90	289.76
Swelling index (%)	15.57	36.47

5. CONCLUSIONS

From the intending discussion and assessment of outcome, it may also be summed up those elements in particular wheat flour stage caused an extremely good impact on spaghetti. The result of existing studies shows that Amaranthus campestris powder can be utilized for the compensation of gluten in spaghetti. Spaghetti samples have been formulated from one of the type aggregates of wheat flour and *Amaranthus campestris* powder. Incorporation of *Amaranthus campestris* and semolina will increase the water absorption capability due to greater fiber content of Amaranthus and protein content of semolina which absorbs higher water compared to control. The spaghetti prepared from the blends of 95% durum wheat flour and 5% Amaranthus have additionally scored higher sensorial acceptability and the incorporated product enriches the fibre content of the developed product with 3.2 g of fibre than regular spaghetti. So, the product can be consumed by Toddlers, women, senior citizens etc.

REFERENCES

[1] N. Sozer, A.C.Dalgic, and A.Kaya. "Thermal, Textural and Cooking Properties of Spaghetti Enriched With Resistant Starch", Journal of Food Engineering, Vol.81, No.2, 2007, pp. 476-484.

[2] A. Sobota, P. Zarzycki, Z. Rzedzicki, E. Sykut-Domańska and A. Wirkijowska, "Effect of Cooking Time on the Texture and Cooking Quality of Spaghetti", Acta Agrophysica, Vol.20, No.4, 2013, pp. 693-703.

[3] N. Gulia, V. Dhaka and B. Khatkar. "Instant Noodles: Processing, Quality, and Nutritional Aspects", Critical Reviews in Food Science and Nutrition, Vol.54, No.10, 2014, pp.1386-1399.

[4] C. Caratini and K.A. Rosentrater, "Developing and Testing Gluten Free Spaghetti Using Quinoa", Journal of Food Research, Vol.8, 2019, pp.20-32.

[5] V. Espinosa-Solis, P.B. Zamudio-Flores, J.M. Tirado-Gallegos, S. Ramírez-Mancinas, G.I. Olivas-Orozco, M. Espino-Díaz and R. Baeza-Jiménez, "Evaluation of Cooking Quality, Nutritional and Texture Characteristics of Pasta Added With Oat Bran and Apple Flour", Foods, Vol. 8, No.8, 2019, pp.299.

[6] S. Chillo, J. Laverse, P. M. Falcone and Matteo Alessandro Del Nobile, "Quality of Spaghetti in Base Amaranthus Wholemeal Flour Added With Quinoa, Broad Bean and Chick Pea", Journal of Food Engineering Vol.84, No.1, 2008, pp.101-107.

[7] Suresh, Lagna and K. Ashok, "Nutritional Activity, Antioxidant and Anti Arthritic Activity of Selected Green Leafy Vegetables", Int. J. Home Sci, Vol.2, No.3, 2016, pp.85-88.

A SYSTEMATIC REVIEW OF BACTERIA BASED SELF HEALING CONCRETE: MACHANICAL, DURABILITY PROPERTIES AND BOMINERALIZATION.

M. Rajendren[1], V. Logumani[2], D.K. Sri Saran[3] and S. Subhashitha[4]
[1,2&3]Department of Civil Engineering,
[4]Department of Bio-Technology,
Bannari Amman Institute of Technology, Sathyamangalam - 638401, Erode Distrct, Tamil Nadu
E-mail: rajendranm@bitsathy.ac.in, logumaniv99@gmail.com,

Abstract

Concrete naturally contains micro cracks and air voids. This allows harmful compounds like chloride and carbon dioxide enter the concrete and destroy THE structures. to avoid the deteriation. The concrete must be reclaimed. Self-healing method is one of the best practices to deal with these situations. The supply of calcium source and urease-production the concrete in calcite precipitates. Bio-mineralization techniques are proven to heal microcracks and air voids in concrete. A continuous hydration process can be used in concrete to bond over newly formed microcracks. Due to combination of calcium carbonate precipitation Bacillus Subtilis and calcium the newly microcracks are formed. The pore structure of the concrete was improved, and bacteria concentrations were controlled for better results. That the use of bacteria can improve the strength and durability of concrete and gives better results than the direct application method. The compressive strength is increase by maximum 12% with 0.5% of calcium lactate and bacteria added to the concrete. Biochemical studies revealed microbiologically Induced CaCO3 precipitation consists of three distinct stages and is independent of the calcium source. Precipitation rate Calcium lactate was twice as high as calcium nitrate, indicating that the organic source of calcium lactate may be high Beneficial to cell function, it is directly related to urease Production and deposition of CaCO3. CaCO3 crystals were present identified as calcite, although the morphological type varies the source of calcium is different. Bacteria also confirmed. The cells served as nucleation sites for crystal formation and growth. The microbial crack healing potential appeared not only at very easy ages but increasing gradually over time that the maximum width of the could be completely healed was up to 450 μm in 120 days. The advantages of using bacteria decrease water penetration and chlorine ion permeability.

1. INTRODUCTION

Aging infrastructure is a major challenge in major economic powers such as the United States and China, requiring huge investment in repair and rehabilitation. For example, 42% of all bridges in the United States are over 50 years old and require an immediate investment of $125 billion in repair and rehabilitation procedures [1]. As a result, in the last few decades. The main repair techniques are the use of self-healing of unreacted cement particles (especially in Ultra High-performance concrete structures) [2]. Polymeric resins (e.g., epoxy, vinyl ester and polyester), Waterproofing chemicals, polyester [3]. Alternative bonding agents (e.g., alkali-activated materials) are practiced [4]. However, In many cases, lack of cost effectiveness [5]. High environmental impacts [6]. Coherent and homogenous scarcity Interfacial transition zone (ITZ), delamination problems (especially for polymer-based materials [7]. Challenges on the real site applications (e.g., liquid activator handling for alkali-activated materials) [8]. Coating is the most recommended and suitable durable protection methods used on concrete surfaces Structures [12]. Three different methods are used to apply microbe-induced curing to concrete, including direct addition of bacteria. In the mixture, incorporating the bacteria into the mixture to keep the bacteria inactive until they are inactivated and spraying or injecting the bacteria on the crack surface [23]. In all these cases, an organic diet is essential to ensure that the cells can grow and react as yeast extract [24]. Although they have been some recent research studies on the production and use of bacterial concrete [15,28]. Most among them mainly focus on the direct effect of bacterial admixture on the mechanical

properties of concrete. In addition, they A mere statement, completely ignoring the microbiological and durability properties and characteristics of bacterial concrete Improved mechanical properties resulting from incorporation of bacterial strains. Gri No et al [29]. The relatively low tensile strength of concrete and the interaction of various load and non-load factors make cracking inevitable. Various factors such as plastic shrinkage, drying shrinkage, thermal stresses, external loading, corrosion of rebar or the combined effects of several factors can cause cracks. For example, microcracks may form as a result of compression but begin to propagate at lower stress levels when an external load is applied. These cracks allow chemicals and moisture to seep into the cracks and weaken the concrete. Cracks can be repaired manually, but manual maintenance and repair operations have several drawbacks, including cost, accessibility, and environmental impact. Currently, various chemical and cement-based repair materials are used. Cement production accounts for about 7% of the world's anthropogenic CO2 emissions, while chemical curing agents pose risks such as material incompatibility, health hazards, and environmental hazards. Microcracks in concrete can start soon after construction or at an advanced stage, and often go unnoticed until they cause serious structural or durability problems. Another burden is the cost of carrying out routine maintenance on the facilities. Finding a long-term crack healing method that is low cost and does not require manual intervention is essential. Self-healing is an emerging concept for providing high-quality materials with the ability to heal damages, and it has received increasing attention in the last decade for use in building structures. As a result, an efficient self-healing mechanism can significantly reduce repair and maintenance work, as well as environmental and financial impacts. Recently, a sustainable mechanism of self-healing using microbiologically induced precipitation of calcium carbonate has been intensively studied for the closure and healing of cracks. Microbial self-healing involves the precipitation of calcium carbonate in cracks through the direct action of bacterial species. Calcium carbonate precipitation by microorganisms is compatible with concrete and the forming process is environmentally friendly. Bacillus subtilis is known to be harmless to humans. Additionally, oxygen is consumed during the process, so it also reduces the chance of reinforcement corrosion. Bacillus species are well suited for use as a self-healing agent in concrete due to their tolerance to moisture, highly alkaline environments, and their ability to form spores. Bacillus has been a frequently used bio-agent for calcite precipitation in research studies. The aim of the research was to assess whether concrete could self-heal biologically by adding bacteria directly to concrete or adding them after being encapsulated in chemical or inorganic compounds.

2. APPLICATION OF BACTERIA

Generally, the crack healing process in bacterial concrete involves crack propagation, bacterial activation, Chemical reaction, production of CaCO3 and final crack sealing [15,23]. However, adequate hydration of concrete a high pH value is required, which may affect microorganisms. In that case, it is necessary to use a specific bacterial culture to function and grow at the high pH level of the concrete medium [30].

2.1 Effect of pH on Alkaliphile Bacteria and Microbial Growth

Most bacteria are growing under and exist at a pH within one or two pH units of the neutral pH 7. In turn, the type of bacteria that can be used in highly alkaline media, Concrete etc. are known as alkaliphiles. This type of bacteria grows best at a pH between 8 and 10. radical alkaliphiles Mechanisms for maintaining protein structure and proton orientation in the acute environment through evolutionary change in lipids force in an alkaline environment [31]. Such properties of alkaliphiles bacteria play an important role in self-healing properties Concrete. An example of alkaliphile bacteria is Bacillus forums, which collects energy for exchange reactions and movement. Na+ ion gradient (Fig:1) illustrates bacterial classification based on growth at different pH levels.

2.2 pH of Concrete and Bacterial Cultivation

Often, environmental factors play an important role in changing the pH of concrete media [30]. The pH in concrete is the negative logarithm of the concentration of active hydrogen ions expressing the degree of alkalinity. Concrete. The hydration process of cementitious materials generally requires high alkalinity to dissolve the mixture materials. Generally, the pH of conventional concrete is in th:e range of 12-13, which is considered a highly alkaline medium [32]. On this basis, it is common practice to consider it if the overall pH does not fall below 9 to 11 the concrete medium is damaged. In this case, if the pH is in the range of 7-9, the concrete it is in the early breakdown stage, whereby surface damage can

sometimes be clearly seen at this pH level. at pH Near 6, severe deterioration of the concrete is evident, and if the overall pH is 4 or less, repair or replacement is required Concrete components or structures are necessary.

3. BACTERIAL CULTIVATION AND ITS INCORPORATION INTO CONCRETE

Bacterial culture refers to the propagation of microorganisms by placing them in a favourable medium Beef extract, peptone, and urea under controlled conditions [36]. After the cultivation stage, the bacteria can be used in concrete by incorporating directly into the concrete mix, freezing, or spraying and direct injection in these methods, Bacterial spores and calcium lactate are added directly to the concrete mixture after the concrete is mixed [15]. The general properties of this concrete remain the same Increases concrete shrinkage using bacteria and calcium lactate. Here calcium lactate is used as food Facilitates healing of small cracks ~0.4 mm wide by bacterial reaction [3 ,16].

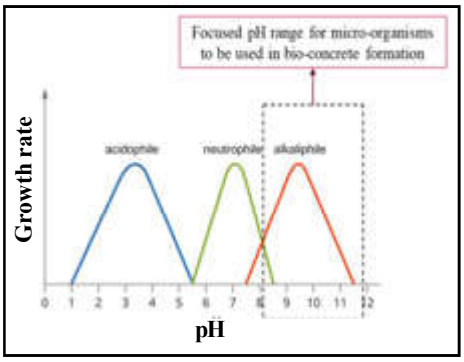

Fig.1 Approximate pH ranges for growth of different types of microorganisms [28]

4. BIOMINERALIZATION

Bacteria attached materials are capable of sealing cracks by forming CaCO3 crystals, which form microcracks and Concrete pores [43]. CaCO3 can be precipitated by a biologically induced mineralization process in the presence of A source of calcium. In this process, carbonate is produced extracellularly by microorganisms through several metabolic pathways. Non-methylotrophic methanogenesis, oxygen and oxidative photosynthesis, organic acid utilization, reduction Calcium sulphate, urea hydrolysis and differential nitrate reduction [44]. (Fig 2) presents the biomineralization process in three steps. (Fig 4) presents a healed crack [45] and (Fig 3) provides further insight into the various modes of biomineralization.

4.1 Autotrophic CaCo3 Precipitation

The word "autotrophic" means that the organism produces something from its own substances, such as carbon dioxide. Mostly uses light as energy. Examples of autotrophic pathways for CaCO3 production are non-methylotrophic methanogenesis, Oxygen and oxidative photosynthesis, which are discussed in the following subsections.

4.2 Non Methylotrophic Methanogenesis

Non-methylotrophic methanogenesis is the process of converting carbon dioxide and hydrogen into methane (Eq. (1). Subsequently, Methane is oxidized anaerobically to carbonate with the help of sulphate acting as an electron acceptor (Eq. 2). This bicarbonate reacts with calcium ions to form CaCO3 (Eq. 3) [27].

$$CO2 + 4H2 \rightarrow CH4 + 2H2O$$

$$CH4 + SO2\text{-}4 \rightarrow HCO\text{-}3 + HS\text{-} + H2O$$

$$Ca2+ + 2HCO\text{-}3 \leftrightarrow CaCO3 + CO2 + H2O$$

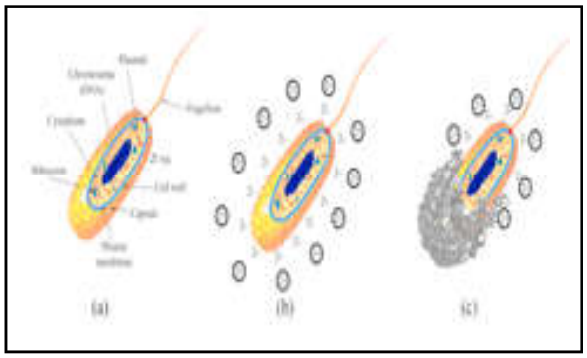

Fig.2 (a) Bacterial structure, (b) negatively charged cell wall and the presence of positively charged ions, and (c) biomineral production by means of binding calcium ions to cell wall [105].

4.3 Anoxygenic Photosynthesis

Figure 4 shows the process of oxidative photosynthesis. In oxidative photosynthesis, hydrogen sulphide acts as an electron donor Therefore, oxygen is not formed. Nevertheless, the oxidative photosynthetic reaction is like that of oxygen photosynthesis [8,9]. Examples of bacteria that undergo oxidative photosynthesis include Halobacterium and Heliobacterium species. Although CaCO3 can be formed by oxidative photosynthesis, it should be noted that this reaction is the only one. Carbon dioxide and light are possible. In other words, for this pathway to be effective in bacterial concretion, it can only be used. Areas of concrete exposed simultaneously to carbon dioxide and light [27].

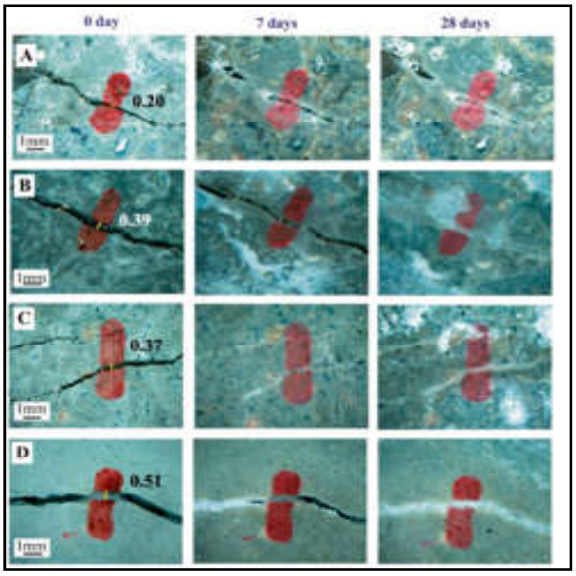

Fig. 3 Calcite precipitation by bacteria in concrete cracks [45]

4.4 Utilization of Organic Acid

Heterotrophic growth of different types of bacterial species on various organic acid salts such as acetate results in production Carbonate minerals [27] In doing so, there are several

A type of bacteria that uses organic acid salts to produce CaCO3. These include Arthrobacter species, Rhodococcus species, and Bacillus species, which are the strains of bacteria most used in bacterial concrete because of their high viability. Alkaline environments. Both Arthrobacter and Rhodococcus species are extremophiles, meaning they can survive in extremely extreme conditions Suitable environments for their use in concrete [48].

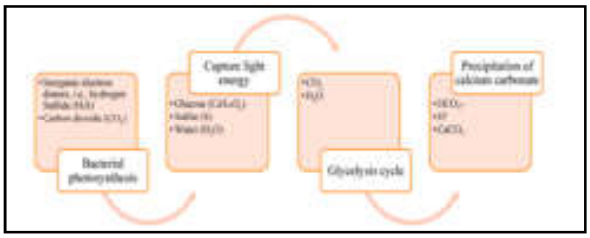

Fig.4 Anoxygenic photosynthesis process

4.5 Reduction of Calcium Sulphate

The sulphur cycle can be used as a pathway to produce CaCO3 by reducing calcium sulphate. For this to happen, a calcium source, all organic matter and sulphate should be present. The first step is the reduction of calcium sulphate to calcium sulphide.

Because this process generally increases the pH of the medium and reduces hydrogen sulphide. It promotes the production of CaCO3 can see [49].

5. BACTERIAL CONCRETE

Many rehabilitation and rehabilitation techniques have been introduced and improved over the past decades Curability and durability properties of damaged concrete. In these techniques, sealants, adhesives, and waterproofing chemicals are used [3]. Generally, in addition to bacteria the mechanical strength and durability of concrete can be increased by filling micro-pores; Therefore, reducing pores that allow water in and Other chemicals seep into the concrete [58]. Methyl methacrylate Recently implemented [57]. However, such chemicals are often expensive, labour intensive, and sometimes hazardous to health Hazards when introducing agents to concrete. In this regard, previous studies [3,22].

5.1 Bacterial Concrete Manufacturing

Bacterial concrete manufacturing process is generally conducted in three stages. In the first step, bacteria are grown A medium with very favourable conditions and adequate nutrition. After the cultivation phase is complete, bacteria are added the concrete medium is placed directly in the mixture or in micro-capsules, which are activated when cracks form [47].

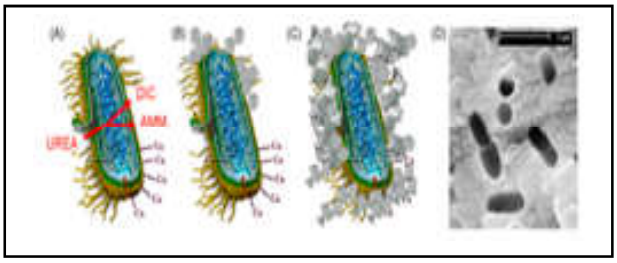

Fig. (a) Urea is added to the cell and produces ammonia, (b) cell is encapsulated by calcium bicarbonate on the surface, (c) concrete closes in on cell and fills the crack, and (d) microscopic image of calcium carbonate coated cells embedded in concrete [47].

5.2 Bacterial Type and Content

Generally, alkaliphilic based bacteria from Bacillus strains are used to make bacterial concrete. Unlike other strains, Bacillus Bacteria are well known to be non-pathogenic and can grow at moderate (mesophilic) temperatures [43]. And can be It can remain dormant for years while withstanding extreme temperatures [59].

As a result of such properties and safety of use, Bacillus megatherium [60], Bacillus mucilaginous [21], Bacillus halodurans [61], Bacillus subtilis [62], Bacillus licheniformis [63,64], Bacillus cohnii [22], Bacillus sphaericus [65], Bacillus pseudofirmus [66], Bacillus cereus [67], and Bacillus pasteuri [68] Bacterial size 103, 105,107 and 109 cfu/ml have been successfully used in concrete. However, a bacterial level of 105 was commonly detected among them Highly suitable and recommended in terms of biomineralization and improvement of physico-mechanical properties of concrete [63 – 68].

5.3 Cement-less Bacterial Concrete

In most cases, the term bacterial concrete refers to the addition of bacterial agents for crack healing purposes. Bacteria form concrete with calcite precipitation as its main binding agent [69,70]. Commonly referred to as bio-cementation, this process also relies on the formation of cementing bridges between solids masses [71]. and has many applications in geotechnical engineering practices such as soil erosion and dust control for purposes [72,73].

6. COMPRESSIVE AND FLEXURAL STRENGTH

The fundamental micro-mechanism for strength restoration and crack healing in bacterial concrete is the transformation of soluble organic matter. Nutrients as inorganic CaCO3 crystals that seal the cracks [21,22]. Recent studies have shown recovery of crack strength by CaCO3 follows a multifactorial criterion approach that can be divided into physical and chemical characteristics in chemistry Characteristics, type, and concentration of bacteria [22]. Another variable affecting the compressive and flexural strength of bacterial concrete is the general nutrient used as feed. A source for bacteria like calcium lactate, calcium nitrate, calcium format, urea and yeast extract Luo and Qian [80].

However, the physical factors affecting the mechanical properties of bacterial concrete are very diverse and include variation in composition Physical properties of composites and cracks. It has been reported in the literature that bacterial concrete follows the same the mechanism of strength gain for normal concrete is that bacteria act as a potential filler in earlier stages Hydration [82.83].

7. MODULUS OF ELASTICITY

Modulus of elasticity refers to the ability of a solid to deform within an elastic stress-strain region without fracture [88-86]. The elasticity of concrete material generally depends on aggregate type and size distribution [87]. This observation may be attributed to the low surface adhesion due to the potential inability of auto-healing in large cracks [94].

8. TOUGHNESS

Toughness is a measure of a material's ability to withstand force and absorb energy without fracture, and is usually is assumed to be the lower part of the stress-strain curve as outlined by Rao et al [43]. Addition of bacteria and nutrients is possible Increase in the slope of the stress strain curve indicates higher hardness in bacterial concrete compared to conventional concrete. Fig 6 Development of high strain and peak stress can be detected in bacterial concrete.

9. EFFECT OF CURING REGIME ON MECHANICAL PROPERTIES

Variation in curing techniques can affect the workability of the concrete mix and adjust the moisture content provided Content in the early stages of abstraction. Generally, the difference between curing regimes is based on temperature, Seal types, and moisture levels (steam and water immersion). In practice, bacterial concrete is cured in water immersion form [95]. Additionally, water curing reduces the overall porosity of hardened concrete by up to 20% [99] and water Up to 10% absorption [100], slightly higher electrical resistivity at 28 days and up to 100% higher electrical resistivity. compared to urea-calcium lactate curing after 150 days of curing [101].

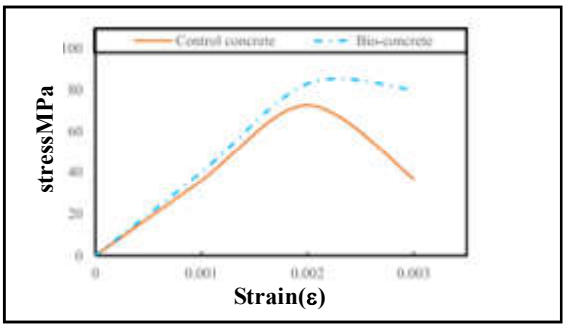

Fig. 6. Stress-strain curve of conventional concrete (control) versus that of bacterial concrete containing Bacillus Subtilis (data from Ref. [43])

10. PHYSICAL AND DURABILITY PROPERTIES

Microbial sealants are a type of waxy technique that involves precipitation of minerals into concrete. Acts as an alternative surface protective treatment (or coating technique) that can be applied to concrete surfaces [102 – 104]. Crack treatments within concrete usually take place in the form of active and passive treatments. In passive treatment, sealants They are injected or sprayed into crack pores to heal or prevent surface cracks [105]. Common concrete test methods are used to measure such durability properties including water permeability [60,101], water absorption [36,108,109], electrical resistance [101,110], chloride permeability [109] and sulphate resistance [111] are used. Each test is described in more detail in the following subsections.

10.1 Porosity Water Absorption and Permeability

Below 20 nm, it is reported to be harmless, and above that it is 200 nm which can affect the mechanical properties of concrete [113]. However, in any form, mercury intrusion porosimeter (MIP) [114], water infiltration and absorption [97], ultrasonic pulse velocity (UPV) [115], and X-ray computed tomography (CT scan) [116] are the techniques most often used to characterize the porosity of bacterial concrete. It was shown that urea-CaCl2 curing results in high Compared to water absorption, water absorption is present not only in bacterial concrete but also in control concrete [100].

10.2 Shrinkage

Length variation through moisture loss, continuous hydration and differential thermal expansion are basic parameters The performance of concrete repair materials may be due to tight adhesion or detachment with previously laid materials Low binding. Drying shrinkage of concrete, length variation due to moisture loss, is usually affected by curing regime, water-to-binder ratio (w/b), and composition content [122]. It is hypothesized that this observation may be due to higher creep and stress relaxation of bacterial concrete. For drying compressive stress, bacteria make concrete more suitable for curing composite materials [124].

10.3 Chloride Resistance

The resistance of concrete to ion transport, which is responsible for corrosion of steel reinforcement and depends on Pore settlement and pore structure [113] can be measured by the rapid chloride penetration (RCP) test [125]. Ensures reduction Penetration of concrete. This observation was confirmed by compressive strength test results, which showed increased strength Also, microstructure compactness was improved by adding bacteria to concrete [13,126]. Ensures reduction Penetration of concrete. This observation was confirmed by compressive strength test results, which showed increased strength Also, microstructure compactness was improved by adding bacteria to concrete [13,126].

11. MATERIAL CHARACTERIZATION

11.1 Chemical Composition Through X-ray Diffractometer Meaning

In addition to joint identification, XRD can be used to determine strain, preferred orientation, and crystallography texture, and grain size of crystalline materials. Crystal structure as a function of XRD when used in glancing angle mode Can get deeper. XRD can also be used on organic materials, for example, to determine the degree of crystallinity of polypropylene fibre as a function of annealing time [136].

11.2 Scanning Electron Microscope

Scanning electron microscopy (SEM) is commonly used for microstructural analysis of concrete surfaces. SEM provides High-resolution images at high magnification levels, through which bacterial components and the bacteria's failure mechanism Concrete can be determined. Gold, silver or chromium plating is usually required and used when making non-conductive materials [123] for SEM experiments.

11.3 Environmental and Economic Challenges

However, the challenges of bacteria Concrete applications are not only related to costs but also to environmental and sustainability impacts. Only a few studies have so far focused on the use of bacteria in concrete through the Life Cycle Assessment (LCA) technique. (e.g., refs. [141,142]), This area can provide a more coherent and in-depth analysis of the environmental consequences of bacteria-based self-healing. Concrete and bio-cementation [141].

12. CONCLUSION AND SUMMARY

In this study, an in-depth study of the effect of adding bacteria to self-healing and calcium carbonate production.

- Microbiological, physio-mechanical and durability properties of concrete are presented. Based on this research study, the following Conclusions can be drawn:

- Crack healing process of bacterial concrete depends on nutrient availability and survival of bacteria. This process, although many studies have been done, some techniques need to be adapted to preserve the species. A major challenge is the large-scale application of self-healing bio-concrete.

- One of the main challenges in preserving bacteria within the concrete medium is the high pH level of concrete. in that respect, only a specific type of bacteria (eg, alkaliphile bacterial strains) is currently used. Among the alkaliphile bacterial strains, the Bacillus spherics, Bacillus pasteurii and Bacillus subtilis are particularly suitable for self-healing applications in the production of bacterial concrete.

- In terms of environmental and economic challenges, bacterial concrete has a significant cost to implement, which is important Due to cultivation, transport and preservation of cells and their nutrition. In addition, in general As discussed in LCA studies, the production of urea, especially during ammonia synthesis, is an energy-intensive process and Nitrogen oxides produce emissions that can result in significantly different impact values based on overall climate change (CO2 production), ozone depletion, acidification and eutrophication values. Further comparative studies in this area could provide additional insights into identifying the most suitable methods for introducing bacteria into cracks Concrete.

REFERENCES

[1] American Society of Civil Engineers (ASCE), "A Comprehensive Assessment of America's Infrastructure", 2021.

[2] K. Wille, A.E. Naaman, S. El-Tawil and G.J. Parra-Montesinos, "Ultra-high-performanceconcrete and Fiber Reinforced Concrete: Achieving Strength and Ductility without Heat Curing", Mater. Struct. Constr.

[3] V. Wiktor and H.M. Jonkers, "Quantification of Crack-Healing In Novel Bacteria-Based Self-Healing Concrete", Cement Concr. Compos.

[4] M. Rezende Schuab, W. Jose dos Santos and P. Henrique Ribeiro Borges, "On the development of MK/BFS Alkali-Activated Materials as Repair Mortars: Performance under Free and Restrained Shrinkage Tests", Construct. Build. Mater.

[5] W. Meng, M. Valipour and K.H. Khayat, "Optimization and Performance of Cost-Effective Ultra-High-Performance Concrete", Mater. Struct. Constr.

[6] T. Stengel, P. Schießl, "Life Cycle Assessment (LCA) of Ultra High-Performance Concrete (UHPC) Structures", Woodhead Publishing Limited, 2013.

[7] D.W. Fowler and D.W. Whitney, "Long-Term Performance of Polymer Concrete for Bridge Decks", 2012.

[8] T. Luukkonen, Z. Abdollahnejad, J. Yliniemi, P. Kinnunen and M. Illikainen, "One-part Alkali-activated Materials: a Review", Cement Concrete, October 2017.

[9] B. Han, L. Zhang, J. Ou, "Smart and Multifunctional Concrete Toward Sustainable Infrastructures", Springer Singapore, Singapore, 2017.

[10] W. Zhang, Q. Zheng, A. Ashour, B. Han, "Self-healing Cement Concrete Composites for Resilient Infrastructures: A Review", February, Compos. B Eng., 2020.

[11] L. Li, Q. Zheng, Z. Li, A. Ashour and B. Han, "Bacterial Technology-enabled Cementitious Composites: A Review, March, Compos. Struct., 2019.

[12] V.G. Papadakis, M.N. Fardis and C.G. Vayenas, "Effect of Composition, Environmental Factors and Cement-Lime Mortar Coating on Concrete Carbonation, Jun. Mater. Struct.

[13] N. Chahal, R. Siddique and A. Rajor, "Influence of Bacteria on the Compressive Strength, Water Absorption and Rapid Chloride Permeability of Fly Ash Concrete", Construct. Build. Mater.

[14] S. Wei, M. Sanchez, D. Trejo and C. Gillis, "Microbial Mediated Deterioration of Reinforced Concrete Structures", Int. Biodeterior. Biodegrad., 2010.

[15] K. Vijay, M. Murmu, S.V. Deo, Bacteria based Self healing Concrete - A Review, Construct. Build. Mater., 2017.

AUTONOMOUS MOBILE ROBOT FOR VISITOR-GUIDANCE

R. Barathan, J. Ajeeth, M. Veerasivakumar and P. Nagarajan
Department of Mechatronics,
Bannari Amman Institute of Technology, Sathyamangalam - 638 401, Erode District, Tamil Nadu
E-mail:nagarajan@bitsathy.ac.in

Abstract

Autonomous Mobile Robot (AMR) is a mobile robot which can autonomously drive itself to reach the specified destination in a dynamically changing environment. For navigation specific destination, the information is given by the user who is not familiar with the place he/she is visiting. In this regard, with the assistance of an AMR they can reach their desired destination with the added information detailing. For the user interface a GUI have been made for giving user inputs and it will give a gist of information about the place which the user wants to visit. The GUI is also developed with many parameters in the Robot Operating System (ROS) navigation stack. These parameters are optimised for more precise motion of navigation. The precise navigation is achieved with sensor fusion of data from wheel encoder and LIDAR. The LIDAR data of the robot aids in avoiding the obstacles while going to the destination. By communicating between GUI and navigation stack in Robot Operating System, autonomous navigation in mobile robot for visitor guidance can be made , so that the visitor can reach out to any places where they want to go, without any worries about knowing each and every pathway to reach their destination.

Keywords: *Autonomous Mobile Robot, Guidance, Obstacle Avoidance, Navigation, Path planning*

1. INTRODUCTION

The paper is about brief knowledge about the development of robot's software that guides the visitor who is newly visiting to the place. It gets the input from the user through the GUI (Graphical User Interface), and navigate them to their desired place autonomously by avoiding obstacles And These types of robots can be used in areas like industrial, military related application, hazardous zone, surveillance purposes, space exploration, etc. In this project simulation and hardware setup of the Autonomous Mobile Robot (AMR) that guides the visitor is developed. The AMR takes the map of the environment with the help of the LiDAR. And the location in the area were shown in the GUI. And getting input it navigate the user to the desired. In this project, robot going to use Robot Operating System (ROS) for basic framework and develop Autonomous Mobile Robot to navigate through the environment. In recent years, AMR are introduced in both commercial and industrial setting.

1.1 Introduction to Robot Operating System

Robot Operating System is an open-source and Meta operating system which provide robotic framework over the OS like Ubuntu, Debian. ROS provides builds and reusable code for different robotic application. ROS is a bunch of software libraries and tools that helps in the building own robot. ROS has active community of robotic enthusiastic. ROS has been widely used in the robotic industry which provide basic nodes and topic for basic robot function. ROS provides reusable programs, debugging tools and visualization tools (2D and 3D) like rqt and Rviz. ROS provides Gazebo where the robot can be simulated in any environment before deploying it the real world. Gazebo is a 3D robotic simulator where the robot can be simulated and tested with different environment. Rviz is tool provide by ROS to 3D visualize the sensor data. It helps to visualise data transmission using the plugin of various available topics. Rviz also for visualization of the maps.

Here in this project, ROS going to be use for the basic frameworks of robot and its tools will be used for visualization.

1.2 Proposed Method

To make the AMR which guides the user and it is operate in dynamic environment the robot is required to get data of its surrounding using sensor LIDAR and generate map for the environment. And this AMR should continuously get information from its environment. Using the acquired data the AMR should update map of the

environment and should calculate the shortest path and avoid the new obstacle. Calculating the shortest path for the destination of robot is tedious and huge task in dynamic environment. So, the path planning algorithm in ROS is customized and the precise and shortest path is identified. For simulation CAD model of AMR should converted into Unified Robotics Description Format (URDF) file and imported to Gazebo for simulation. For real time AMR is developed from scratch. The mapping and navigation of the both simulation and real time is visualized through Rviz.

2.DESIGN OF MOBILE ROBOT

2.1 Designing Cad Model of Autonomous Mobile Robot

CAD model of the AMR can be done by using the fusion 360 design software. First select the required components that are going to be used. And the dimensions of the components are measured. And the dimension of the robot is defined. Then the rough draft of the design is created and the created design is analysed and modifications were made. Then the hardware required for the robot is designed through software. Then the required components are assembled. The assembly can be made by using certain criteria. The criteria were explained in the next part. Then the full assembly of the robot is made. Figure 1 shows the CAD model of the robot.

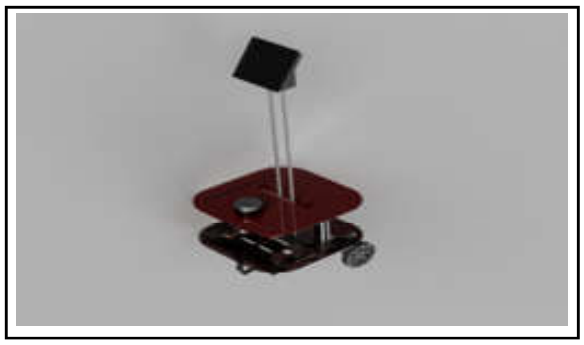

Fig.1 CAD model of autonomous mobile robot

2.2 Design To URDF Conversion

- To convert cad model to URDF(unified robot description format) we want to follow some criteria that are discussed below
- Define the plane axis in the format shown in the figure 2 like z axis in the facing top and the robot front is to be faced in the x axis and the y axis in the side of the robot

Fig. 2 Plane definition for modelling

- Then the base frame of the robot is to be designed this base frame is parent link of the robot other link are child link of the robot so the base frame is clearly designed and assembled
- Then the designed wheel is imported to the current file and the wheels are attached to the base frame as a revolute joint because the wheels are to be moved in circular motion this is one of the child_link to the base frame.
- And LiDAR design is imported to the file and the LiDAR is attached to the base frame as a rigid joint this also one of the child_link to the base frame
- The design of the IMU is imported and attached to the base frame as rigid joint
- The robot mid-point is to be placed to the origin of the graph in the fusion software
- The robot is to be aligned just above the x axis so in the gazebo the robot was positioned in a correct position.
- After all this process we want export the robot in the URDF file format

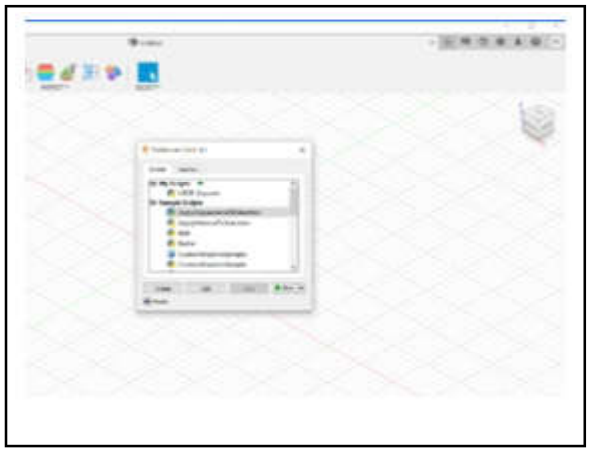

Fig.3 URDF builder

- For that URDF exporter is used and the URDF file is successfully exported by the exporter.
- The robot mid-point is to be placed to the origin of the graph in the fusion software
- The robot is to be aligned just above the x axis so in the gazebo the robot was positioned in a correct position.
- After all this process we want export the robot in the URDF file format.

Fig. 4 URDF builder

- For that URDF exporter is used and the URDF file is successfully exported by the exporter.

3. SIMULATION AND WORKING

3.1 Environmental Setup

- Install UBUNTU 20 in NVIDIA Jetson Board controller.
- Next install Noetic full version in Ubuntu OS by using command line " sudo apt install Robot Operating System-noetic-desktop-full" which will have the image shown below Figure 5.

Fig.5 Noetic-version of robot operating system

- After installation create workspace using the command "mkdir -p ~/catkin_ws/src", "cd ~/catkin_ws/", "catkin_make" this command will convert a simple directory to Robot Operating System workpace.
- The convertion of workspace will be similar as shown in Figure 6.

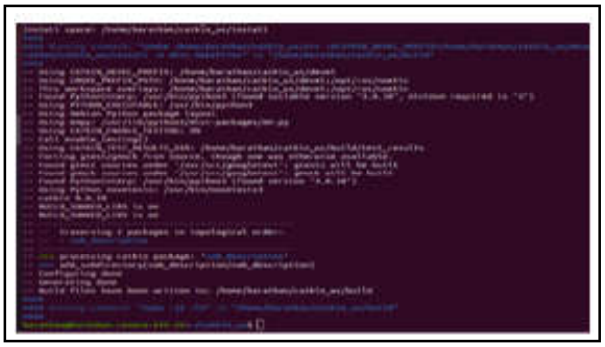

Fig.6 Compilation of workspace

- Then place the converted URDF file in "catkin_ws/src" .
- Next open new terminal type "cd catkin_ws"and next "catkin_make".
- Next modify some of the parameters and to add some plugins to make robot - URDF model to communicate with Robot Operating System and it can move accordingly with data which comes through Robot Operating System, which the user defined in backend,
- Git Clone mapping packages form github for mapping and planning paths for AMR. There are two main types packages for mapping one is G-Mapping where it used encoder and LiDAR output for mapping and other one is Hector-Mapping which is completely dependent only on LIDAR output. To work with G-mapping first need to clone Packages from github using the command.
- "git clone https://github.com/Robot Operating System-perceptio/slam_gmapping.git" command in catkin_ws/src and then come to catkin_ws by "cd .." command and then type catkin_make compile it in the Robot Operating System workspace.
- Finally create a launch file and set parameters for local-costmap and global-costmap which are used while in the simulation

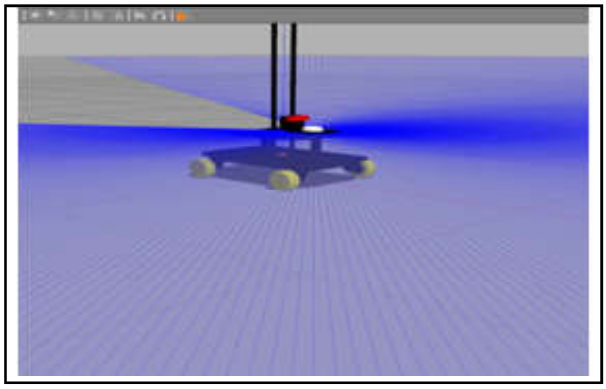

Fig 7 Simulation setup

The environment setup is ready now, if any complication while cloning packages then refer to Robot Operating System.org.com to get rid of errors and implement the process, make sure that no errors while compiling the packages and building the system. All the links given above are taken from opensource sites Robot Operating System.org and Github.com.

3.2 Navigation Stack

- Navigation Stack is a function in RVIZ which is a software to visualize the data from the GAZEBO simulator
- NAV_STACK makes the Mobile robot move to the desired position, NAV_STACK subscribes the information of odometry and sensors data, odemetry is the position feedback from the encoder motors and sensor data from LiDAR sensor and NAV_STACK publishes the velocity command to mobile robot to move accordingly. For Navigation Stack the pre-requisite is the robot must work with the Robot Operating System, robot should publish the sensor data of correct message type (e.g., std_msgs.msg.string).
- navigation stack requires correct implementation of differential drive and mobile robot base shape in CAD model for accurate navigation of robot in the environment. The differential drive is one of main factors for robot motion, it determines the velocity of the robot by controlling the mobile base by sending the velocity values (x, y,).
- The shape of mobile robot should be square or circular because the NAV_STACK will work with best performances while the mobile base is square or circular in shape, because when the robot moves along the path to reach the desired position at that the robot should be in shape that symmetry to another half of the robot, and the robot should not be in large rectangular in size, because it could be more difficult, while move along in path that contains doorways.
- By interfacing SLAM and Navigation Stack the Enhanced D* algorithm has been developed.

3.3 Configuring Parameters

3.3.1 Local costmap

It help to set the range of obstacles around the robot to avoid the obstacle to reach the desired position, which can be done by configuring the following parameters:

- Min_acce (minimum acceleration of robot while detection of obstacles)
- Max_acce (maximum acceleration of to be moved when no obstacle has detected)
- Radi (radius of robot)
- Height (height of our robot)

These are the some parameters, have be to change according to robot configuration, remaining parameter are set to be default in local costmap

3.3.2 Global Costmap

Configure the global costmap as default static map to dynamic map and other parameter to be set as default.

All other parameters should be set to be default value as mentioned in Robot Operating System website.

3.4 Overall Block Diagram

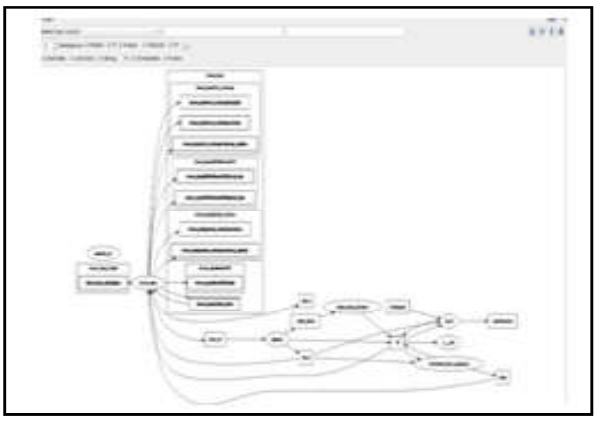

Block diagram represents the communication between nodes by the help of topics

3.5 Simulator (Gazebo) / Visualizer (RVIZ)

3.5.1 Gazebo

Gazebo is a simulator used to simulate the robot in a given environment that has been specified in a launch file

3.5.2 RVIZ

Rviz is a visualizer used to visualize the robot with each and every detailed parameter that has been published from the robot.

3.6 Simulation

TEST_1 : First autonomous navigation of the AMR is done in simulation

TEST 1

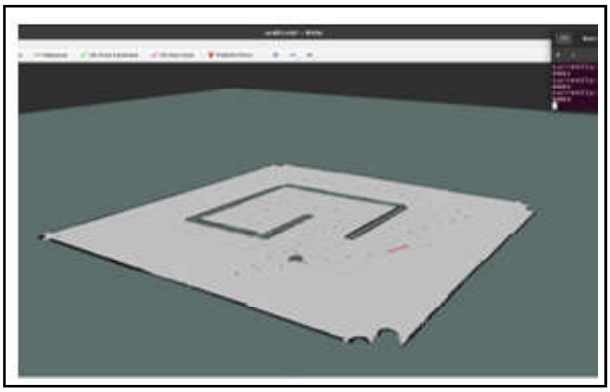

Fig.8 Navigation stage 1

With the help of nav_stack , point out the position in the given environment by using a 2d nav goal in Rviz and the robot navigate to the point autonomously by creating a shortest path and by avoiding obstacles.

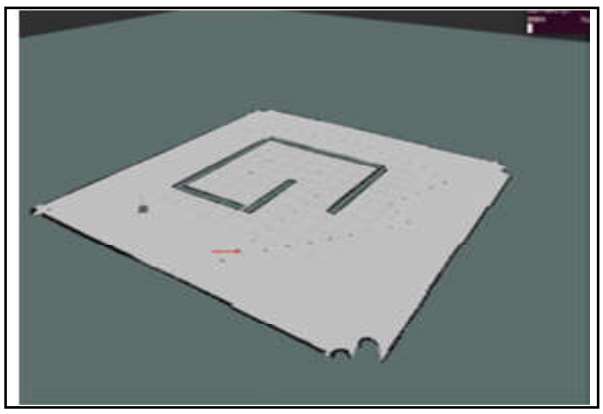

Fig.9 Navigation stage 2

- In second case the point is given by using move_base action server,client which is the pre build action server in Robot Operating System using a piece of code the point for the robot to navigate was given and the robot navigate to the point autonomously.Our robot works perfectly in more complex static environment, so we have tested our robot in a frequently changing environment, the outputs shown below figure 8,9
- After that the GUI and the software simulation is get interfaced and the user enter the input through GUI and the robot autonomously navigate to the point and also by avoiding obstacles.

4. CREATING GUI

4.1 GUI

Graphical user interface helps the user in finding, understanding and using a device. GUI is a bridge between user and backend code. GUI presents contents

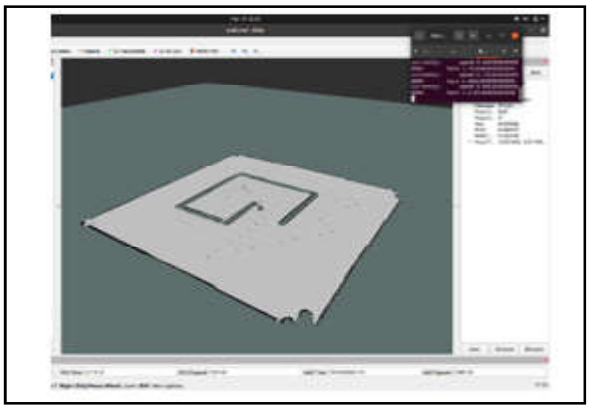

Fig.10 Navigation stage 3

Here in this project, GUI will help the user to select the location where the user likes to go and it will communicate with the robot and set the goal position. In this project, Kivy, KivyMD libraries are used to develop GUI which are open-source python libraries that help in developing user interfaces on windows, macOS, Linux and Android.

Fig.11 Home screen

SHINROS is the name of the robot, here in the GUI, figure 4.1 is the launch screen, which consists of gif for logo, button, labels, when user click the screen, the button bind which call the callback function the screen manager and switch the current screen to mode selection screen.

4.2 Mode Selection Screen

In the Mode selection screen, the user can select either the visitor or the admin mode. The respective button will call the respective screen and the screen manager will make it as the current screen. As in figure 4.2, there are two buttons, rectangular button which will call respective screen

The visitor mode screen is the main part of the GUI because the user can select the desired locations where he/she likes to go.

Fig 12 Mode selection

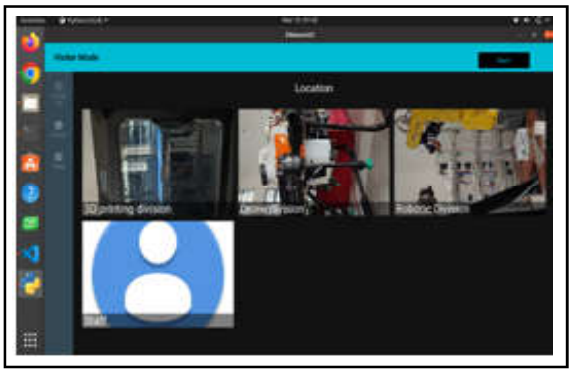

Fig.13 visitor mode

The screen comes with a toolbar where the visitor mode title and back button will be displayed.The back button helps the user to switch back to the user selection screen. On the left side, navigation rail is added, which consists of location list, about, and help which helps the user to navigate on the screen. In the centre part of the screen, the list of the available locations will be shared. The users can select the location, when they select the location, tile binding will call the function to publish the coordinator of goal location using ROS framework. The node will publish coordinates in geometry-msg/ pose format.

4.3 Admin Login Popup Screen

This popup window is the admin login screen, the admin is needed to authenticate for further access. The password will be verified, if the user enters the wrong password, the access will be denied.

4.4 Admin Location Adding Screen

Admin screen will contain tabbed bar using which the user can change in between adding and removing tabs. In the add new location tab, the tab consists of Name, Description, Image (file location/path in system). The add location button will add the location to list.

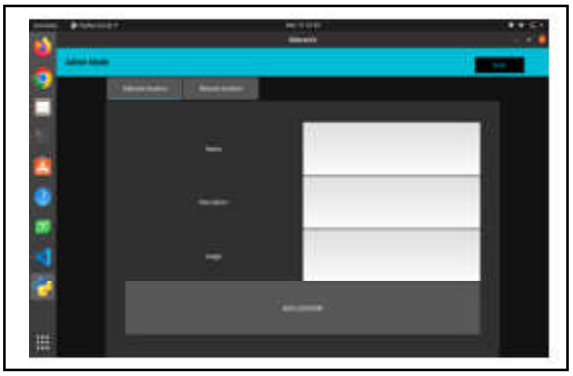

Fig.14 Admin location adding

4.5 Admin Location Removing Screen

In the remove location tab, the tab consists of Name. The remove location button will be removed from the location list. The name will be searched in the location list and it will be removed from the list

Fig.15 Admin login popup screen

5. AUTONOMOUS NAVIGATION

5.1 Mapping

For mapping in the real time, the lidar scan data and the odometry data is needed. All the requirements for the mapping was done and here in this project slam gmapping algorithm was used. Using slam gmapping the 2D occupancy grid map was created, from using a laser and floor data.

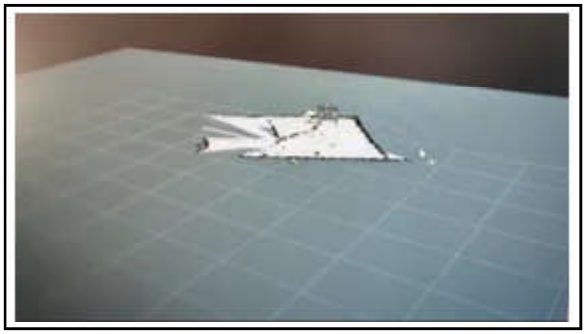

Fig.16 Mapping output

5.2 Navigation Stack Setup

Navigation is the most important one in Mobile robot to drive to a specific position . In Autonomous mobile robot the navigation is done with the help of a navigation stack which has many file systems like local planner, global planner, costmaps, navigation planners, path planners , localization etc.

The some of the implemented files systems are local and global planner and with costmaps, let's see a brief look about the terms and parameters used in the file system.

5.3 Navigation Parameters

5.3.1 Global Planner

Global planner with create a long path with the help of the data from the map of the environment, it does not use any sensor data to detect any obstacle in the path way.

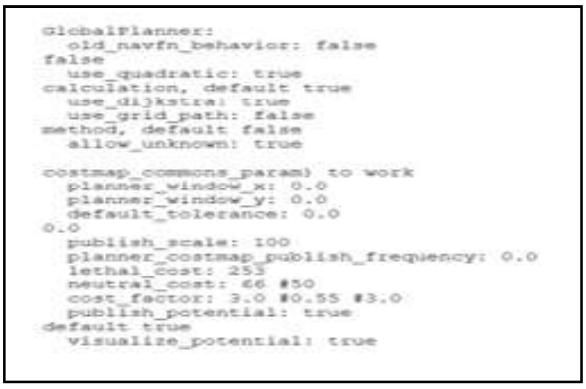

Fig.17 Global planner

5.3.2 Global Costmap

It's a sub map created with the data from the original map to drive the robot safely in the corners and sharp edges of the walls and things around the robot.

5.3.3 Local Planner

Local planner will take the data from the sensors which is attached in robot and that will creates a new path to the obstacle in the way. Local planner gets data from multiple sensors like Lidar, Depth camera etc.

5.3.4 Local Costmap

It's also a small map which have been created with the data from the sensor and marks the obstacles in the map to avoid the crash and it helps local planner to plan the path easily.

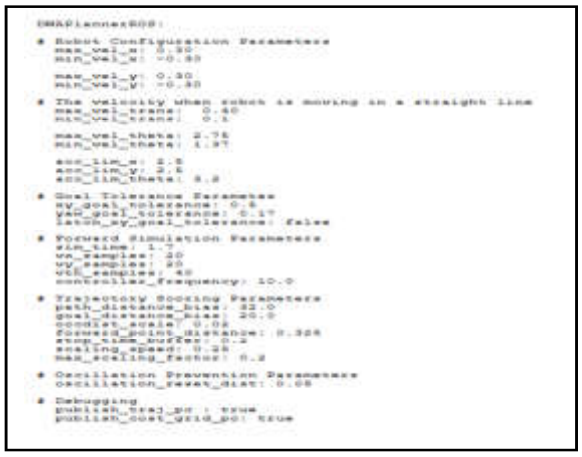

Fig.18 Local planner

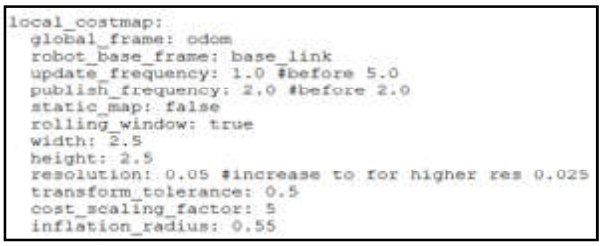

Fig.19 Local costmap

5.4 Localization

It's a most important thing in navigation, because for the navigation the robot should know where it is at the environment at any point of time. So, for navigation use AMCL (Adaptive Monte Carlo Localization**)** for localization.

5.5 ACML Localization

The ACML uses the sensor data from IMU, Odometry and tf data from the rviz to localize the robot in that environment. Finally with all planner and cost maps data path have been planned, the path planning is planned with the help of ROS system packages.

5.6 Autonomous Navigation

With the help of all these parameters autonomous navigation was done. First the generated map was loaded in the Rviz with map server node. And then the point for robot to reach was given by using 2d nav goal and the robot reaches the point. And then the point was given by using a piece of code using move base client server. The robot will successfully reach the point.

5.7 Interacing Hardware and Software

In this step the point was given by the robot by using user interface created in this project. The robot gets the

input from the user and the robot navigates to that point and successfully the autonomous navigation was done by getting input from the GUI.

6. CONCLUSION

With help of Robot Operating System, an open source autonomous navigation of mobile robot is controlled. A wheeled robot is navigated autonomously in unknown environment and avoid dynamic obstacles using LIDAR and encoder data. The autonomous mobile robot is developed, that is capable of guiding the visitor who is new to the place. The AMR receives user input as point location to the robot by GUI, then autonomously navigates the visitor to that point. The nav_stack in Robot Operating System helps to overcome the difficulties in navigation of robot model (URDF model) for visualisation of robot, hence using Robot Operating System with a nav_stack robot can autonomous navigates with the information from GUI.

REFERENCES

[1] Afanasyev, Ilya & Sagitov, Artur & Magid and Evgeni, "ROBOT OPERATING SYSTEM-Based SLAM for a Gazebo-Simulated Mobile Robot in Image-Based 3D Model of Indoor Environment", Advanced Concepts for Intelligent Vision Systems, Vol.938, 2015.

[2] Dieter Hoetzer "Collision Avoidance System and Method" Publication of US20100063736A1 Application filed by Robert Bosch GmbH Assigned to ROBERT BOSCH GMBH, ROBERT BOSCH LLC.

[3] Giuseppe Fragapane, Rene de Koster, Fabio Sgarbossa and Jan Ola Strandhagen, "Planning and Control of Autonomous Mobile Robots for Intralogistics: Literature Review and Research Agenda", European Journal of Operational Research, Vol.294, No.2, 2021.

[4] Hutabarat, Dony & Rivai, Muhammad & Purwanto, Djoko &Hutomo and Harjuno, "LIDAR-based Obstacle Avoidance for the Autonomous Mobile Robot", 12th International Conference on Information & Communication Technology and System (ICTS), 2019.

[5] Hmaid, Taheri & Bing, Qiao & Nurallah and Ghaeminezhad "Kinematic Model of a Four Mecanum Wheeled Mobile Robot" International Journal of Computer Application, Vol.113, No.3, 2015 .

[6] M. Köseođlu, O. M. Celik and O. Pektas, "Design of An Autonomous Mobile Robot based on Robot Operationg System", International Artificial Intelligence and Data Processing Symposium (IDAP), doi: 10.1109/IDAP.2017.8090199., 2017, pp. 1-5.

[7] Lentin Joseph March, "Robot Operationg System Robotic Projects", published by Packt Publishing Ltd, 2017, pp. 186-200.

[8] Matteo Munaro, Filippo Basso, Stefano Michieletto and Enrico Pagello, University of Padova, "A Software Architecture for RGB-D People Tracking Based on Robot Operationg System Framework for a Mobile Robot", From ResearchGate under Mobile Robotics, published in January 2013.

[9] R.S.Pol and M.Murugan, "A Review on Indoor Human Aware Autonomous Mobile Robot Navigation Through a dynamic environment survey of different path planning algorithm and methods", International Conference on Industrial Instrumentation and Control (ICIC), doi: 10.1109/IIC.2015.7150956, 2015, pp. 1339-1344.

[10] K.Rahul Sharma, "Design and Implementation of Path Planning Algorithm for Wheeled Mobile Robot in a Known Dynamic Environment", International Journal of Research in Engineering and Technology, Vol.02, No.06, Jun 2013.

[11] Sukkpranhachai Gatesichapakorn Kasetsart University, Thailand, Jun Takamatsu Nara Institute of Science and Technology, Japan, Miti Ruchanurucks Kasetsart University, Thailand, "Robot Operating System based Autonomous Mobile Robot Navigation Using 2D LiDAR and RGB-D Camera", Published in First International Symposium on Instrumentation, Control, Artificial Intelligence, and Robotics (ICA-SYMP), 2019.

A STUDY ON AWARNESS OF E-BANKING SERVICES AMONG COLLEGE STUDENTS

M. Freddy Chris and K. Gokul
Department School of Management Studies
Bannari Amman Institute of Technology, Sathyamangalam - 638 401, Erode District, Tamil Nadu

Abstract

Banking has evolved as a critical service business in this era of global competitiveness. The banking sector has increased its operations in response to client demand. Moreover, the segmentation, structuring of activities and scope of banks has changed in response to developments in the global economy. Insurance and foreign transactions are added to the financial and investment operations. The technology revolution has increased the use of advanced information and communication tools, which have supplanted manual financial transactions. E- banking is not a new issue in today's world, but it has increased the banking sector's business by 4.6 percent solely owing to technology improvements. This report is an attempt to investigate the awareness of e-banking facilities among college students aged 18 to 25 who live and study in rural locations.

Keywords: *Awareness, E-Banking, E-Banking Technology and Services*

1. INTRODUCTION

A bank is a financial entity that offers a variety of financial services to its customers. It is extremely important in the evolution of society. It receives funds from a variety of sources in the form of deposits and investments, and then disburses them to various businesses in the form of debts and loans. It has a significant impact on economic growth. The concept of electronic banking is a new millennium concept. It is the use of electronic technology to conduct banking transactions. E-banking refers to the use of electronic technology to provide financial services to customers at their homes, offices, and on the go. It means that customers can access financial services from anywhere and at any time; there are no geographical or time restrictions.

1.1 Different Types of E-Banking Services

- ATM
- NEFT/RTGS
- Internet Banking
- Mobile Banking
- SMS Banking
- Telephone Banking
- Cards Facility

1.2 Need of the Study

In today's society, the terms "e-banking" and "e-commerce" are quite prevalent. In most cities, all banks now provide e-banking services. E-banking services do not have any geographical restrictions. However, the usefulness of e-banking is contingent on knowledge of e-banking services and information on e-banking services.

2. OBJECTIVES OF THE STUDY

- To investigate students' awareness of e-banking.
- To determine whether students use bank-provided e-banking services.
- E-banking services are popular among college students

3. REVIEW OF LITERATURE

Akshaya Kumar Bhandary, 2021, "Prospects and Challenges of E-banking: A Perception Research" was the title of the study. The study's goal is to learn how clients feel about E-banking. Electronic banking has evolved in recent years, with new distribution channels such as the Internet and mobile services being used. Enterprises began to use E-banking in the mid-1990s, when it first became available. Digital banking has risen at a quicker rate after demonetization in 2016. The majority of Indian banks have built E-banking and mobile

banking websites to provide consumers with online access to nearly all banking products. E-banking has become a commonplace method of obtaining safe and convenient financial services. The biggest barrier to electronic banking adoption is assuring financial security.

Kishor Ananda Patil, 2019, In the banking industry, e-banking is a typical revolution. It featured Internet Banking, ATMs, credit and debit cards, NEFT, RTGS, and a variety of other e-banking delivery methods. It is beneficial to both banks and customers. There is no time restriction on it. Customers can access the form from any location and at any time. It merely requires a computer or smartphone with internet access. This study will use a structured questionnaire.

P. Vijay Shankar and S. T. Surulivel, 2018, E-banking consumers must be aware of all of their bank's services in order to get the most out of their e-banking services. This research study is an attempt to better understand the level of knowledge among users who utilise e-banking features in their daily lives. The research is being carried out with the assistance of 138 student volunteers who use their e-banking services for a variety of purposes. The research is conducted using a questionnaire that has 30 questions about e-banking awareness. The gathered primary data was examined for reliability and sample adequacy, yielding an overall reliability of 88.2 percent for the construct and a sampling adequacy of 75.1 percent for the collected samples.

Dr. V. Sangeetha, 2018, Internet Banking enables anytime access to the customer to give the customer's anytime access to their banks. Customers could check out their account details, get their bank statements, perform transactions like transferring money to other accounts and pay other bills sitting in the comfort of their homes and offices. However, the biggest limitation of Internet Banking is the requirement of the PC with an internet connection. Mobile Banking addresses the fundamental limitation of internet banking, as it reduces the customer requirement to just a mobile phone. Mobile usage has seen explosive growth in most of the Asian economics like India, China and Korea. The main reason that Mobile Banking scores over Internet Banking are that it enables, 'Anywhere, Anytime banking.' This paper highlights the awareness of customers towards the e-banking services provided by the banks.

4. ANALSIS AND INTERPRATATION

4.1 Reliability Test

Valid instruments and reliable research are the necessary conditions to obtain a high-quality research result. Reliability is a measure to indicate that a reliable instrument to be used as means of collecting data is considered good. So, it is necessary to test the reliability and validity of the data's used in the study.

Cronbach's alpha is a measure of scale reliability. It is a function of the number of items in a test, the average covariance between the pair of items and the variance of the table. Cronbach's alpha range is from 0 to 1, the higher values will indicate greater reliability and consistency of the data whereas with lesser value the data is less reliable and consistent.

Case Processing Summary

		N	%
Cases	Valid	122	62.6
	Excluded[a]	73	37.4
	Total	195	100.0

Reliability Statistics

Cronbach's Alpha	N of Items
.797	23

INTERPRETATION

The above table shows that there is greater level of reliability in the data collected and therefore there is consistency too. We come to this decision as the Cronbach's Alpha from the test conducted is said to be 0.797.

4.2 SPERMANN RANK CORRELATION TEST

Spearman's rank correlation measures the strength and direction of association between two ranked variables. It basically gives the measure of monotonicity of the relation between two variables i.e., how well the relationship between two variables could be represented using a monotonic function.

Correlations

			How often do you use E Banking services	Have you ever faced any difficulties in E banking Services
Spearman's rho	How often do you use E Banking services	Correlation Coefficient	1.000	.095
		Sig. (2-tailed)	.	.185
	Have you ever faced any difficulties in E banking Services	Correlation Coefficient	.095	1.000
		Sig. (2-tailed)	.185	.
		N	195	195

How often do you use E Banking services and have you ever faced any difficulties in E banking services

HYPOTHESIS: There is no significant between How often do you use E Banking services and have you ever faced any difficulties in E banking services.

HYPOTHESIS: There is no significant relationship between Most preferred payment method and how much would you like to rate an e banking services.

INTERPRETATION: As per the correlation output table the test significant value is .993 which is greater than the significant P value (0.05).
Hence, we accept null hypothesis.

4.3 Mann Whitney Test

Mann Whitney U test is used to compare difference between two independent groups when the dependent variable is either ordinal or continuous, but not normally distributed.

INTERPRETATION: As per the correlation output table the test significant value is .185 which is greater than the significant P value (0.05).
Hence, we accept null hypothesis.

Most preferred payment method and how much would you like to rate an E banking services

Correlations:

Expectation in banking services and Gender Ranks

	Gender	N	Mean Rank	Sum of Ranks
Expectation in banking services	Male	114	100.77	11488.00
	Female	80	92.84	7427.00
	Total	194		

Test Statistics[a]

	Expectation in banking services
Mann-Whitney U	4157.000
Wilcoxon W	7427.000
Z	-.994
Asymp. Sig. (2-tailed)	.320

HYPOTHESIS: There is no significant difference between the Gender and Expectation in banking services.

INTERPRETATION: As per Mann-Whitney output table the test asymptotic significant value is 0.320 which is greater than the significant P value (0.05).
Hence, we accept null hypothesis.

Frequency of Visiting the Branch and Gender

Ranks

	Gender	N	Mean Rank	Sum of Ranks
Frequency of visiting the branch	Male	113	90.82	10263.00
	Female	80	105.73	8458.00
	Total	193		

Test Statistics[a]

	Frequency of visiting the branch
Mann-Whitney U	3822.000
Wilcoxon W	10263.000
Z	-1.996
Asymp. Sig. (2-tailed)	.046

HYPOTHESIS: There is no significant difference between the gender and Frequency of visiting the branch.
INTERPRETATION: As per Mann-Whitney output table the test asymptotic significant value is 0.46 which is greater than the significant P value (0.05).
Hence, we accept null hypothesis.

4.4 Kruskal Wallis Test

Kruskal Wallis Test is a non-parametric test which have been used when the assumptions for one-way Anova is not been met. Both these tests are done to find out the statistical difference between the continuous dependent variable by categorical independent variable. For Kruskal Wallis the independent variables group must be 51 more than two. Kruskal Wallis can be used for both continuous and ordinal dependent variable. The P-Value for Kruskal Wallis is 0.05

Preferred Banking experience is delivered and Qualification

Ranks

	Qualification	N	Mean Rank
Preferred Banking experience is delivered by	UG	123	95.73
	PG	65	99.00
	Others	7	128.57
	Total	195	

Test Statistics[a,b]

	Preferred Banking experience is delivered by
Chi-Square	3.054
df	2
Asymp. Sig. (2-tailed)	..217

HYPOTHESIS: There is no significant difference between the response Qualification and Preferred banking experience is delivered.

INTERPRETATION: As per Kruskal- Walli's output table the test asymptotic significant value is .217 which is greater than the significant P value (0.05).
Hence, we accept null hypothesis.

Frequency of visiting the branch and qualification

Ranks

	Qualification	N	Mean Rank
Preferred Banking experience is delivered by	UG	123	102.63
	PG	65	91.33
	Others	7	78.64
	Total	195	

	Frequency of visiting the branch
Chi-Square	3.053
df	2
Asymp. Sig. (2-tailed)	..217

HYPOTHESIS: There is no significant difference between the response in qualification and frequency of visiting the branch.
INTERPRETATION: As per Kruskal – Walli's output table the test asymptotic significant value is .217 which is greater than the significant P value (0.05).
Hence, we accept null hypothesis.

Most preferred payment method and qualification

Ranks

	Qualification	N	Mean Rank
Most preferred payment method	UG	123	93.18
	PG	65	106.26
	Others	7	106.00
	Total	195	

Test Statistics[a,b]

	Most preferred payment method
Chi-Square	3.053
df	2
Asymp. Sig. (2-tailed)	.260

HYPOTHESIS:
There is no significant difference between the response in qualification and Most preferred payment method.

INTERPRETATION:
As per Kruskal – Walli's output table the test asymptotic significant value is .260 which is greater than significant P value (0.05).
Hence, we accept null hypothesis.

4.5 CHI – SQUARE TEST

A Chi – Squared test is a statistical hypothesis test that is valid to perform when the last statistic is chi-squared distributed under the null – hypothesis, Specifically Pearson's chi-squared test and variants thereof.

Chi- square test between Age and Do you enjoy any of the following with your primary bank [Mobile Banking].

Crosstabulation

			Do you enjoy any of the following with your primary bank [Mobile Banking]		Total
			Yes	No	
Age	18-25	Count	158	20	178
		Expected Count	158.8	19.2	178.0
	26-35	Count	12	1	13
		Expected Count	11.6	1.4	13.0
	35-45	Count	4	0	4
		Expected Count	3.6	.4	4.0
Total		Count	174	21	195
		Expected Count	174.0	21.0	195.0

Chi-Square Tests

	Value	df	Asymp. Sig. (2-sided)
Pearson Chi-Square	.651a	2	.722
Likelihood Ratio	1.092	2	.579
Linear-by-Linear Association	.616	1	.432
N of Valid Cases	195		

Symmetric Measures

		Value	Asymp. Std. Errora	Approx. Tb	Approx. Sig.
Nominal by Nominal	Phi	.058			.722
	Cramer's V	.058			.722
Interval by Interval	Pearson's R	-.056	.044	-.784	.434c
Ordinal by Ordinal	Spearman Correlation	-.050	.055	-.694	.489c
N of Valid Cases		195			

Null Hypothesis: There is no statistical difference between Age and Do you enjoy any of the following with your primary bank [Mobile Banking]

INTERPRETATION: In this test, the significant level between Age and Do you enjoy any of the following with your primary bank [Mobile Banking] than the expected P value which is 0.05. Thus, we accept the null hypothesis.

Chi - Square test between Age and Do you prefer E banking than traditional banking.

Crosstabulation

			Do you prefer E banking than Traditional Banking		Total
			Yes	No	
Age	18-25	Count	148	29	178
		Expected Count	148.8	29.2	178.0
	26-35	Count	10	3	13
		Expected Count	10.9	2.1	13.0
	35-45	Count	4	0	4
		Expected Count	3.3	.7	4.0
Total		Count	163	32	195
		Expected Count	163.0	32.0	195.0

Chi-Square Tests

	Value	df	Asymp. Sig. (2-sided)
Pearson Chi-Square	1.208[a]	2	.547
Likelihood Ratio	1.819	2	.403
Linear-by-Linear Association	.054	1	.816
N of Valid Cases	195		

Symmetric Measures

		Value	Asymp. Std. Errora	Approx. Tb	Approx. Sig.
Nominal by Nominal	Phi	.079			.547
	Cramer's V	.079			0547
Interval by Interval	Pearson's R	-.017	.059	-.232	.817[c]
Ordinal by Ordinal	Spearman Correlation	.007	.072	.101	.919[c]
N of Valid Cases		195			

Null Hypothesis: There is no statistical difference between Age and Do you prefer E banking than traditional banking.

INTERPRETATION: In this test, the significant level between Age and Do you prefer E banking than traditional banking than the expected P value which is 0.05. Thus, we accept the null hypothesis.

5. SUGGESTION

- The banks may concentrate and increase their technological proficiency by focusing on transaction speed and online banking services.
- The majority of respondents believe that the availability of 24*7 services connectivity becomes a concern, and that the problem should be detected swiftly to avoid any system server downtime.
- Amount debited & credited notification is not received for the time but check in another way so solve the issue of banking services.

6. CONCLUSION

Based on the facts above, it is possible to infer that technology has had a significant impact on youngsters, pushing them to conduct banking in a creative manner. They are well-versed in all kinds of digital modes of banking. ATMs were the most popular, followed by internet banking, credit cards, and mobile banking, while credit cards had the greatest drop page rate, followed by mobile banking, and smart cards. The usage of ATMs and online banking varies greatly across age groups, with young people leading the way, but it is low for credit cards and mobile banking. It has also been shown that the use of ATMs and internet banking is increasing Dependent on education, with a high rate of adoption among the highly educated. Income is strongly related to the adoption of ATMs, online banking, and credit cards, with higher income groups leading the way, but the trend is different with mobile banking, demonstrating that it is the least expensive e-banking delivery channel.

REFERENCES

[1] https://globalpresshub.com/index.php/AJEFM/article/view/1207
[2] https://doi.org/10.1504/IJEF.2009.027848
[3] https://www.academia.edu/download/55959543/IJNTR03010004.pdf
[4] https://www.indian journals.com/ ijor.aspx?target=ijor :ijrss&volume =7&issue=1 &article=018
[5] https://www.emerald.com/insight/content/doi/10.1108/IJBM-12-2014-0175/full/html?fullSc=1&mbSc=1&fullSc=1
[6] https://www.academia.edu/download/30882133/E-Banking_innovations_trends_in_India.pdf

DESIGN AND IMPLEMENTATION OF CHATGPT: A NEURAL LANGUAGE MODEL FOR CONVERSATIONAL AI

K. Gunalan
Department of Computer Technology
Bannari Amman Institute of Technology, Sathyamangalam - 638 401, Erode District, Tamil Nadu
E-mail: gunalank@bitsathy.ac.in

Abstract

A sophisticated language model called ChatGPT can recognise genuine language and generate dialogue that sounds like actual conversations. It uses deep learning methods to process textual data and is based on the GPT-3.5 and GPT-4 architecture. By learning from vast volumes of text data, ChatGPT generates responses depending on the context and previous messages in a discussion. It integrates techniques like attention mechanisms, neural networks, and language modelling to produce coherent and applicable responses. ChatGPT is a helpful tool for many natural language processing activities, including question-answering, text summarization, and language translation, thanks to its comprehensive capabilities. In general, ChatGPT is an effective tool for enhancing user experiences due to its ability to understand and produce natural language.

Keywords: *ChatGPT, GPT-3, LLMs, LSTM, OpenAI API*

1. INTRODUCTION

The introduction of Large Language Models, the ground-breaking self-attention mechanism that made it possible to train GPT-3, and Reinforcement Learning From Mortal Feedback are covered in the machine learning replicas that power ChatGPT[1]. Then, we delve into the cutting-edge method that made ChatGPT exceptional: Reinforcement Learning From Human Feedback.[1, 2]

Fig. 1 Introduction of LLM Source [3]

2. LARGE LANGUAGE MODELS

ChatGPT is an enlargement of the Vast Language Model class of automated learning Natural Language Processing models (LLMs) [1, 2]. Huge amounts of textual information are ingested by LLMs, which then infer associations between words in the text. As computer power has improved over the past few years, these models have expanded. LLMs get more powerful as their input datasets and parameter space get bigger. [1, 2]

Figure 2 LLMs Source [3]

Predicting a word in a string of words is a prerequisite for training language models. The two most frequent observations of this are next-token prediction and masked language modelling. [1, 2]

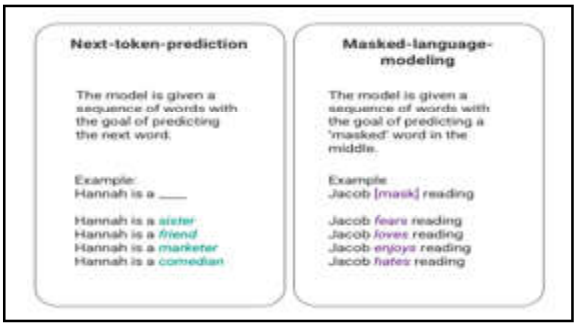

Fig.3 Large Language Models Source[1, 2]

In this fundamental method of sequencing, which is frequently implemented using a Long-Short-Term-Memory (LSTM) model, the model fills in the gap with the word that is statistically most likely given the context. Its sequential modelling structure has two main drawbacks. [1, 2]

Fig.4 Long-Short-Term-Memory Source [3]

- The model is unable to assign a higher value to certain surrounding words than to others. While "reading" may be most frequently associated with "hates" in the example above, "Jacob" in the database may be such an avid reader that the model should give "Jacob" more weight than "reading" and chose "love" instead of "hates."[2]
- Instead of processing the input data as a whole corpus, each individual piece of data is processed in turn. It follows that when an LSTM is trained, the context window is fixed and only extends beyond a single input for a number of steps in the sequence. As a result, the intricacy of word associations and the meanings that can be inferred are constrained.[2]

Transformers were first created in 2017 by a Google Brain team in response to this problem. Transformers can process all input data concurrently, in contrast to LSTMs. The model can assign variable weights to various input data components in connection to any point of the language sequence by use of a self-attention mechanism. This innovation made it possible to considerably improve the meaning that LLMs convey and to analyse much larger datasets.[2]

3. GPT AND SELF-ATTENTION

In 2018, openAI released GPT-1, the first of its Generative Pre-training Transformer (GPT) models. GPT-2, GPT-3, and InstructGPT were the most recent additions to the models' evolution, which had been ongoing since 2019[2]. The greatest advancement in the evolution of the GPT model occurred before the system started using human feedback. This is because improvements in computational efficiency allowed GPT-3 to be trained on a larger amount of data than GPT-2, which gave it a more varied knowledge base and the ability to handle a wider range of tasks[2].

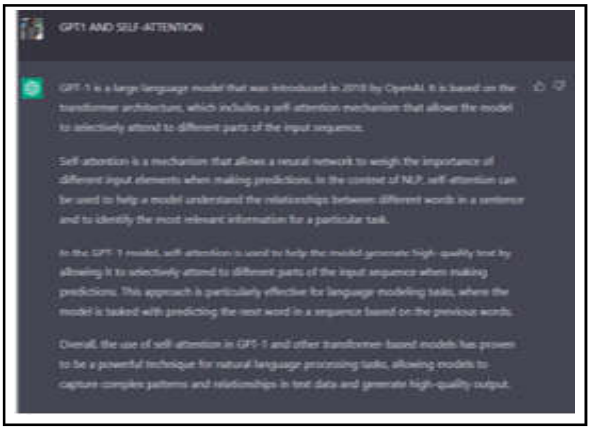

Fig.5 GPT1 Self-attention Source [3]

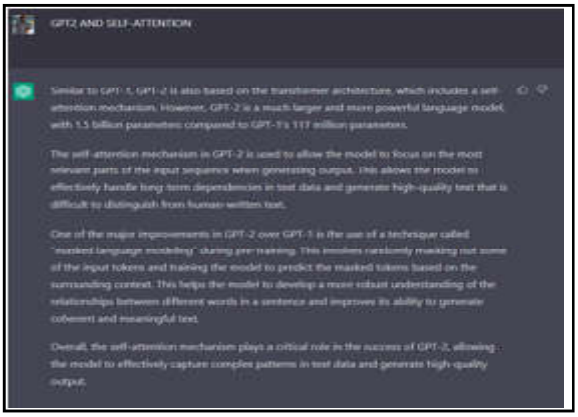

Fig.6 GPT2 Self-attention Source[3]

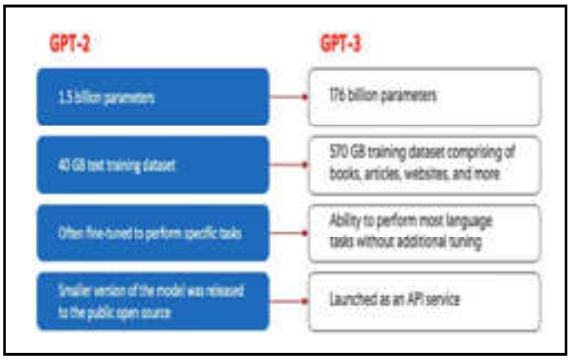

Fig.7 Comparison of GPT-2 (left) and GPT-3 (right) Source [1, 2]

Each and every GPT model has a transformer architecture, which consists of a decoder to create the output sequence and an encoder to process the input sequence[1, 2]. A multi-head self-attention mechanism

is present in both the encoder and decoder that enables the model to differentially weight different portions of the sequence in order to infer meaning and context. In order to comprehend the relationships between words and create more understandable responses, the encoder also makes use of masked-language modelling.

Tokens (items of text, which can be a word, sentence, or other grouping of text) [1, 2] are transformed into vectors that represent the token's relevance in the input sequence by the self-attention process that powers GPT. The model, thus,

- For each token in the input sequence, a query, key, and value vector is created.
- Using the dot product of the two vectors, determine how similar the query vector from step one is to each token's key vector.
- By passing the result of step 2 into a softmax function, normalised weights are produced.
- Creates a final vector by multiplying the weights from step 3 by the value vectors of each token, which represents the significance of the token within the sequence.

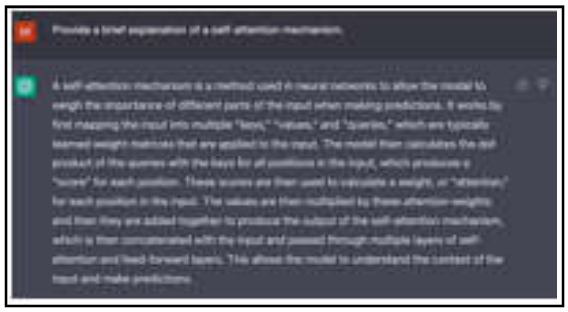

Fig.8 Self-attention Source [3]

The GPT's "multi-head" attention mechanism is an advancement of self-attention. The model iterates this technique numerous times in parallel rather than carrying out steps 1-4 only once, creating a fresh linear projection of the query, key, and value vectors each time. The model is able to comprehend sub-meanings and more intricate linkages within the input data by increasing self-attention in this way.

Although GPT-3 made significant strides in natural language processing, it has a limited capacity to match user intentions. GPT-3, for instance, could result in outputs that,

Fig.9 GPT3 Self-attention Source [3]

- They are not helpful if they do not adhere to the user's clear instructions.
- Include hallucinations that are based on false or unreliable facts.
- Lack of interpretability makes it challenging for people to comprehend how the model came to a specific conclusion or prediction.
- Incorporate damaging, offensive, or prejudiced stuff that spreads misinformation and is toxic or biassed.

To address some of these built-in problems of traditional LLMs, innovative teaching approaches were incorporated in ChatGPT.

Fig.10 GPT4 Self-attention Source [3]

4. GPT AND GPT-4?

OpenAI, a firm supported by Microsoft Corp., unveiled GPT-4, a potent update to ChatGPT. The GPT-4 programme can adopt a dialogic conversational position and provide superior information, facts, and analysis in response to queries. Users of ChatGPT can alter the chatbot's tone and delivery style, unlike the technology's prior incarnation, which had a fixed tone and aesthetic.

GPT-4 is a "multimodal" tool, able to respond to both text and image commands to produce information. The potential for collaboration and creativity is really high in this most recent edition of Chat GPT. It can also create, edit, and improve writing projects for both artistic and practical reasons, such as creating screenplays and songs

or understanding a user's writing style. It suggests that a text generator with strong analytical capabilities and the capacity to form views can take on the role of a lawyer at one point, a chemistry expert at another, and so on.

And among GPT-4's many features are:

- More than 50 specialists contributed to the development of GPT-4, the most recent step in OpenAI's endeavour to scale up deep learning, including AI safety and security.
- Our internal analyses show that GPT-4 is 82% less likely to reply to requests for content that is not permitted and 40% more likely to produce factual responses than GPT-3.5.
- GPT-4 can tackle complex problems because of its extensive general knowledge and problem-solving abilities.
- GPT-4, the most advanced system in OpenAI, produces safer and more informative answers.
- With use in the actual world, GPT-4 will be continuously reviewed and modified. GPT-4's sophisticated reasoning and command-following skills accelerated safety work.
- The production of training data for classifier iterations in training, assessments, and monitoring is facilitated by GPT-4.
- GPT-4's infrastructure also makes it possible for it to be delivered to people all around the world because it was trained on Microsoft Azure AI supercomputers.

GPT-4 is available on ChatGPT Plus as well as as an API that programmers can use to build applications and services. GPT-4 can process both text and image inputs, but only the text-input feature will be available to ChatGPT Plus subscribers and software developers, and there will be a waiting. One can update their account model from GPT-3.5 default to GPT-4 for a $20 monthly subscription cost. And a user who choose the subscription plan will have access to new features earlier, receive more frequent updates, and receive quicker response times.

GPT-4's acknowledged drawbacks, such as social prejudices, hallucinations, and hostile prompts, are still being worked on. OpenAI is making a lot of effort to encourage transparency, user education, and broader AI literacy in an effort to help shape the GPT model in response to a noticeable increase in users.

5. TRAINING METHODS

In order to get started, ChatGPT is trained using dialogue datasets, including demonstration data, where human annotators show examples of what a chatbot assistant should say in response to given cues. Using supervised learning, this data is utilised to fine-tune GPT3.5, creating a policy model that can create several responses when given prompts. The best responses to a prompt are then ranked by human annotators, and this information is utilised to train a reward model. The policy model is then iteratively improved using reinforcement learning and the reward model.[4]

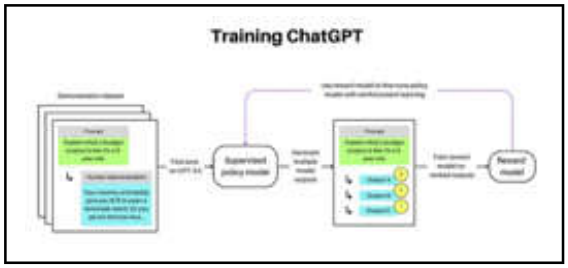

Fig. 11 Traning ChatGPT Source [4]

In a nutshell, Reinforcement Learning from Human Feedback (RLHF), a technique for adding human feedback to enhance a language model during training, is used to train ChatGPT. Instead of only predicting the next word in a phrase using a corpus of general training data, like GPT-3, this enables the model's output to align to the job desired by the user.[4]

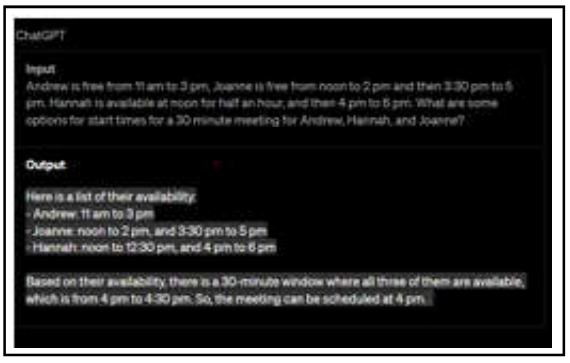

Fig.12: GPT Source [5]

The exact method used to train GPT-4 by OpenAI is still a secret. "Details on the architecture (including model size), hardware, training compute, dataset construction, training procedure, or similar" are not included in their Technical Report. What is known is that GPT-4 is a transformer-style generative multimodal model that was trained on data that was both openly available and licenced from a third party before being adjusted using RLHF. Incidentally, OpenAI did divulge information on

their improved RLHF methods, which increase model accuracy and decrease the likelihood that answers may stray outside of safety margins.[4]

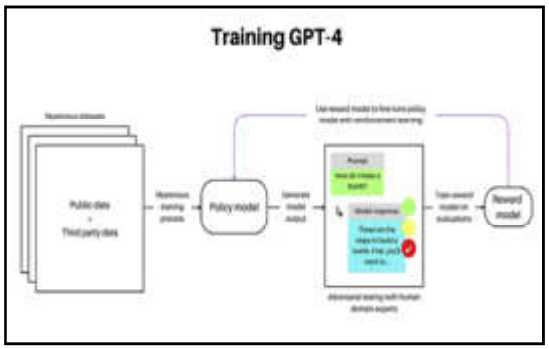

Fig.13 Traning ChatGPT4 Source [4]

GPT-4, in contrast to ChatGPT, which only accepts text, allows prompts that include both text and graphics and responds with text. Sadly, the ability to use image inputs is not currently accessible to the general public as of the publication of this article.

5.1 Performance

As comparison to GPT-3.5, OpenAI reports a considerable improvement in safety performance for GPT-4 (from which ChatGPT was fine-tuned). It is unclear at this moment, nevertheless, whether the GPT-4 model itself or the additional adversarial testing is to blame for the decrease in replies to requests for prohibited content, the decrease in the production of poisonous content, and the improvement in responses to sensitive themes.[4]

Also, GPT-4 performs better than GPT-3.5 on the majority of human-administered academic and professional exams. In contrast to GPT-3.5, which received a score in the 10th percentile on the Uniform Bar Test, GPT-4 received a score in the 90th percentile. Moreover, GPT-4 greatly beats its predecessor on benchmarks for conventional language models and other SOTA models (although sometimes just barely).[4]

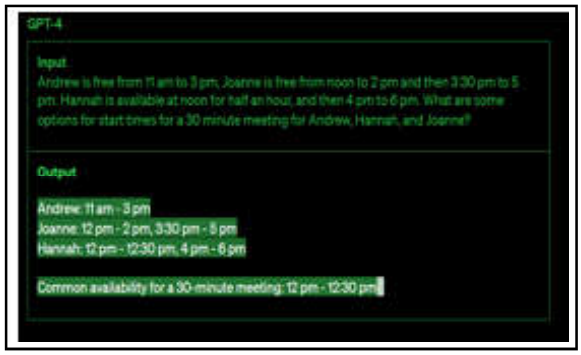

Fig.14 GPT 4 Source[5]

5.1.1 Step 1: Supervised Fine Tuning (SFT) Model

The initial step in the process was to fine-tune the GPT-3 model by employing 40 contractors to provide a supervised training dataset, in which each input has a predetermined outcome from which the model may learn. The Open API was used to gather inputs, or prompts, from actual user entries. After that, the labelers responded appropriately to the prompt, producing a known output for each input. This new, supervised dataset was subsequently used to enhance the GPT-3 model, resulting in GPT-3.5, also known as the SFT model.[4]

Just 200 prompts could originate from a single user ID in order to enhance diversity, and any prompts that had lengthy common prefixes were eliminated. The last step was the removal of all prompts holding personally identifiable information (PII).[4]

Labelers were requested to produce sample prompts to fill out categories for which there was little genuine sample data after gathering prompts from the OpenAI API. The interest categories included

- Simple requests: any random question.
- Few-shot instructions are those that have several question/response pairings.
- User-based prompts: relate to a particular use-case for the OpenAI API that was requested.

Labelers were instructed to try their best to deduce what the user's instruction was when producing answers. The primary three methods for information requests are discussed in the study.

- Clearly: "Tell me about..."
- Write another narrative about the same subject based on these two samples of stories.
- Continue: Given the beginning of a tale, complete it.

13,000 input/output samples were generated via the combination of OpenAI API prompts and handwritten labeler instructions. These samples were used to train the supervised model.[4]

5.1.2 Step 2: Reward Model

The SFT model produces better aligned responses to user prompts following step 1's training. The next improvement involves developing a reward model, whose model inputs consist of a sequence of questions and

answers and whose output is a scaler value known as a reward. To take advantage of Reinforcement Learning, in which a model learns to create outputs to maximise its reward, the reward model is necessary (see step 3).[4]

Labelers are shown 4 to 9 SFT model outputs for a single input prompt in order to train the reward model. Students are required to create combinations of output ranking starting with the best and working their way down.

Overfitting resulted from adding each combination to the model as a single datapoint (failure to extrapolate beyond seen data). Each group of rankings was used as a single batch datapoint for building the model to tackle the problem.

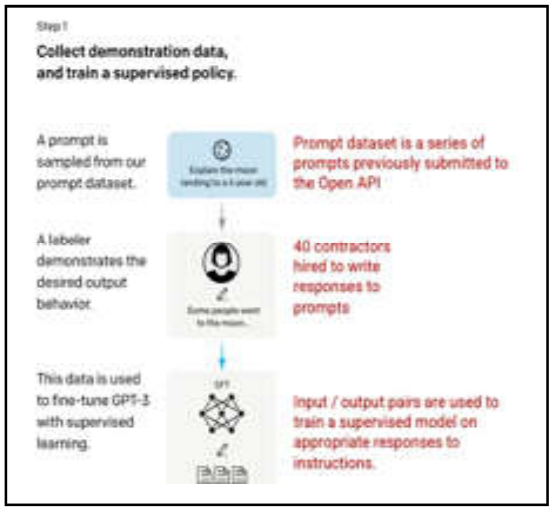

Fig. 15 Supervised Fine Tuning (SFT) Model Source[1, 2]

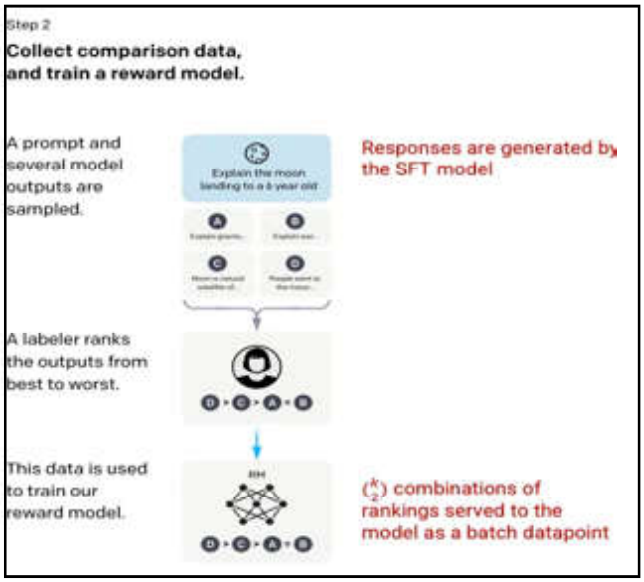

Fig.16 Collect Comparison Data Source [1, 2]

5.1.3 Step 3: Reinforcement Learning Model

The model receives a random cue in the last stage and responds with an answer. The response is produced using the "policy" that the model learned in step 2 of the training process. The policy is an approach the computer has learned to adopt to accomplish its objective, in this example, maximising its reward. A scaler reward value is then established for the prompt and response pair using the reward model created in step 2 as a basis. The model then incorporates the reward to modify the policy. [1, 2]

Proximal Policy Optimization (PPO), a mechanism used to update the model's policy as each response is produced, was first introduced by Schulman et al. in 2017. A per-token Kullback-Leibler (KL) penalty from the SFT model is included in PPO. The KL divergence penalises excessive distances and gauges how similar two distribution functions are. In order to prevent over-optimizing the reward model and departing too significantly from the human intention dataset, using a KL penalty in this instance decreases the distance that the replies can be from the SFT model outputs developed in step 1. [1, 2].

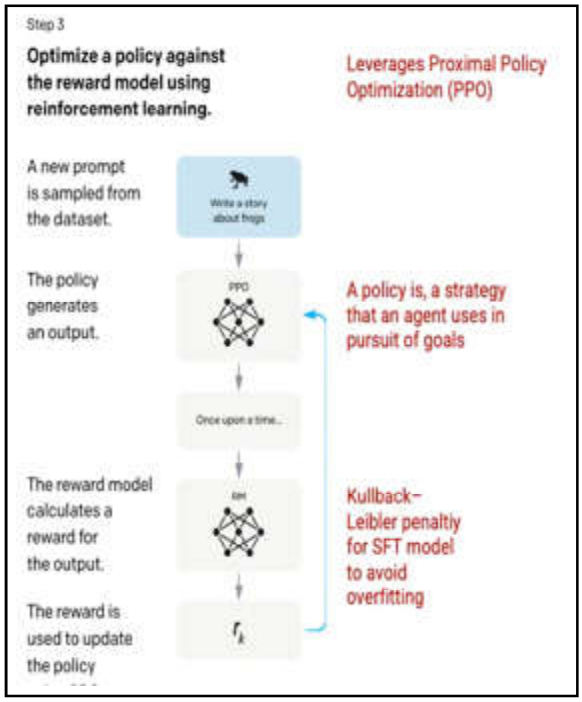

Fig.17 Optimize the policy Source [1, 2]

Although this hasn't been done a lot in practise, it is possible to repeatedly go through steps 2 and 3 of the process.

Fig.18 Reinforcement Learning Model Source [2]

6. EVALUATION OF THE MODEL

By reserving a test set during training that the model hasn't seen, the model is evaluated. A series of analyses are performed on the test set to check whether the model is more aligned than its forerunner, GPT-3. [1, 2]

Helpfulness: The capacity of the model to deduce and implement user instructions. 85 3% of the time, labelers chose InstructGPT outputs over GPT-3 outputs. [1, 2]

Sincerity: The model's propensity for hallucinations. When evaluated using the TruthfulQA dataset, the PPO model generated outputs that demonstrated marginal increases in truthfulness and informativeness. [1, 2]

Harmlessness: The model's capacity to stay away from offensive, disparaging, and demeaning material. With the use of the RealToxicityPrompts dataset, harmlessness was evaluated. Three different scenarios were used to conduct the test. [4]

- When instructed to respond respectfully, the number of toxic reactions significantly decreased.
- Without any context for respect, asked to respond: no discernible improvement in toxicity.
- A toxic reaction was requested, and the results were noticeably more harmful than the GPT-3 model.

7. CONCLUSION

In conclusion, ChatGPT is an advanced language model built on the GPT-3.5 architecture that uses deep learning techniques to understand and generate natural language. It learns from vast amounts of textual data and uses attention mechanisms, neural networks, and language modeling to produce coherent and relevant responses in a conversation. Its advanced capabilities make it an effective tool for various natural language processing tasks, including language translation, text summarization, and question-answering. With its ability to understand and generate natural language, ChatGPT has the potential to revolutionize communication and enhance user experiences in a range of domains, from customer service and education to entertainment and healthcare.

Fig.19 Reinforcement Learning Model Source [3]

Fig.20 Reinforcement Learning Model Source [3]

We go over ChatGPT and GPT-4's training procedures, performance and capabilities, limitations and hazards, as well as their key parallels and distinctions.

GPT-4 purports to be an improved version of ChatGPT that now accepts image and text inputs and claims to be safer, more accurate, and more creative, despite the fact that we know very little about the model architecture and training techniques behind it. However, as GPT-4 is only a part of the ChatGPT Plus subscription, we will have to trust OpenAI's word for it.

With the publication of ChatGPT and GPT-4 only a few months apart, the competition to develop the most precise and dynamic big language models has

accelerated. As we traverse this fascinating but quickly changing terrain of massive language models, it is crucial to be educated about the developments, hazards, and limitations of these models.

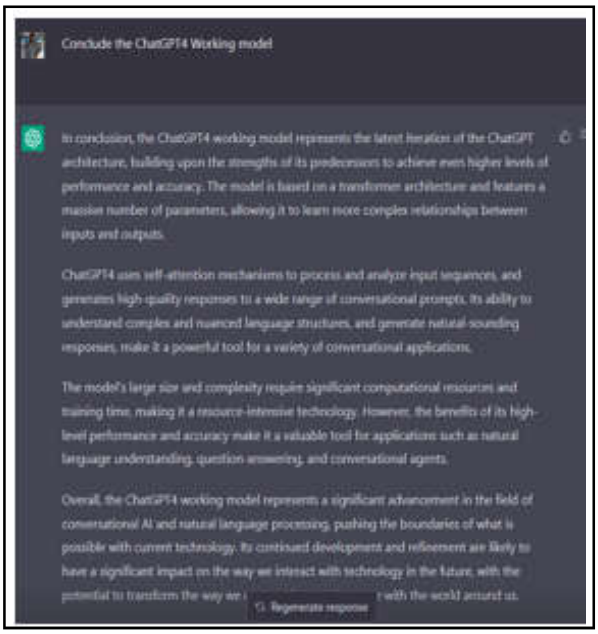

Fig.21 Reinforcement Learning Model Source [3]

Fig.22 Reinforcement Learning Model Source [3]

As the technology behind ChatGPT continues to advance, we can expect even more impressive capabilities from this powerful language model in the future.

REFERENCES

[1] L.Ouyang,*et al*., "Training Language Models to Follow Instructions with Human Feedback", Advances in Neural Information Processing Systems, Vol.35, 2022, pp.27730-27744.
[2] M. Ruby, "How ChatGPT Works: The Model Behind The Bot", 2023.
[3] ChatGPT. Screenshots from ChatGPT. 2023.
[4] M.Newhauser, "GPT-4 vs.ChatGPT: An Exploration of Training, Performance, Capabilities, and Limitations", 2023.
]5] OpenAI's. GPT-4 is OpenAI's Most Advanced System, Producing Safer and More Useful Responses, 2023.

HYBRID STRUCTURE OF PURE ZnO, ZnO:NiO, ZnO:SnO2 NANO COMPOSITES

B. Sharanya Shree, T. Preethi, S.V. Tharanprabu and S. Ashokan
Department of Physics, Advanced Material Research Lab,
Bannari Amman Institute of Technology, Sathyamangalam - 638 401, Erode District, Tamil Nadu
E-mail: ashopudur@yahoo.com

Abstract

Pure ZnO, NiO nanoparticles and ZnO:NiO nanocomposite are successfully synthesized by co-precipitation and mechanical mixture method respectively. The structural, optical and electrical studies were carried out for the prepared samples. X-ray diffraction of the synthesized nanocomposites confirms that the synthesized nanocomposites crystalize in their respective crystal structure without any deviation and no impurity phases have been observed. The average crystalline size and dislocation density were found to be 33nm and $0.001001m^{-2}$. A red shift in the absorption band edge of ZnO nanocomposites is observed while adding SnO_2 and NiO nanoparticles. UV-Vis absorption spectra shows ZnO nanocomposites are highly transparent in the visible region which is the characteristic of a wide band gap metal oxides. The absorbance of the sample was found to be increased for nanocomposites compared to pure ZnO nanoparticles. In order to study the electrical conductivity, I-V characteristics of ZnO nanoparticles is studied.

Keywords: *Conductivity, Nanocomposites, XRD*

1. INTRODUCTION

Metal oxides are an interesting class of materials intensively investigated nowadays, and displaying unique properties including mechanical stress tolerance, high optical transparency, exceptional carrier mobilities, etc. Several metal oxide nanomaterials have been reported in recent years, however, the most investigations are focused on low-cost, abundant, and nontoxic. Zinc oxide (ZnO), titanium dioxide (TiO_2), tungsten oxide (WO_3), copper oxides (CuO and Cu_2O), and tin oxides (SnO and SnO_2) have all these prerequisites, as well as some of them being environment friendly, easily produced and can be integrated in distinct applications [1,2].

With the development of science and technology, researchers are able to synthesis and explore micro-level materials for numerous applications. In particular, nanosized materials offer unique and special properties which gives huge scope for researchers to investigate.

The researchers have been focused on the nanostructured II-VI semiconductors due to their excellent properties in luminescence and the photo-electrochemistry. In thrust of preparing novel materials, scientists are attempting to develop inorganic/organic hybrid materials to modify the composition and the particle size as per contraption [3].

Nanostructured metal oxide materials attracted a lot of attention due to their potential optical, magnetic, electrical and catalytical properties which can be used in many promising applications. Among a various transition metal oxides Zinc oxide (a wide band gap n-type semiconductor material) founds wide range of applications than that of others. Zinc oxide possess unique properties like direct and wide band gap (Eg= 3.37 eV) and high exciton binding energy (60 meV). This high value of exciton binding energy allows an efficient excitonic emission even at room temperature and thus assures the possibility to obtain low threshold and high efficiency photonic devices [4-6].

Nickel oxide (NiO) a p-type semiconductor (Eg=3.5 eV) possesses high hole concentration, high hole mobility, and low lattice mismatch with ZnO, which facilitates the formation of p-n heterojunction with ZnO [7].

Recently, electrospun and thermal oxidization methods have been reported for the preparation of NiO- ZnO heterojunctions with enhanced photocatalytic activities [8, 9]. Uddin et al. have reported photocatalytic properties of ZnO/SnO_2 nanostructures for degradation of organic dyes. The heterojunction structure between ZnO/SnO_2 plays very important role in improving its sensing

properties [10]. Humidity sensing depends on the reaction induced water vapor molecules absorbed on sample surface. ZnO, NiO and SnO2 nanoparticles were prepared by co-precipitation and hybrid structure such as ZnO:NiO and ZnO:SnO2 composites are made by mechanical mixture method. The prepared nanocomposite samples have been characterized by various physical characterization techniques and have been reported.

2. MATERIALS AND EXPERIMENTAL METHODS

Zinc acetate dehydrate ((CH3COO) Zn.2H2O, Himedia), Sodium hydroxide (NaOH, Merck), iso- propyl alcohol (Sigma-Aldrich), acetone (Sigma-Aldrich) was used without further purification as they were of analytical grade. In the present work, nanoparticles were synthesized by chemical precipitation method.

2.1 Synthesis of ZnO Nanoparticles by Chemical Precipitation Method

The aqueous solution of (CH3COO) Zn.2H2O (0.1 M) was prepared in a cleaned round bottomed flask. Then 0.2 M of NaOH solution were added and stirred with the above mentioned precursor solution. The nanoparticles solution was prepared with continuous stirring for 2 hrs at 60^{O}C (750 rpm). The large quantity of milky white precipitate is yielded from the transparent solution. The obtained precipitate was centrifuged at 4500 rpm for 5 mins. and washed 3-4 times with de-ionized water and acetone. The precipitated samples were dried in hot air oven at 75^{O}C for 6 hrs. The prepared samples were grinded and finally characterized to confirm the presence of Zinc oxide nanoparticles.

2.2 Synthesis of SnO_2 and NiO nanoparticles

For SnO2 synthesis, first 0.01M of SnCl2. 2H2O, (1.1M) of NaOH, (0.002M) of CTAB were dissolved in 35 mL of de-ionized water and stirred at 2000 rpm for 30 mins at room temperature. Then the solution was transferred to a Teflon-lined stainless-steel autoclave with 50 mL capacity. The autoclave was placed in muffle furnace and heated to 140°C for 5 hours. After cooling to room temperature, the black precipitates obtained were washed 3-4 times with de-ionized water and absolute ethanol by centrifugation (4500 rpm), and then dried at 60°C for overnight in air to obtain the final black SnO_2 powders.

For the pure NiO nanoparticles synthesis, NiCl2·6H2O and NaOH were taken in the desired molarity of 0.1M. Then aqueous solution of $NiCl_2 \cdot 6H_2O$ was stirred for 20 min. The pH value was adjusted to 10 by using NaOH solution. Once pH value of solution has attained 10, the solution is allowed to stir for 4 hours. The precipitates were centrifuged and washed with De-ionized water 3-4 times. Samples were dried at 80°C for 8 hours in hot air oven. Finally, the dried powders were calcined at 550°C to obtain NiO Nanoparticles.

2.3 Preparation of Hybrid Nanocomposites

The prepared ZnO nanoparticles were annealed at 400^{O}C for 2 hrs in Muffle furnace. A 0.6g of ZnO and 0.6 mg of SnO_2 nanoparticles were mixed by mechanical mixture method and annealed at 400^{O}C for 2 hours. Finally, the hybrid nanocomposites powder is obtained and the same process was continued with ZnO and NiO nanoparticles. Finally, the dried hybrid nanocomposites were finely-grinded by using a mortar.

Fig. 1 Preparation of (a) ZnO without annealing, (b) ZnO, (c) ZnO:SnO2 and (d) ZnO:NiO nanocomposites annealing with 400^{O}C.

3. RESULTS AND DISCUSSION

The prepared powdery ZnO, ZnO:NiO and ZnO:SnO_2 hybrid nanocomposites are characterized by structural, optical, and electrical studies.

3.1 Structural Analysis (XRD)

X-ray diffraction pattern of ZnO, ZnO:NiO and (c) ZnO:SnO2 nanocomposites are shown in Figure 2 (a-c). All the diffraction peaks are well matched with the standard card values (JCPDS No:36-1451) which correspond to hexagonal wurtzite structure of ZnO. The peaks at angle (2θ) 31.84^{o}, 34.38^{o}, 36.25^{o}, 47.50^{o}, 56.54^{o}, 62.85^{o}, 66.38^{o}, 67.94^{o}, 69.16^{o}, 72.51^{o} and 76.93^{o} correspond to reflections from (1 0 0), (0 0 2), (1 0 1), (1 0 2), (1 1 0), (1 0 3), (2 0 0), (1 1 2), (2 0 1), (0 0 4) and (2 0 2) are shown in Figure 2a.

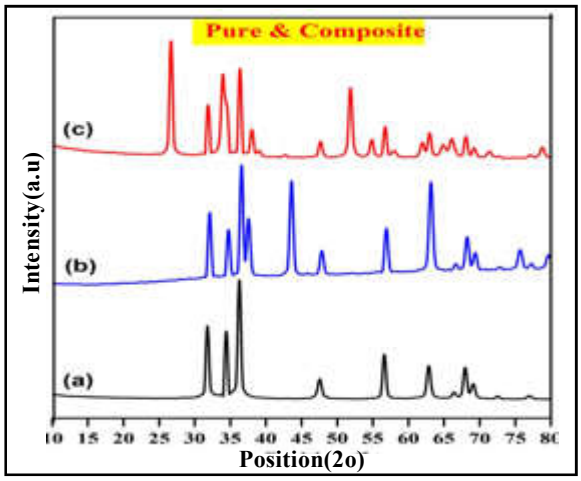

Fig. 2 XRD pattern of (a) ZnO nanoparticles (b) ZnO:NiO and (c) ZnO:SnO² nanocomposites

No extra peak of any other phases is detected in the diffraction patterns which confirm the high purity of the obtained ZnO. The observed highly intense peaks of the sample shows good crystalline nature of the obtained nanoparticles [11].

In the ZnO:NiO nanocomposites the two distinct face-centered cubic and hexagonal structures were identiыed at annealing temperature of 400^{O}C and is shown in Figure 2b. The diffraction peaks can be indexed to cubic structure of NiO (JCPDS 78-0643) and hexagonal structure of ZnO (JCPDS 36-1451), respectively.

The diffraction peaks remain sharp and no other characteristic peaks for impurities are present. As can be expected, the XRD patterns of the ZnO:SnO_2 nanocomposite shown in Figure 2c, contain diffraction peaks from both hexagonal wurtzite ZnO (JCPDS 76-0704) and tetragonal SnO_2 (JCPDS 71-0652). The existence of ZnO and SnO_2 in their corresponding crystalline phases confirms the formation of nanocomposites rather than alloy.

The average crystallite size of the hybrid composite is estimated using the Scherrer's equation (1):

$$D=k\lambda/\beta\cos\theta \quad (1)$$

where, λ is the X-ray wavelength (1.5406 E), k is the shape factor (constant value ~ 0.89), D is the average diameter, θ is the Bragg angle in degrees and β is the line broadening measured by half- height in radian. The dislocation density (δ) can be evaluated from Williamson and Small man's formula (2),

$$\delta=1/D^2 \quad (2)$$

The average crystallite size and dislocation density of the prepared ZnO nanopowders is found to be 33 nm and 0.001001m^{-2}, respectively.

Further, ZnO nanoparticle has good luminescent properties and high light sensitive and therefore it is very attractive materials for opto-electronic applications.

Table 1 XRD patterns of pure ZnO, ZnO:NiO and ZnO:SnO_2 nanocomposites

ZnO Nanopowders		ZnO:NiO Hybrid Nanocomposites		ZnO:SnO2 Hybrid Nanocomposites			
Pos.[°2Th.]	hkl	Pos.[°2Th.]	hkl	Pos.[°2Th.]	hkl	Pos.[°2Th.]	hkl
31.84	1 0 0	32.2398	1 0 0	26.6812	1 1 0	58.0104	0 0 2
34.38	0 0 2	36.6688	1 0 1	31.9169	1 0 0	62.0173	1 0 3
36.25	1 0 1	37.5288	1 1 1	33.9469	1 0 1	62.9750	3 1 0
47.50	1 0 2	43.5625	2 0 0	34.5175	0 0 2	64.7942	1 1 2
56.54	1 1 0	47.8579	1 0 2	36.3398	1 0 1	66.0653	2 0 0
62.85	1 0 3	56.7671	1 1 0	37.9995	2 0 0	68.0324	1 1 2
66.38	2 0 0	63.0908	2 20	47.6571	1 0 2	69.1616	3 1 1

3.2 Optical Absorbance Analysis (UV)

The optical properties of ZnO nanoparticles are studied by analyzing the UV-Vis spectra. Optical absorption spectra of nanoparticles were recorded in the spectral range from 200 nm - 600 nm using UV-Vis-NIR spectrophotometer (JASCO V-770). The UV-Vis absorption spectra for pure ZnO, ZnO:NiO and ZnO:SnO_2 nanocomposites were recorded at room temperature are given Figure 3.

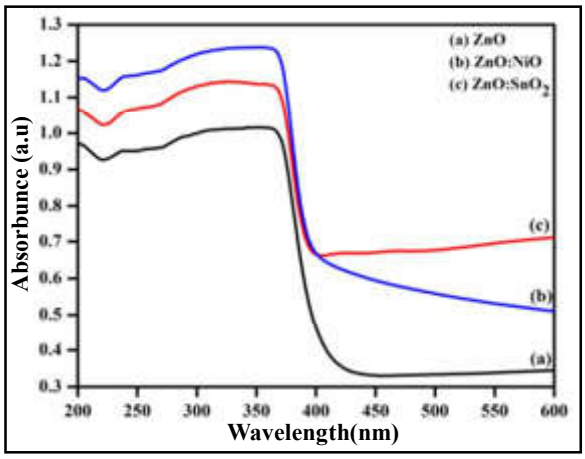

Fig. 3 UV-Vis absorbance spectra of (a) ZnO, (b) ZnO:NiO and (c) ZnO:SnO2 nanocomposites

Figure 3(a) shows two individual absorption bands at ~238 nm and ~315 nm for ZnO nanoparticles. The Figure 3 (b & c) shows absorbance spectra around 239 and 362 nm. A red shift in absorption band edge is observed on adding NiO and SnO_2, which can be ascribed to the well-known quantum size effect.

It is observed that for the hybrid nanocomposites absorbance band is shifted from 315 to 362 nm and all the bands are attributed to p - p* transitions. The band gap of ZnO nanoparticles were estimated using the transition rate equation for direct band gap semiconductor [12]. The absorption coefficient for direct transition is given by the equation (3):

$$\alpha h\nu = A(h\nu - E_g)^n \qquad (3)$$

where hν = photon energy, α = absorption coefficient ($\alpha = 4\theta\pi k/\lambda$; k is the absorption index or absorbance, λ is the wavelength in nm), E_g=band gap energy, A=constant, n=a constant which depends on the probability of transition. The direct band gap energies were calculated by plotting Tauc's plot between $(\alpha h\nu)^2$ versus photon energy (hν) for ZnO nanoparticles.

The calculated absorption band gap value is in the range of 2.3eV-3.94 eV.

3.3 Optical Emission Analysis (PL)

Photoluminescence spectra was observed using PL spectrometer (JASCO-FP 8300). Figure 4 shows the emission spectra of pure ZnO and ZnO:NiO, ZnO:SnO_2 nanocomposites recorded at room temperature. In Figure 4(a) PL spectra shows four-emission bands at around ~296 nm, ~384 nm, ~414 nm and ~464 nm. While for nanocomposites (Figure 4 (b,c)) the peaks are shifted to ~304 nm, ~397 nm, ~417 nm and ~467 nm. All spectra show a peak around 296 nm resulting due to electron transfer from valence band (VB) to conduction band (CB) that could be the origin of any emission. The peak observed at 384 nm from the excitonic recombination corresponding to the near band-edge emission of ZnO.

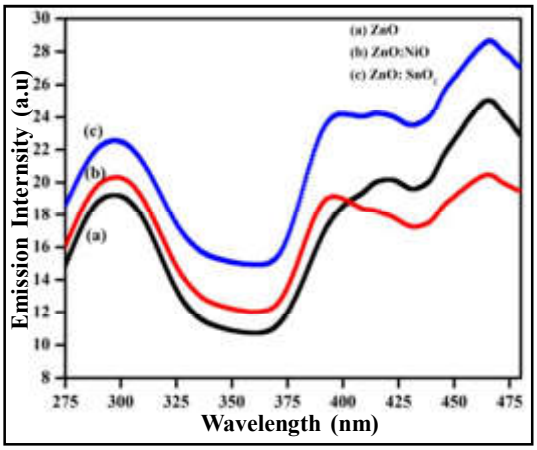

Fig. 4 PL spectra of (a) ZnO, (b) ZnO:NiO and (c) ZnO:SnO2 nanocomposites

The peak centered at ~395 nm corresponds to UV emission which was attributed to inter band radiative transition. The peak observed around 416 nm and 466 nm corresponds to blue emission, which is due to transition of electrons from shallow levels to the acceptor levels above the valence band.

Table 2 PL Emission Spectra Peaks

Samples	Peak1(nm)	Peak2(nm)	Peak3(nm)	Peak4(nm)
ZnO	296	384	414	464
ZnO:NiO	302	395	416	466
ZnO:SnO2	304	397	417	467

The band gap energy is calculated using the formula given below, $E_g = (h*c)/\lambda$. The band gap values of ZnO, ZnO:NiO and ZnO:SnO2 nanocomposites are 3.2eV, 3.17eV and 3.1 eV.

The bandgap energy is decreased for ZnO nanocomposites in comparison with pure ZnO nanoparticles.

3.4 Electrical Studies

Electrical conductivity measurements are carried out for the prepared samples in the room temperature range using Keithley electrometer 6517B. Fig. 5 shows the I-V characteristics of ZnO nanoparticles. From that it has been observed that the current varies linearly with voltage which indicates ohmic behavior of ZnO nanoparticles. The conductivity of the samples was estimated using the formula (4),

$$\alpha = (I \times L) / (2\pi S) \quad (4)$$

where, I is the current, V is the voltage, S is the distance between the probes. The conductivity decreases with increase in resistivity. The calculated electrical conductivity value of ZnO nanoparticles is $4.02*10^{-06}$ S/cm.

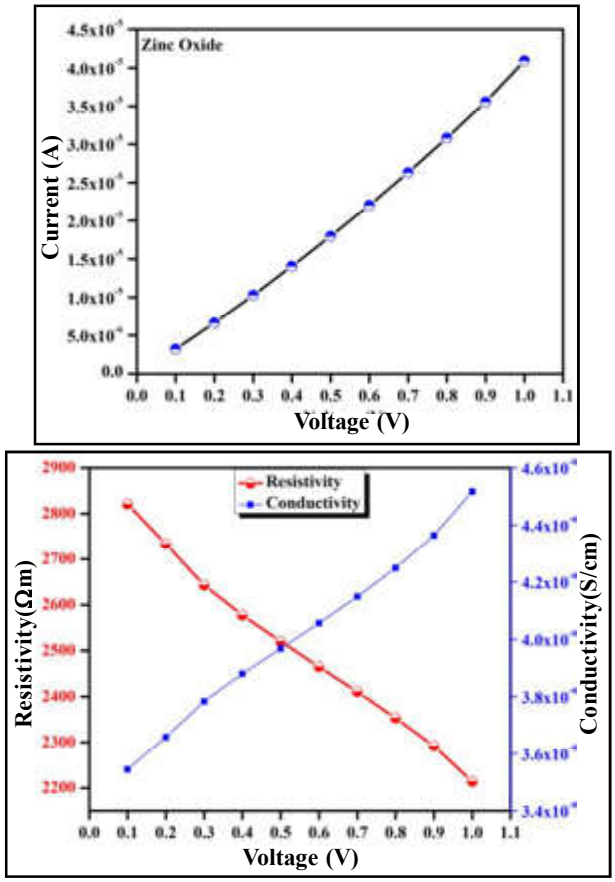

Fig. 5 I - V characteristics of ZnO nanoparticles and (b) Electrical resistivity vs. conductivity

4. CONCLUSION

Pure ZnO, NiO, SnO_2 nanoparticles, ZnO:NiO and ZnO:SnO_2 nanocomposites were prepared by coprecipitation and physical mixing of the obtained nanopowders. The structural, optical and electrical properties of the synthesized nanocomposites have been studied. X-ray diffraction pattern confirms the existence of synthesized nanoparticles in their corresponding crystal system. PL spectra show that the main emission band is observed in UV and visible region. The band gap values of ZnO, ZnO:NiO and ZnO:SnO_2 nanocomposites are 3.2eV, 3.17eV and 3.1 eV. The bandgap energy is decreased for ZnO nanocomposites in comparison with pure ZnO nanoparticles. The quantum confinement effect in ZnO is important for UV optoelectronic device applications. From the electrical conductivity studies it is observed that ZnO nanoparticles obey ohmic nature of the material and the measured conductivity values is found to be $4.02* 10^{-06}$ S/cm.

REFERENCES

[1] S. Ameen, M. S. Akhtar, S. G. Ansari, O. Yang and H.S.Shin, "Electrophoretically Deposited Polyaniline/ZnO Nanoparticles for p–n Heterostructure Diodes", Superlattices and Microstructures, Vol.46, 2009, pp.872-880.

[2] A.A. Othman, "Sonochemically Synthesized ZnO Nanosheets and Nanorods: Annealing Temperature Effects on the Structure, and Optical Properties", Ceramics International, Vol.43, 2017, pp.527-533.

[3] S. Kumar, N. Jaggi, R.Nigam and V.Kundu, "Sol–gel Synthesis of ZnO–SnO2 Nanocomposites and their Morphological, Structural and Optical Properties", J Mater Sci: Mater Electron, Vol.2, 2016.

[4] K. Raja, "Synthesis, Structural and Optical Properties of ZnO and Ni-doped ZnO Hexagonal Nanorods by Co-precipitation Method", Spectrochim. Acta-Part A Mol. Biomol. Spectrosc, Vol.120, 2014, pp.19-24.

[5] N. A. Salahuddin, "Synthesis and Characterization of ZnO Nanotubes by Hydrothermal Method", International Journal of Scientific and Research Publications, ISSN 2250-3153, Vol.5, 2015.

[6] N. Kamarulzaman, M.F. Kasim and R.Rusdi, "Band Gap Narrowing and Widening of ZnO Nanostructures and Doped Materials", Nanoscale Res Lett, Vol.10, 2015, pp.346.

[7] P. Dai, T. Yan, X. Yu, Z.Bai and M.Wu, "Two-solvent Method Synthesis of NiO/ZnO Nanoparticles Embedded in mesoporous SBA-15: Photocatalytic Properties Study", Nanoscale Research Letters, Vol.11, 2016, pp.226.

[8] J. N. Li, F. Zhao, L. Zhang, M. Y. Zhang, H. F. Jiang and S. Li *et al*, "Electrospun Hollow ZnO/ NiO Heterostructures with Enhanced Photocatalytic Activity", RSC Adv. Vol.5, 2015, pp.67610-612.

[9] C.Z. Luo, D.L.Li, W.H.Wu, Y.P. Zhang and C.X.Pan, "Preparation of Porous Micro-nano-structure NiO/ZnO Heterojunction and its Photocatalytic Property", RSC Adv, Vol.4, 2014, pp.3090-5.

[10] M.T. Uddin, Y. Nicolas, C. Olivier, T. Toupance, L. Servant, M. M. Muller, H. J. Kleebe, J. Ziegler and W. Jaegermann, "Nanostructured SnO_2-ZnO Heterojunction Photocatalysts Showing Enhanced Photocatalytic Activity for the Degradation of Organic Dyes, Vol.51, 2012, pp.7764-7773.

[11] Y. Volokitin, J. Sinzig, L. J. Jongh, M. N. Vargaftik and I. I. Moiseevi II, "Quantum-size Effects in the Thermodynamic Properties of Metallic Nanoparticles, Nature, Vol.384,1996, pp.621-623.

[12] G.N. Narayana, "Effect of Annealing Temperature on Structural, Optical and Electrical Properties of Hydrothermal Assisted Zinc Oxide Nanorods", Thin Solid Films, Vol.598, 2016, pp.39-45.

EFFICIENT CHARACTER RECOGNITION AND STORAGE OF TYPE-WRITTEN AND HAND-WRITTEN DOCUMENTS

V. Sri Vigna Hema and L. Priya
Department of Information Technology,
Bannari Amman Institute of Technology, Sathyamangalam - 638 401, Erode District, Tamil Nadu
E-mail:vignahema@gmail.com

Abstract

In reality, there is a huge demand for storing and retrieving information to a storage disk from the various datum available in handwritten documents or images to utilize the information by means of computers. We can achieve the same by simply scanning the required documents and uploading it in an image format. The main problem comes in the re-utilizing these data, it would be very difficult to manipulate these query text, that are necessary. Optical Character Recognition comes into play to achieve this functionality. The main objective of OCR is to achieve modifications of any form of text-containing documents into editable format for deeper processing. The OCR can be differentiated into two types by considering the input format, these include OCR for handwritten characters and for typewritten characters. This editable extracted text is finally imported into the SQL Server database for effective usage of data. Here, SQL Server database is already maintained for specific departments and thus claiming its effectiveness.

Keywords: *Database, Next.js, OCR, Optical Character Recognition, React.js, SQL Server*

1. INTRODUCTION

The efficient character recognition and storage of type-written and hand-written documents system offers functionality to quick access and maintenance of user desired information that can be arranged and edited as per desired need. The application enables various uses namely monitoring of results and performance of certain value-based departments. They could also be used for sharing desired data to multiple users just by scanning documents.

With a computer system, the system can maintain nearly hundreds of records per day, making it quicker and more precise. When necessary, the system will also allow searching for specific information. This software application is created in a way that it can accommodate any future fundamental CRUD activities that can be carried out on necessary data requirements.

Consider an MNC or a low-level cottage industry, instead of manually updating their profit data or worker's information or certain details about the project, they can just easily scan their documents with the help of the application and import the same into the database.

Overall, the web app is a unique and innovative online platform that offers a novel approach to extract predefined information from scanned images and documents that can be stored in a database for effective usage. This information is stored in a database for effective CRUD operations.

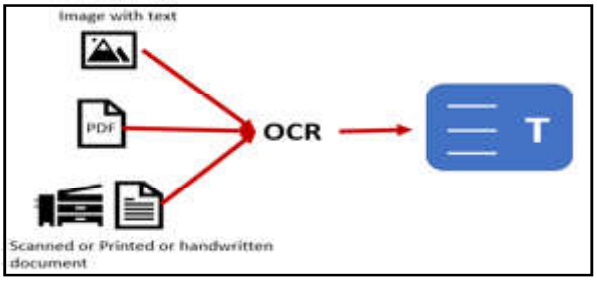

Fig.1 OCR

1.1 Advantages of the Proposed Method

The effective character recognition and storage of type-written and hand-written document web app has several advantages over traditional OCR methods and other data extraction apps. Here are some of the benefits

Increased Accuracy: It can recognize text accurately, reducing the risk of human error associated with manual data entry.

Cost Savings: It can reduce the cost associated with paper-based document storage and retrieval. Digitizing

documents reduces the need for physical storage space and makes it easier to search and retrieve information.

Accessibility: It can make printed or handwritten text accessible to people with visual impairments, as the text can be read aloud by screen reading software.

Searchability: Once text has been digitized using OCR, it can be searched and sorted electronically, making it easier to find specific information within a document.

Scalability: It can be used to digitize large volumes of documents quickly and efficiently, making it ideal for businesses or organizations with large amounts of data to manage.

1.2 Application of the Proposed Method

Document Scanning and Management: It can be used to digitize paper documents, allowing them to be stored electronically and easily searched, sorted, and retrieved.

Data Entry: It can be used to automate the data entry process, reducing the time and cost associated with manual data entry.

Banking and Finance: It can be used to read checks, bills, and other financial documents, helping to automate financial transactions and reduce errors.

Healthcare: It can be used to convert patient records, medical histories, and other documents into digital format, making them easily accessible and searchable.

Retail: OCR can be used to scan and recognize product information, such as barcodes and price tags, improving inventory management and customer service.

2. METHODOLOGY

2.1 Existing System

The methodology of OCR is commonly used, many applications implement the technology of OCR but an effective way for manipulation of databases has not been provided. Nowadays applications implementing OCR for typewritten text are capable of copying the extracted text and can modify the same.

Existing systems may take maintenance of the system erroneously, because of the overly processed data. This project overcomes these problems by extracting only the desired information and these information are editable that can be modified according to user's wish and is finally automatically updated to the database.

2.2 Drawbacks

Drawbacks of the system are given below.
The system requires a lot of manpower for maintaining information. So the process is time consuming Reports generation is difficult since the maintenance is manual and also it leads to error prone results No convenient way to store the extracted information.

2.3 Proposed System

The Proposed system implements an application in order to solve these problems, where data is stored in a database and data can be viewed at any time. Effective CRUD operations are made possible on the extracted text. An efficient system should be developed, with the aim of ensuring that data free from redundancy are feasible. The extracted data should be precise and should not take a lot of time to be processed.

The proposed scheme should encourage multiple organizations and educational institutions to adapt the applications in order to manage their huge database. The web app will be built using react.js running on next.js, the proposed system contains two segments. The first segment titled 'Type-written text extraction' is built in typescript with the help of tesseract API which is used to achieve the OCR capabilities and uses prisma ORM in order to connect with the database.

The second segment titled 'Hand-written character recognition' is built using python along with its libraries (tensorflow-keras, numpy, bidict) in order to model a convolutional neural network that consists of sequential layers.

2.4 Features

The system will automatically update the database with the extracted text of specific importance. The extracted information can later be altered or modified using UI.

Through the system, databases can be maintained for various fields and sharing of these databases is made easy. The extracted text can also be edited before updating into the database. Current entries in the database

can also be viewed, there is a specific button in the application just to see the important information in the database. Being a web application, the storage takes very little space and thanks to tesseract API the processing time is also reduced. The images selected or captured can be cropped into more concentrated areas thanks to the open source matine API.

2.5 Implementation Details

The web app will be built into two segments one for recognition for type-written documents and another for hand-written documents.
Front End : Reactjs.
For Type-written document Segments: typescript and tesseract API.
For Hand-written Character Recognition Segment:Python(libraries:numpy,tensorflow,bidict).
Database: Microsoft SQL server.

2.5.1 Front End

The web app is developed using react.js. Next.js and create-react-app is installed.

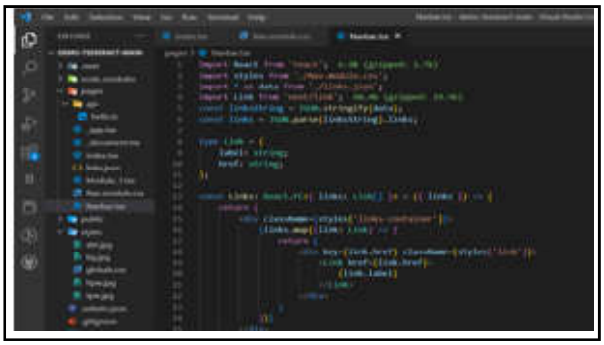

Fig.2 Import statements

Each segment routes are stored as a json format that is looped using map function and the navbar is made. Initially a navbar is created.

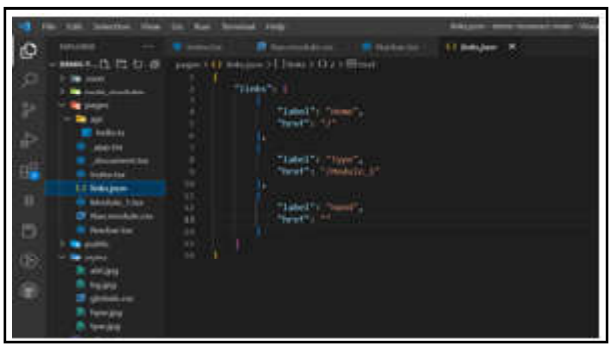

Fig. 3 Route links as json

Bootstrap is used for styling. Individual cards are created using bootstrap.

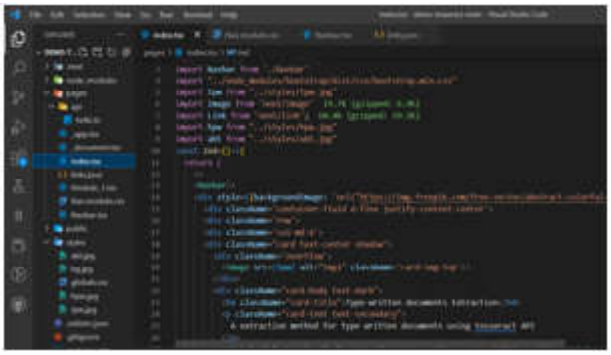

Fig. 4 individual cards

2.5.2 Back End (Type-written Text Extraction)

The Type-written segment is built using matine and tesseract API.

Fig. 5 tesseract API

The render is then altered.

2.5.3 Back End (Hand-written Character Recognition)

The Type-written segment is built using python and its libraries (numpy,bidict,flask,tensorflow-keras). Html pages are created and is routed correspondingly.

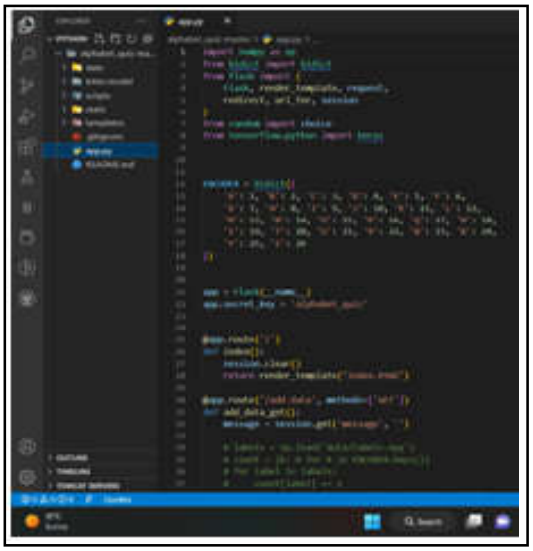

Fig.7 Bidict implementation

A canvas is created using css and html elements which is used to acquire pixels from the canvas and is then processed through the neural network saved as a local state and is then the character is determined using the bidict numpy array.

Fig.8 canvas

2.5.4 Database

Microsoft SQL server is the database used here. A new database and a table is created. The table is then customized with an example usage. Here the connection to the sql server is achieved by using prisma. Prisma is an open source next-generation ORM. The connection pool is altered for localhost connection and the schema. prisma is edited regarding the same.

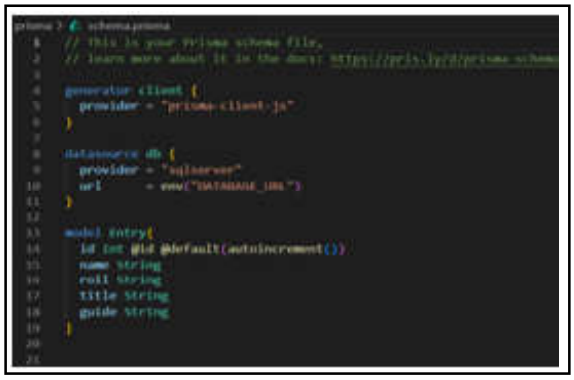

Fig.9 prisma schema

3. RESULTS AND DISCUSSION

3.1 Results

Following a review of the system's needs, the system will be developed. Even someone with basic computer expertise will be able to utilize the system because it will be designed in an approachable way with helpful messages for the user.

Since the system was created using effective technologies, it is entirely menu-driven and very user-friendly. Error messages that are appropriate are given to guide the user in a suitable and user-friendly way.

Tables are designed with primary keys and foreign keys in order to establish relationships between tables. In order to get ideas for implementation, the design part has been done. Development and testing has been completed.

3.2 Discussion

- To increase the text extraction accuracy and lower the amount of mismatches, tesseract API is implemented and additional extraction of data can be done.
- To improve user engagement and database management, the app might provide new features or sharable options.
- To assure only legal data are processed and prevention of sharing of illegal data can be easily identified and suitable officers can be alarmed of this situation can be made possible in future case.

4. CONCLUSION

Finally, the efficient character recognition and storage of type-written and hand-written documents app is a

cutting-edge solution to the age-old problem of data entry and maintenance. The app's features and functionality, such as its extraction algorithm, search and filter features, database tools, verification and safety measures, provide users with a dependable and efficient way to store and extract their data and also share their database.

While there is always room for improvement, this web app has the potential to revolutionize the traditional text extraction process by providing users with a convenient, safe, and efficient way to extract it. The success of the app is ultimately determined by user satisfaction and engagement, which can be achieved through ongoing optimization and improvement of its design and functionality.

Overall, this web app is a promising storage and character recognition method with the potential to significantly improve the lives of many organizations looking for automation data entry.

5. FUTURE SCOPE

Efficient Character Recognition and Storage of type-written and hand-written documents system offers functionality to quick access and maintenance of user desired information that can be arranged and edited as per desired need. The application enables various uses namely monitoring of results and performance of certain value-based departments. They could also be used for sharing desired data to multiple users just by scanning documents.

There are various scopes for future works in the same, imagine if a blind person uses this application we can create a module that can consist of sensors or audio equipment which will be able to convey the database information in a suitable format. The database used here can be altered for major sharing between users features.

In short, there are a lot of upgrades to be made and features could be added in the application. Being an emerging technology, research regarding the same is currently being pursued by many scholars and researchers.

REFERENCES

[1] R.Morais, V. Le, T. Tran, B. Saha, M. Mansour and S.Venkatesh, "Learning Regularity in Skeleton Trajectories for Anomaly Detection in Videos", in Proceedings of the IEEE Conference on Computer Vision and Pattern Recognition, 2019, pp.11996-12004.

[2] S.S.Paliwal, D.Vishwanath, R.Rahul, M.Sharma and L.Vig, "Tablenet: Deep Learning Model for End-To-End Table Detection and Tabular Data Extraction from Scanned Document Images", in International Conference on Document Analysis and Recognition (ICDAR), IEEE, 2019, pp.128-133.

[3] P. Riba, A. Dutta, L. Goldmann, A. Fornes, O. Ramos and J.Llados, "Table Detection in Invoice Documents by Graph Neural Networks", in International Conference on Document Analysis and Recognition (ICDAR), IEEE, https://doi.org/10.1109/ICDAR.2019.00028, Sep 2019, pp.122-127.

[4] Y.F. Zhou, R.H. Jiang, X. Wu, J.Y. He, S. Weng and Q.Peng, "Branchgan: Unsu-pervised Mutual Image-to-Image Transfer with a Single Encoder and Dual Decoders", IEEE Transactions on Multimedia, 2019.

[5] Mathilde Caron, Ishan Misra, Julien Mairal, Priya Goyal, Piotr Bojanowski and Armand Joulin, "Unsupervised Learning of Visual Features by Contrasting Cluster Assignments", In NeurIPS, 2020.

[6] Sungha Choi, Joanne T Kim and Jaegul Choo, "Cars Can't Fly Up In the Sky: Improving Urban-Scene Segmentation via Height-Driven Attention Networks", In CVPR, 2020.

[7] Ting Chen, Simon Kornblith, Mohammad Norouzi and Ge- offrey Hinton, "A Simple Framework for Contrastive Learning of Visual Representations", In ICML, 2020.

[8] Olivier Henaff, "Data-effcient Image Recognition with Contrastive Predictive Coding", In ICML, 2020.

[9] Xia Li, Yibo Yang, Qijie Zhao, Tiancheng Shen, Zhouchen Lin and Hong Liu, "Spatial Pyramid Based Graph Reasoning for Semantic Segmentation", In CVPR, 2020.

[10] R. Reeve Ingle, Yasuhisa Fujii, Thomas Deselaers, Jonathan Baccash and Ashok C. Popat, "A Scalable Handwritten Text Recognition System", ArXiv, abs/1904.09150, 2019.

Indian Journal of Engineering, Science, and Technology (IJEST)

(ISSN: 0973-6255)
(A half-yearly refereed research journal)

Information for Authors

1. All papers should be addressed to The Editor-in-Chief, Indian Journal of Engineering, Science, and Technology (IJEST), Bannari Amman Institute of Technology, Sathyamangalam - 638 401, Erode District, Tamil Nadu, India.
2. Two copies of manuscript along with soft copy are to be sent.
3. A CD-ROM containing the text, figures and tables should separately be sent along with the hard copies.
4. Submission of a manuscript implies that : (i) The work described has not been published before; (ii) It is not under consideration for publication elsewhere.
5. Manuscript will be reviewed by experts in the corresponding research area, and their recommendations will be communicated to the authors.

Guidelines for submission

Manuscript Formats

The manuscript should be about 8 pages in length, typed in double space with Times New Roman font, size 12, Double column on A4 size paper with one inch margin on all sides and should include 75-200 words abstract, 5-10 relevant key words, and a short (50-100 words) biography statement. The pages should be consecutively numbered, starting with the title page and through the text, references, tables, figure and legends. The title should be brief, specific and amenable to indexing. The article should include an abstract, introduction, body of paper containing headings, sub-headings, illustrations and conclusions.

References

A numbered list of references must be provided at the end of the paper. The list should be arranged in the order of citation in text, not in alphabetical order. List only one reference per reference number. Each reference number should be enclosed by square brackets.

In text, citations of references may be given simply as "[1]". Similarly, it is not necessary to mention the authors of a reference unless the mention is relevant to the text.

Example

[1] M.Demic, "Optimization of Characteristics of the Elasto-Damping Elements of Cars from the Aspect of Comfort and Handling", International Journal of Vehicle Design, Vol.13, No.1, 1992, pp. 29-46.

[2] S.A.Austin, "The Vibration Damping Effect of an Electro-Rheological Fluid", ASME Journal of Vibration and Acoustics, Vol.115, No.1, 1993, pp. 136-140.

SUBSCRIPTION

The annual subscription for IJEST is Rs.600/- which includes postal charges. To subscribe for IJEST a Demand Draft may be sent in favour of IJEST, payable at Sathyamangalam and addressed to IJEST. Subscription order form can be downloaded from the following link http:// www.bitsathy.ac.in./ ijest.html.

For subscription / further details please contact:

IJEST
Bannari Amman Institute of Technology
Sathyamangalam - 638 401, Erode District, Tamil Nadu Ph: 04295 - 226340 - 44
Fax: 04295 - 226666 E-mail: ijest@bitsathy.ac.in Web:www.bitsathy.ac.in

Indian Journal of Engineering, Science, and Technology
Volume 15, Number 1&2, January - December 2021

CONTENTS